Université Lille I - Sciences et Technologies

Laboratoire de Mécanique de Lille (UMR CNRS 8107)

Ecole Doctorale SPI Lille Nord-de-France

Année 2010 - N° d'ordre : 40444

THESE

Pour obtenir le grade de

Docteur de l'Université Lille I - Sciences et Technologies

Discipline : Génie Civil

Présentée par

Adrian ROZANSKI

Sur la représentativité, la taille minimale du VER et les propriétés effectives de transport des matériaux composites aléatoires

Soutenue publiquement le 8 Décembre 2010 devant le jury composé de

M. C. BOUTIN, Directeur de recherche CNRS, ENTPE,	Président
M. D. KONDO, Professeur, Université Paris 6,	Rapporteur
M. W. PULA, Professeur, Université Technologique de Wroclaw	Rapporteur
M. D. LYDZBA, Professeur, Université Technologique de Wroclaw	co-directeur de thèse
M. J.F. SHAO, Professeur, Université de Lille I,	Directeur de thèse

Acknowledgements

Résumé :

Dans cette thèse, on s'intéresse à quelques aspects spécifiques des matériaux composites aléatoires : la taille minimale du volume élémentaire représentatif et la détermination des propriétés effectives de transport. L'objectif principal est de proposer une méthode numérique efficace permettant une détermination rapide des propriétés effectives. Les propriétés de type transport sont considérées. Il est montré que cette classe de propriétés peuvent être déterminées soit en réalisant des calculs sur un échantillon de grande taille soit en faisant moyenne sur un nombre suffisant de petites réalisations de microstructures. Cependant, pour un type de microstructure donné, la taille des ces petites réalisations ne peut pas être inférieure à une certaine limite minimale. Celle-ci est fortement influencées par plusieurs facteurs tel que type de microstructure, fractions volumiques des constituants, contrastes de propriétés entre phases, nombre de réalisation et précision acquise.

Par ailleurs, deux types de représentativités sont étudiées : représentativité géométrique et celle en rapport avec les propriétés de transport. Par conséquent, deux critères distincts de taille minimale sont proposés en se basant sur des propriétés des fonctions de corrélation à deux-points. Comparant à d'autres méthodes proposées dans de large littératures, le critère proposé ici comporte un avantage car il tient compte de la morphologie de microstructure. En conséquence, des calculs numériques comme ceux par les éléments finis ne sont pas nécessaires pour la détermination de la taille minimale de REV. La validation de la méthodologie proposée est effectuée sur plusieurs exemples de microstructures 2D.

Abstract

The thesis focuses on random composites, in particular, relates to problems such as: representativity, the minimum size of a representative volume element (RVE) and the determination of effective transport parameters. Its main objective is to formulate a computationally efficient method which would allow for quick - i.e. without a large number of numerical calculations - determination of effective properties.

Within the work effective properties of transport type are considered. It is shown that this particular type of effective properties can be estimated either by performing calculations over one large sample or by averaging over sufficient number of microstructure realizations, which are significantly smaller in size. Nevertheless, the size of the sample can not be taken as small as one may wish. It appears that, for a given type of microstructure, there exist a threshold value of RVE size – in order to properly predict effective properties of composite material, one can not take into account a sample which is smaller than the minimum one. In other words, if one analyses the RVE which is not large enough (smaller than the critical - minimum - size) then the effective property, which is determined as the mean value averaged over sufficient number of realizations, does not coincide with the response determined for infinite sample. It is shown that this critical size of RVE is strongly affected by several parameters. These are as follows: microstructure type, volume fractions of constituents, contrast in mechanical properties of composite phases, number of performed realizations as well as a desired accuracy.

Furthermore, within the work, two separate types of representativity are introduced, i.e. geometrical representativity and representativity with respect to overall transport properties. Two distinct criterions for the minimum size of RVE – with respect to microstructure geometry and to overall transport properties - are formulated basing on the properties of the two-point correlation function. Comparing to other methods proposed in wide literature, the criterion formulated in the thesis, gives an advantage, i.e. the condition utilizes a microstructure morphology, and therefore, in order to determine the minimum size of RVE none numerical calculations like those of FE are necessary.

A validation of proposed methodology is performed on several examples of 2D microstructures. These are: random checkerboard, Ising model microstructure, system of overlapping disks, system of non-overlapping disks, Debye models as well as two microstructures of real materials, i.e. Fontainebleau sandstone and boron-carbide/aluminum composite.

Contents

1. Introduction

Composites are complex materials (such as concrete, soils, rocks, foams, wood, etc.) in which two or more distinct, structurally complementary substances, are combined to produce one material of overall properties usually not present in any individual component. For instance, consider two isotropic materials, such that one of them is highly conductive while the latter is an insulator. Combining these two materials in alternating layers in a laminate structure (see Fig. 1.1) results in an original overall behaviour of the material. The composite exhibits strong anisotropy having high conductivity in direction parallel to layers whereas in direction normal to layers it posses insulating property. The laminate microstructure is of a deterministic type.
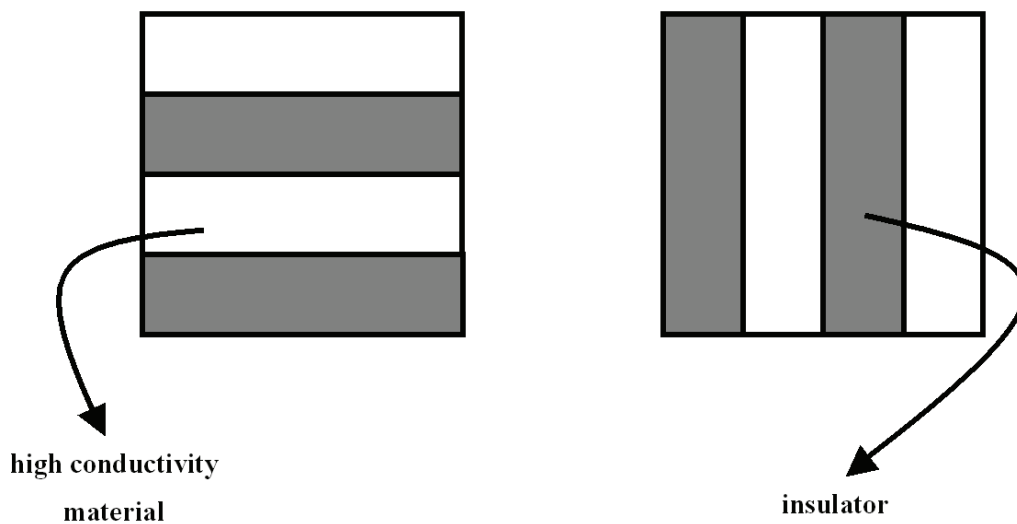
Fig. 1.1. Anisotropic composite which is produced by combining two materials – highly conductive one and an insulator.

The thesis focuses on random composites which - as distinguished from deterministic ones - exhibit limited information regarding the material. This is due to fact that, in case of random composites, the information on composite microstructure is given in terms of statistical measures, so such information like spatial distribution or geometry of composite constituents are usually only partially available since perfect description of random structure involves an infinite number of microstructure descriptors. The simplest level of information – usually available – are the volume fractions of constituents and a macroscopic isotropy if a microstructure does not possess any preferential direction of components ordering.

Within last 25 years numerical calculations, like those of finite element or finite volume, regarding effective properties determination have became accepted as the ones which provide most accurate results. In case of numerical approach, the process of effective properties determination –

averaging process – takes place over statistically representative sample of composite, i.e. representative volume element. Nevertheless, in many cases the computations over representative volume element are very often extremely large. This is due to fact that aforementioned sample of material should contain a large number of microheterogeneities to be treated as representative one for given composite.

The aim of this work is the formulation of computationally efficient method of effective properties determination of random two-phase composite materials. Focus is on transport properties – classes of transport properties considered in this work are widely discussed in next chapter. It is shown that effective properties can be estimated either by performing calculations over one large sample or by averaging over sufficient number of microstructure realizations significantly smaller in size, however not too small. It appears that there exists, for a given type of microstructure, the minimum size of RVE that one can not use smaller in order to properly predict effective properties of composite material. In other words, if the RVE is taken too small in size then the effective property calculated as the mean value averaged over sufficient number of realizations does not coincide with the response determined for infinite sample. This critical size of RVE appears to be affected by several parameters: type of microstructure, volume fractions of phases, contrast in mechanical properties of composite constituents, number of performed realizations as well as a desired accuracy. The original criterion for the minimum size of RVE is formulated in the thesis basing on the properties of microstructure descriptor, namely the two-point correlation function. The advantage of the condition proposed in this work comparing to other methods proposed in literature is that for the determination of RVE size none numerical calculations like those of Finite Element Method or Finite Volume Method are necessary.

A validation of proposed criterion is performed on several 2D microstructures. These are split into two groups: *random cell models* and *reconstructed microstructures*. Within the first group there are: random checkerboard, Ising model microstructure, system of overlapping disks, system of non-overlapping disks. In case of *reconstructed microstructures* we consider theoretical microstructure like Debye and modified Debye models as well as two microstructures of real materials, i.e. Fontainebleau sandstone and boron-carbide/aluminum composite.

The thesis is organized as follows. In chapter 2 some basics of continuum micromechanics are provided, i.e. a micro-macro passage as well as the boundary value problem concerning the diffusion process (other classes of transport processes as well) in heterogeneous media are formulated. Section 2.2 recalls both the rigorous bounds and direct estimations of effective thermal

conductivity of random heterogeneous media. Relations regarding bounds of Voigt/Reuss and those due to Hashin and Shtrikman as well as direct estimations like Maxwell's approximation, Mori-Tanaka model or self-consistent scheme are provided. In section 2.3 the notion as well as a wide literature regarding representative volume element are presented.

Chapter 3 deals with statistical descriptors of microstructure, namely *n*-point probability and lineal-path functions. The main focus is, however, on the two-point probability function which plays a central role in this work. Then some preliminary studies on notion and minimum size of RVE are performed. Particulate random microstructure is investigated, namely a random checkerboard. Such structure possesses some advantages as: simple analytical form of probability distribution, closed form equation of a local porosity variance and finally its simple microstructure geometry enables fast determination of composite overall properties. The properties like volume fraction, two-point correlation function and effective thermal conductivity coefficient are examined. It is shown that overall properties can be determined either by performing calculations over one large sample or by averaging over sufficient number of significantly smaller samples. To determine the overall value of volume fraction one can use the sample of arbitrary small size, provided that a large number of sample realization is performed. This does not hold true, however, for the overall properties as two-point probability function and effective thermal conductivity. There exists a critical RVE size which can not be decreased. For the random checkerboard microstructure this minimum RVE size is almost of the same value irrespective if it concerns the two-point correlation function or the effective thermal conductivity. A problem regarding determination of the sufficient number of realization is discussed also in this chapter. For this purpose the Central Limit Theorem and the Chebyshev's Inequality are recalled in section 3.2.2.

The crucial results of the thesis are presented in the next chapters. The condition for the minimum RVE size to be representative with respect to the two-point correlation function is formulated in chapter 4. The criterion is developed based on a random variable, so called, local volume fraction. It is shown that necessary condition is that the variance of aforementioned variable can not exceed assumed error tolerance in order the RVE does satisfactory reflect microstructure geometry. Evaluation of the local volume fraction variance is proposed to carry out by Monte Carlo technique which details are also briefly outlined. Finally, numerical validation of the minimum RVE size condition proposed is provided in section 4.3 where a sequence of different types of random microstructures are numerically tested.

The condition for the minimum RVE size to be representative with respect to overall transport properties is formulated in chapter 5. The development of the criterion follows that one presented in

chapter 4 where the criterion of minimum RVE size has been proposed with respect to microstructure geometry. This time, however, new random variables are used, namely local Voigt as well as local Reuss estimates. Slightly modified form of the two-point correlation function is also introduced in order to reflect conductivity properties of the composite constituents. Chapter ends with qualitative and quantitative investigations of minimum RVE size for random checkerboard microstructure. Some comparisons between minimum RVE sizes with respect to microstructure geometry and with respect to effective thermal conductivity are also presented.

In chapter 6 the condition for RVE size, formulated in chapter 5, is numerically tested. Once more a sequence of different types of random microstructures, the same as for validation of the criterion proposed in chapter 4, is used for validation of the criterion proposed for the minimum RVE size to be representative with respect to overall transport properties. The numerical calculations have been performed using own numerical procedure. The formulation of the numerical method – based on the finite volume scheme – as well as mesh density analysis are therefore also provided.

In chapter 7 general conclusions are formulated. Note, however, that detailed remarks regarding all aspects considered within this work are provided after each chapter.

2. Continuum micromechanics

Micromechanics of heterogeneous materials enables one to predict their macroscopic properties on the basis of both geometries and properties of phases which constitute the material. More precisely, continuum micromechanics is the analysis of overall mechanical response of composite material, for given microstructure and macroscopic load states. It consists in determining the "macroscopic" constitutive relation between properly averaged field variables as well as overall properties being material constants of the constitutive relations obtained (Fig. 2.1). The volume averaging process takes place over statistically representative sample of material which is referred to as the *representative volume element* (RVE), while overall properties are referred to as the *effective properties*.

$$\left\langle \sigma_{ij} \right\rangle = C_{ijkl}^{eff} \left\langle \varepsilon_{kl} \right\rangle$$

$$C^{(1)} \qquad C^{(2)} \qquad C^{eff}$$
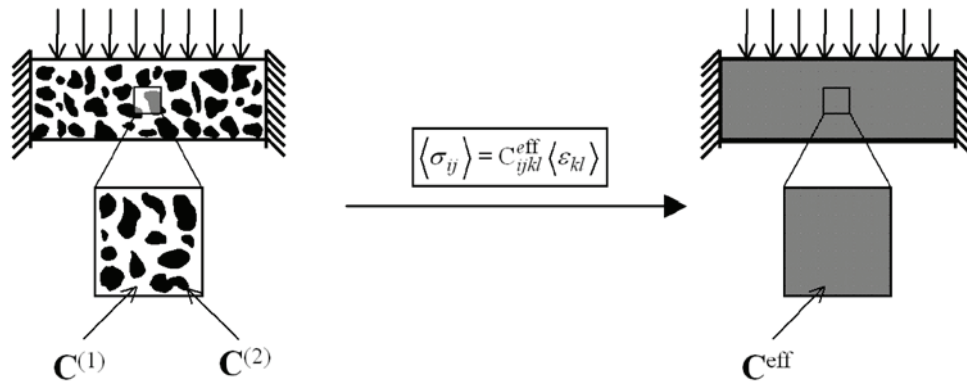
Fig. 2.1. The concept of effective properties

In a particular case of heterogeneous media, i.e. with periodic microstructure, the RVE is simply a periodic unit cell and the effective properties determination consists in solving a boundary value problem stated for this unit cell and then properly averaging the solution obtained. Then - for such media - given the geometry and properties of phases the effective properties can be determined in the unique manner. On the other hand, considering random media one possesses usually only limited statistical information about the material, i.e. the spatial distribution and geometry of composite phases are very often not given; typically, the simplest level of available information is the volume fraction of phases. Therefore, in case of random media, one can evaluate the rigorous bounds or estimates of effective properties in terms of given statistical information (Dormieux et.al. 2006; Milton, 2002; Łydżba, 2002). Then, a fundamental problem of micromechanics appears, i.e. to understand how effective properties depend on the microstructure.

In order to illustrate the fact of microstructure importance, consider now a two-phase material having the same volume fraction of constituents, i.e.: $\phi_1 = \phi_2 = \phi$ (left panel of Fig. 2.2). Assume that

the black phase is highly conductive relative to the white phase. On the other hand, the right panel of Fig. 2.2. presents the same microstructure, however, the phases are interchanged. It is easy to note that due to the connectivity of matrix the right panel microstructure has the higher conductivity even though both composites have the same volume fraction. This implies that effective properties depend also on higher-order statistical information, e.g. shapes and orientations of inclusions, connectivity of phases, spatial distributions of inclusions, etc. In fact, it was shown in the pioneering paper of Brown (Brown, 1955) that this dependence involves, even for a macroscopically isotropic material, an infinite set of correlation functions that statistically characterize the composite. Brown, in his general formula, used as statistical measures so called *n*-point correlation functions.
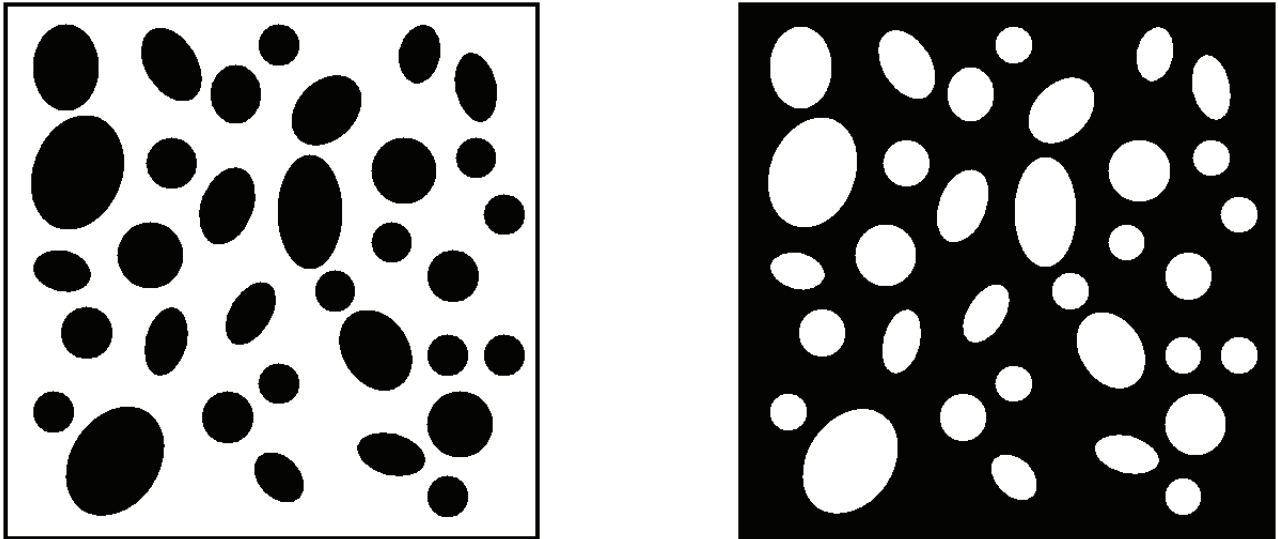
Fig. 2.2. Phase interchanged microstructures with volume fraction $\phi = 0.5$

The general formula, which expresses the effective property in terms of components' properties and microstructure statistical information, can be therefore presented as follows:

$$\mathbf{K}^{\text{eff}} = f\left(\mathbf{K}_1, \mathbf{K}_2, ..., \mathbf{K}_n; \phi_1, \phi_2, ..., \phi_n; \mathbf{\Psi}\right) \tag{2.1}$$

where $\mathbf{\Psi}$ represents the functionals of higher-order microstructure statistical descriptors (presentation of the descriptors is postponed to chapter 3). In practice, the infinite amount of information can never be obtained, and therefore, one has to rely on the limited number of microstructure information.

As mentioned in Introduction the purpose of this work is the formulation of computationally efficient numerical method of effective transport properties determination. The methodology outlined within this work is devoted to random media and is provided for solving steady state boundary value problems of heat flow, electrical current and transfer of solute (Table 2.1). Following the effective properties definition, any of aforementioned effective property, which is

generally denoted as $\mathbf{K}^{\text{eff}}$, is defined by linear relation between an average of local flux $\mathbf{F}$ and an average of local intensity $\mathbf{G}$, i.e.:

$$\mathbf{F} = \mathbf{K}^{\text{eff}}\mathbf{G} \tag{2.2}$$

For instance, in case of heat flow, averaged flux $\mathbf{F}$ represents the heat flux and the intensity $\mathbf{G}$ is the averaged gradient of temperature.

Table 2.1. Classes of transport problems (Sviercoski, 2007)

Heat flow	Electrical current	Transfer of solute
Temperature: T Conduction Coeff. $\lambda(x)$ $q = \lambda(x)\nabla T$ Fourier's law	Voltage: V Specific Coeff. $\sigma(x)$ $q = \sigma(x)\nabla V$ Ohm's law	Concentration: C Diffusion Coeff. $D(\text{x})$ $q = D(x)\nabla C$ Fick's law

2.1. Micro-Macro passage

The micro-macro transition, i.e. development of a macroscopic description from that at the micro-level, consists of transforming the latter, through appropriate averaging over RVE procedure, into a framework in which only the macroscopic variables (averaged variables) are employed. To do a complete transformation between different observation scales, the microscopic description needs, in general, to be supplemented by suitable boundary conditions at the peripheries of RVE. These conditions should reflect, as closely as possible, the actual state of RVE within the considered medium (Suquet, 1987).

Incorporation of specific boundary conditions in the local description is often referred to as "closing hypothesis". It allows isolating RVE from its environment and, thus, narrowing the scope of analysis to the examination of mechanical characteristics of RVE alone. For composite solids, for instance in case of heat conduction process, the simplest and most frequently employed closing hypothesis is the assumption of uniform heat flux or uniform temperature gradient state. However, such hypothesis is justified only when the size of individual inhomogenities is small compared to dimensions of RVE. In case of periodic media, i.e. when the material structure can be reconstructed based on a single RVE cell, the boundary conditions incorporate the local periodicity of the considered physical fields.

The micro-macro passage is simply illustrated by an example of stationary diffusion process in a heterogeneous medium which occupies the volume V. However, as mentioned before, other transport problems can be investigated in the same manner.

The micro-scale description of diffusion process is based on:

- constitutive equation (Fick's law) for each phase of composite:

$$q_i = -D \frac{\partial C}{\partial x_i} \quad \text{in } V, \tag{2.3}$$

- mass conservation equation:

$$\frac{\partial q_i}{\partial x_i} = 0 \qquad \text{in } V, \tag{2.4}$$

where q_i is a x_i component of the mass flux vector of the diffusing substance, C is the concentration and D is the diffusion coefficient, each constituent of composite is characterized by its own value of diffusion coefficient. The flux is said to be continuous at the interfaces between constituents.

The concentration of substance at any point within the volume V can be defined as:

$$C = \left\langle \frac{\partial C}{\partial x_i} \right\rangle \left(x_i - z_i^c \right) + \left\langle C \right\rangle + \overline{C} \tag{2.5}$$

where $<*>$ is the volume averaging operator, $\left\langle \dfrac{\partial C}{\partial x_i} \right\rangle$ is the macroscopic gradient of concentration

$\left\langle C \right\rangle$. The coordinates z_i^c specify the location of the centroid of RVE, while $\overline{C}$ is so-called corrector term. The presence of corrector function $\overline{C}$ in formula (2.5) is the result of local heterogeneity of considered medium. This function is constrained by $\left\langle \overline{C} \right\rangle = 0$, which can be formally proved by averaging (2.5) and noting that $\left\langle y_i - z_i^c \right\rangle = 0$.

Substituting the Fick's law (2.3) together with (2.5) in (2.4), one obtains:

$$\begin{cases} -\dfrac{\partial}{\partial x_i} \left(D \left\langle \dfrac{\partial C}{\partial x_i} \right\rangle + D \dfrac{\partial \overline{C}}{\partial x_i} \right) = 0 & \text{in } V \\ \text{boundary conditions} & \text{on } \partial V \end{cases} \tag{2.6}$$

Now, the boundary conditions for RVE are typically formulated by assigning specific values to corrector or its gradient. For a periodic structure, the periodicity of corrector function is postulated; whereas for a random media, the specific value of its gradient preserving the uniform flux or simply vanishing of the corrector.

Assigning, for example, a zero value to the corrector along boundaries of RVE and noting that the boundary value problem (2.6) possesses a linear form, thus, $\overline{C}$ depends linearly on the macroscopic gradient $\left\langle \dfrac{\partial C}{\partial x_i} \right\rangle$, i.e.

$$\overline{C} = A_i \left\langle \frac{\partial C}{\partial x_i} \right\rangle \tag{2.7}$$

where A_j is the solution of (2.6) corresponding to macroscopic gradient with its *j*-component equal to one and the remaining ones equal to zero. Then, the formula which relates the local value of concentration gradient to its macroscopic counterpart can be established:

$$\frac{\partial C}{\partial x_j} = P_{ij} \left\langle \frac{\partial C}{\partial x_i} \right\rangle \tag{2.8}$$

where $P_{ij} = \left(\delta_{ij} + \frac{\partial A_i}{\partial x_j} \right)$ is referred to as the localization operator. Relation (2.8) allows now to express the macroscopic flux of diffusing substance as a function of the macroscopic concentration gradient, i.e.:

$$\left\langle q_i \right\rangle = -D_{ij}^{\text{eff}} \left\langle \frac{\partial C}{\partial x_j} \right\rangle \tag{2.9}$$

where $D_{ij}^{\text{eff}} = \left\langle D P_{ij} \right\rangle$.

Relation (2.9) represents the macroscopic constitutive equation which describes the diffusion process in a medium that is homogeneous at the macro-scale. The tensor D_{ij}^{eff} is the effective (homogenized) diffusion tensor. In case of deterministic microstructure expression (2.9) is simply the linear relation between volume averaged local flux and the volume average of local intensity. Nevertheless, when random media are considered, expression (2.9) becomes the relation between ensemble averages of local fields (Milton, 2002). The approach concerning random media is outlined further in this work.

It has to be marked that depending on the boundary condition applied, the following inequalities hold true (Suquet,1987; Sab, 1992):

$$D_F^{eff} \leq D_\#^{eff} \leq D_G^{eff}$$

where $D_\#^{eff}$ represents the diffusion coefficient evaluated at the periodic conditions, D_F^{eff} and D_G^{eff} correspond to the uniform flux and uniform gradient boundary conditions, respectively. If RVE is large enough then these values coincide. This implies that "true" effective property of composite corresponds to the asymptotic value, with increasing size of RVE, independently of the conditions type applied at the boundaries of RVE. Furthermore, the periodic boundary condition leads to the faster convergence to that value (see for instance Kanit et.al, 2003), so in the following

parts of the thesis only periodic boundary conditions are used, whenever numerical calculation is performed.

2.2. Rigorous bounds and existing models

For random media the distribution of constituents and their geometry are not strictly defined, i.e. only limited statistical information is available. Typically, the primary information which can be obtained is that on volume fractions of individual constituents. Furthermore, if there is no preferred arrangement of constituents, i.e. the structure is not ordered, the other statistical information available is that stipulating the isotropy of the medium at the macro-scale. Since the statistical information is incomplete, only the estimates of effective properties and the range of their admissible values can be provided.

In this section the rigorous bounds as well as some direct estimates of effective transport properties are briefly discussed. The exhaustive presentation of this subject one can find in several books (Dormieux et.al., 2006; Dormieux and Ulm, 2005; Milton, 2002; Torquato, 2002).

The theorems are presented for the case of thermal conductivity (heat transfer) problem (note that all the formulas provided above are valid for other transport problems presented in Table 2.1).

The oldest micromechanical models which take into account only the volume fractions of composite phases are those due to Voigt and Reuss. These models are very simple and may be interpreted, for macroscopic linear properties of composites, as upper and lower bound, respectively. These bounds take into account only the volume fractions of composite phases, thus they are quite wide and provide basic qualitative information. The effective conductivity tensor $\boldsymbol{\lambda}^{\mathrm{eff}}$ is bounded from above by the arithmetic mean and from below by the harmonic mean of phase conductivities:

$$\left\langle \boldsymbol{\lambda}^{-1} \right\rangle^{-1} \leq \boldsymbol{\lambda}^{\mathrm{eff}} \leq \left\langle \boldsymbol{\lambda} \right\rangle \tag{2.10}$$

More sophisticated bounds for a two phase composite were developed in 1963 by Hashin and Shtrikman (Hashin & Shtrikman, 1963). These bounds, beyond the volume fraction of constituents, incorporates, in addition, the macroscopic isotropy of composite. The *d*-dimensional Hashin-Shtrikman bounds on λ^{eff} for two-phase isotropic media are as follows:

$$\left\langle \lambda \right\rangle - \frac{\phi_1 \phi_2 \left(\lambda_2 - \lambda_1 \right)^2}{\left(\lambda_1 \phi_2 + \lambda_2 \phi_1 \right) + (d-1) \lambda_1} \leq \lambda^{\mathrm{eff}} \leq \left\langle \lambda \right\rangle - \frac{\phi_1 \phi_2 \left(\lambda_2 - \lambda_1 \right)^2}{\left(\lambda_1 \phi_2 + \lambda_2 \phi_1 \right) + (d-1) \lambda_2} \tag{2.11}$$

where ϕ_i and λ_i are the volume fraction and conductivity of phase *i*, respectively, whereas $\left\langle \lambda \right\rangle = \lambda_1 \phi_1 + \lambda_2 \phi_2$. The bounds (2.11) are established with following assumption: $\lambda_2 \geq \lambda_1$.

The general bounds on the effective conductivity λ^{eff} of multicomponent, d-dimensional and macroscopically isotropic composites are also known. In case of composite consisting of p phases we have:

$$\left(\sum_{i=1}^{p}\phi_i\left((d-1)\lambda_{\min}+\lambda_i\right)^{-1}\right)^{-1}-\lambda_{\min}\leq\lambda^{\text{eff}}\leq\left(\sum_{i=1}^{p}\phi_i\left((d-1)\lambda_{\max}+\lambda_i\right)^{-1}\right)^{-1}-\lambda_{\max} \tag{2.12}$$

where $\lambda_{\min}$ and $\lambda_{\max}$ are the smallest and the largest phase conductivities, respectively. Note that in case of $p=2$ relation (2.12) simply reduces to (2.11). Furthermore, the bounds (2.12) were shown by Milton (1981c) to be realizable.

More complex bounds which involves higher-order statistical information as well as bounds for macroscopically anisotropic composites can be found in the wide literature. For more details see e.g. Willis (1977), Milton (1981a, 1981b), Milton (2002), Torquato (1985), Sen & Torquato (1989), Torquato (2002).

Within last fifty years a lot of direct estimations of effective properties were also developed. The Maxwell approximation, self-consistent scheme (Zaoui, 1987), Mori-Tanaka and Kuster-Toksöz models (Dvorak & Benveniste 1992; Suquet 1997), to mention only a few, all have a notable place in the field of micromechanics. These methods are based on the solution of the problem of a single inclusion immersed in an infinite homogeneous body. The presentation below is limited to spherical inclusion immersed in a composite matrix. Ellipsoidal inclusions as well as anisotropic arrangement of constituents are exhaustively treated, for instance, in the book of Dormieux et.al. (2006).

In case of composite consisting of (p-1) constituents, all of the spherical shape, immersed in the constituent being the matrix, the Maxwell's approximation is given in the following form (Milton, 2002).:

$$\frac{\lambda_M-\lambda^{\text{eff}}}{2\lambda_M+\lambda^{\text{eff}}}=\sum_{i=1}^{p-1}\frac{\phi_i\left(\lambda_M-\lambda_i\right)}{2\lambda_M+\lambda_i} \tag{2.13}$$

where λ_M stands for the matrix conductivity coefficient. Maxwell's approximation is an explicit scheme, in the sense that the effective conductivity coefficient is obtained directly from the values of constituents parameters. Furthermore, if the conductivity coefficients of inclusions are smaller/larger than the value corresponding to the matrix, λ_M, then the estimate from Maxwell's scheme is identical to upper/lower bounds of Hashin-Shtrikman.

Like the Maxwell's scheme, the Mori – Tanaka model has been formulated for composite media in which one of the constituents forms the matrix, while the remaining ones are the inclusions (Dormieux, 2006). Once again, considering the multicomponent composite which consists of (p-1) spherical inclusions the Mori – Tanaka gives following estimate for effective conductivity:

$$\lambda^{\mathrm{eff}} = \frac{\displaystyle\sum_{i=1}^{p} \frac{3\phi_i \lambda_i \lambda_M}{2\lambda_M + \lambda_i}}{\displaystyle\sum_{i=1}^{p} \frac{3\phi_i \lambda_M}{2\lambda_M + \lambda_i}} \tag{2.14}$$

Even though the formulations within Maxwell's approximation and Mori-Tanka model are different, in case of spherical inclusions they yield the same estimate of effective properties.

On the contrary to Maxwell's and Mori – Tanaka's models the self-consistent scheme is an implicit one, i.e. the assessment of λ^{eff} requires the solution to an implicit equation. For spherical inclusions the formula is given as follows:

$$\sum_{i=1}^{p} \phi_i \frac{\lambda_i - \lambda_M}{\lambda_i + 2\lambda_M} = 0 \tag{2.15}$$

All direct estimations presented above are, in many cases, very efficient. Nevertheless, the deficiencies of these estimates are also well known, e.g. the Maxwell approximation as well as Mori-Tanaka scheme give good prediction if the volume fraction of inclusions is not too large; the failure of self consistent scheme appears when very large contrast in properties is studied.

Consider two-phase composite with high contrast in constituents' properties, $\dfrac{\lambda_2}{\lambda_1} \to \infty$, then relation (2.15) reduces to:

$$\frac{\lambda^{\mathrm{eff}}}{\lambda_1} = \left(1 - 3\phi_2\right)^{-1} \tag{2.16}$$

Therefore phase 2 (spherical inclusions) will percolate at the volume fraction of $\phi_2^{\mathrm{per}} = \dfrac{1}{3}$ (Fig. 2.3). Note that this critical value of volume fraction does not depend on the statistical information regarding the microstructure. On the other hand it is shown in Torquato (2002) that the percolation threshold for spherical inclusions strongly depends on the microstructure, i.e. in case of overlapping spheres the critical volume fraction is $\phi_2^{\mathrm{per}} \approx 0.29$, whereas for "hard-spheres" $\phi_2^{\mathrm{per}} \approx 0.64$.

Assuming now that phase 2 consists of perfectly insulating spheres, i.e. $\dfrac{\lambda_2}{\lambda_1} \to 0$ relation (2.15) yields

$$\frac{\lambda^{\mathrm{eff}}}{\lambda_1} = 1 - \frac{3}{2}\phi_2 \tag{2.17}$$

Relation (2.17) implies that the volume fraction of phase at which it no longer conduct is $\phi_2^{per} = \dfrac{2}{3}$ (Fig. 2.4). Once again the value of critical volume fraction ϕ_2^{per} does not depend on the microstructure.
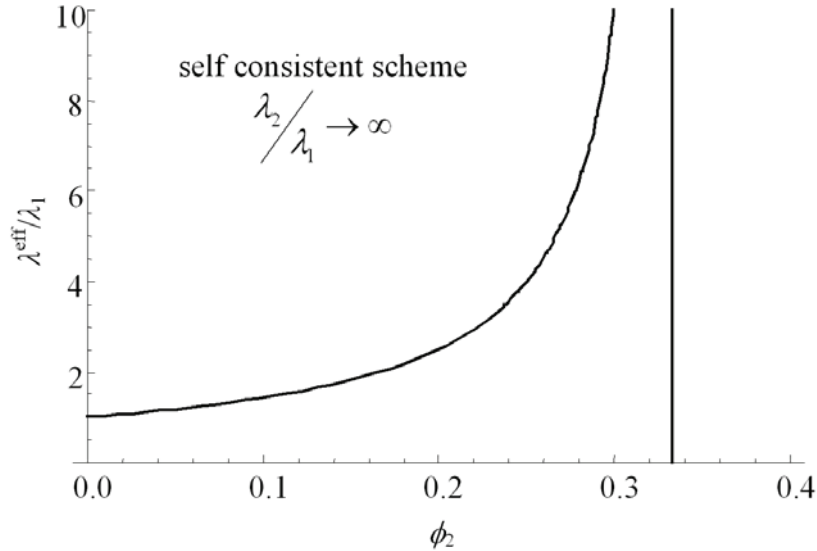
Fig. 2.3. Self consistent estimate for two-phase composite with high conductive spherical inclusions (phase 2)
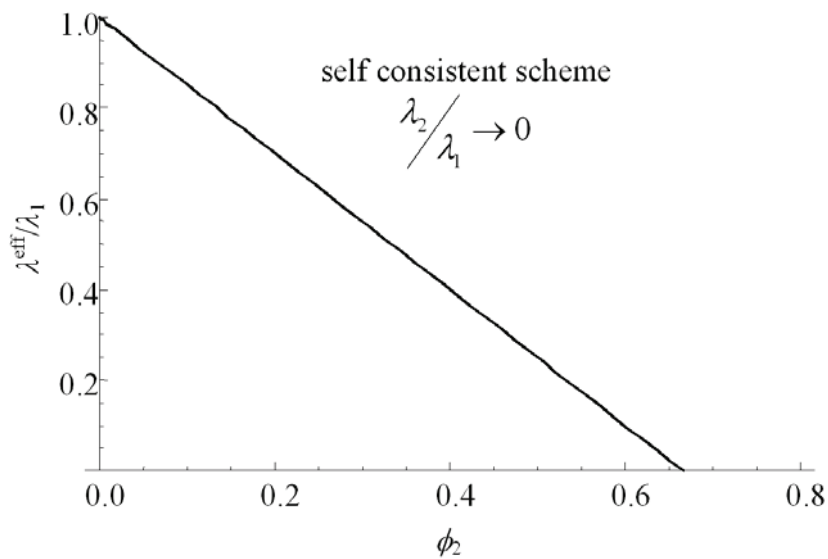
Fig. 2.4. Self consistent estimate for two-phase composite with perfectly insulating spherical inclusions (phase 2)

2.3. Representative volume element

Due to the deficiencies of direct estimates as well as due to the rapid development of computer techniques within last decades it is now accepted that numerical simulations are necessary in order to obtain more accurate mechanical responses. Within the numerical approach the notion of RVE as well as its quantitative definition are of paramount importance.

The RVE is usually regarded as a volume of heterogeneous body which is small enough from a macroscopic point of view and simultaneously large enough in order to contain sufficient number of inhomogenities to be representative. Some definitions of a RVE, used by scientists for different purposes, can be found in Stroeven *et al*. (2004) and Gitman *et al.* (2007), e.g.

- *"The RVE is a model of material to be used to determine the corresponding effective properties for the homogenized macroscopic model. The RVE should be large enough to contain sufficient information about the microstructure in order to be representative, however it should be much smaller than the macroscopic body"*; (Hashin, 1983).

- *"The RVE is the smallest material volume element of the composite for which the usual spatially constant (overall modulus) macroscopic constitutive representation is a sufficiently accurate model to represent a mean constitutive response"*; (Drugan & Willis, 1996).

- *"The RVE is defined as the minimum volume of laboratory specimen such that the results obtained from this specimen can still be regarded as representative for a continuum"*; (van Mier, 1997).

Note that all the definitions above provide quite strict information concerning the RVE, however, none of them gives precise information on its size. Hence, for practical purposes they are useless. In other words, if one wants to consider, say transport properties of composite materials, the definitions of RVE do not provide the information on how large sample should be taken into account? RVE is clearly defined only in case of materials with periodic microstructure – it is simply the periodic unit cell and effective properties can be established in the unique manner provided that the geometry and properties of phases are known.

On the other hand, for random media, the notion of RVE is meaningful only if the statistical error of analysed effective property is assumed. In other words, the quantitative definition of RVE, which usually involves microstructure information, must be established in the way that effective properties are determined with given error tolerance relative to the response of the real body. Furthermore, in case of random media, RVE can be established only for statistically homogeneous materials. Thus, if mechanical response of material which "shows" localisation is considered, a RVE cannot be determined due to looseness of statistical homogeneity. Note, the definition of statistical homogeneity is provided in next chapter.

A lot of attempt has been made in order to quantify the RVE on the basis of statistical and numerical analysis. Gusev (1997) used Monte-Carlo (MC) simulations for the generation of statistically independent realizations of periodic elastic composite consisted of disordered non-

overlapping spheres. The scatter in the results, i.e. averaged properties has been investigated. In (Stroeven *et al*., 2004) statistical calculations of numerical experiments are performed in order to quantify the size of RVE for composites that consist of particles in a matrix material. Several criterion as well as statistical tool, namely the *Student-t* distribution, have been taken into account in order to quantify the size of RVE. Gitman *et al.* (2007) proposed the quantification of RVE on the basis of the simple *Chi-square* statistical criterion, whereas Grufman *et al.* (2007) formulated the methodology based on the Kolmogorov *goodness-of-fit* test.

Evaluation of RVE size with accounting the microstructure information as well as the estimation of effective properties based on the RVE size determined have been extensively studied by (Povirk, 1995), (Zeman & Sejnoha, 2001), (Graham & Yang, 2003), (Du & Ostoja-Starzewski, 2006). Kanit *et al.* (2003) have proposed a method of numerical determination of the size of RVE on the basis of the microstructural descriptor, namely the integral range (the definition of integral range can be found in (Lantuéjoul, 2002)). The authors claimed that the size of RVE *"must be considered as a function of five parameters: the physical property, the contrast of properties, the volume fractions of components, the wanted relative precision for the estimation of the effective property and the number of realizations of the microstructure associated with computations that one is ready to carry out"*. The validation of the methodology concerning two materials from food industry was performed by Kanit *et al.* (2006). Thomas *et al.* (2008) focused on the determination of RVE for anisotropic composite with high-fiber volume fraction. Three different properties (fiber area fraction, pair correlation function, effective thermal conductivity) were considered in order to establish the size of RVE.

A separate problem is performing numerical calculations over RVE. Even though RVE is usually significantly smaller than the real material, nevertheless, in many cases, the calculations are often still extremely large. It results from the fact that RVE should contain a large number of heterogeneities to be representative. Additionally the response of RVE should be independent of the type of prescribed boundary conditions (Sab, 1992) - it also supports the large size of RVE. Some studies were performed in order to reduce the CPU time: Zohdi *et al.* (2001) proposed a method of regular partition of global domain into non-overlapping sub-domains; in Kanit *et al.* (2003) it was shown that effective properties can be evaluated not only by numerical simulations on large samples but also by considering rather smaller volumes with sufficient number of realizations.

2.4. Remarks

In this chapter some basics of continuum micromechanics were provided. It appeared that effective transport properties for deterministic microstructure are simply defined by linear relation between volume averaged local flux and a volume average of local intensity. It was mentioned, however, that in case of random media one must take into account the ensemble averages.

In section 2.2 the rigorous bounds as well as direct estimations regarding effective thermal conductivity of random heterogeneous media were outlined. Bounds such as Reuss and Voigt are usually quite wide and provide rather poor qualitative information, whereas those due to Hashin and Shtrikman are the tightest ones providing that the macroscopic isotropy and volume fractions of constituents are the only data known. It was shown that both Maxwell's (2.13) and Mori-Tanka's (2.14) schemes are explicit ones and even though the formulations of these models are different they yield the same estimate of effective properties when composite with spherical inclusions is considered. On the contrary, the assessment of effective conductivity coefficient on the basis of self consistent scheme is more complicated task – it requires the solution to an implicit equation (2.15).

It was shown that in some cases direct estimations reveal some deficiencies, e.g. self consistent can produce spurious results when large contrast in properties is applied. In that case numerical simulations have appeared to be necessary in order to obtain proper macroscopic responses. Therefore, the notion of RVE is of paramount importance, however, the problem concerning the appropriate size of RVE and corresponding error of estimate appears. Then, the primary questions are: *how large should be the sample to be "sufficiently large"*? and *what error of effective properties estimate one gets by averaging over such volume?* The wide literature on the problem of RVE size determination on the basis of statistical and numerical analysis is provided in section 2.3.

In general, the effective properties of random media are strongly affected by mechanical properties of phases, their volume fractions and – what is most important – statistical information beyond the one contained in volume fraction. Simple example of phase interchanged microstructures with 50% volume fraction of phases (Fig. 2.2) shows, for instance, the importance of phases connectivity. Furthermore, one can simply imagine that in many cases the answers for some basic questions regarding the composite phases, like:

- *what are their shapes and sizes?*
- *what are their orientations?*

- *how spatially distributed they are?*
- *etc.*

could be of paramount importance. Statistical descriptors which provide considerable information on the random microstructure are briefly outlined in chapter 3.

As mentioned, within this work only transport properties are considered, however, in the wide literature, the relations between two different classes of properties, e.g. elastic modulus and electrical conductivity can be found (Bristow, 1960; Levin, 1967; Berryman & Milton, 1988). When the measurement of some mechanical properties is a difficult task such relations enables one to estimate them in terms of the others. For instance Zhao *et al.* (2006) examined the cross-property relations for planar two-phase composites using both analytical approaches and the digital-based finite element implementation. Focus was based on studying how the microstructure affects the correlation between elastic module and conductivity.

3. Random microstructure: statistical descriptors, representativity

As mentioned in previous chapter the effective transport properties for random media are simply defined by linear relation between ensemble averages of local flux and of local intensity. Therefore in order to reflect the nature of random media, first, some basic definitions are provided. Let (Ω, Ψ, P) be some probability space which consists of set Ω which is a sample space, Ψ representing a σ-algebra of subsets of Ω, and a measure P on (Ω, Ψ). Clearly, Ω can be considered as a set of outcomes, Ψ is a set of events, and P is a probability measure such that $P(\Omega) = 1$. To illustrate these basic definitions, consider now flipping (once) a coin. Then, the possible outcomes are heads (H) and tails (T). Hence $\Omega = \{H, T\}$ and $P(\Omega) = 1$ - we have fifty percent chance of tossing either heads or tails. The σ-algebra Ψ contains 4 events: {H} - heads, {T} – tails, {} – neither heads nor tails, {H, T} – heads or tails, and the appropriate probabilities are as follows: $P(\{H\}) = P(\{T\}) = 0.5$; $P(\{\}) = 0$; $P(\{H, T\}) = 1$.

Consider now the sample of random heterogeneous material being a realization of a specific random process. Then, the ensemble is regarded as a collection of large number of realizations of a random medium, such that these realizations are different in the view of microscopic scale, while within the point of view of macroscopic details the realizations are identical (for further reference, see: Beran 1968; Drugan & Willis, 1996; Sejnoha & Zeman, 2000). Recalling now the sample space Ω, we denote a single realization within Ω as ω. The probability density of ω in Ω is described as $p(\omega)$.

Following Torquato (2002) the medium can be characterized by a random variable $\eta(\mathbf{x}; \omega)$, called the structure function. Note, in general η depends additionally on time t, i.e. $\eta(\mathbf{x}, t; \omega)$. For instance such variable can be applied if one studies the evolution of microstructure, e.g. investigating the process of concrete leaching. Within this work only static microstructures are considered and hence η is said to be independent of time and then the ensemble average of $\eta(\mathbf{x}; \omega)$, at given localization $\mathbf{x}$, is defined as:

$$\overline{\langle \eta(\mathbf{x}) \rangle} = \int_{\Omega} \eta(\mathbf{x}; \omega) p(\omega) d\omega \tag{3.1}$$

Following definition (3.1) one can easily observe that determination of ensemble average of $\eta(\mathbf{x}; \omega)$, in a given localization $\mathbf{x}$, requires the generation of all realizations forming ensemble, then evaluation of $\eta(\mathbf{x}; \omega)$ for each realization ω and at least averaging over all realizations. This cumbersome procedure causes that it is meaningful to introduce the ergodic hypothesis which allows replacing ensemble averaging with volume averaging providing that the volume tends to infinity. Note that, volume averaging is meaningful when the statistical homogeneity of medium is provided, i.e. there is no preferred origin in the system (see Fig. 3.1) and then the ensemble average of $\eta(\mathbf{x}; \omega)$ given by relation (3.1) is invariant under translation of the space origin by constant value of $\mathbf{y}$ (Torquato & Stell, 1982):

$$\overline{\left\langle \eta\left(\mathbf{x}_1, \mathbf{x}_2, ..., \mathbf{x}_n\right)\right\rangle} = \overline{\left\langle \eta\left(\mathbf{x}_1 - \mathbf{y}, \mathbf{x}_2 - \mathbf{y}, ..., \mathbf{x}_n - \mathbf{y}\right)\right\rangle} = \overline{\left\langle \eta\left(\mathbf{x}_{12}, ..., \mathbf{x}_{1n}\right)\right\rangle} \tag{3.2}$$

Note that relation (3.2) is obtained with the assumption $\mathbf{y}=\mathbf{x}_1$ and $\mathbf{x}_{ij}=\mathbf{x}_j\text{-}\mathbf{x}_i$. Now, adopting the ergodic hypothesis, the ensemble average of $\eta(\mathbf{x}; \omega)$ can be replaced by volume average in the limit that the volume tends to infinity:

$$\overline{\left\langle \eta\left(\mathbf{x}\right)\right\rangle} = \left\langle \eta\left(\mathbf{x}\right)\right\rangle = \lim_{V \to \infty} \frac{1}{V} \int_V \eta\left(\mathbf{x}+\mathbf{y}\right) d\mathbf{y} \tag{3.3}$$
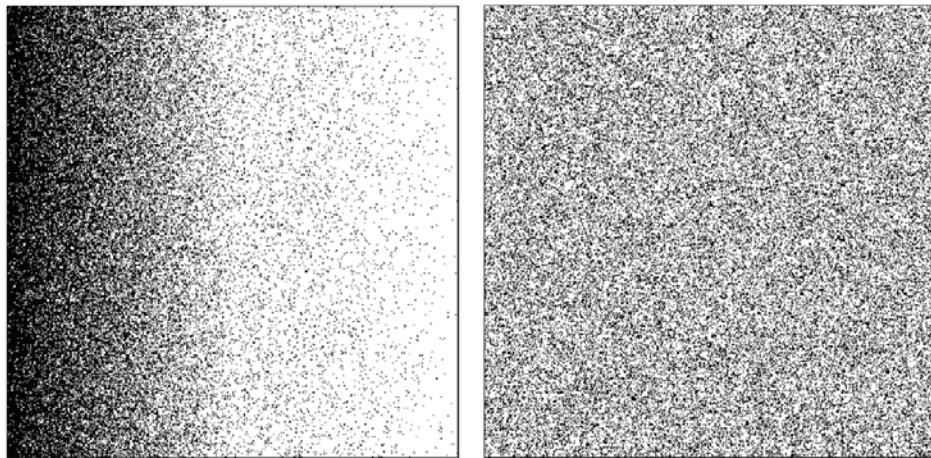
Fig. 3.1. Two examples of random media: a.) statistically inhomogeneous medium; b.) statistically homogeneous and isotropic medium

Relation (3.3) gives the possibility of considering only one arbitrary realization providing that the sample volume is infinite. Hence recalling now expression (2.9) it can be seen that in case of engineering applications such theory is meaningless, unless one allows the error tolerance of estimation, then the reasonable size of sample can be taken into account and "sufficiently large" sample can be examined. Nevertheless, the primary question can be formulated: *how large should be the sample to be treated as the "sufficient"(representative) one for given error of estimate?* The answer for this question, on the basis of analytical considerations and numerical calculations, is studied further in this work.

As a remark, it should be noted that microstructure presented in the right panel of Fig. 3.1 is a statistically homogeneous and isotropic one. For statistically isotropic media the ensemble average is not only independent of the position of the coordinate but also of the coordinate system rotation. Then, the ensemble average of $\eta(\mathbf{x}; \omega)$ depends only on distances $r_{ij} = \left\| \mathbf{x}_{ij} \right\|$

$$\overline{\left\langle \eta\left(\mathbf{x}_{12}, ..., \mathbf{x}_{1n}\right)\right\rangle} = \overline{\left\langle \eta\left(r_{ij}\right)\right\rangle} \tag{3.4}$$

where $i=1, ... , n$ and $j=1, ... , n$.

3.1. Statistical microstructure descriptors

It was mentioned in previous chapter that microstructure has a significant influence on the values of effective properties of random media, and therefore, the ability to describe the details of random microstructure is of particular importance. By the details of microstructure we usually mean the phase volume fractions, orientations, sizes, shapes, connectivity, spatial distribution, etc. Within this chapter some functions which statistically describe the microstructure are provided. The focus is on *n-point probability* and the *lineal path* functions. Moreover, the former function – in further considerations - is used to determine the size of the sample which can be treated as the representative one for given random microstructure.

In what follows a two-phase random medium is considered, however, the generalizations to *n*-phase media can be obtained in the obvious way. A realization ω of two-phase random medium is presented in Fig. 3.2. Note that the volume V is composed of two disjoint regions: phase 1 which occupies a region $\mathcal{V}_1(\omega)$ of volume fraction ϕ_1 and phase 2 occupying a region $\mathcal{V}_2(\omega)$ of volume fraction ϕ_2. The interface between two regions is denoted as $\partial \mathcal{V}(\omega)$.
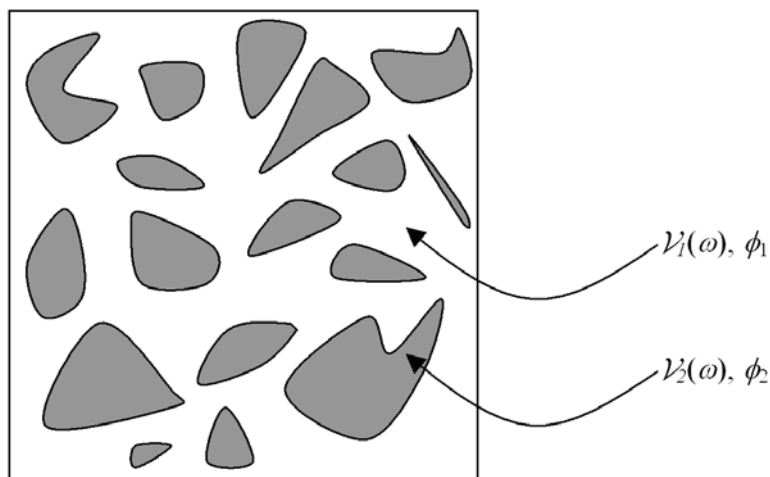
Fig. 3.2. Realization ω of a two-phase random medium

Introduce now a structure function $\eta(\mathbf{x}; \omega)$, for phase i, such that:

$$\eta(\mathbf{x};\omega) = I^{(i)}(\mathbf{x};\omega) = \begin{cases} 1, & \text{if } \mathbf{x} \in \mathcal{V}_i(\omega) \\ 0, & \text{otherwise} \end{cases} \tag{3.5}$$

Note, the relation (3.5) is just the indicator function, i.e. for fixed $\mathbf{x}$ it has only two possible values: 0 or 1, depending on the realization ω. For brevity, in what follows, ω is dropped from notation, and therefore, in case of two-phase medium it is evident that:

$$I^{(1)}(\mathbf{x}) + I^{(2)}(\mathbf{x}) = 1 \tag{3.6}$$

We focus now on the *n*-point probability function, also called the *n*-point correlation function. This function denotes the probability that *n* points at positions $\mathbf{x}_1$, $\mathbf{x}_2$, ..., $\mathbf{x}_n$ are found in phase *i*. According to its definition $S_n^{(i)}$ can be expressed in terms of probability that the indicator function is 1 for all points $\mathbf{x}_1$, $\mathbf{x}_2$, ..., $\mathbf{x}_n$, i.e.

$$S_n^{(i)}(\mathbf{x}_1, \mathbf{x}_2, ..., \mathbf{x}_n) = P\left(I^{(i)}(\mathbf{x}_1) = 1, I^{(i)}(\mathbf{x}_2) = 1, ..., I^{(i)}(\mathbf{x}_n) = 1\right) \tag{3.7}$$

On the other hand, the *n*-point probability function is the expectation of the product $I^{(i)}(\mathbf{x}_1)I^{(i)}(\mathbf{x}_2)...I^{(i)}(\mathbf{x}_n)$ (Brown, 1955; Torquato & Stell, 1982):

$$S_n^{(i)}(\mathbf{x}_1, \mathbf{x}_2, ..., \mathbf{x}_n) = \overline{\left\langle I^{(i)}(\mathbf{x}_1)I^{(i)}(\mathbf{x}_2)...I^{(i)}(\mathbf{x}_n)\right\rangle} \tag{3.8}$$

In what follows we assume that the medium is statistically homogenous, i.e. there is no preferred origin in the system, and therefore, the probability given by relation (3.7) is invariant under translation of the space origin by constant value of $\mathbf{y}$:

$$P\left(I^{(i)}(\mathbf{x}_1) = 1, I^{(i)}(\mathbf{x}_2) = 1, ..., I^{(i)}(\mathbf{x}_n) = 1\right) =$$
$$= P\left(I^{(i)}(\mathbf{x}_1 + \mathbf{y}) = 1, I^{(i)}(\mathbf{x}_2 + \mathbf{y}) = 1, ..., I^{(i)}(\mathbf{x}_n + \mathbf{y}) = 1\right) \tag{3.9}$$

Furthermore, in case of statistically homogenous media, the *n*-point probability function $S_n^{(i)}$ depends only on relative displacements $\mathbf{x}_{ij}$, i.e.:

$$S_n^{(i)}(\mathbf{x}_1, \mathbf{x}_2, ..., \mathbf{x}_n) = S_n^{(i)}(\mathbf{x}_1 + \mathbf{y}, \mathbf{x}_2 + \mathbf{y}, ..., \mathbf{x}_n + \mathbf{y}) = S_n^{(i)}(\mathbf{x}_{12}, ..., \mathbf{x}_{1n}) \tag{3.10}$$

where $\mathbf{y} = \mathbf{x}_1$ and $\mathbf{x}_{ij} = \mathbf{x}_j - \mathbf{x}_i$.

As mentioned, when the statistical homogeneity of random medium is assumed then it is meaningful to define volume averages of considered quantities, and therefore, following the ergodic hypothesis (3.3) the *n*-point probability function can be expressed as:

$$S_n^{(i)}(\mathbf{x}_{12}, ..., \mathbf{x}_{1n}) = \lim_{V \to \infty} \frac{1}{V} \int_V I^{(i)}(\mathbf{y}) I^{(i)}(\mathbf{y} + \mathbf{x}_{12})...I^{(i)}(\mathbf{y} + \mathbf{x}_{1n}) d\mathbf{y} \tag{3.11}$$

Hereafter, the primary attention is limited to one- and two-point probability functions since they are only used in the following parts of the thesis.

Note that on the basis of above assumptions ((3.10) and (3.11)) the one-point probability (the probability of finding phase i in location $\mathbf{x}$) is constant and simply equals the volume fraction of phase i, i.e.:

$$S_1^{(i)} = \phi_i \tag{3.12}$$

Therefore, for statistically homogeneous and ergodic media, the one-point probability for phase i can be considered as its volume fraction in the composite.

According to the relation (3.11) the two-point probability function for phase i is given as follows

$$S_2^{(i)}(\mathbf{x}_{12}) = \lim_{V \to \infty} \frac{1}{V} \int_V I^{(i)}(\mathbf{y}) I^{(i)}(\mathbf{y} + \mathbf{x}_{12}) d\mathbf{y} \tag{3.13}$$

Nevertheless, further simplification arises when the medium is assumed to be statistically isotropic. Then $S_2^{(i)}(\mathbf{x}_1, \mathbf{x}_2)$ reduces in a following way:

$$S_2^{(i)}(\mathbf{x}_1, \mathbf{x}_2) = S_2^{(i)}(r_{12}) = S_2^{(i)}(r) \tag{3.14}$$

where $r = r_{12} = \|\mathbf{x}_{12}\|$. It is evident that in the same manner higher order probability functions can be expressed. For example the three-point probability have the form:

$$S_3^{(i)}(\mathbf{x}_1, \mathbf{x}_2, \mathbf{x}_3) = S_3^{(i)}(r_{12}, r_{13}, r_{23}) = S_3^{(i)}(r, s, t) \tag{3.15}$$

In the equation above $s = r_{13} = \|\mathbf{x}_{13}\|$ and $t = r_{23} = \|\mathbf{x}_{23}\|$.

In Fig. 3.3 the geometrical interpretation of one-, two- as well as three-point probability is provided. Note, all the interpretations are provided for both statistically homogeneous and isotropic media. Hence, $S_1^{(i)}$ can be interpreted as the probability that a randomly placed point, within the volume V, lies in $\mathcal{V}_i$ (Fig. 3.3 A). The two-point probability for phase i, $S_2^{(i)}$, is the probability that two ends of a line segment of length r lie in $\mathcal{V}_i$ when randomly placed in the sample (Fig. 3.3 B). In the same manner the geometrical meaning of three-point probability, $S_3^{(i)}$, for phase i is easily formulated: it is the probability that all three vertices of a triangle are found in $\mathcal{V}_i$ when randomly placed in the volume V (Fig. 3.3 C).

Note that the general geometrical interpretation of n-point probability for statistically homogeneous and isotropic media can also be provided. Assume that $F_n^{(i)}$ is a polyhedron with n vertices located at $\mathbf{x}_1$, $\mathbf{x}_2$, ..., $\mathbf{x}_n$. Then, following (Torquato, 2002) $S_n^{(i)}$ *can be interpreted as the*

probability that all n vertices of $F_n^{(i)}$ lie in $\mathcal{V}_i$ when the polyhedron is randomly placed in the volume, i.e. over all translations and solid-body rotations of the polyhedron.

(A)　　　　　　　　(B)　　　　　　　　(C)

$$S_1^{(i)} \qquad\qquad S_2^{(i)}(r) \qquad\qquad S_3^{(i)}(r,s,t)$$
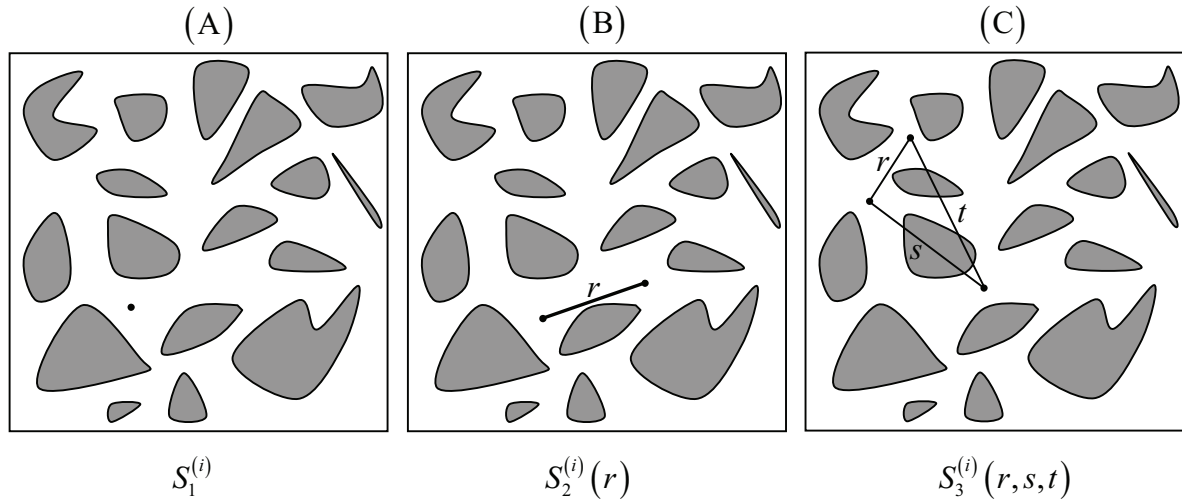
Fig. 3.3. Geometrical interpretation of probabilities

3.1.1. Two-point probability

Within this work special attention is focused on microstructural descriptor, namely the two-point probability $S_2^{(i)}$. This correlation function is widely used by scientists for different purposes, i.e.: determination of effective mechanical properties of random media (see e.g. Berrymann & Blair, 1986; Zeman & Sejnoha, 2001; Różański *et al.* 2008; Torquato & Sen, 1990), evaluation of the rigorous bounds of mechanical properties (Brown, 1955; Milton, 2002), 2D as well as 3D reconstruction of random composites (Yeong & Torquato, 1998a, 1998b), numerical determination of the size of RVE for random media (Łydżba & Różański 2009; Różański & Łydżba 2009; Różański *et al.* 2009).

Basing on geometrical interpretation of two-point probability provided in previous section, one can easily found that for statistically homogeneous and isotropic media this function can be simply obtained via Monte-Carlo simulations, i.e. by randomly tossing the line segment of length *r* and counting the fraction of times the end points are found in the phase for which the correlation function is evaluated. Furthermore, this function, when determined for phase *i*, provides information of how the end points of line segment are correlated within the microstructure.

Once again we consider a two-phase random medium which is assumed to be statistically isotropic and ergodic one. For such media, following relations exist:

$$S_2^{(1)}(r) = \phi_1 - \frac{1}{2} S_2^{(12)}(r)$$

$$S_2^{(2)}(r) = \phi_2 - \frac{1}{2} S_2^{(12)}(r) \tag{3.16}$$

$$S_2^{(1)}(r) + S_2^{(12)}(r) + S_2^{(2)}(r) = 1$$

where $S_2^{(12)}(r)$ is the probability of finding two end points of line segment r simultaneously in different phases. Note that according to (3.16) the two-point probability function for all phases can be determined providing that this function is given only for one arbitrary phase.

The two-point probability function for phase i attains its maximum value of ϕ_i at $r=0$ and usually decays with $r \to \infty$ to asymptotic value of ϕ_i^2, if microscopic structure of the composite possesses no long-range order,

$$\lim_{r \to 0} S_2^{(i)}(r) = \phi_i \tag{3.17}$$

and

$$\lim_{r \to \infty} S_2^{(i)}(r) = \phi_i^2 \tag{3.18}$$

In what follows three examples of different, two-phase microstructures are studied in order to exhibit the sort of information which can be provided by two-point probability. All microstructures (Fig. 3.4) are type of binary image composed of 90,000 pixels such that black (white) pixel is denoted as phase 1 (phase 2). The microstructures A and B have the volume fraction $\phi_2=0.25$, whereas microstructure C has approximately equal volume fraction of constituents.

For each microstructure the two-point probability for phase 2 is determined by simple Monte Carlo simulations, i.e. for given distance r, two points are randomly thrown in the microstructure and successful hits (two points found in phase 2) are counted and divided by total number of throws:

$$S_2^{(2)}(r) = \frac{n_s(r)}{n_T} \tag{3.19}$$

where $n_s(r)$ is the number of successful hits and n_T denotes the total number of throws. Then utilising relations (3.16) the two-point probability for phase 1 is determined. Both $S_2^{(1)}(r)$ and $S_2^{(2)}(r)$ are presented graphically in Fig. 3.4. Note that in each case S_2 is plotted against the value of d which expresses the number of pixels, i.e. $r = dl$, where l is the length of pixel side.
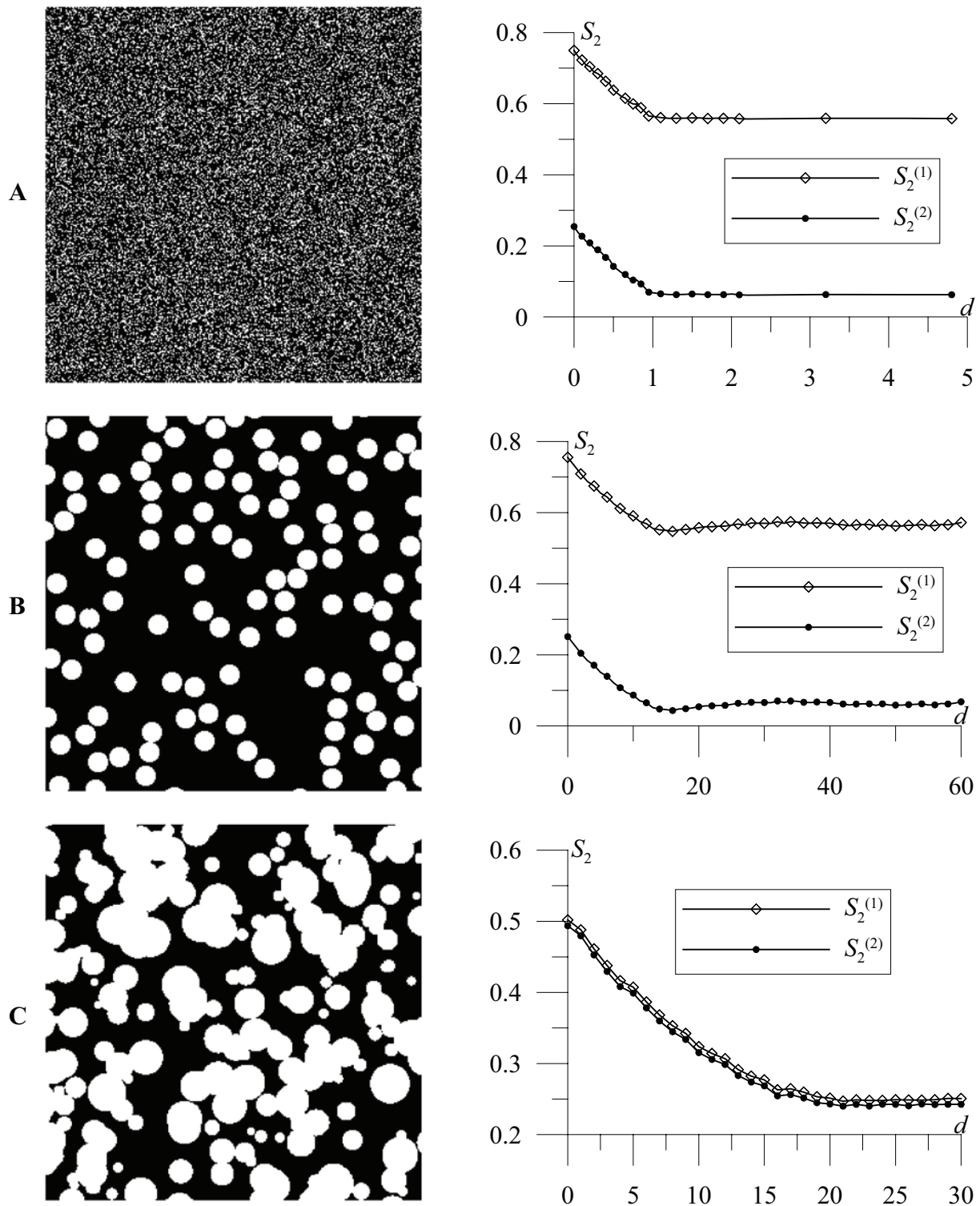
Fig. 3.4. Two-point probability functions and their associated microstructures: A – random checkerboard, B – system of nonoverlapping disks, C – system of overlapping disks.

Observing results (Fig. 3.4) one can simply notice that only in case of system of non-overlapping disks (B) two-point probability $S_2(r)$ exhibits noticeable periodic oscillations with decreasing amplitude. It results from the fact that the disks are spatially correlated, i.e. the position of j-disk is dependent on the positions of all disks which have been placed in the microstructure before. Note

that the periodicity of $S_2(r)$ is roughly equal to d=16 which is also the size of the disks diameter $D \approx 16l$. Therefore $S_2(r)$ provides information on the size of particle diameter.

In case of random checkerboard (A) as well as a system of overlapping disks (C) $S_2^{(i)}(r)$ decays to its asymptotic value ϕ_i^2 at r=l and $r \approx 20l$, respectively. In both cases $S_2(r)$ rather belies the fact that there are significantly larger particles in the microstructure than l (A) and $20l$ (C). Note that particles create clusters which are appreciably larger than l (Fig. 3.4 A) and $20l$ (Fig. 3.4 C). However, $S_2(r)$ exhibits no periodic oscillations which indicates that particles of certain "characteristic" size (l for (A) and $20l$ for (C)) are spatially uncorrelated.

As mentioned $S_2^{(i)}(r)$ provides information of how the end points of line segment of length r are correlated within the microstructure. The limit of $S_2^{(i)}(r)$ for $r \to \infty$ is equal to the square of the volume fraction of phase i (3.18). Nevertheless, if this limit is reached before $r \to \infty$, say for certain value $r = r*$, then the points within the microstructure with a distance larger that $r*$ are not correlated.

The two-point probability provides, in addition, the information on specific surface s of the system which is defined as the interface area per unit volume. The slope of $S_2(r)$ at the origin is related to the specific surface s by following relation (Berryman & Milton, 1988; Torquato, 2002):

$$s = -4 \frac{d}{dr} S_2^{(i)}(r) \Big|_{r=0} \qquad (3.20)$$

Note that (3.20) is valid for two-dimensional digitised and isotropic media for which r takes discrete values. The result for continuous values of r has been first established by Debye *et al.* (1957). Berrymann & Blair (1986) have demonstrated the application of Debye's result with Kozeny-Carman relation in order to obtain estimates of fluid permeability. Furthermore, the relationship between s and $S_2(r)$ for anisotropic porous media has been established by Berrymann (1987).

3.1.2. Lineal-path function

As shown in previous section, in some cases, the two-point probability does not well exhibit clustering and percolation information. Another useful quantity, which statistically describes the microstructure is the lineal-path function (Lu & Torquato, 1992). More details as well as applications of this microstructural descriptor can be found in the works of Quintanilla & Torquato (1996) and Yeong & Torquato (1998a, 1998b).

In case of statistically isotropic media the lineal-path function for phase i, $L^{(i)}(r)$, gives the probability that a line segment of length r lies wholly in phase i when randomly thrown into the sample. Thus, lineal-path function contains higher level of connectedness information than two-point probability, because the latter concerns only two end points of line segment.

$L^{(i)}(r)$ is a monotonically decreasing function of r and following limiting values exist:

$$L^{(i)}(0) = \phi_i \qquad (3.21)$$

$$L^{(i)}(\infty) = 0 \qquad (3.22)$$

Furthermore, due to fact that lineal-path function denotes the value of probability, it is evident that for two-phase random media:

$$L^{(1)}(r) + L^{(12)}(r) + L^{(2)}(r) = 1 \qquad (3.23)$$

where $L^{(12)}(r)$ is the probability that line segment of length r lies in two phases simultaneously when randomly thrown into the sample; in other words, it is the probability that a line segment of length r intersects the interface between two phases when randomly placed in the structure.

The lineal-path function was determined for both phases of three different types of microstructures (Fig. 3.5 – note the microstructures are the same as in case of two-point probability). As previously, for given phase, the lineal-path function was evaluated by simple Monte Carlo simulations, i.e. a line segment of length r was randomly thrown into the sample and successful hits (whole line lies in phase i) were counted and divided by total number of throws, i.e.

$$L^{(i)}(r) = \frac{n_s(r)}{n_T} \qquad (3.24)$$

Note that in case of microstructures (A) and (B) the connectedness of phase 1 (black phase) is much larger than phase 2 (white phase) (Fig. 3.5). The confirmation of this fact can be easily found in Fig. 3.5. where lineal-path is plotted against d. Note that in case of (A) and (B) we have that: $L^{(1)} \geq L^{(2)}$ for all values of d. For instance, in case of microstructure (B), when the length of line segment is r=10l, $L^{(1)} = 0.558$ whereas $L^{(2)} = 0.069$.

Observing the microstructure depicted in Fig. 3.5. (C) it can be seen that connectivity of black phase is insignificantly larger comparing to the white one. Note that the lineal-path function determined for this microstructure confirms that the connectedness of both phases is approximately on the same level, i.e. for all values of d $L^{(1)} \approx L^{(2)}$.

As mentioned in previous section the two-point probability determined for microstructure (C) (Fig. 3.4 C) did not provide useful information on particles clustering - certain characteristic size of

particle was indicated. Note that more details on phase connectedness are exhibited by the "tail" of lineal-path function which gives information about the largest lineal-paths in phase *i*.
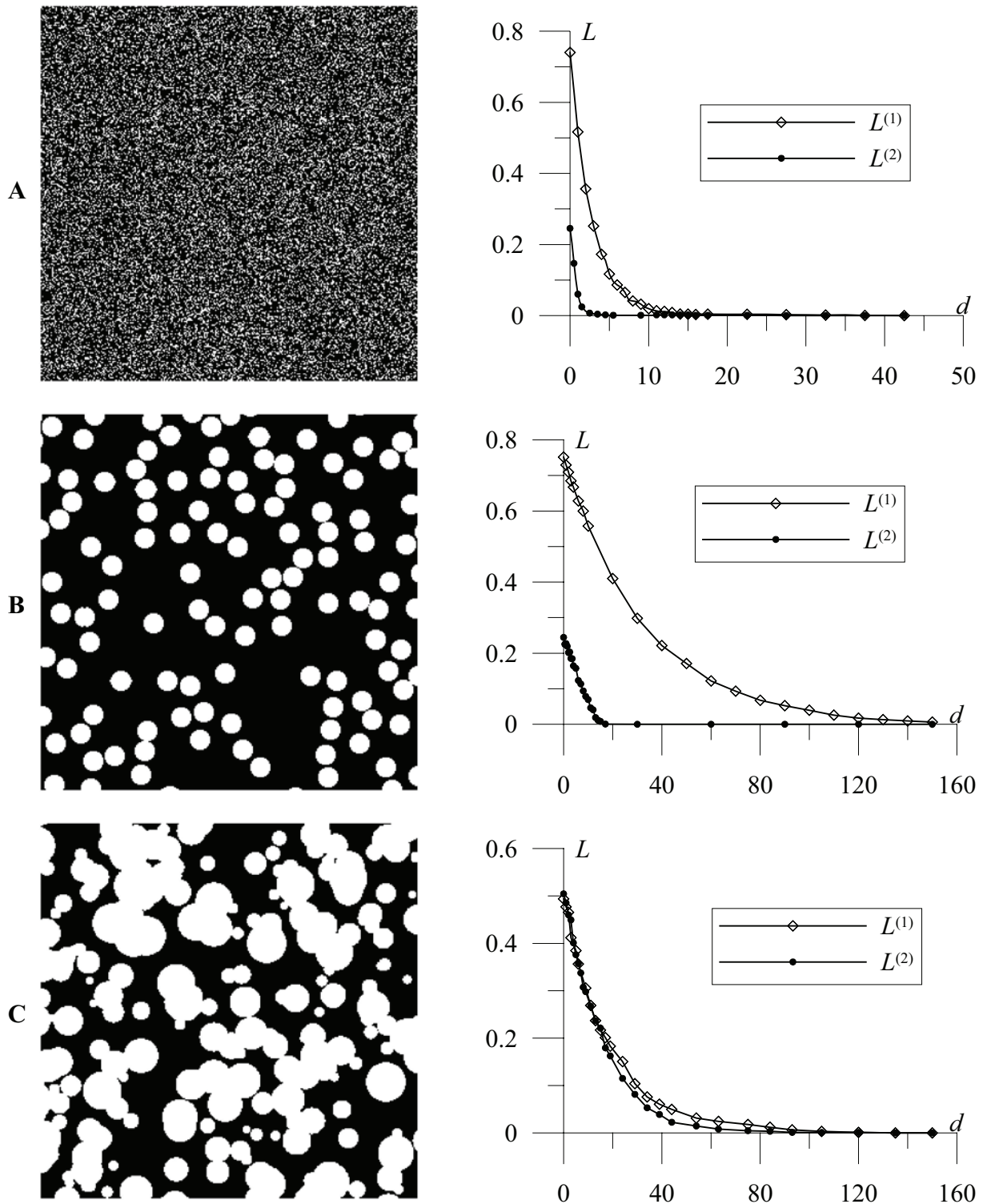
Fig. 3.5. Lineal-path functions and their associated microstructures: A – random checkerboard, B – system of nonoverlapping disks, C – system of overlapping disks.

3.2. Representativity

As mentioned in previous chapter RVE is usually regarded as a volume of heterogeneous body which is small enough from a macroscopic point of view and simultaneously large enough in order to contain sufficient number of inhomogenities to be *representative*. In case of periodic media the definition of RVE is unique - it is simply the periodic unit cell. On the contrary, for random composite materials, formulation of the quantitative definition of RVE is not an easy task - the size of RVE strongly depends on the microstructure of considered media.

It is evident that in case of random media the best choice would be the sample of infinite size – then all possible microstructure realizations would be contained within RVE. Nevertheless, such approach is useless for engineering applications. Hence, one has to choose the finite size sample for which the analyzed property can be evaluated with given error tolerance relative to the response of the real body.

3.2.1. Sampling window

In many cases numerical calculations over finite size RVE can be very often still extremely large. On the other hand, as it will be shown further in this chapter, it is possible to estimate effective properties either by averaging over one large sample or by averaging over certain (sufficient) number of significantly smaller samples – sampling windows. This approach has been proposed by Kanit *et al.* (2003) who claims that: "*the effective properties can be determined for large volumes and small number of realizations; conversely, smaller volumes can be used providing that a sufficient number of realizations are considered*". For further references, see also (Łydżba & Różański, 2007; Różański *et al.*, 2008; Różański *et al.*, 2009).

Sampling window is a certain region of finite volume Ω_0 whose centroid is located at **x**. Note that the location of aforementioned window is random (Fig. 3.6). Having certain number of such samples, say *n* sampling windows*,* the analyzed property is classically estimated as the mean value averaged over all considered realizations, i.e.

$$\overline{\mu^{\text{eff}}} = \frac{1}{n}\sum_{j=1}^{n}\mu_j \tag{3.25}$$

where μ_j is the property evaluated for *j*-window (random realization of microstructure).

It should be emphasized that within such approach some difficult questions appear, i.e.:

- *what is the appropriate size of sampling window?*

- *how many microstructure realizations (sampling windows) should be taken into account?*

- *what is the error of such estimation?*

The answers to above questions are of paramount importance and will be widely discussed in this work. Note that having answers to above questions one can formulate a slightly different definition of RVE, i.e. the one which involves the size of the sample, number of realizations to be performed as well as an error of estimation.
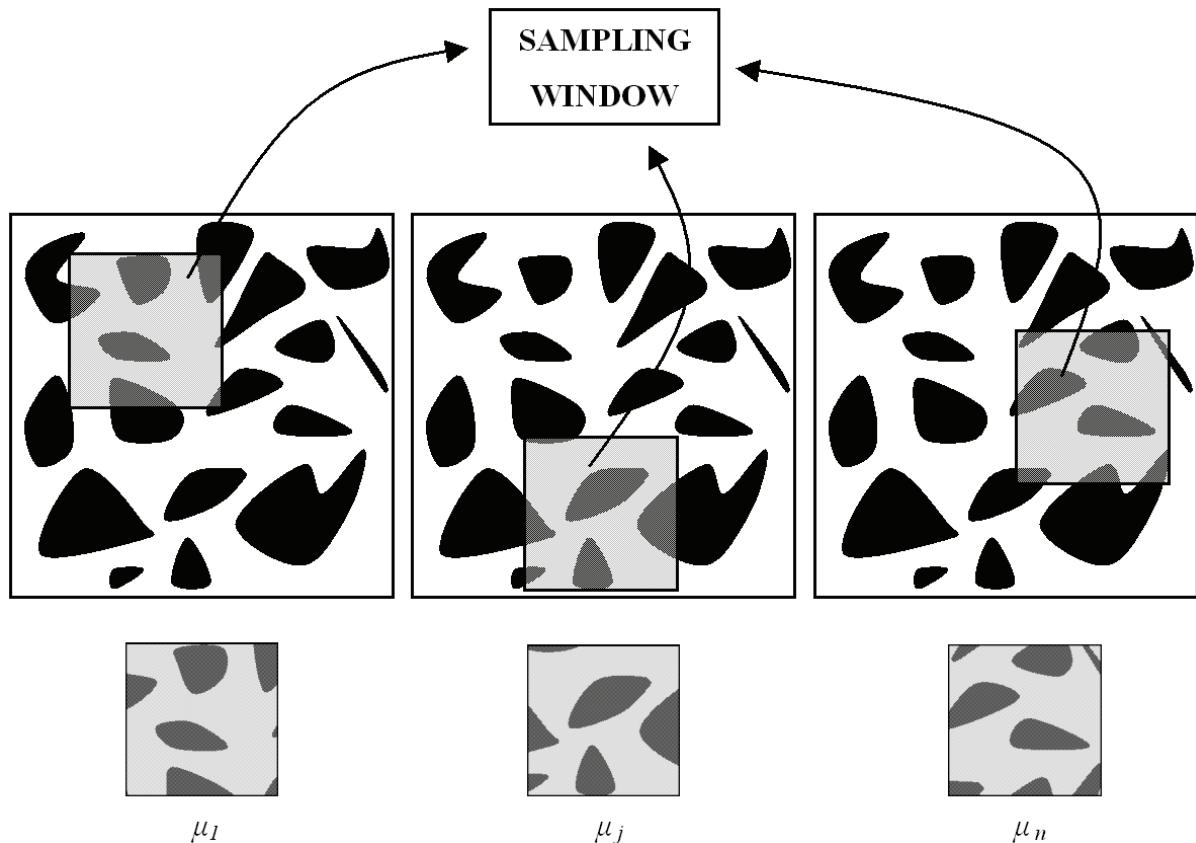
Fig. 3.6. Sampling windows

It should be mentioned that within this approach periodicity of the sample is assumed. It means that each randomly located sampling window is extended to infinity by periodic arrangement such that the window is regarded as the unit cell which is repeated in all directions forming the infinite continuous body (Fig. 3.7).

The fact of sampling window periodicity has a strong influence on the determination of effective geometrical as well as mechanical (transport) properties. For instance, consider the process of the two-point probability determination – it consists in random throwing of two points in the microstructure such that first of them always falls in the region Ω_0 while the remaining one (particularly in case of large distance r) can fall outside the region of the sample. Then, the periodicity conditions are recalled and the coordinates of this point are simply evaluated by periodic

translation. This procedure is used in this work each time when this microstructural descriptor is evaluated.

It will appear further in this work that in order to answer the question concerning the size of sampling window the reasonable choice is to take into account the two-point probability function. The methodology is provided in chapter 4. Furthermore, it will be shown that sufficient number of realizations and error of estimate can be established on the basis of both statistical and probabilistic tools contained within the Monte-Carlo methodology.
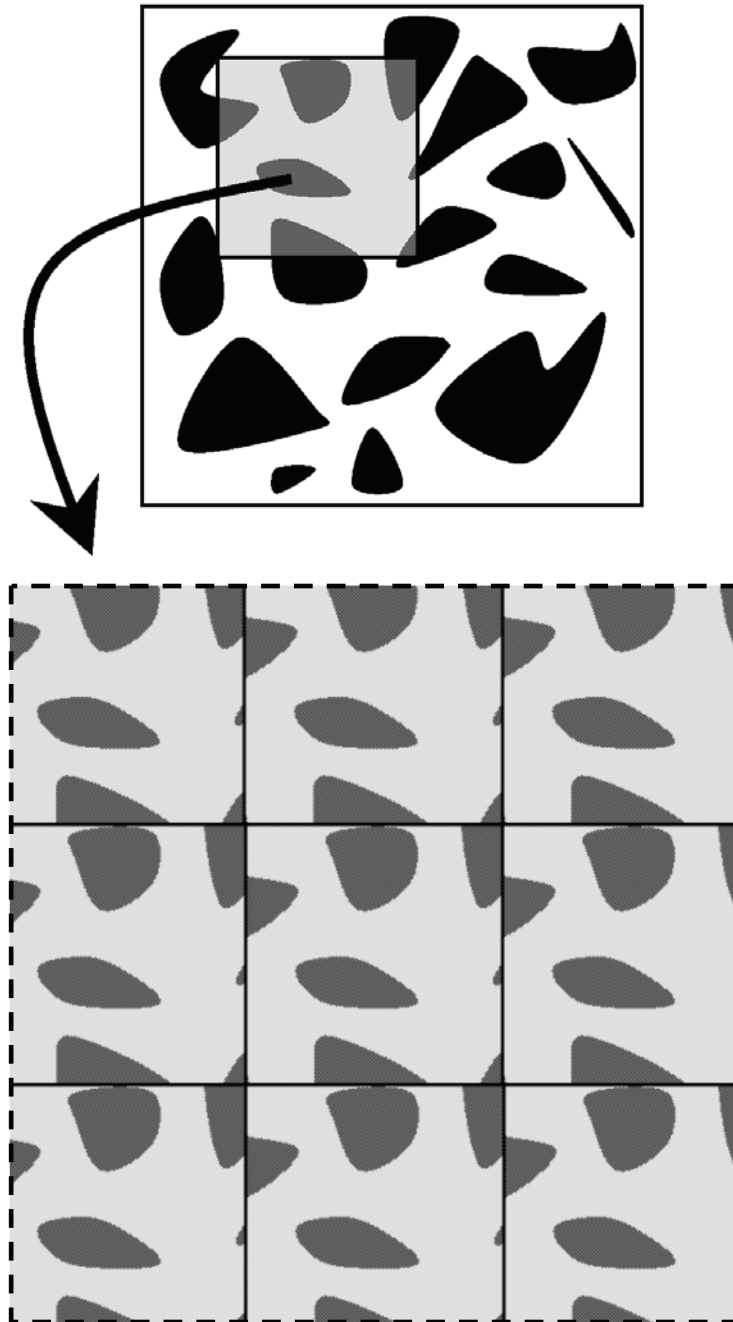
Fig. 3.7. Periodic arrangement of single unit cell (sampling window)

3.2.2. Central limit theorem (CLT) and Chebyshev's Inequality

The primary question of Monte Carlo techniques as well as the problem of evaluation estimator (3.25) is: *when the sampling should be stopped in order to obtain the good estimate of* μ^{eff}? The answer to above question is of paramount importance when playing with Monte Carlo methods. In what follows the Central Limit Theorem and the Chebyshev's Inequality are briefly discussed.

To begin with, let us recall some definitions of convergence of random variables, i.e.:

<u>Definition 1 (convergence in distribution)</u>: Let $\{X_1, X_2, ...\}$ be a sequence of random variables, and let X be a random variable. Suppose that X_n has cumulative distribution function F_n , and X has cumulative distribution function F. We say that sequence $\{X_1, X_2, ...\}$ *converges in distribution*, or weakly, to random variable X if

$$\lim_{n \to \infty} F_n(t) = F(t) \tag{3.26}$$

at every value t where F is continuous.

<u>Definition 2 (convergence in probability)</u>: Let $\{X_1, X_2, ...\}$ be a sequence of random variables, and let X be a random variable. Then sequence $\{X_1, X_2, ...\}$ is said to *converge in probability* to X if for every $\varepsilon > 0$

$$\lim_{n \to \infty} P(|X_n - X| > \varepsilon) = 0 \tag{3.27}$$

With the mode of convergence in distribution, we increasingly expect to see the next outcome in a sequence of random experiments becoming better and better modelled by a given probability distribution. The basic idea of the convergence in probability is that the probability of an "unusual" outcome becomes smaller and smaller as the sequence progresses.

It has to be marked that the convergence in probability implies the convergence in distribution, so weaker form of convergence is that one in distribution.

Using Monte Carlo simulations, we estimate the expectation value of analysed property by the mean value obtained from n sampling experiments performed, i.e. $\bar{X} = n^{-1} \sum_{i=1}^{n} X_i$. The theorem presented below justified correctness of the MC prediction.

<u>Theorem 1 (Weak Law of Large Numbers)</u>: Let X_1, X_2, … be a sequence of independent and identically distributed random variables, each with mean μ and variance σ^2. Then for every $\varepsilon > 0$,

$$\lim_{n\to\infty} P\left(\left| \frac{1}{n}\sum_{i=1}^{n} X_i - \mu \right| > \varepsilon \right) = 0 \tag{3.28}$$

The Weak Law of Large Numbers ensures that the Monte Carlo estimator converges in probability to the expectation value of a quantity being estimated so, in vocabulary of statistics, the Monte Carlo estimator is consistent. The above theorem, however, does not give any information about actual statistics of $\overline{X} = n^{-1}\sum_{i=1}^{n} X_i$, even the convergence in probability implies the convergence in distribution, so the latter is therefore assured by this theorem. This is what the Central Limit Theorem answers, namely:

<u>Theorem 2 (Central Limit Theorem)</u>: Let X_1, X_2, … be a sequence of independent and identically distributed random variables, each with mean μ and variance σ^2. Let

$$Z_n = \frac{n^{-1}\sum_{i=1}^{n} X_i - \mu}{\sigma/\sqrt{n}} \tag{3.29}$$

then Z_n converges in distribution to Z, where Z is a standard normal random variable.

In other words, the Central Limit Theorem says that mean of independent identically distributed random variables can be approximated by a standard normal distribution, for a large number n.

Now, we formulate the following problem: the estimator of μ^{eff} given by (3.25) should satisfy the following condition

$$P\left(\left| \overline{\mu^{\text{eff}}} - \mu^{\text{eff}} \right| \le \varepsilon_{abs} \right) \ge 1 - \alpha \tag{3.30}$$

where ε_{abs}>0 and 0<α<1 are the absolute error and the significance level, respectively. The values of ε_{abs} as well as α are a priori known.

Let us transform the relation (3.30) as:

$$P\left(\left| \frac{\overline{\mu^{\text{eff}}} - \mu^{\text{eff}}}{\sigma/\sqrt{n}} \right| \le \frac{\varepsilon_{abs}}{\sigma/\sqrt{n}} \right) \ge 1 - \alpha \tag{3.31}$$

According to the CLT, the distribution of random variable $\dfrac{\overline{\mu^{\text{eff}}} - \mu^{\text{eff}}}{\sigma/\sqrt{n}}$ can be approximated by the standard normal distribution, for large values of n, therefore the inequalities (3.31) implies:

$$\Phi\left(\frac{\varepsilon_{abs}}{\sigma/\sqrt{n}} \right) \ge 1 - \frac{\alpha}{2} \tag{3.32}$$

or equivalently:

$$n \geq \left(\frac{\sigma}{\varepsilon_{abs}}\right)^2 \left(\Phi^{-1}\left(1-\frac{\alpha}{2}\right)\right)^2 \tag{3.33}$$

where $\Phi(*)$ is the cumulative distribution function of standard normal random variable.

In many cases it is more accurate, however, to use the relative error instead of absolute one. In such case the inequality (3.33) becomes:

$$n \geq \left(\frac{\sigma}{\mu^{\text{eff}}\varepsilon_{rel}}\right)^2 \left(\Phi^{-1}\left(1-\frac{\alpha}{2}\right)\right)^2 \tag{3.34}$$

where

$$\varepsilon_{rel} = \frac{\varepsilon_{abs}}{\mu^{\text{eff}}} \tag{3.35}$$

Let us now examine qualitatively the result (3.34) stated above. The significance level is typically assumed as: 5%, 3% or 1% , which corresponds to: α=0.05, α=0.03 and α=0.01, respectively. These values, according to the table of standard normal distribution, imply: $\Phi^{-1}\left(1-\frac{0.05}{2}\right)=1.96$, $\Phi^{-1}\left(1-\frac{0.03}{2}\right)=2.17$ and $\Phi^{-1}\left(1-\frac{0.01}{2}\right)=2.575$. Substituting these values to the inequality (3.34) lead to:

$$n \geq \begin{cases} n_{5\%} = (1.96)^2 \left(\dfrac{\sigma}{\mu^{\text{eff}}\varepsilon_{rel}}\right)^2 \\[2ex] n_{3\%} = (2.17)^2 \left(\dfrac{\sigma}{\mu^{\text{eff}}\varepsilon_{rel}}\right)^2 \\[2ex] n_{1\%} = (2.575)^2 \left(\dfrac{\sigma}{\mu^{\text{eff}}\varepsilon_{rel}}\right)^2 \end{cases} \tag{3.36}$$

According to the inequality (3.30), the correctness of the Monte Carlo estimator $\overline{\mu^{\text{eff}}}$ is assured only with some probability value. The significance levels assumed above imply:

$$P\left(\left|\frac{\overline{\mu^{\text{eff}}}-\mu^{\text{eff}}}{\mu^{\text{eff}}}\right| \leq \varepsilon_{rel}\right) \geq \begin{cases} 0.95 & \text{for } n \geq n_{5\%} \\ 0.97 & \text{for } n \geq n_{3\%} \\ 0.99 & \text{for } n \geq n_{1\%} \end{cases} \tag{3.37}$$

It is evident that, with increasing the number of sampling this probability will also increase. Furthermore it should be noted that *n*, as a number of sampling windows, has to be an integer value, and therefore, in order to determine its value the ceiling function of (3.33) or (3.34) should be

evaluated (ceiling function, usually denoted as $\lceil x \rceil$, is the smallest integer not less than x). It should be also clearly pointed out, that one has to carefully apply the values (3.36) since they have been obtained with assumption of large value of n. This assumption has been crucial in deriving the inequalities (3.33) and (3.34), since it permitted to approximate distribution of MC estimator $\overline{\mu}^{\text{eff}}$ by the standard normal distribution. Therefore, if the number n, given by (3.36), is not large enough then the statement (3.37) is not valid, in general. In such case the number n can be determined from the Chebyshev's inequality as is presented below.

<u>Theorem 3 (Chebyshev's Inequality)</u>: Let X be a random variable with mean μ and variance σ^2. Then

$$P\left(|X - \mu| > \varepsilon\right) \leq \frac{\sigma^2}{\varepsilon^2} \tag{3.38}$$

Notice that for independent and identically distributed random variables X_i, with mean μ and variance σ^2, the following relations hold true:

$$E\left(n^{-1}\sum_{i=1}^{n} X_i\right) = n^{-1}\sum_{i=1}^{n} E(X_i) = \mu \tag{3.39}$$

$$Var\left(n^{-1}\sum_{i=1}^{n} X_i\right) = n^{-2}\sum_{i=1}^{n} Var(X_i) = \frac{\sigma^2}{n} \tag{3.40}$$

In the relations above the operators $E(*)$ and $Var(*)$ denote an expectation and variance, respectively.

Applying (3.39) and (3.40) in Chebyshev's Inequality, one gets:

$$P\left(\left|n^{-1}\sum_{i=1}^{n} X_i - \mu\right| > \varepsilon\right) \leq \frac{\sigma^2}{\varepsilon^2 n} \tag{3.41}$$

The relation above implies, of course, that:

$$P\left(\left|n^{-1}\sum_{i=1}^{n} X_i - \mu\right| \leq \varepsilon\right) \geq 1 - \frac{\sigma^2}{\varepsilon^2 n} \tag{3.42}$$

Comparing inequalities (3.42) and (3.30) one immediately concludes that:

$$n \geq \frac{1}{\alpha}\left(\frac{\sigma}{\varepsilon_{abs}}\right)^2 \tag{3.43}$$

or

$$n \geq \frac{1}{\alpha}\left(\frac{\sigma}{\varepsilon_{rel}\mu^{eff}}\right)^2 \tag{3.44}$$

For the significance levels investigated above, the inequality (3.44) leads to the following relation:

$$P\left(\left|\frac{\overline{\mu^{\mathrm{eff}}}-\mu^{\mathrm{eff}}}{\mu^{\mathrm{eff}}}\right|\leq\varepsilon_{rel}\right)\geq\begin{cases}0.95 & \text{for } n\geq n_{5\%}=\dfrac{100}{5}\left(\dfrac{\sigma}{\varepsilon_{rel}\mu^{\mathrm{eff}}}\right)^{2}\\[2em]0.97 & \text{for } n\geq n_{3\%}=\dfrac{100}{3}\left(\dfrac{\sigma}{\varepsilon_{rel}\mu^{\mathrm{eff}}}\right)^{2}\\[2em]0.99 & \text{for } n\geq n_{1\%}=\dfrac{100}{1}\left(\dfrac{\sigma}{\varepsilon_{rel}\mu^{\mathrm{eff}}}\right)^{2}\end{cases} \tag{3.45}$$

It is obvious that number n derived from the Chebyshev's inequality is few times larger than that one from the Central Limit Theorem, since CLT uses information on standard normal distribution, in addition. In the following chapters, the simulation number is always evaluated according CLT. Whenever n has been appeared to the author not enough large then the simulation result was verified by increasing, in addition, sampling number according to that required by the Chebyshev's inequality.

Let us denote the expectation value, corresponding to some definite value N of sampling window, by μ_{N}^{eff}. The theorems presented above do only assure convergence in probability of MC estimator to the value μ_{N}^{eff} and not to the value μ_{∞}^{eff}, which is the property of random medium to be determined. This problem is investigated in a following section.

3.2.3. Analytical results: checkerboard

Determination of the appropriate size of sampling window was indicated in section 3.2.1 to be a fundamental problem of the proposed methodology. It is evident that such observation window should be sufficiently large in order to be representative for given random microstructure. Moreover, as it will be shown in further considerations, the size of window is strongly affected by the type of analyzed property. For instance, if one considers transport properties and the size of sampling window is not large enough then averaging over sufficient (or even infinite) number of realizations does not lead to effective properties. Hence the size of the sample should be chosen reasonably and very carefully (the results which point at this problem can be found in (Kanit *et al.* 2003; Różański *et al.* 2008; Różański & Łydżba 2009; Różański *et al.* 2009). On the other hand, in case of geometrical property, namely the volume fraction, the mean value does not depend on the size of the sample – if the sufficient number of realizations is carried out the mean value is always equal to the macroscopic value of the volume fraction.

Even though this work deals with transport parameters, in addition, geometrical properties, namely the volume fraction as well as two-point probability, are studied. The motivation for studying geometrical properties stems from the fact that the results of these examinations are fundamentals for further considerations. All of aforementioned properties are investigated for a particular two-phase microstructure, namely random checkerboard (Fig. 3.8). Due to simple generation procedure this type of microstructure can be described statistically in an analytical way. Its numerical reconstruction is as follows: pseudo-random number uniformly distributed in the range 0 to 1 is generated for each pixel. Then, if random number is less than given value of probability p the pixel is filled with black color, otherwise the white color is assigned. Note that, in a following example, black pixels are treated as inclusions (phase 2) with volume fraction $\phi_2=\phi$, contrary to white pixels which are defined as matrix (phase 1) with volume fraction $\phi_1=1-\phi$.

It should be mentioned that throughout this work all pseudo-random numbers are generated using the Marsaglia-Zaman generator which is a part of Mathematica software (Mathematica, 2008). More details concerning Marsaglia-Zaman and other generators as well as its quality checks can be found in (Janke, 2002).

Fig. 3.8. Some examples of random microstructures: 40x40, 60x60, 80x80, respectively.

Note that the process of random checkerboard generation can be described by Bernoulli trials (Feller, 1961). In what follows, we define the appearance of black pixel as a success having constant probability p. Then, the generation process is a sequence of N^2 (total number of pixels in a sample) independent success/failure experiments, each of which yields success with probability p. Following (Feller, 1961) we have that the number of successes (black pixels) S_{N^2} has a binomial distribution with expectation

$$E\left(S_{N^2}\right) = N^2 p \qquad (3.46)$$

and variance

$$Var\left(S_{N^2}\right) = N^2 p\left(1-p\right) \tag{3.47}$$

Volume fraction

It is evident that $\phi = \dfrac{S_{N^2}}{N^2}$ and hence, utilising (3.46) and (3.47), we simply obtain:

$$E\left(\phi\right) = p \tag{3.48}$$

and

$$Var\left(\phi\right) = \frac{p\left(1-p\right)}{N^2} \tag{3.49}$$

Note that the expected value of the volume fraction (3.48) is equal to the value of probability p, regardless of N.

Now, in order to determine the estimator of (3.48), we employ the methodology outlined in section 3.2.1. Hence, we consider a set of n sampling windows (realizations of random checkerboard). For each j-realization the volume fraction of phase 2 is ϕ_j. Then, the overall volume fraction of black cells is estimated as the mean value averaged over n sampling windows, i.e.:

$$\overline{\phi} = \frac{1}{n}\sum_{j=1}^{n}\phi_j \tag{3.50}$$

Defining $S_{N^2}^{j}$ as the number of black pixels within j-realization as well as S_n as the total number of black cells, such that $S_n = \displaystyle\sum_{j=1}^{n} S_{N^2}^{j}$, relation (3.50) can be rewritten in the following form:

$$\overline{\phi} = \frac{S_n}{nN^2} \tag{3.51}$$

In order to evaluate the value of estimator (3.51) it is necessary to determine sufficient number of realizations n which has to be performed. The problem can be solved by making use of Central Limit Theorem (CLT), however, we use a slightly different approach utilizing the properties of binomial properties. Thus, we require that $\overline{\phi}$ should be in a following range:

$$E\left(\phi\right)\left(1-\varepsilon\right) \le \overline{\phi} \le E\left(\phi\right)\left(1+\varepsilon\right) \tag{3.52}$$

where $\varepsilon > 0$ is the given error of estimation.

Substituting (3.48) as well as (3.51) in the relation (3.52) leads to:

$$nN^2 p\left(1-\varepsilon\right) \le S_n \le nN^2 p\left(1+\varepsilon\right) \tag{3.53}$$

Therefore, the problem of estimating n can be formulated as follows: there exist such n that the probability that S_n satisfies (3.53) is larger or equal to $1-\alpha$. i.e.

$$\forall(\alpha > 0, N > 0), \quad \exists n \Rightarrow P\left(nN^2 p(1-\varepsilon) \leq S_n \leq nN^2 p(1+\varepsilon)\right) \geq 1-\alpha \tag{3.54}$$

On the other hand one can notice that relation above is the probability that S_n lies between two limits and hence (3.54) can be rewritten in the following form (Feller, 1961):

$$\forall(\alpha > 0, N > 0), \quad \exists n \Rightarrow \left\{ \sum_{i=i_{min}}^{i=i_{max}} \binom{nN^2}{i} p^i (1-p)^{(nN^2-i)} \right\} \geq 1-\alpha \tag{3.55}$$

where

$$\begin{aligned} i_{min} &= \left\lfloor nN^2(1-\varepsilon)p \right\rfloor + 1 \\ i_{max} &= \left\lfloor nN^2(1+\varepsilon)p \right\rfloor \end{aligned} \tag{3.56}$$

Note, in the relations above $\lfloor * \rfloor$ stands for the integral part of $*$, whereas $\binom{nN^2}{i}$ is the binomial coefficient defined as:

$$\binom{nN^2}{i} = \frac{nN^2!}{i!(nN^2-i)!} \tag{3.57}$$

The sufficient number of realizations n can be determined by calculating the sum in (3.55). It can be seen that the value of n is influenced by the size of sampling window N, value of probability p as well as by the significance level α. Some numerical calculations were carried out and the results are summarized in Table 3.1.

Observing the results (Table 3.1) one can simply notice that the greater value of p the smaller value of n is required. Furthermore, for given value of probability p, n is decreasing when the size of the sample is increasing. The error of estimation also strongly influences the number of realizations, i.e. for $\varepsilon=0.03$ the number of realizations is significantly larger (for all values of N) when compared to the case of $\varepsilon=0.05$.

Numerical simulations were performed in order to determine the value of volume fraction estimator (3.50). The study was carried out for three different values of volume fraction p, i.e. 0.1, 0.3, 0.5. The number of performed realizations corresponds to the error of estimation $\varepsilon=0.03$ (see Table 3.1). In Figures 3.9-3.11 the fluctuations of volume fraction about its average value are provided for three different values of p as well as three chosen sizes of sampling windows. Furthermore Figures 3.12, 3.13 as well as 3.14 show the value of estimator (3.50) plotted against

the number of performed realizations. It can be seen that as the number of realizations n increases the value of estimator (3.50) converges towards the volume fraction p.

Table 3.1. Sufficient number of realizations n determined for different values of sample size N, probability p and estimation error ε.

N	Number of realizations n					
	p=0.1		p=0.3		p=0.5	
	ε=0.03	ε=0.05	ε=0.03	ε=0.05	ε=0.03	ε=0.05
1	38417	13705	9952	3540	4264	1501
2	9551	3431	2486	885	1056	381
4	2389	859	619	225	263	96
6	1065	385	275	100	119	44
8	600	217	155	57	67	25
10	384	139	99	36	43	16
12	267	97	70	25	30	11
14	197	71	51	19	22	8
16	150	55	39	15	17	6
18	119	43	31	12	14	5
20	96	35	25	9	11	4
300	1	1	1	1	1	1
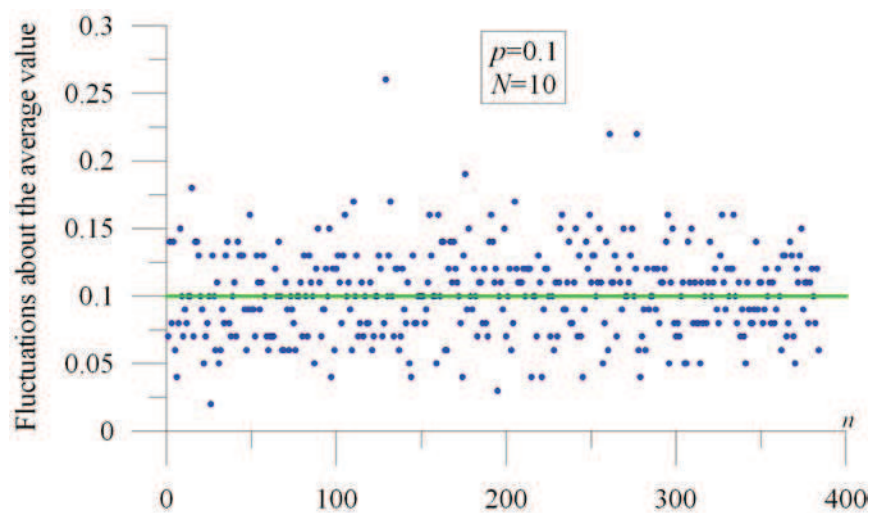
Fig. 3.9. Fluctuations about the average value of volume fraction; p=0.1 and N=10
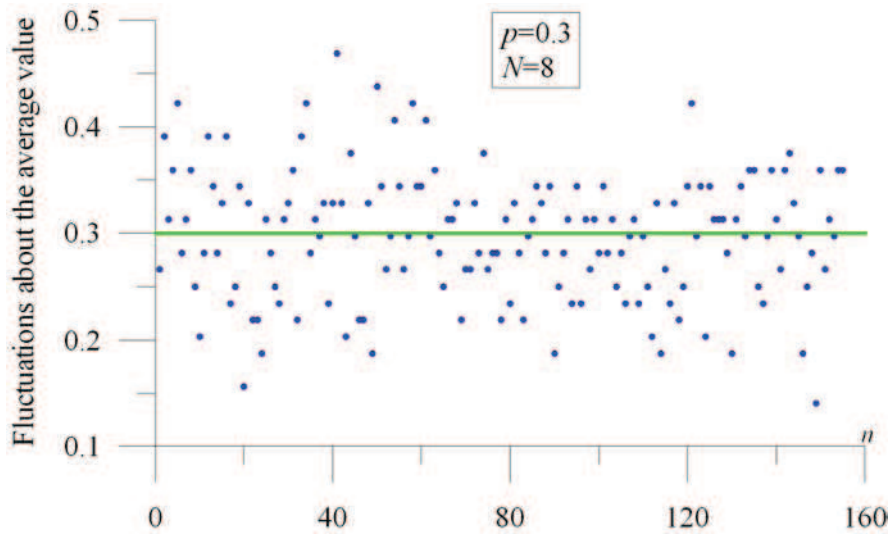
Fig. 3.10. Fluctuations about the average value of volume fraction; p=0.3 and N=8
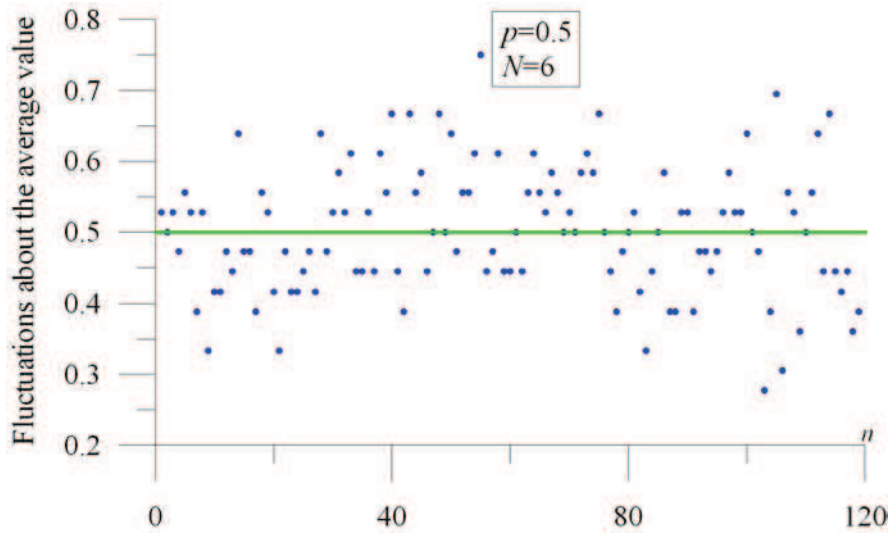
Fig. 3.11. Fluctuations about the average value of volume fraction; p=0.5 and N=6
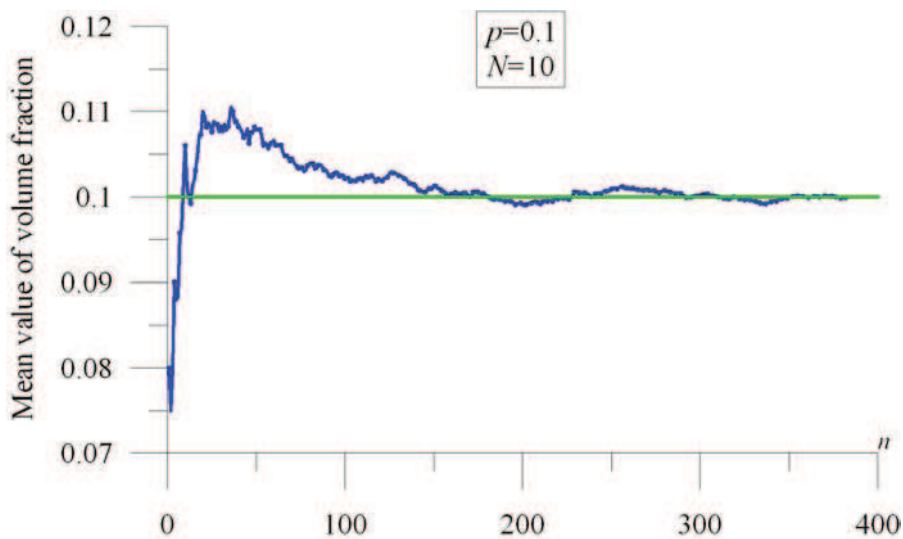
Fig. 3.12. The value of estimator (3.50) plotted against the number of performed realizations; p=0.1 and N=10.
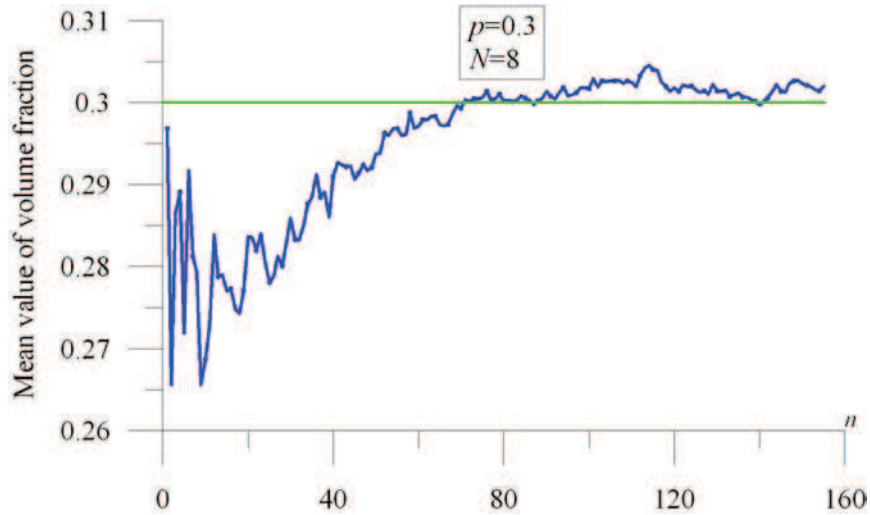
Fig. 3.13. The value of estimator (3.50) plotted against the number of performed realizations; p=0.3 and N=8.
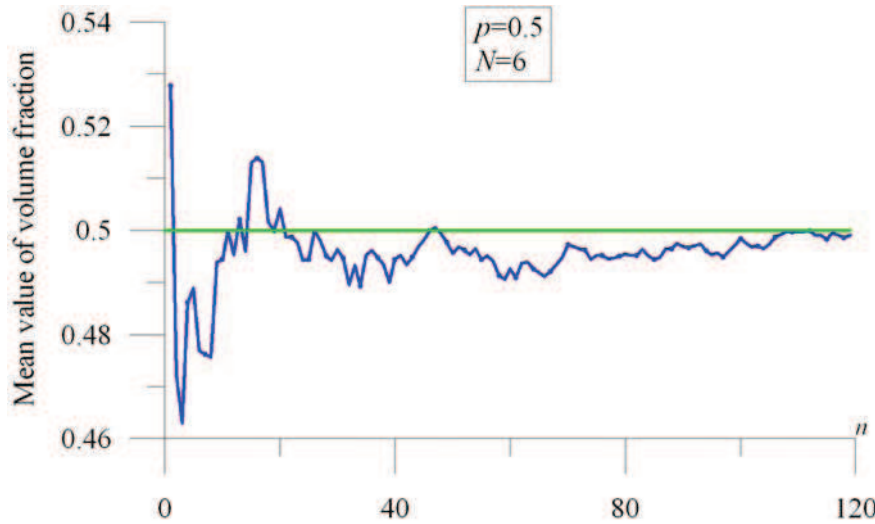
Fig. 3.14. The value of estimator (3.50) plotted against the number of performed realizations; p=0.5 and N=6.

Figures 3.12, 3.13 as well as 3.14 confirm the analytical solution, i.e. relation (3.48). However, this fact is more noticeable in Figures 3.15-3.17 where the mean value of volume fraction – determined for sufficient number of realizations (see Table 3.1) - is plotted against the size of sampling window N. It can be noticed that even though the volume fraction varies from sample to sample, the mean value of volume fraction does not depend on the size of sampling window N. The mean values obtained for small sample sizes as well as for large N are in a very well agreement.

Due to fact that the mean value does not depend on the size of sampling window, (rather on the number of performed realizations) none conclusions respecting the representativity of the sample can be drawn. On the other hand, one can notice that the variance of volume fraction strongly depends on the size of window (Figs. 3.18-3.20), i.e. it is decreasing when the sample size is increasing. Hence, it seems that a quantitative understanding of how the volume fraction fluctuates, as the sampling window is moved from point to point in the sample, is of paramount importance.
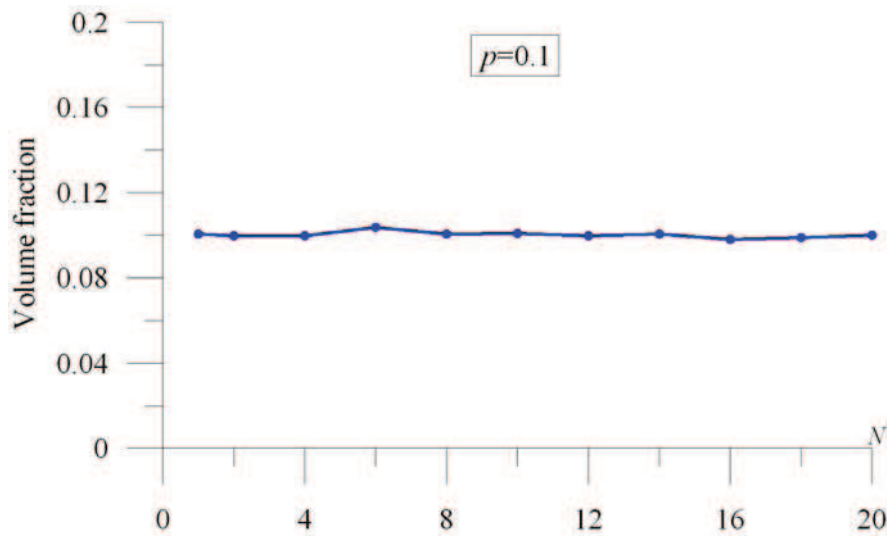
Fig. 3.15. Mean value of volume fraction plotted against the size of sampling window *N* (*p*=0.1).
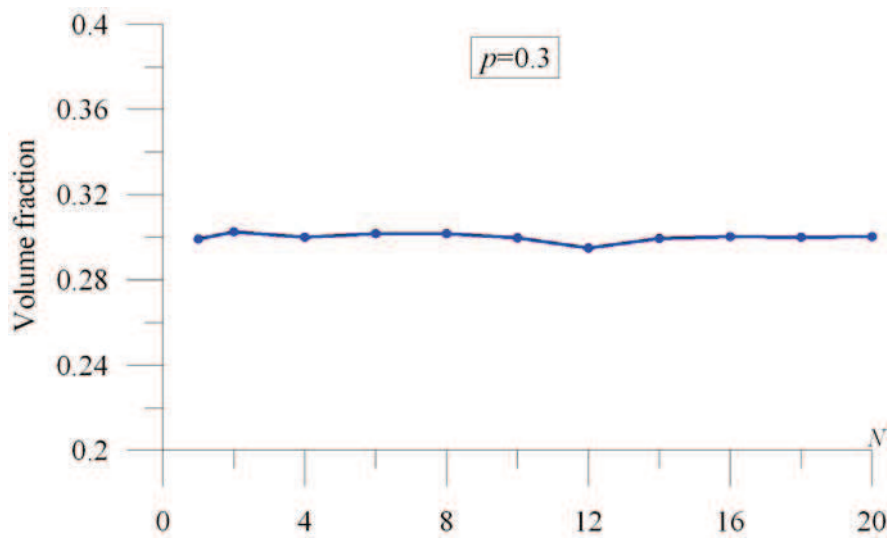
Fig. 3.16. Mean value of volume fraction plotted against the size of sampling window *N* (*p*=0.3).
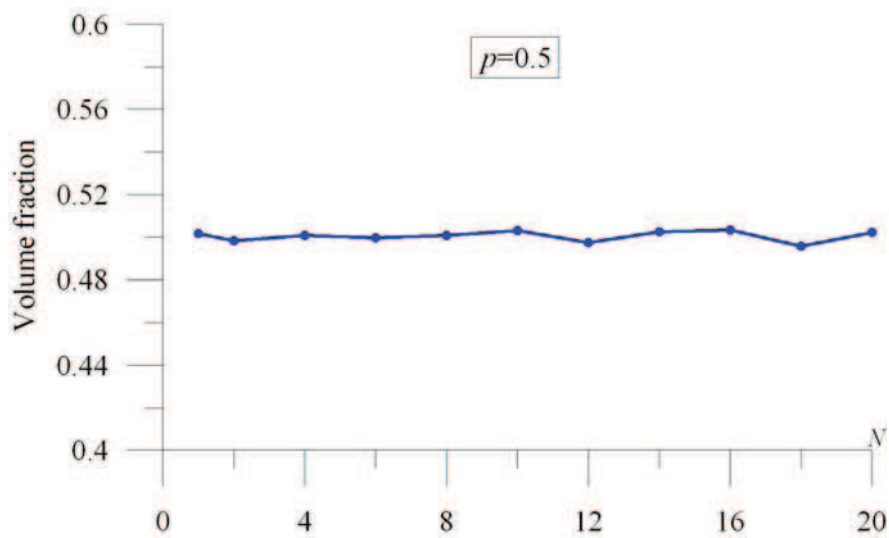
Fig. 3.17. Mean value of volume fraction plotted against the size of sampling window *N* (*p*=0.5).
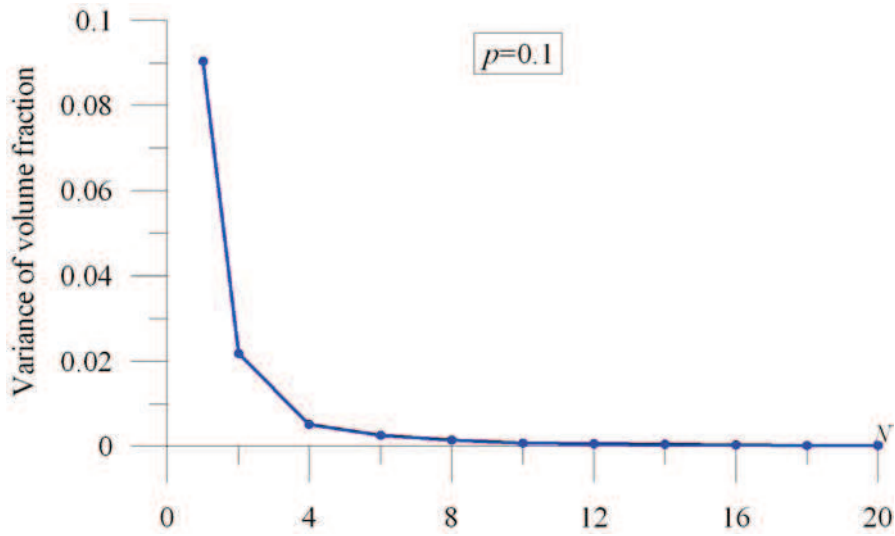
Fig. 3.18. Variance of volume fraction plotted against the size of sampling window N (p=0.1).
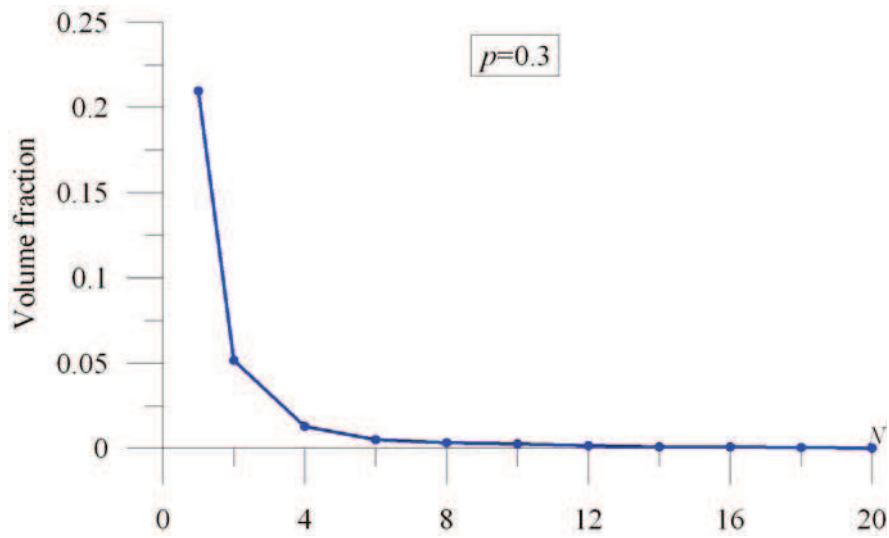
Fig. 3.19. Variance of volume fraction plotted against the size of sampling window N (p=0.3).
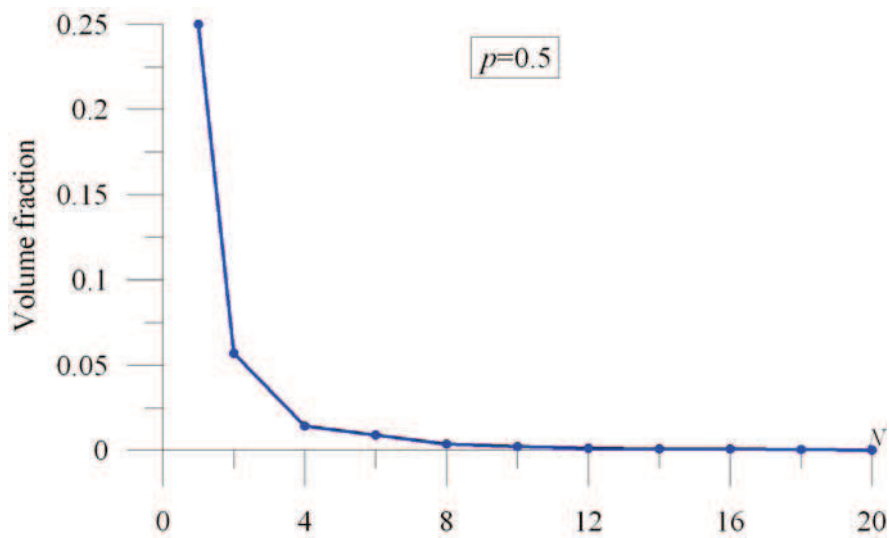
Fig. 3.20. Variance of volume fraction plotted against the size of sampling window N (p=0.5).

Two-point probability

In this section we investigate whether the conclusions found for volume fraction could be extended to the two-point probability. Once again we consider a set of *n* sampling windows (realizations of random checkerboard). For each *j*-realization the two-point (phase 2) probability function is determined via relation (3.19) and is denoted as $S_{2,j}^{(2)}$. Then, the overall two-point probability is estimated as the mean value averaged over *n* sampling windows, i.e.:

$$\overline{S_2^{(2)}} = \frac{1}{n}\sum_{j=1}^{n} S_{2,j}^{(2)} \tag{3.58}$$
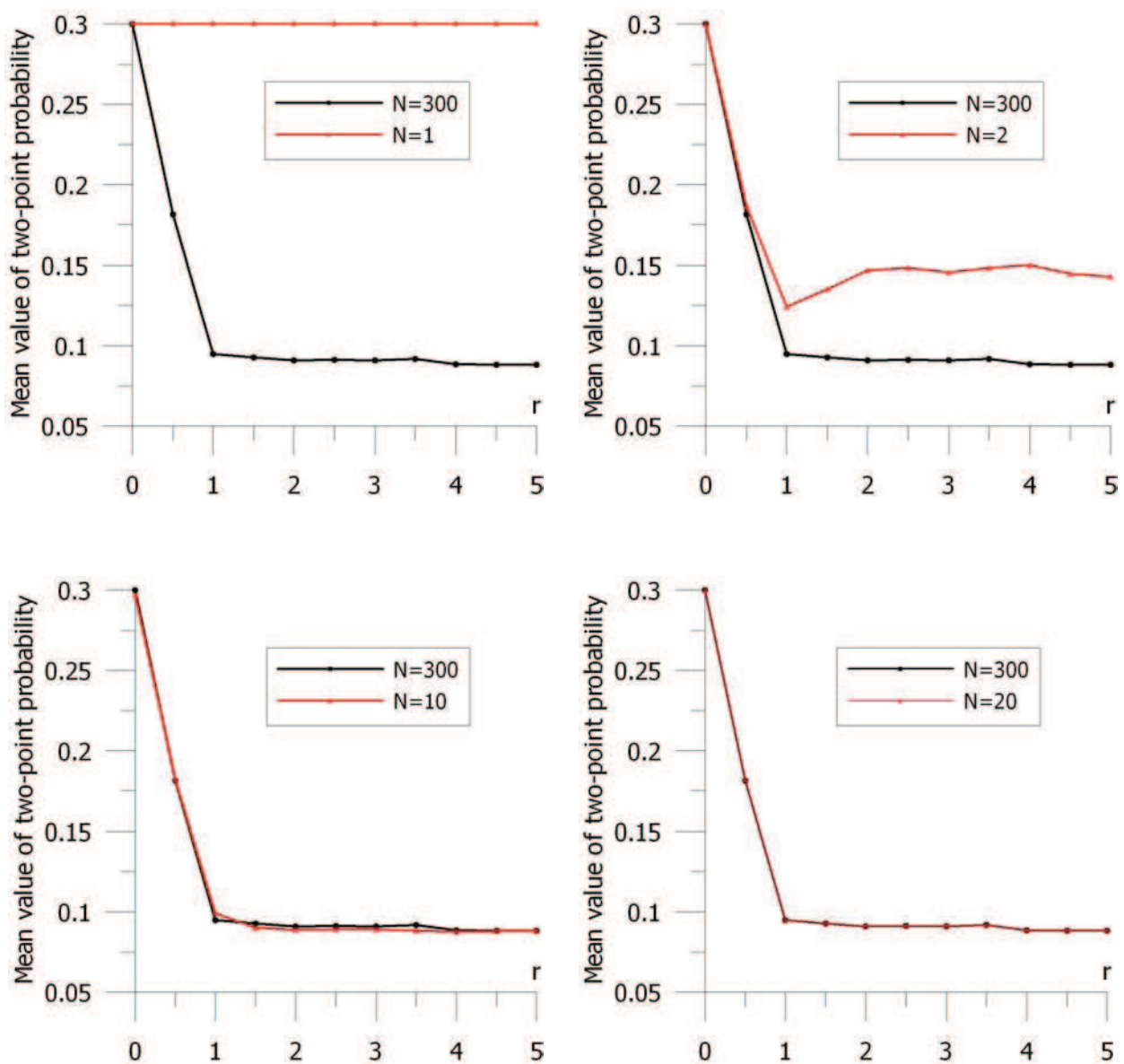
Fig. 3.21. Mean values of two-point probability corresponding to different sizes of sampling windows plotted against the distance *r* (in pixels).

Figure 3.21 presents the mean values of the two-point probability determined for different values of sampling windows size, i.e. $N=1$, $N=2$, $N=10$, $N=300$. The results correspond to the checkerboard with the volume fraction $\phi=0.3$. Note that on the horizontal axis the length of distance r is presented as a function of the number of pixels.

It can be seen that in case of $N=1$ and $N=2$ the mean values are different and do not converge towards the result obtained for larger window i.e. one realization of $N=300$ sample. Furthermore, in case of $N=1$ the two-point probability is constant and equal to the volume fraction $p=0.3$. We see that for $N=10$ the mean value only slightly differs from the two-point probability value determined for large sample ($N=300$). In case of $N=20$ both results are in a very well agreement. Therefore the relation observed for volume fraction cannot be extended to the two-point probability: the mean value of two-point probability does not only depend on the number of realizations but primarily is strongly affected by the size of the sample.

Transport properties

In what follows we focus on the transport properties considering the problem of thermal conductivity. Therefore we attribute different conductivities to the composite constituents: $k_M=0.009$ [W/mK] for matrix (white cells) and $k_I=0.25$ [W/mK] for inclusion (black cells). The microstructure with volume fraction of black cells $p=0.3$ is studied. Once again we consider a set of n microstructure realizations (sampling windows). The thermal conductivity coefficient, for j-th microstructure realization k_j, is determined using numerical method which is presented in chapter 6 of this work. Then the mean value $\overline{k}$ is estimated on the basis of (3.25), i.e.

$$\overline{k} = \frac{1}{n}\sum_{j=1}^{n} k_j \tag{3.59}$$

First, we analyze the smallest possible sampling window size, i.e. $N=1$ (one pixel). Thus, for each realization, only two outcomes are possible: black cell (the property k_I) appears with probability p while the appearance of white cell (thermal conductivity k_M) has the probability 1-p. Therefore, basing on the properties of binomial distribution, the expected value of thermal conductivity coefficient can be determined as follows:

$$\mathrm{E}(k) = \sum_{t=0}^{N^2} k_t \frac{N^2!}{t!(1-t)!} p^t (1-p)^{N^2-t} = \sum_{t=0}^{1} k_t \frac{1}{t!(1-t)!} p^t (1-p)^{1-t} = k_I p + k_M (1-p) \tag{3.60}$$

In the equation above k_t is the thermal conductivity coefficient associated with the event that t black cells appears. Note that the right side of Eq. (3.60) simply expresses the bound of Voigt.

Substituting the values of thermal conductivity k_I and k_M in the relation (3.60) we have that the analytical result, in case of $N=1$, is

$$\mathrm{E}(k) = 0.0813 \ [\mathrm{W/mK}] \tag{3.61}$$

The numerical calculations were also performed and the mean value of thermal conductivity coefficient $\overline{k}$ given by relation (3.59) was determined. This quantity is displayed, as a function of n, in Figure 3.22. One can simply notice that the mean value of thermal conductivity coefficient converges towards the analytical result (bound of Voigt) (3.61). Furthermore, if the number of realizations n is greater than 6,000 it only slightly differs from the analytical solution.
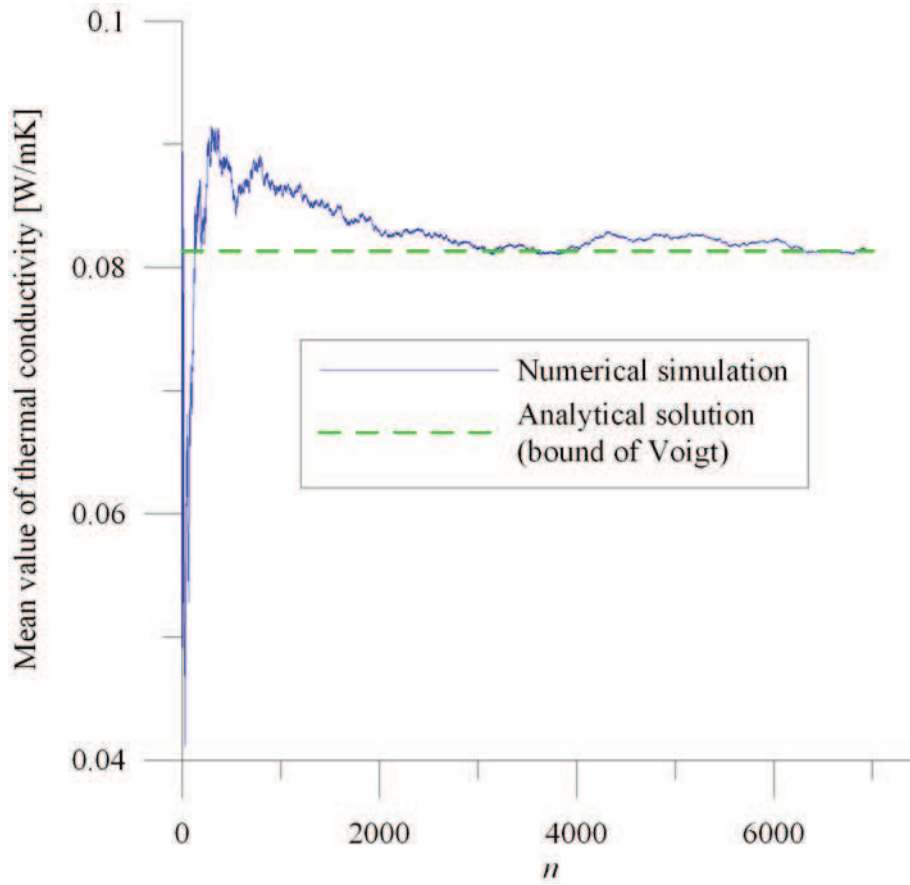
Fig. 3.22. Mean value of thermal conductivity $\overline{k}$ [W/mK] ($N=1$) against the number of performed realizations n

In the same manner, both the analytical and numerical solutions, can be obtained for greater sizes of sampling windows. However, there is some inconvenience when the analytical solution is performed for $N>1$ - the number of possible microstructure outcomes is given by 2^{N^2}. Nevertheless, in case of $N=2$, the analytical solution is still easy to perform because it consists of only 16 realizations. The possible microstructure realizations, in case of $N=2$, are presented in Fig. 3.23.

The analytical solution, in case of $N=2$, is as follows:

$$E(k) = \sum_{t=0}^{N^2} k_t \frac{N^2!}{t!(N^2-t)!} p^t (1-p)^{N^2-t} = \sum_{t=0}^{4} k_t \frac{4!}{t!(4-t)!} p^t (1-p)^{4-t} \tag{3.62}$$

In order to determine (3.62) the values of k_0, k_1, k_2, k_3, k_4 were previously calculated. These are as follows: k_0 and k_4 are simply equal to k_M and k_I, respectively; the method outlined in chapter 6 was used to evaluate k_1 and k_3 (k_1=0.0149 [W/mK], k_3=0.1514 [W/mK]); in case of t=2 one can notice that 6 different types of pixel arrangements are possible (see Fig. 3.23) - four of them have the solution simply described by Voigt and Reuss bounds, whereas two microstructures possess phase-inversion symmetry and its property is equal to $\sqrt{k_M k_I}$ and hence the value of k_2 is the mean of these 3 results, i.e.: k_2=0.0648 [W/mK]. Substituting the values of k_t in the relation (3.62) we have that:

$$E(k) = 0.0389 \text{ [W/mK]} \tag{3.63}$$

Once again the numerical simulations were performed and the results are presented in Figure 3.24. One can observe that as the number of realizations n is greater than 2,500-3,000 the mean value only slightly differs from the analytical solution.
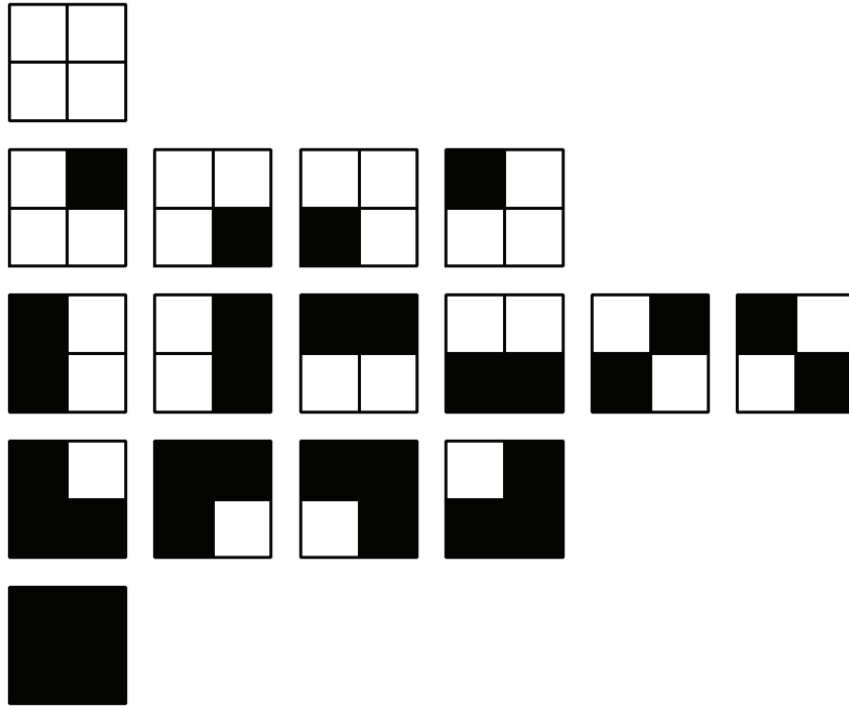
Figure 3.23. Possible microstructure realizations in case of N=2

The most important is, however, that the results obtained in case of N=1 as well as N=2 are different. This fact indicates strong dependence of thermal conductivity coefficient on the size of sampling window. Furthermore, this relation is similar to the one established for the two-point probability function. This fact is emphasized in Fig. 3.25, where the mean value of thermal

conductivity is plotted against the size of the sample. Additionally, the result of numerical calculations performed for one realization of large sample (*N*=300) is also presented.

Figure 3.25 shows that the mean value of thermal conductivity coefficient does not only depend on the number of performed realizations rather on the size of the sampling window. For small samples the average value is close to the bound of Voigt whereas for larger samples the solution converges towards the effective thermal conductivity and is close to the one determined for single realization of *N*=300 sample.
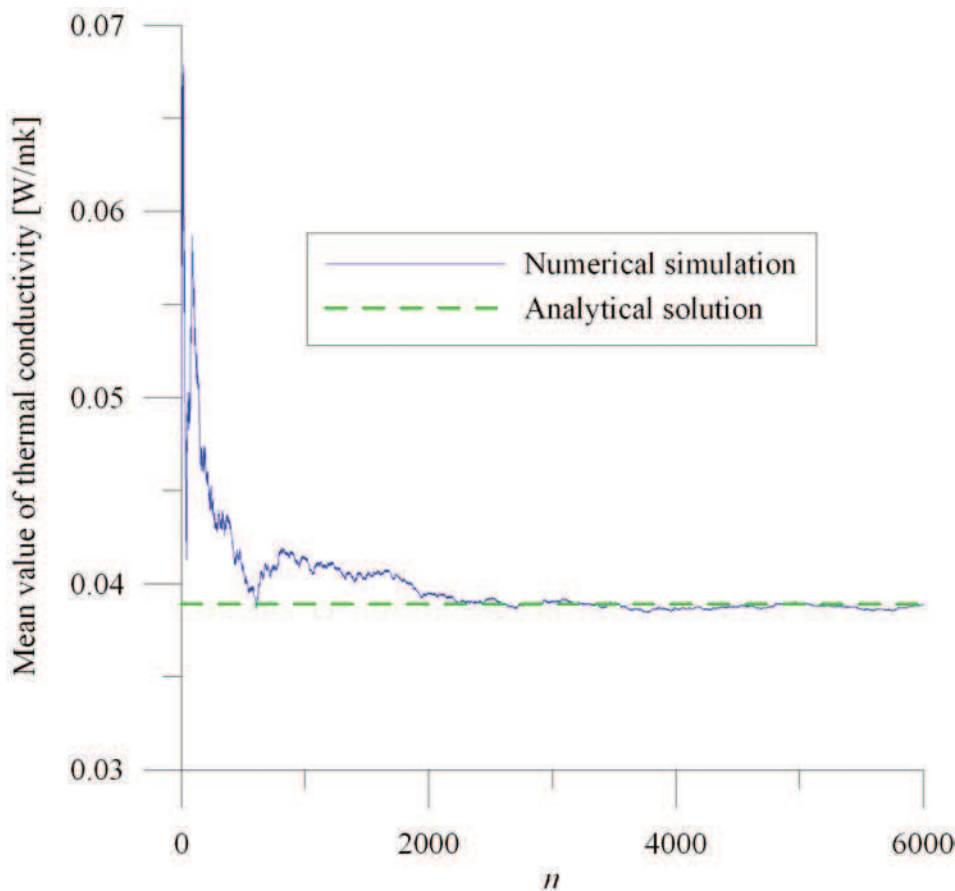
Fig. 3.24. Mean value of thermal conductivity $\overline{k}$ [W/mK] (*N*=2) against the number of performed realizations *n*

Thus, we have to notice that transport properties can be simply evaluated either by considering small samples with sufficient (usually large) number of realizations or by performing even one calculation over large sample – it confirms the results obtained by Kanit *et al.* (2003). Nevertheless, there exist some threshold value of the sample size below which the mean value does not converge towards the solution obtained in case of large sample (*N*=300). In case of considered example this threshold value of the sample size is approximately $N \simeq 8 \div 10$ (Fig. 3.25) – only for $N \geq (8 \div 10)$ the mean value is in a very well agreement with the solution obtained for large size of window.

Note, that this threshold value corresponds to the one established for the geometrical property, namely the two-point probability - see Fig. 3.21 where the mean value of two-point probability, in case of *N*=10, only slightly differs from the two-point probability value determined for one realization of large sample (*N*=300). Therefore, comparing the sizes of sampling windows established for different properties we can expect that two-point probability could be successfully used in order to determine the minimum sample size for the problem of effective transport properties.
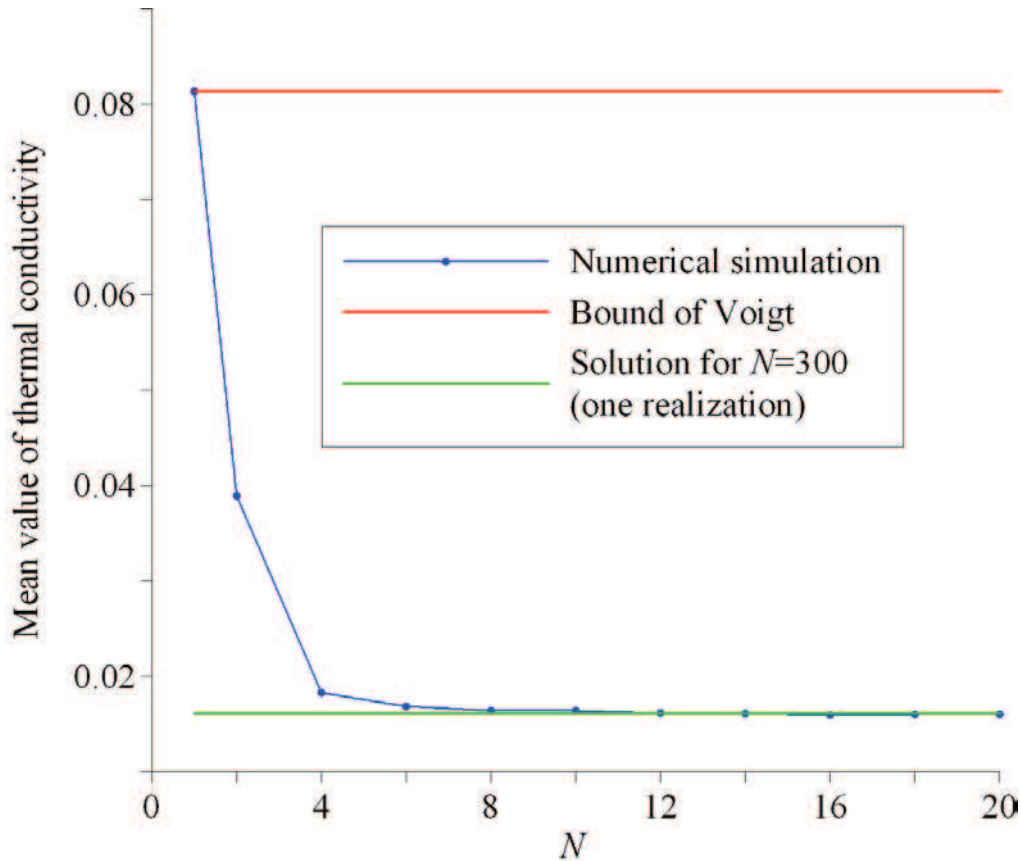
Fig. 3.25. Mean value of thermal conductivity $\bar{k}$ [W/mK] plotted against the size of sampling window

3.3. Remarks

Within this chapter only two microstructural descriptors, namely 2-point probability as well as lineal-path function have been presented. Nevertheless, there exist a large number of other correlation functions which characterize the microstructure morphology. In Torquato (2002) the microstructure descriptors like *Chord-Length Density Function*, *Pore-Size Function*, *Nearest-Neighbor Functions*, *Point/q-Particle Correlation Functions*, *Surface/Particle Correlation Functions* as well as its applications to the mechanics of random media are provided.

As mentioned, RVE for random composite material is usually regarded as a volume of heterogeneous body which is small from a macroscopic point of view and simultaneously large enough to be able to contain sufficient number of inhomogenities to be representative. For random media the formulation of the quantitative definition of RVE is not an easy task – it strongly depends on the microstructure as well as on the considered effective property. Theoretically, the best choice would be the infinite size of RVE, however, for practical applications one has to assume the finite size of RVE such that the considered property is evaluated with given error tolerance relative to the response of the real body.

It is, however, possible to estimate effective properties either by performing calculations over one large sample or by averaging over sufficient number of significantly smaller samples – so called *sampling windows*. Then, the analyzed property is classically estimated as the mean value – relation (3.25). The problem of estimating the sufficient number of realizations (sampling windows), which one has to carry out, is solved by the application of *Central Limit Theorem* – relations (3.33) or (3.34).

A separate problem is the determination of the size of the sampling window. It was shown that the size of the window strongly depends on the type of analyzed property. Basing on numerical as well as analytical solutions provided for the particular type of microstructure, namely random checkerboard, some conclusions regarding the representativity can be stated. These are as follows:

- the mean value of volume fraction does not depend on the size of sampling window; performing the sufficient number of realization one always gets the macroscopic value of the volume fraction p, regardless of the size of sampling window N,

- the variance of volume fraction strongly depends on the sample size – it is decreasing as the size N is increasing,

- the mean value of two-point probability is strongly affected by the size of the sample; in case of $N=1$ this quantity is constant and simply equals the volume fraction of considered phase,

- as the size of sampling window is increasing the mean value of two-point probability converges towards the two-point probability determined for one realization of large sample ($N=300$),

- strong dependence of thermal conductivity coefficient on the size of sampling window was also indicated; in case of $N=1$ the mean value of thermal conductivity converges towards the bound of Voigt,

- as the size of sampling window is increasing the mean value of thermal conductivity is decreasing and converges towards the result obtained for one realization of large sample (N=300); it was shown that there exist some threshold value of the sample size N below which the mean value of thermal conductivity does not converge towards the result evaluated in case of N=300 sample,

- the threshold value of sampling window size corresponds to the one established for the two-point probability,

- comparing the sizes of sampling windows which are representative in the view of two-point probability and effective thermal conductivity one can expect that two-point probability could be successfully used for the determination of the minimum sample size in case of the problem of evaluating the effective transport properties,

Note that on the basis of conclusions above, a slightly different definition of RVE can be formulated: RVE is a function of the analyzed property, size of the sample, sufficient number of realizations which has to be performed as well as an error of estimation. The formulation of the conditions for RVE size to be representative according to geometry and overall transport properties are provided in chapter 4 and 5, respectively.

4. Formulation of the condition for RVE size to be representative with respect to microstructure geometry

4.1. Local volume fraction fluctuations

As mentioned in previous section, when moving sampling window from point to point, the volume fraction of phases strongly fluctuates, although the "overall" volume fraction for statistically homogeneous media is constant. This problem has been extensively studied by (Lu & Torquato, 1990; Quintanilla & Torquato, 1997; Quintanilla & Torquato, 1999).

Following above references we define so called *local volume fraction* as the volume fraction of the phases, say phase 1, contained in sampling window with position $\mathbf{x}$. In other words the local volume fraction is the fraction of the window which lies in phase 1 (Fig. 4.1) and is denoted as $\xi(\mathbf{x})$. Although the macroscopic volume fraction of phase 1, ϕ_1, is constant, the concentration ξ is a random variable which ranges from 0 to 1 (see Fig 4.1).
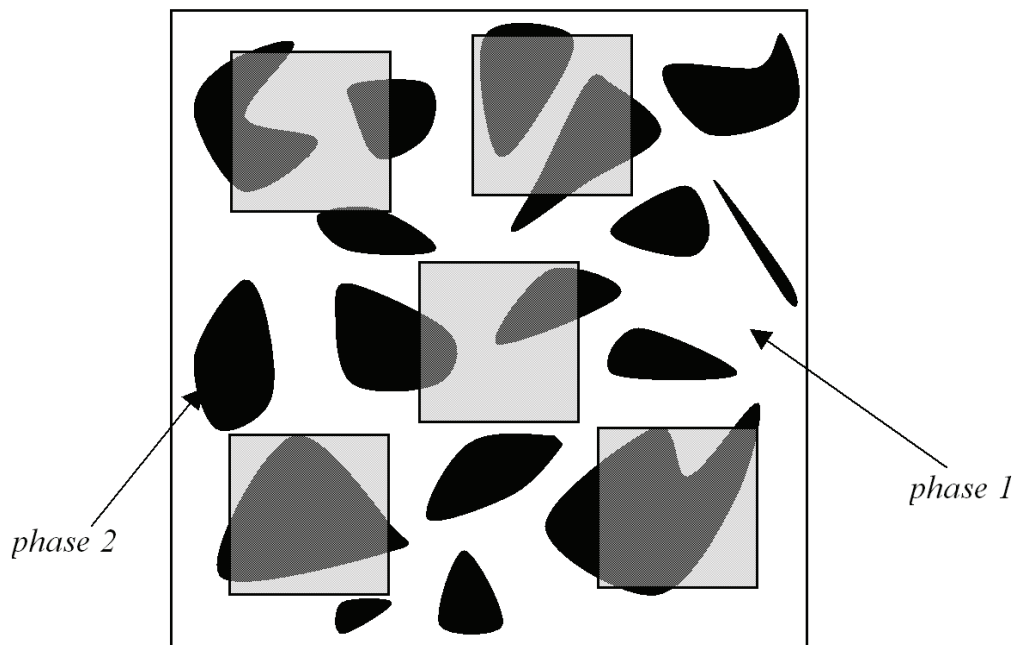
Fig. 4.1. A schematic depicting the local volume fraction which is the fraction of sampling window lying in phase 1.

In what follows, we consider the volume fraction of phase 1 contained in the sampling window $\Omega_0(\mathbf{x})$ whose centroid is located at $\mathbf{x}$. As mentioned, the volume fraction of phase 1 contained in

$\Omega_0(\mathbf{x})$ fluctuates when the window is moved from point to point. Hence, the local volume fraction $\xi(\mathbf{x})$ can be defined as follows:

$$\xi(\mathbf{x}) = \frac{1}{\|\Omega_0\|} \int_{\Omega_0(\mathbf{x})} I^{(1)}(\mathbf{y}) d\mathbf{y} \tag{4.1}$$

where $I^{(1)}(\mathbf{y})$ is the indicator function expressed by (3.5).

Introduce now a new function, i.e. sampling window indicator function which has the form:

$$\theta^{(i)}(\mathbf{x}, \mathbf{y}) = \begin{cases} 1, & \text{if } \mathbf{y} \in \mathcal{V}_i \cap \Omega_0(\mathbf{x}) \\ 0, & \text{otherwise} \end{cases} \tag{4.2}$$

Note that (4.2) can be rewritten as

$$\theta^{(i)}(\mathbf{x}, \mathbf{y}) = I^{(i)}(\mathbf{y}) H(\mathbf{y} - \mathbf{x}) \tag{4.3}$$

where

$$H(\mathbf{y} - \mathbf{x}) = \begin{cases} 1, & \text{if } (\mathbf{y} - \mathbf{x}) \in \Omega_0(0) \\ 0, & \text{otherwise} \end{cases} \tag{4.4}$$

Then, utilising (4.2) as well as (4.3) the definition (4.1) takes the form:

$$\xi(\mathbf{x}) = \frac{1}{\|\Omega_0\|} \int_{\Omega} I^{(1)}(\mathbf{y}) H(\mathbf{y} - \mathbf{x}) d\mathbf{y} \tag{4.5}$$

Recalling now the ergodic hypothesis one can equate the ensemble average of ξ to the volume average in the limit of infinitely large volume and hence it is easy to show that (Lu & Torquato, 1990)

$$\overline{\langle \xi \rangle} = \phi_1 \tag{4.6}$$

In previous section, where the numerical example of random checkerboard was studied, it was shown that the variance of volume fraction strongly depends on the size of the sampling window. It is a decreasing function of the size of the window. Therefore, a quantitative understanding of how the volume fraction fluctuates, when the window is moved from point to point in the sample, is very important. Therefore, in what follows, a variance associated with $\xi(\mathbf{x})$ is studied.

Following the definition of the variance and utilising (4.6) we have that

$$Var(\xi) = \overline{\langle \xi^2 \rangle} - \left(\overline{\langle \xi \rangle} \right)^2 = \overline{\langle \xi^2 \rangle} - \phi_1^2 \tag{4.7}$$

One can simply notice that in order to calculate the variance of ξ, first the quantity $\overline{\langle \xi^2 \rangle}$ has to be determined. Utilizing (4.5) the quantity $\overline{\langle \xi^2 \rangle}$ can be simply expressed as:

$$\overline{\left\langle \xi^2 \right\rangle} = \left\langle \overline{\frac{1}{\left\| \Omega_0 \right\|^2} \int_\Omega I^{(1)}(\mathbf{x}+\mathbf{r}) H(\mathbf{r}) d\mathbf{r} \int_\Omega I^{(1)}(\mathbf{x}+\mathbf{z}) H(\mathbf{z}) d\mathbf{z}} \right\rangle \tag{4.8}$$

Once again, taking into account the ergodic hypothesis, the relation (4.8) can be presented in the following form:

$$\overline{\left\langle \xi^2 \right\rangle} = \lim_{\|\Omega\| \to \infty} \frac{1}{\|\Omega\|} \frac{1}{\|\Omega_0\|^2} \int_\Omega \int_\Omega \int_\Omega I^{(1)}(\mathbf{x}+\mathbf{r}) I^{(1)}(\mathbf{x}+\mathbf{z}) H(\mathbf{r}) H(\mathbf{z}) d\mathbf{r} d\mathbf{z} d\mathbf{x} \tag{4.9}$$

Following the definition of two-point probability, given by (3.13), we see that $\overline{\left\langle \xi^2 \right\rangle}$ can be expressed in terms of two-point probability function, i.e.

$$\overline{\left\langle \xi^2 \right\rangle} = \frac{1}{\|\Omega_0\|^2} \int_\Omega \int_\Omega S_2^{(1)}(\mathbf{r}-\mathbf{z}) H(\mathbf{r}) H(\mathbf{z}) d\mathbf{r} d\mathbf{z} \tag{4.10}$$

Utilising the substitution $\mathbf{t} = \mathbf{r} - \mathbf{z}$, the above relation takes the form

$$\overline{\left\langle \xi^2 \right\rangle} = \frac{1}{\|\Omega_0\|^2} \int_\Omega \int_\Omega S_2^{(1)}(\mathbf{t}) H(\mathbf{r}) H(\mathbf{r}-\mathbf{t}) d\mathbf{r} d\mathbf{t} \tag{4.11}$$

and therefore, in what follows, we focus on determination of the quantity $\vartheta_{int}(\mathbf{t},a,b)$ defined as:

$$\vartheta_{int}(\mathbf{t},a,b) = \int_\Omega H(\mathbf{r}) H(\mathbf{r}-\mathbf{t}) d\mathbf{r} \tag{4.12}$$

Relation (4.12) is the intersection volume of two sampling window regions whose centroids are separated by the displacement $\mathbf{t}$. Furthermore, a and b are the lengths of window sides (see Fig. 4.2).
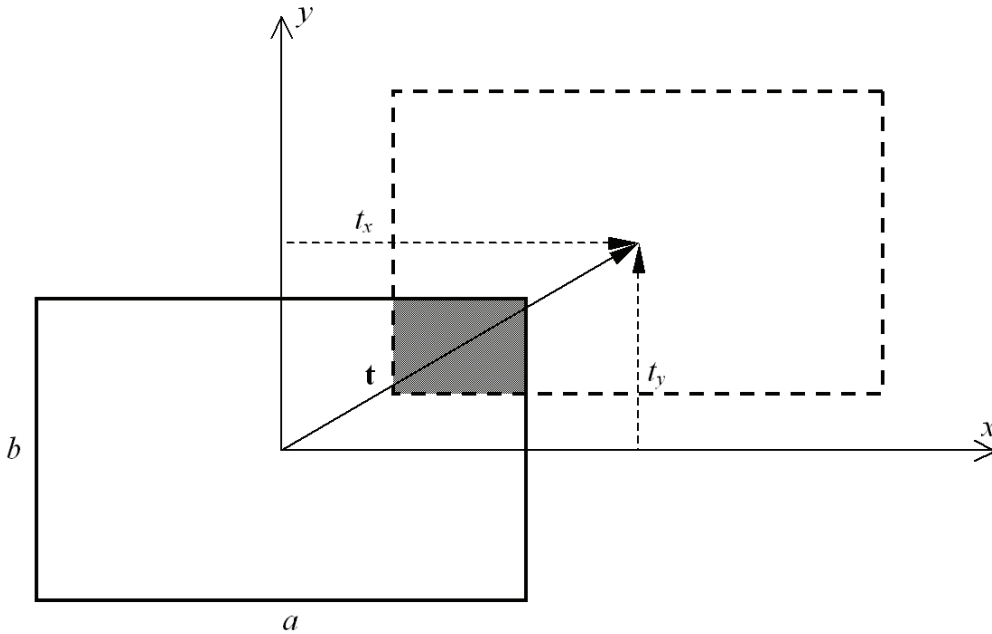
Fig. 4.2. Two sampling windows whose centroids are separated by the displacement $\mathbf{t}$

Using the notations presented in Fig. 4.2 one can notice that $\vartheta_{int}(\mathbf{t}, a, b)$ can be expressed as follows:

$$\vartheta_{int}(\mathbf{t}, a, b) = \left(a - |t_x|\right)\left(b - |t_y|\right)1\left(a - |t_x|\right)1\left(b - |t_y|\right) \tag{4.13}$$

where $1(x)$ is the Heaviside step function.

Note that

$$\int_{\Omega} \vartheta_{int}(\mathbf{t}, a, b)\, dt = \int_{-a}^{a}\int_{-b}^{b}\left(a - |t_x|\right)\left(b - |t_y|\right)1\left(a - |t_x|\right)1\left(b - |t_y|\right)dxdy = \left\|\Omega_0\right\|^2 \tag{4.14}$$

and therefore

$$\frac{1}{\left\|\Omega_0\right\|^2}\int_{\Omega} \vartheta_{int}(\mathbf{t}, a, b)\, dt = 1 \tag{4.15}$$

Utilising (4.11) as well as (4.15) the variance of local volume fraction, defined by (4.7), can be presented as:

$$Var(\xi) = \frac{1}{\left\|\Omega_0\right\|^2}\int_{\Omega}\left(S_2^{(1)}(\mathbf{t}) - \phi_1^2\right)\vartheta_{int}(\mathbf{t}, a, b)\, dt \tag{4.16}$$

Furthermore, substituting (4.13) in the relation (4.16), we have that:

$$Var(\xi) = \frac{1}{\left\|\Omega_0\right\|^2}\int_{\Omega}\left(S_2^{(1)}(\mathbf{t}) - \phi_1^2\right)\left(a - |t_x|\right)\left(b - |t_y|\right)1\left(a - |t_x|\right)1\left(b - |t_y|\right)dt \tag{4.17}$$

In case of 2D problem, it is easy to write (4.17) in the following, final form:

$$Var(\xi) = \frac{4}{\left\|\Omega_0\right\|^2}\int_{0}^{a}\int_{0}^{b}\left(S_2^{(1)}(\mathbf{t}) - \phi_1^2\right)\left(a - t_x\right)\left(b - t_y\right)dxdy \tag{4.18}$$

4.2. RVE representativity according to two-point probability

It has been shown above that local volume fraction fluctuates when sampling window is moved from point to point. The study of these fluctuations can be performed by calculating their variance. Relation (4.18) gives the possibility to determine the variance of ξ in case of planar (2D) problems with rectangle sampling window. However, in the analogical way, different shapes of sampling window can be considered by suitable modification of relation (4.13).

Note that in the relation (4.18), the two-point probability function for phase 1, $S_2^{(1)}$, plays a central role, i.e. given the values of two-point probability one can simply estimate the variance of

local volume fraction ξ and, moreover, as it will be shown further in this section, a condition regarding the representativity of the sample can be formulated.

First, we should explain what is a meaning of "the sample to be representative with respect to geometry". As it has been discussed in previous sections, the perfect mathematical description of random microstructure geometry involves an infinite number of statistical measures. In what follows we restrict our consideration to only one microstructure statistical descriptor, i.e. the two-point probability function. Therefore, throughout further consideration a following definition of sample representativity with respect to microstructure geometry is adopted:

Definition 3: A sample is representative, with respect to geometry, if based on a knowledge of sample geometry, one can obtain a satisfactory replica of the two-point correlation function of random composite (statistically homogeneous), with definite value of statistical error tolerance.
The above definition is, in the framework of Monte Carlo simulation, interpreted in an extended sense, in the thesis. Let $\{V_1, V_2, ...\}$ be a sequence of samples of the same finite size and let $\{f_1(r), f_2(r), ...\}$ be a sequence of two-point correlation function corresponding to samples' microstructure. The replica is evaluated as the MC estimator of two-point correlation function, i.e.:

$$\overline{f}(r) = n^{-1} \sum_{i=1}^{n} f_i(r) \tag{4.19}$$

and the sample is said to be representative with respect to geometry if:

$$\max \left| \lim_{n \to \infty} \overline{f}(r) - S_2(r) \right| \le \varepsilon \tag{4.20}$$

The symbol ε represents assumed error tolerance.

The two-point probability function decays to the asymptotic value of ϕ^2, at r being large enough, Therefore, one can determine - for given error of estimation ε - the correlation length, $l_c(\varepsilon)$, which can be defined as:

$$\forall r \ge l_c(\varepsilon) \Rightarrow \left| \frac{S_2(r) - \phi^2}{\phi^2} \right| \le \varepsilon \tag{4.21}$$

It is evident that the size of the sample should be equal to or larger than the correlation length $l_c(\varepsilon)$.

Before further considerations are provided some remarks have to be depicted, first. As mentioned in section 3.1.1, in case of isotropic media, the two-point probability function exhibits certain properties, particularly at the limits of r (see Eqs. (3.17) and (3.18)). In Fig. 4.3 a qualitative

plot of two different kind of the two-point probability function is presented. Note that the points in which S_2 attains the values of ϕ_1 and ϕ_1^2 are denoted as the *fixed points*, since they are common for any of the two-point correlation function, irrespective of the microstructure to which it corresponds. Therefore, a sample, to be representative with respect to the geometry, should necessarily preserve the fixed points of the two-point correlation function. The first fixed point, $S_2 = \phi$ at $r=0$, is always assured, since the mean value of volume fraction converges towards the macroscopic volume fraction , regardless of the sample size used (see previous chapter). On the other hand, whether the mean value of S_2 fits the remaining fixed point, ϕ^2, depends on the size of the sample. The consideration presented below aims at the deriving necessary condition for this sample size.
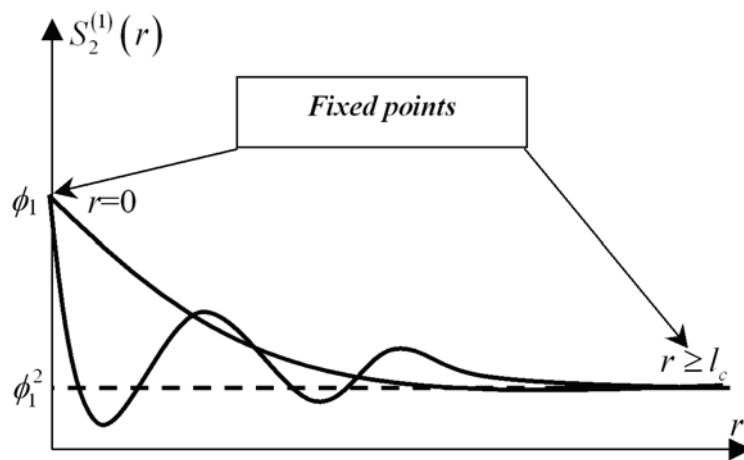
Fig. 4.3. A qualitative plot of the two-point probability function for an arbitrary microstructure

As it has been presented in section 3.1.1, evaluation of two-point probability can be successfully done by simple Monte Carlo simulations, i.e. for given distance *r*, two points are randomly thrown in the microstructure and successful hits (two points found in phase) are counted and divided by total number of throws. Then, the value of two-point probability is estimated according to relation (3.19). If one works, however, with digital images of microstructure, this procedure can lead to large computational cost. On the contrary, Yeong & Torquato (1998a) proposed - for isotropic digitised systems - more accurate procedure, which appears to be more efficient, and furthermore, it produces a smoother S_2 profile comparing to the random sampling outlined in section 3.1.1. The methodology is briefly outlined in a following. Consider a binary $N \times N$ image of an arbitrary random microstructure (Fig. 4.4 presents case corresponding to *N=6*). We attribute to each pixel only one of two possible values: 0 or 1. Therefore the digital image can be expressed by a square matrix $\mathbf{A}_{[N \times N]}$, in such way, that each element of matrix $\mathbf{A}$ is equal to 0 or 1, i.e.: $A[i,j]=1$ if pixel "contains" the phase for which the two-point probability is going to be evaluated. Indices, *i* and *j* correspond to the localization of the pixel within the image and denote the number of a row and a

column, respectively. In Fig. 4.4 the digital image and corresponding matrix $\mathbf{A}_{[6\times6]}$ for white pixels (phase 1) are presented. In the same manner the matrix $\mathbf{B}_{[6\times6]}$ for the black phase – the number 0 and 1 are interchanged (see Fig. 4.3).

$$\mathbf{A} = \begin{bmatrix} 0 & 1 & 1 & 1 & 0 & 0 \\ 0 & 1 & 0 & 1 & 1 & 1 \\ 1 & 1 & 1 & 1 & 0 & 1 \\ 0 & 1 & 0 & 0 & 1 & 1 \\ 1 & 0 & 1 & 0 & 1 & 1 \\ 1 & 1 & 1 & 1 & 1 & 0 \end{bmatrix}$$

$$\mathbf{B} = \begin{bmatrix} 1 & 0 & 0 & 0 & 1 & 1 \\ 1 & 0 & 1 & 0 & 0 & 0 \\ 0 & 0 & 0 & 0 & 1 & 0 \\ 1 & 0 & 1 & 1 & 0 & 0 \\ 0 & 1 & 0 & 1 & 0 & 0 \\ 0 & 0 & 0 & 0 & 0 & 1 \end{bmatrix}$$
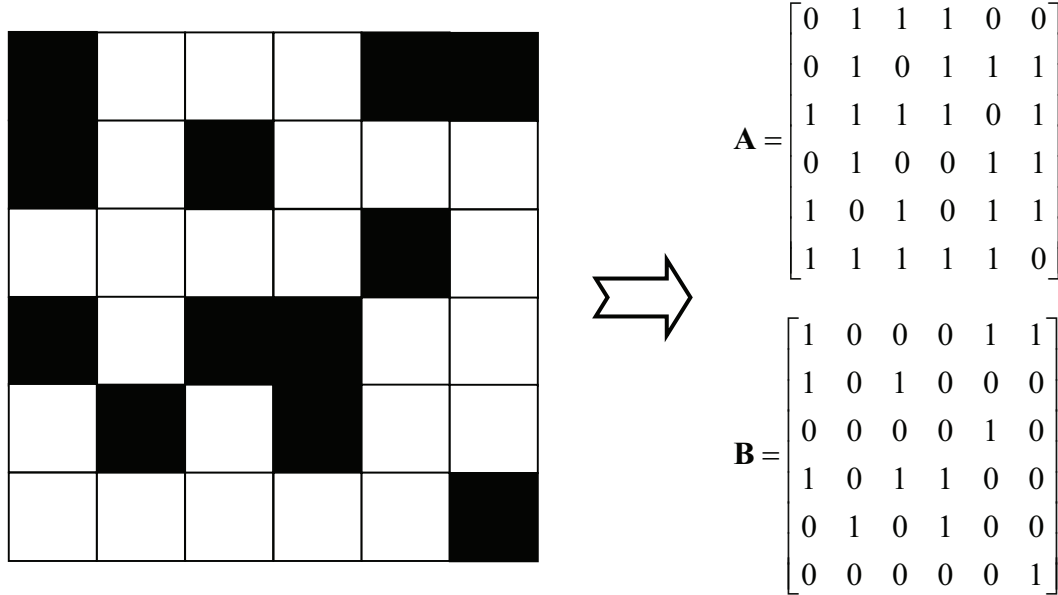
Fig. 4.4. An arbitrary binary image and corresponding (0, 1) matrices: $\mathbf{A}$ and $\mathbf{B}$.

Then, the two-point correlation functions for white and black phase can be expressed as:

$$S_2^{(1)}(r) = \frac{1}{N^2} \sum_{j=1}^{N} \sum_{i=1}^{N} \frac{A[i,j]\big(A[i,j+r]+A[i+r,j]\big)}{2} \qquad r=1,2,...$$

(4.22)

$$S_2^{(2)}(r) = \frac{1}{N^2} \sum_{j=1}^{N} \sum_{i=1}^{N} \frac{B[i,j]\big(B[i,j+r]+B[i+r,j]\big)}{2} \qquad r=1,2,...$$

Geometrical interpretation of this procedure is as follows: $S_2^{(1)}(r)$ is evaluated by translating a line segment of length r (in pixels) at a distance of one pixel at a time and spanning the whole image. Each time the end points of r are located at the pixel centers. The number of successful events, such that two end points of line segment of length r are found in phase 1, are counted and divided by the total number of trials. Note that by the assumption of system isotropy sampling is performed along two orthogonal directions: rows and columns. It should be mentioned that hereafter each time when the two-point correlation function is determined this procedure is utilized.

Recall now the relation (4.21) and the conclusion that the size of the sample, expressed in terms of pixels, should be equal to or larger than the correlation length, i.e. $N \geq l_c(\varepsilon)$. In what follows, we consider the sample that is a little bit larger than the correlation length (Fig. 4.5), and hence, we assume that the sample size is:

$$N_{\min} = l_c(\varepsilon) + \delta \qquad (4.23)$$

It was mentioned, in section 3.2.1, that each sampling window is extended to infinity by periodic arrangement such that the window is regarded as the unit cell, which is repeated in all directions forming the infinite continuous body (see Fig. 3.7).
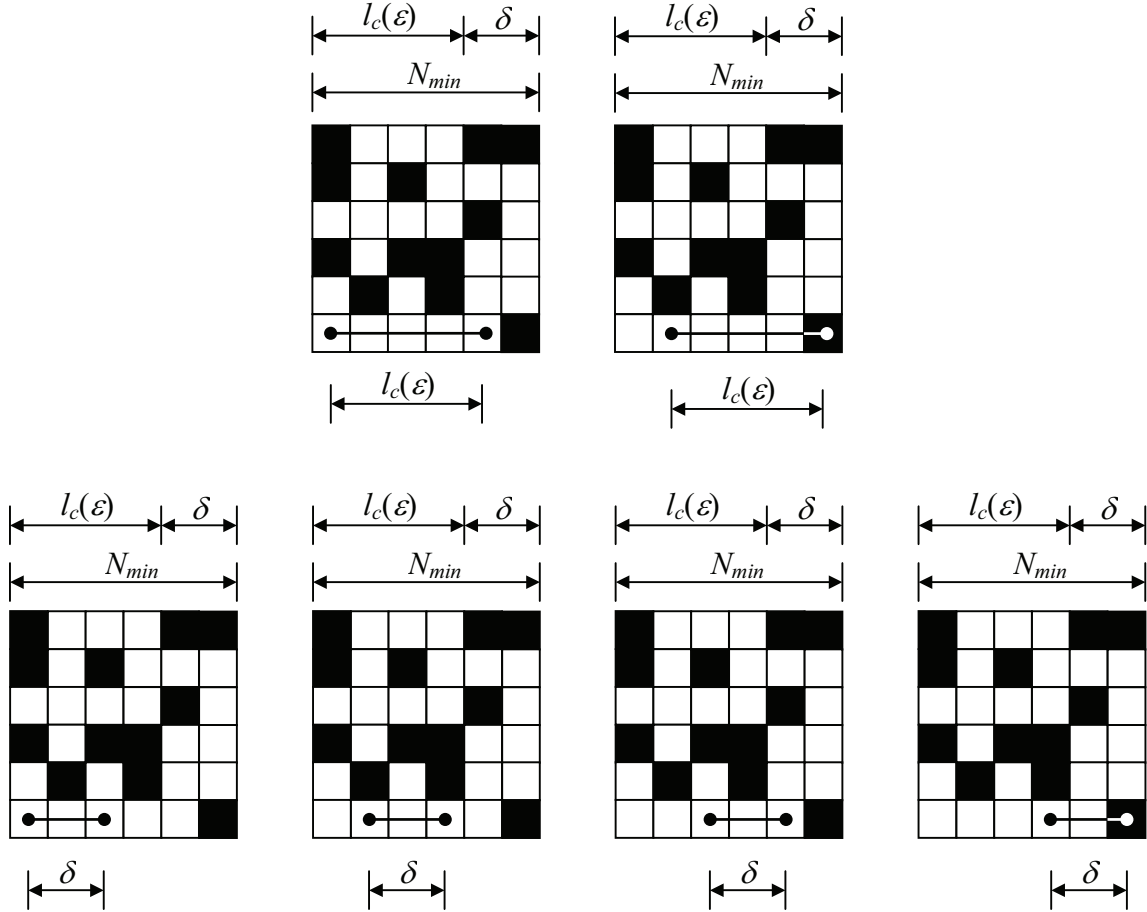
Fig. 4.5. Sampling window and a procedure of two-point probability determination.

Using the relation (4.22) as well as the periodicity condition, it can be shown that:

$$S_2^{(i)}\left(l_c(\varepsilon)\right) = \frac{\delta}{N_{\min}} S_2^{(i)}\left(l_c(\varepsilon)\right) + \left(1 - \frac{\delta}{N_{\min}}\right) S_2^{(i)}(\delta) \qquad (4.24)$$

Geometrical interpretation of relation (4.24) is presented in Fig. 4.5. Note that as the line segment is translated at a distance of one pixel the volume fraction of "events" corresponding to $S_2^{(i)}\left(l_c(\varepsilon)\right)$ is

$\dfrac{\delta}{N_{\min}}$ (see top of Fig. 4.5). When the end point of line segment r falls outside the sample, then, on the basis of periodicity conditions, the two-point probability is a function of the line segment of

length δ. Furthermore, the volume fraction of "events" corresponding to $S_2^{(i)}(\delta)$ is $\left(1-\dfrac{\delta}{N_{min}}\right)$ (see bottom of Fig. 4.5).

The relation (4.24) implies:

$$\left(1-\frac{\delta}{N_{min}}\right)S_2^{(i)}\left(l_c\left(\varepsilon\right)\right)=\left(1-\frac{\delta}{N_{min}}\right)S_2^{(i)}\left(\delta\right) \tag{4.25}$$

It is evident that this is fulfilled, up to a tolerance error ε, by any δ such that

$$\delta \geq l_c\left(\varepsilon\right) \tag{4.26}$$

since, according to the correlation length definition (4.21):

$$\forall r \geq l_c\left(\varepsilon\right) \Rightarrow S_2^{(i)}\left(r\right) \approx S_2^{(i)}\left(l_c\left(\varepsilon\right)\right) \tag{4.27}$$

Substituting (4.26) in the relation (4.23) one gets:

$$N_{min} \geq 2l_c\left(\varepsilon\right) \tag{4.28}$$

It should be noted that in the same manner the two-point probability for perpendicular direction could be studied. As a result one gets that the size of the sample, namely the number of pixels in a column (for digitised system), should also satisfy the relation (4.28). In general, if the sample is a rectangle with sides a and b (see Fig. 4.2), both a and b should be equal to or larger than $2l_c\left(\varepsilon\right)$.

Now, let us consider a sequence of sampling windows of the same definite size. The size of sampling window is such that it fulfils the constraint (4.28). Let $f_i\left(r\right)$ be a two-point correlation function corresponding to i-th sampling window and let ξ_i be a local volume fraction of the phase considered, within this window. Therefore, one can expect that

$$f_i\left(r \geq l_c\left(\varepsilon\right)\right) = \xi_i^2 \tag{4.29}$$

Hence, the Monte Carlo estimator:

$$\overline{\xi^2} = n^{-1}\sum_{i=1}^{n}\xi_i^2 \tag{4.30}$$

converges in probability to the expectation value corresponding to the definite size N_{min} of the sampling window, i.e.:

$$\overline{\xi^2} \xrightarrow{\text{Pr}} \left\langle \overline{\xi^2} \right\rangle_{N_{min}} \tag{4.31}$$

It becomes obvious, that to preserve the second fixed point $(S_2\left(l_c\left(\varepsilon\right)\right)=\phi^2)$ of the two-point correlation function, the expectation value has to verify:

$$\frac{\left|\left\langle \xi^2 \right\rangle_{N_{min}} - S_2\left(l_c\left(\varepsilon\right)\right)\right|}{S_2\left(l_c\left(\varepsilon\right)\right)} \leq \varepsilon \tag{4.32}$$

where ε is used as a relative error.

Since $\overline{\left\langle \xi \right\rangle}_{N_{min}} = \overline{\left\langle \xi \right\rangle}_\infty = \phi$, therefore one gets:

$$\frac{\left|\overline{\left\langle \xi^2 \right\rangle}_{N_{min}} - S_2\left(l_c\left(\varepsilon\right)\right)\right|}{S_2\left(l_c\left(\varepsilon\right)\right)} = \frac{\left|\overline{\left\langle \xi^2 \right\rangle}_{N_{min}} - \phi^2\right|}{\phi^2} = \frac{\left|\overline{\left\langle \xi^2 \right\rangle}_{N_{min}} - \overline{\left\langle \xi \right\rangle}_{N_{min}}^2\right|}{\overline{\left\langle \xi \right\rangle}_{N_{min}}^2} = \frac{Var\left(\xi\right)}{\overline{\left\langle \xi \right\rangle}^2} \leq \varepsilon \tag{4.33}$$

The constraint (4.33) is the second necessary condition, in addition to (4.28), which the sampling window has to verify in order to preserve the fixed points of the two-point probability function.

It is evident that in case of two-phase microstructure the sample should be simultaneously representative according to both phases. Thus, if we define the local volume fraction of phase 2 as $\psi\left(\mathbf{x}\right)$, by the analogy, one can write then:

$$\frac{Var\left(\psi\right)}{\overline{\left\langle \psi \right\rangle}^2} \leq \varepsilon \tag{4.34}$$

and finally

$$\mathrm{Max}\left(\frac{Var\left(\xi\right)}{\overline{\left\langle \xi \right\rangle}^2}, \frac{Var\left(\xi\right)}{\overline{\left\langle \psi \right\rangle}^2}\right) \leq \varepsilon \tag{4.35}$$

Note that (4.35) comes from the two-phase media property – the variance of local volume fraction for phase 1 is equal to that for phase 2, i.e.: $Var\left(\xi\right) = Var\left(\psi\right)$.

The size of the sample can be associated with $\left\|\Omega_0\right\| = ab$. Utilizing (4.35) as well as (4.28) the condition for minimum size of the sample, which can be treated (with respect to microstructure geometry) as a RVE, is as follows:

$$\left\|\Omega_0\right\|^* \geq \max\left[\left\|\Omega_0\right\|_\xi; \left\|\Omega_0\right\|_\psi; \left\|\Omega_0\right\|_{l_c}\right] \tag{4.36}$$

where:

$$\left\|\Omega_0\right\|_\xi = \frac{2}{\phi_1}\sqrt{\frac{\int_0^a\int_0^b\left(S_2^{(1)}\left(t\right) - \phi_1^2\right)\left(a - t_x\right)\left(b - t_y\right)dxdy}{\varepsilon}} \tag{4.37}$$

$$\left\|\Omega_0\right\|_\psi = \frac{2}{\phi_2}\sqrt{\frac{\int_0^a\int_0^b\left(S_2^{(1)}\left(t\right) - \phi_1^2\right)\left(a - t_x\right)\left(b - t_y\right)dxdy}{\varepsilon}} \tag{4.38}$$

and

$$\left\|\Omega_0\right\|_{l_c} = 4 l_c^2 \left(\varepsilon\right) \tag{4.39}$$

Note that relations (4.37) and (4.38) are obtained by substituting (4.18) and (4.6) in the relation (4.35). They should be interpreted as follows:

$$\text{find } a \text{ and } b \text{ such that:} \quad ab = \frac{2}{\phi} \sqrt{\frac{\int_0^a \int_0^b \left(S_2^{(1)}(t) - \phi^2\right)\left(a - t_x\right)\left(b - t_y\right) dx dy}{\varepsilon}} \tag{4.40}$$

The closed-form of the two-point correlation function is available only for a few certain types of microstructure. Therefore, the equation (4.40) requires a numerical solution, in general. Section 4.3.2 proposes, for that purpose, making use of procedure based on Monte Carlo integration scheme.

The condition (4.36) derived above is a necessary condition to preserve fixed points of two-point correlation function. It seems, however, reasonable to state that this condition assures, in addition, a satisfactory replica of the entire two-point probability function. This stems from the fact that the second fixed point, i.e. ϕ^2 at $r = l_c\left(\varepsilon\right)$, represents value at the distance $l_c\left(\varepsilon\right)$ which is a measure of the longest range order of particular microstructure. Therefore, if the size of the window applied allows for mapping this point, so shorter range orders should be also properly reproduced. Thus it is proposed that the condition (4.36) is also a necessary and sufficient condition for the sample size to be representative with respect to geometry. Validity of this proposition is investigated numerically in section 4.3, where calculations are performed for a sequence of different random microstructures.

A practical use and preliminary results of the criterion (4.36) are depicted below, where an example of random checkerboard is, once again, investigated. Thus, we focus on the determination of the minimum number of pixels for the sample to be representative for this particular type of microstructure.

First, we focus on the correlation length l_c. In Fig. 4.6 the two-point probability, determined on the basis of relation (4.22), is presented. One can simply notice, that the correlation length is equal to one pixel, i.e. $l_c = 1$, regardless of volume fraction p. Therefore, utilising (4.39) we have that:

$$\left\|\Omega_0\right\|_{l_c} = 4 \tag{4.41}$$
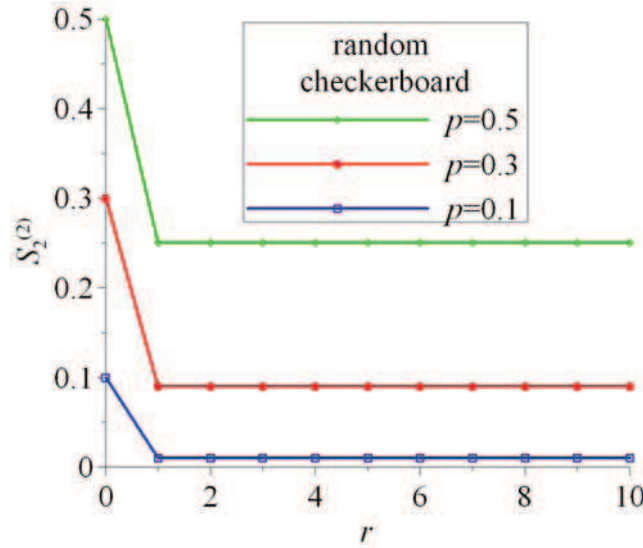
4.6. Random checkerboard two-point probability function against the distance *r* (in pixels)

In order to determine the values of $\|\Omega_0\|_\xi$ and $\|\Omega_0\|_\psi$ the relations regarding the local volume fraction expectation as well as its variance have to be utilized. Thus, substituting (3.48) as well as (3.49) in the relation (4.35) it can be shown that:

$$\|\Omega_0\|_\xi = \frac{p}{(1-p)\varepsilon} \tag{4.42}$$

and

$$\|\Omega_0\|_\psi = \frac{(1-p)}{p\varepsilon} \tag{4.43}$$

Therefore, according to relation (4.36), the minimum size of RVE (expressed as the number of pixels within the sample) for random checkerboard can be presented as follows:

$$\|\Omega_0\|^* \geq \max\left[\frac{p}{(1-p)\varepsilon};\frac{(1-p)}{p\varepsilon};4\right] \tag{4.44}$$

Assuming that a RVE is a square shape digital image, one can express the size of RVE in terms of the number of pixels in a row and in a column, $N^* = \sqrt{\|\Omega_0\|^*}$. Hence

$$N^* \geq \max\left[\sqrt{\frac{p}{(1-p)\varepsilon}};\sqrt{\frac{(1-p)}{p\varepsilon}};2\right] \tag{4.45}$$

In Fig. 4.7 the number of pixels, given by $\|\Omega_0\|^* = (N^*)^2$, is plotted against the volume fraction *p*. The minimum size of RVE was determined for three different values of ε, i.e.: 0.01, 0.03, 0.05. We can observe that the larger value of ε the smaller sample size is determined to be representative. Furthermore, note that the condition is a symmetrical function of *p* - the symmetry axis is in *p*=0.5.
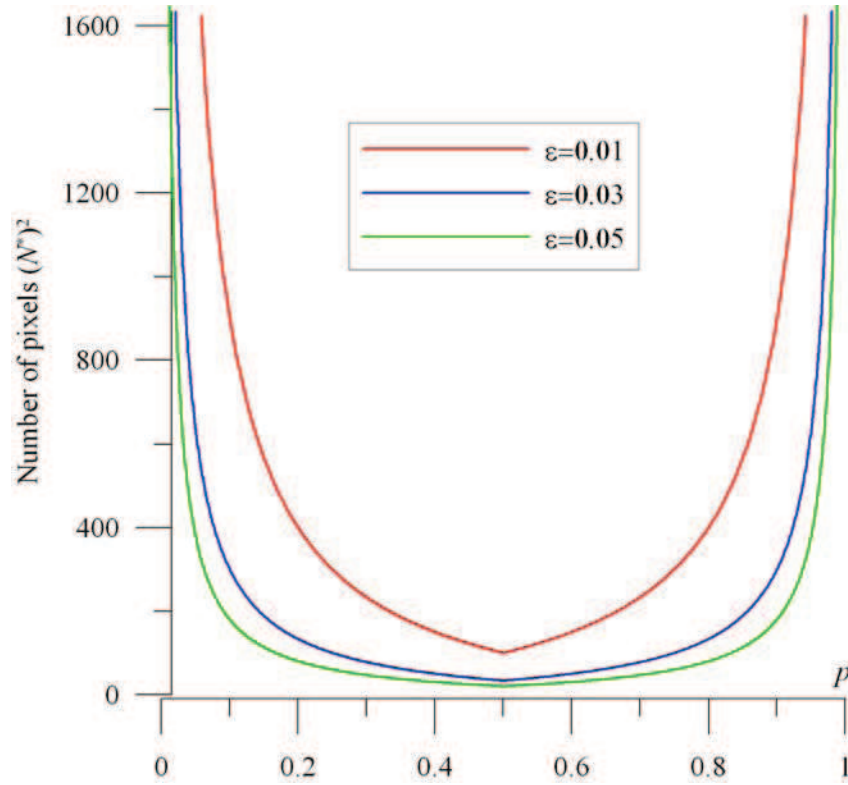
Fig. 4.7. The minimum size of RVE $\left\|\Omega_0\right\|^*$ plotted against the volume fraction p.

It should be noted that in case of random checkerboard the correlation length l_c exhibits a short range and therefore the criterion which influences the size of RVE is the one given by (4.35). Furthermore, due to fact that RVE is a digital image consisting of some number of pixels the value of N^* has to be an integer value.

4.3. Numerical validation of the RVE size condition

In this section numerical simulations are provided in order to validate the proposed methodology of RVE size determination. Few different types of two-phase microstructures, split into 2 groups, are considered. First one is so-called *random cell models* group (section 4.3.3), where following types of microstructures can be found: random checkerboard, system of overlapping disks, system of non-overlapping disks, *Ising* model based microstructure.

Another group (section 4.3.4) is consisted of microstructures obtained by the reconstruction procedure (Yeong & Torquato, 1998a, 1998b). Within this group reconstructions of theoretical models (e.g. Debye random medium) as well as real materials (Fontainebleau sandstone, boron-carbide/aluminum) are provided. For that purpose the Mathematica software reconstruction algorithm, created in the *Institute of Geotechnics and Hydrotechnics of Wroclaw University of Technology*, is utilized. Note that the reconstruction procedure is briefly outlined in section 4.3.4.

For all groups of microstructures the sizes of RVE are evaluated on the basis of geometrical criterion given by (4.36). The results are carried out for different values of volume fractions. Furthermore, the RVE sizes are determined for varied values of error ε.

It should be mentioned, however, that the main difficulty in determining the size of RVE is evaluation of integral given by (4.18). In case of random checkerboard the variance of local volume fraction as well as its expectation is expressed by analytical formulas. Therefore, as it was shown in previous section, determination of the RVE size for this particular type of microstructure is an easy task. On the other hand, for an arbitrary random microstructure the variance of local volume fraction is unknown and has to be numerically evaluated.

Within this work, in order to evaluate the value of integral (4.18), Monte Carlo based approach is proposed. Therefore, before the numerical validation of RVE size condition is provided, first, some basics of MC integrating as well as simple numerical example are depicted.

4.3.1. Basics of Monte Carlo integrating

Despite the widespread use of MC method it is rather impossible to find its unique definition in the literature. For instance, Fehske *et al.* (2008) have formulated a very general definition, which characterizes MC as a numerical method involving random numbers in a significant way. More precise definition has been provided by (Kalos & Whitlock, 2008) - MC is the method that "*involves deliberate use of random numbers in a calculation that has a structure of a stochastic process. By stochastic process, we mean a sequence of states whose evolution is determined by random events. In a computer, these are generated by a deterministic algorithm that generates a sequence of pseudorandom numbers, which mimics the properties of truly random numbers*".

MC is mostly applied to the problems, which have the random nature. It was first used by scientists working on the development of nuclear weapons in 1940s. However, what is remarkable, the method can be successfully applied to the problems with clearly deterministic (no probabilistic) content. Furthermore, if one considers numerical methods, which rely on n-point evaluations in d-dimensional space for determination of an approximate solution, then, if d increases, MC method reveals computational efficiency in comparison to other methods. This is due to fact that absolute error of MC estimate decreases as $n^{-\frac{1}{2}}$ whereas for other methods it decreases as $n^{-\frac{1}{d}}$, at best (Fishman, 1996).

In order to outline the basics of MC methods, within this section, a fundamental problem is considered, i.e. how to estimate the value of the integral

$$I = \int_{\Omega} f(x) dx \qquad (4.46)$$

over certain region Ω utilising MC technique? It will be presented that clearly deterministic problem (4.46) can be interpreted as the probabilistic (stochastic) one.

We start our considerations with the simplest MC simulation, so-called *"hit-or-miss"* MC. Suppose that one wish to estimate (4.46) over interval $[a,b]$, i.e.

$$I = \int_{a}^{b} f(x) dx \qquad (4.47)$$

Assume that within $[a,b]$ interval function $f(x)$ satisfies following inequality:

$$0 \le f(x) \le c \qquad (4.48)$$

From the probabilistic point of view, if X and Y are assumed to be uniform random variables within $[a,b]$ and $[0,c]$, respectively, then

$$I = P\big(Y \le f(X)\big) A \qquad (4.49)$$

where A denotes the area of rectangle: $A = (b-a)c$.

Estimation of I, based on *"hit-or-miss"* approach, consists in generating a large number of uniformly distributed random numbers x_i and y_i such that $a \le x_i \le b$, $0 \le y_i \le c$. Then the estimator of I has the following form:

$$\tilde{I} = \frac{n_{hits}}{n} A \qquad (4.50)$$

where n_{hits} is the number of ordered pairs (x_i, y_i) such that $y_i \le f(x_i)$, n is the total number of pairs (x_i, y_i).

We observe that the estimator of I is unbiased, i.e.

$$E\big(\tilde{I}\big) = I \qquad (4.51)$$

and furthermore the variance of *"hit-or-miss"* estimate is:

$$Var\big(\tilde{I}\big) = \frac{I(A-I)}{n} \qquad (4.52)$$

Note, above relations are the result of the fact that the number of hits has the binomial distribution, which is the discrete probability distribution of successes (hits in our case) in a sequence of n independent experiments, each of which yields success with probability $p = \dfrac{I}{A}$. For more details concerning the binomial distribution the reader is referred to (Feller, 1961).

Another MC approach for estimating (4.46) is so-called "*crude*" MC. This approach is also referred to as the "*sample mean*" MC or simply the "*Monte Carlo Method*". In what follows we consider a random variable Y with support on Ω, having the probability mass function or probability density function $p(y)$ such that:

$$p(y) > 0 \qquad (4.53)$$

and

$$\int_{\Omega} p(y)dy = 1 \qquad (4.54)$$

Then the expectation of a function $g(y)$ is

$$E\big(g(Y)\big) = \int_{\Omega} g(y)p(y)dy \qquad (4.55)$$

If we define the function $g(y)$ as

$$g(y) = \frac{f(y)}{p(y)} \qquad (4.56)$$

then the expected value of $g(y)$ given by relation (4.55) equals the integral (4.46), i.e.:

$$E\big(g(Y)\big) = \int_{\Omega} f(y)dy = I \qquad (4.57)$$

Therefore the result of above integration can be approximated by $\hat{I}$, which is an estimator of $E\big(g(Y)\big)$. The approach consists in taking the random sample, Y_1, Y_2, ..., Y_n of n random draws from the density function $p(y)$ and then computing the mean of $g(Y)$ over the sample, i.e.:

$$\hat{I} = \frac{1}{n}\sum_{i=1}^{n} g(Y_i) \qquad (4.58)$$

One can simply notice that

$$E\big(\hat{I}\big) = E\left(\frac{1}{n}\sum_{i=1}^{n} g(Y_i)\right) = \frac{1}{n}\sum_{i=1}^{n} E\big(g(Y_i)\big) = \frac{1}{n}\sum_{i=1}^{n} I = I \qquad (4.59)$$

which implies that the estimator $\hat{I}$ is unbiased. Furthermore it is easy to prove that:

$$Var\big(\hat{I}\big) = \frac{1}{n}\int_{\Omega}\big(g(y) - I\big)^2 p(y)dy \qquad (4.60)$$

Once again we wish to estimate integral of function $f(x)$ given by relation (4.47). Assume that Y is a uniformly distributed random variable, and hence, using the following density function:

$$p(x) = \frac{1}{b-a} \qquad (4.61)$$

we obtain:

$$I = (b-a)E(f(X))\tag{4.62}$$

Therefore the "*crude*" MC estimate of *I* and its variance are as follows:

$$\hat{I} = \frac{(b-a)}{n}\sum_{i=1}^{n} f(Y_i)\tag{4.63}$$

$$Var(\hat{I}) = \frac{b-a}{n}\left[\int_a^b (f(x))^2\, dx\right] - \frac{I^2}{n}\tag{4.64}$$

We focus now on evaluating the difference between the variance of "*hit-or-miss*" approach and the one of "*crude*" estimate. Utilising (4.52) , (4.64) and the inequality (4.48) we have that:

$$Var(\tilde{I}) - Var(\hat{I}) = \frac{(b-a)}{n}\int_a^b f(x)(c - f(x))\, dx \;\; \geq 0\tag{4.65}$$

Therefore $Var(\tilde{I})$ is always greater or, at the most, equal to $Var(\hat{I})$ and hence, the "*crude*" MC is never less efficient than the "*hit-or-miss*" approach.

There exist a large number of MC approaches which cause the reduction of MC estimate variance, e.g. "*stratified sampling*", "*antithetic variates*", "*control variates*", to mention only a few. Nevertheless, most common as well as very useful is the "*importance sampling*" technique. It improves the efficiency of estimation by sampling more often in the regions of space Ω that have the larger contribution to the integral.

Within the "*importance sampling*" approach we introduce the "*importance function*" $w(x)$ which is the probability density function. We have that:

$$I = \int_\Omega g(y)p(y)\,dy = \int_\Omega f(y)\,dy = \int_\Omega \frac{f(x)}{w(x)}w(x)\,dx\tag{4.66}$$

Then, the "*importance sampling*" estimate of *I* has the following form:

$$\breve{I} = \frac{1}{n}\sum_{i=1}^{n}\frac{f(X_i)}{w(X_i)}\tag{4.67}$$

It should be mentioned that within the interval of integration $w(\mathrm{x})$ should be similar to $f(\mathrm{x})$. The "*importance sampling*" function can be determined by minimizing the variance of $\breve{I}$ given by:

$$Var(\breve{I}) = \frac{1}{n}\left[E\left(\left[\frac{f(x)}{w(x)}\right]^2\right) - I^2\right]\tag{4.68}$$

Note that (4.68) is minimized by fixing $w(x) = \dfrac{f(x)}{I}$. Nevertheless, in many cases, I is not a

priori known (we want to estimate the value of I). Thus, it is reasonable to choose $\dfrac{f(x)}{w(x)}$ to be a

constant (Torquato, 2002).

Consider, for example, the integral:

$$I = \int_0^1 \frac{e^x - 1}{e - 1} dx \qquad (4.69)$$

We use three different MC approaches in order to estimate (4.69). Table 4.1 summarizes the values of estimators as well as their standard deviations determined for different number of realizations *n*. Note, in case of importance sampling $w(x) = 2x$. The analytical solution of (4.69) is *I*=0.418023.

We see that the "*importance sampling*" approach appears to be more accurate estimate than those of two other techniques ("*hit-or-miss*" and "*crude*" MC). Note that for each number of realizations *n* the standard deviation is the largest in case of "*hit-or-miss*" approach whereas the smallest one is obtained for "*importance sampling*".

Table 4.1. Monte Carlo estimates of (4.69) and associated standard deviations

n	"hit-or-miss" Monte Carlo		"crude" Monte Carlo		"importance sampling"	
	$\tilde{I}$	$\sigma_{\tilde{I}}$	$\hat{I}$	$\sigma_{\hat{I}}$	$\breve{I}$	$\sigma_{\breve{I}}$
10	0.6000	0.06992	0.4338	0.02228	0.435123	0.01058
30	0.6000	0.03502	0.4545	0.00912	0.433852	0.00451
50	0.5200	0.02373	0.4594	0.00637	0.430013	0.00299
70	0.4857	0.01788	0.4615	0.00527	0.423803	0.00223
100	0.4300	0.01272	0.4324	0.00401	0.422845	0.00162
500	0.4260	0.00258	0.4308	0.00099	0.420361	0.00033
1000	0.4350	0.00136	0.4265	0.00054	0.418285	0.00017
5000	0.4278	0.00032	0.4206	0.00012	0.418126	0.00004
10000	0.4178	0.00016	0.4193	0.00006	0.418097	0.00002

4.3.2. Numerical evaluation of local volume fraction variance

It was shown in previous section that MC methods can be successfully applied to the problems with clearly deterministic (no probabilistic) content. Thus, in order to evaluate the integral (4.18) the MC based approach is proposed. Hereafter, we assume that RVE is a square consisted of N^2 pixels (N in a row and column).

Therefore, the variance of local volume fraction given by (4.18) can be rewritten in a following form:

$$Var(\xi) = \frac{4}{\|\Omega_0\|^2} \int\limits_0^N \int\limits_0^N \left(S_2^{(1)}\left(\sqrt{x^2 + y^2} \right) - \phi_1^2 \right)(N-x)(N-y)\, dxdy \qquad (4.70)$$

One can simply notice that:

$$\frac{4}{\|\Omega_0\|^2} \int\limits_0^N \int\limits_0^N (N-x)(N-y)\, dxdy = \left[\frac{2}{N^2} \int\limits_0^N (N-x)\, dx \right]\left[\frac{2}{N^2} \int\limits_0^N (N-y)\, dy \right] = 1 \qquad (4.71)$$

and therefore the function

$$p(x,y) = p(x)p(y) \qquad (4.72)$$

where

$$p(x) = \frac{2}{N^2}(N-x)$$
$$p(y) = \frac{2}{N^2}(N-y) \qquad (4.73)$$

can be treated as the probability density function in Ω_0. Substituting (4.73) in the relation (4.70) we can express the variance of local volume fraction in the following form:

$$Var(\xi) = \int\limits_0^N \int\limits_0^N g(x,y)p(x)p(y)\, dxdy = E\big(g(X,Y)\big) \qquad (4.74)$$

Note that in the relation above

$$g(x,y) = \left(S_2^{(1)}\left(\sqrt{x^2 + y^2} \right) - \phi_1^2 \right) \qquad (4.75)$$

Thus, estimation of considered integral consists in generating random numbers X_i and Y_i from the density functions $p(x)$ and $p(y)$ and then computing the mean of $g(x, y)$, i.e.:

$$Var(\xi) \approx \frac{1}{n}\sum_{i=1}^n g(X_i, Y_i) \qquad (4.76)$$

As mentioned, in order to evaluate the value of (4.76) pseudo random numbers from non-uniform distribution has to be drawn. Following (Janke, 2002) this problem is divided into two parts. First, a simple generator is used to generate uniformly distributed random numbers, which in a second step are transformed to follow the required distribution. In what follows, so-called inverse method is utilized (Janke, 2002).

The non-decreasing cumulative distribution function (CDF) of $p(x, y)$ is as follows:

$$Q(X,Y) = \int_0^X \int_0^Y \frac{2}{N^2}(N-x)\frac{2}{N^2}(N-y)\,dxdy \tag{4.77}$$

Note, that $Q(X, Y)$ can be expressed in the equivalent form, i.e.:

$$Q(X,Y) = Q(X)Q(Y) = \int_0^X \frac{2}{N^2}(N-x)\,dx \int_0^Y \frac{2}{N^2}(N-y)\,dy \tag{4.78}$$

Calculating the integrals in relation (4.78) one gets:

$$Q(X) = 1 - \frac{(N-X)^2}{N^2}$$

$$Q(Y) = 1 - \frac{(N-Y)^2}{N^2} \tag{4.79}$$

The functions above are presented graphically in Fig. 4.8 (the plots correspond to the one pixel case, i.e. $N=1$). Note that CDF always grows monotonically from 0 to 1, such that Q values are uniformly distributed (Janke, 2002) (see Fig. 4.8). Therefore, the problem of generating the numbers of an arbitrary distribution consists in drawing a uniformly distributed random number, say RN, such that $RN = Q(X)$ and, if the inverse function exists (is known in the analytical way), setting $X = Q^{-1}(RN)$.

It is evident that in case of relations (4.79) the inverse functions exist and have following form:

$$X(Q) = N\left(1 - \sqrt{1-Q(X)}\right) \tag{4.80}$$

and

$$Y(Q) = N\left(1 - \sqrt{1-Q(Y)}\right) \tag{4.81}$$

Therefore the estimator of the integral (4.74) (variance of the local volume fraction) can be rewritten as:

$$Var(\xi) \approx \frac{1}{n}\sum_{i=1}^n g(X(Q_i), Y(Q_i)) = \frac{1}{n}\sum_{i=1}^n \left(S_2^{(1)}\left(\sqrt{X(Q_i)^2 + Y(Q_i)^2}\right) - \phi_1^2 \right) \tag{4.82}$$

where the values of Q_i are obtained from the uniform distribution in the interval $[0,1]$, while $X(Q_i)$ as well as $Y(Q_i)$ are the non-uniformly distributed random numbers determined via relations (4.80) and (4.81).
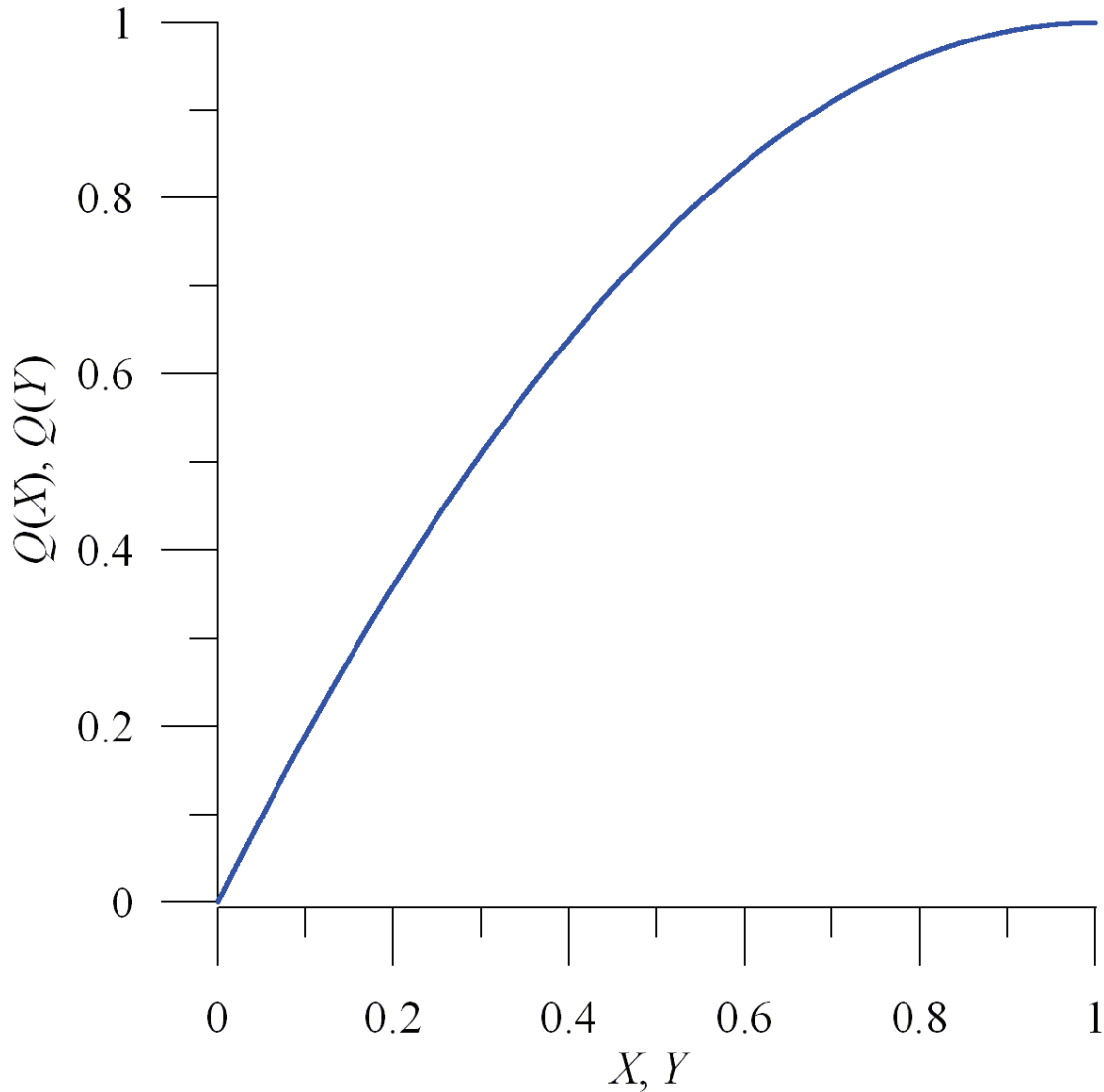
Fig. 4.8. Cumulative distribution functions $Q(X)$ and $Q(Y)$ given by (4.79)

In order to verify the method formulated above the variance of local volume fraction, for random checkerboard, was evaluated. This quantity, as a function of N, is displayed in Fig. 4.9. Furthermore, the analytical solution (3.49) is also presented.

Comparing analytical and numerical results one can notice that, mainly in case of small values of N, the analytical solution is underestimated. The influence of this fact on the numerical procedure of RVE size determination is studied in next section.
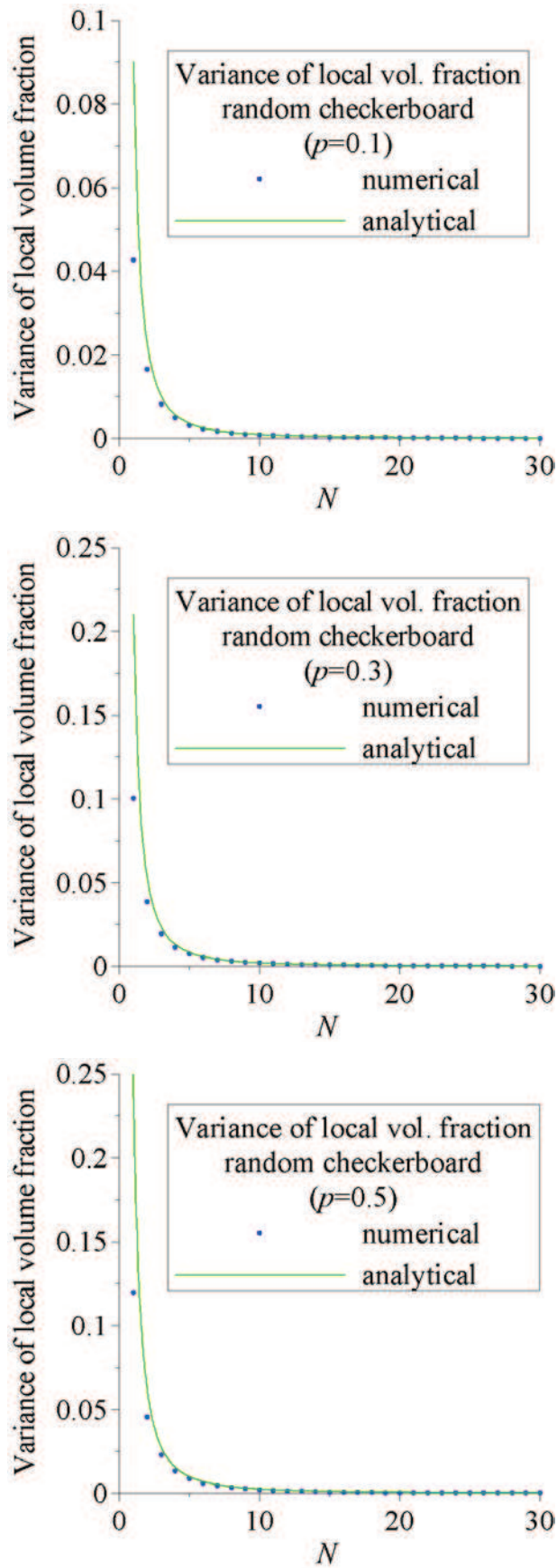
Fig. 4.9. Variance of local volume fraction for random checkerboard – analytical and numerical results

4.3.3. Random cell models

<u>Random checkerboard</u>

We begin our considerations with random checkerboard microstructure which was described, in details, in section 3.2.3 Three digital images ($N \times N = 500 \times 500$ pixels) of random checkerboard corresponding to different values of volume fraction are presented below (Fig. 4.10).
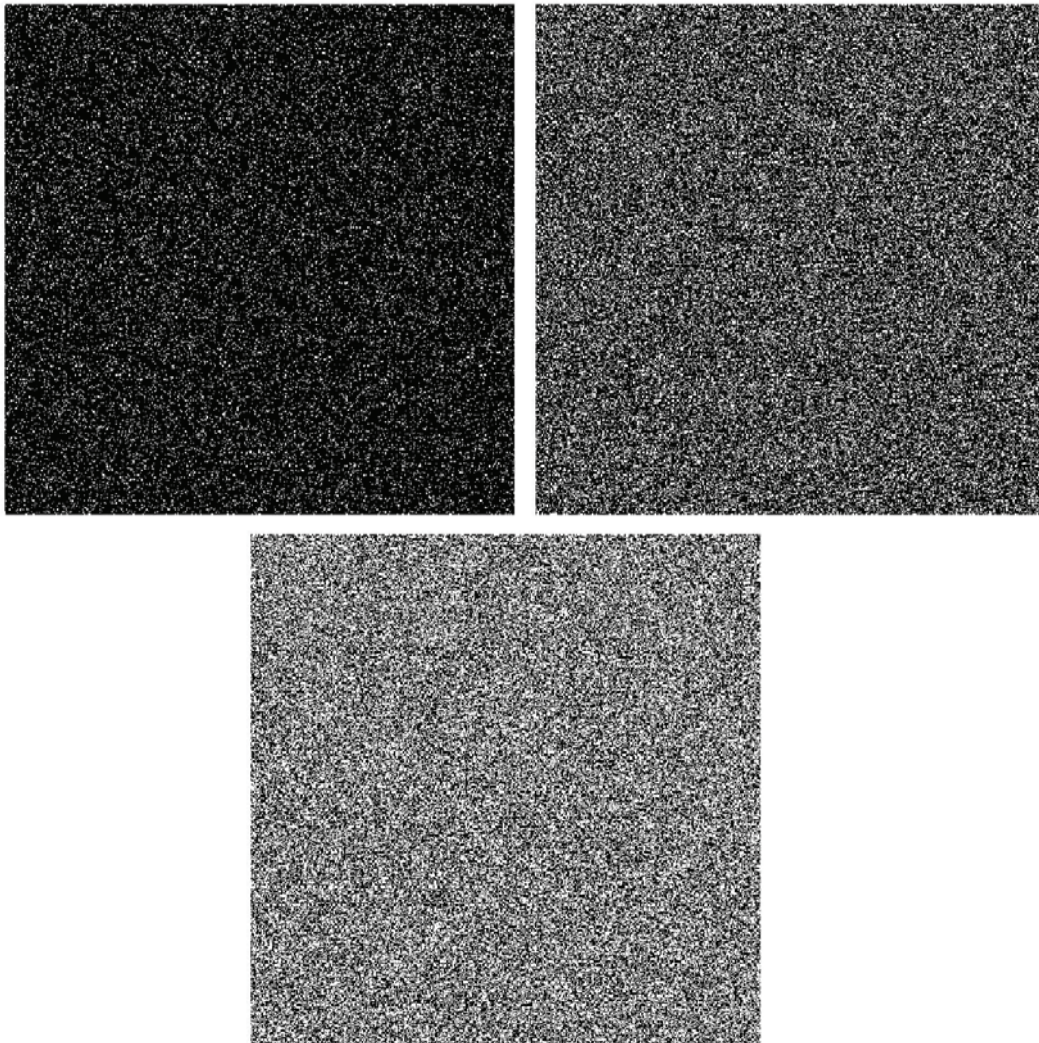
Fig. 4.10. The digital images (500×500 pixels) of random checkerboard with different volume fraction of phase 1 - top left: ϕ_I=0.1, top right: ϕ_I=0.3, bottom: ϕ_I=0.5.

In spite of some results concerning random checkerboard were discussed and presented graphically in section 4.2 (see Fig. 4.7), in order to be more legible, they are provided once again

and collected in Table 4.2 and 4.3. Each table corresponds to fixed value of relative error ε, i.e. 3% and 1%. The results corresponding to different values of volume fraction are provided.

Table 4.2. RVE size corresponding to error ε= 3% (random checkerboard microstructure)

ϕ_1	N^* analytical	N^* numerical
0.1	18	16
0.2	12	12
0.3	9	9
0.4	8	7
0.5	6	6

Table 4.3. RVE size corresponding to error ε = 1% (random checkerboard microstructure)

ϕ_1	N^* analytical	N^* numerical
0.1	30	27
0.2	20	20
0.3	16	16
0.4	13	13
0.5	10	10

Tables 4.2 and 4.3 provide the results of both analytical and numerical approach. The RVE sizes are expressed in terms of the number of pixels in a row and in a column. Observing the results, it can be seen, that only in case of ϕ_1=0.1 the numerical solution underestimates the analytical one. For other values of volume fraction both results are in a very well agreement. Furthermore, it should

be emphasized that in case of random checkerboard, the correlation length l_c exhibits a short range and therefore the results concerning the size of RVE stem from the relation (4.35).

It was shown in section 3.2.3 that the mean value (averaged over sufficient number of realizations) of two-point probability depends on the size of the sample – for too small samples the mean value does not converge towards the original $S_2^{(i)}$ function determined for large digital image (see Fig. 3.21).

Therefore, in what follows, we check whether mean values of two-point probability, $\overline{S_2^{(1)}}$, determined for previously established RVE sizes are in agreement with original functions obtained for digital images displayed in Fig. 4.10. In other words, we verify whether the mean value of two-point probability, $\overline{S_2^{(1)}}$, fits the fixed points, and hence, whether it can be treated as the *replica* of original $S_2^{(1)}$ function. The results of calculations are presented graphically in Figs. 4.11-4.13. Observing results, one can see that the original function $S_2^{(1)}$ as well as the mean value (replica), $\overline{S_2^{(1)}}$, are in a very well agreement, regardless of the value of volume fraction ϕ_1. Note that the simulations were performed only for the RVE sizes collected in Table 4.3 (ε=1%).
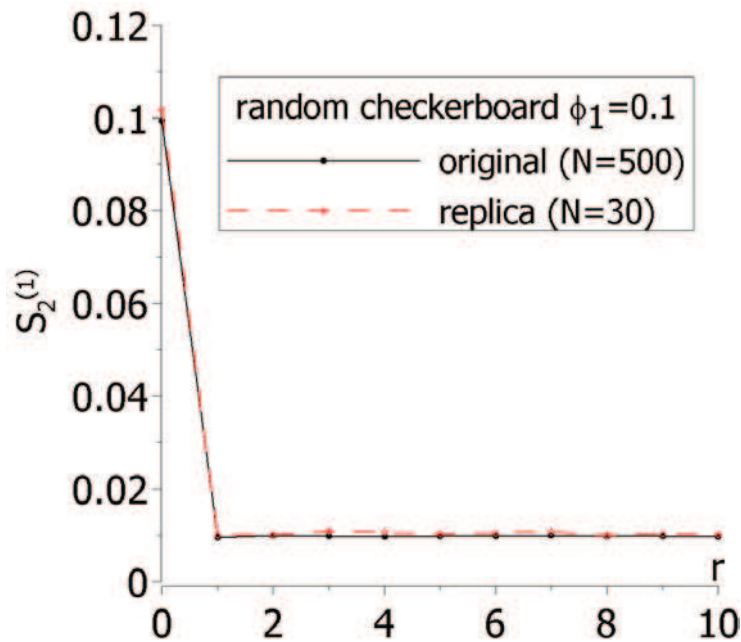
Fig. 4.11. Original $S_2^{(1)}$ and its replica - random checkerboard, ϕ_1=0.1.
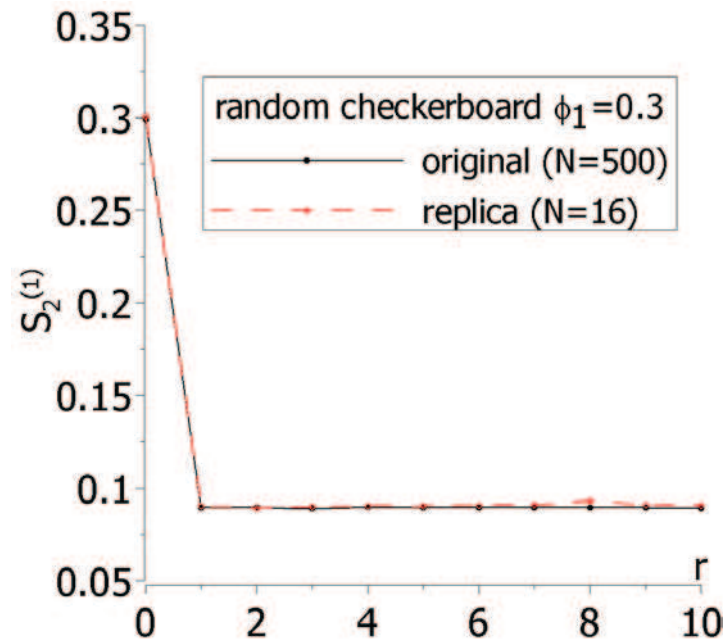
Fig. 4.12. Original $S_2^{(1)}$ and its replica - random checkerboard, ϕ_1=0.3.
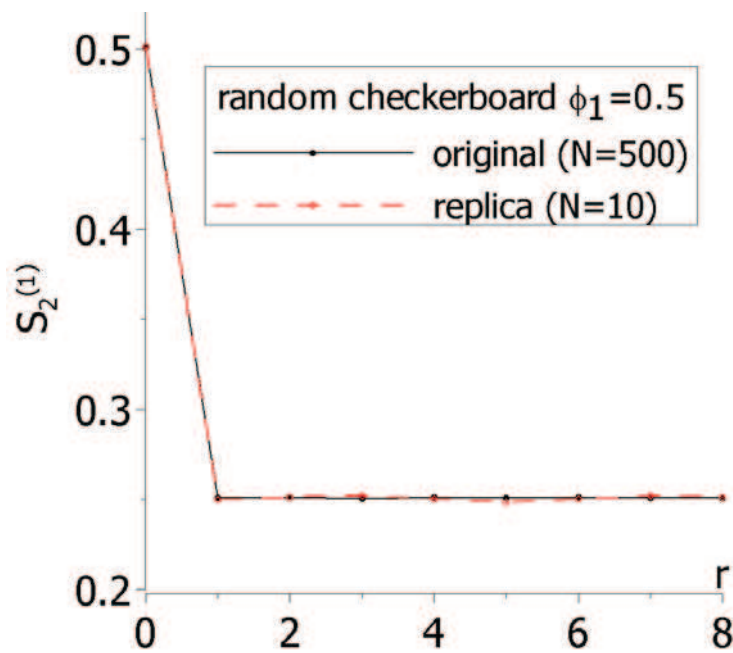
Fig. 4.13. Original $S_2^{(1)}$ and its replica - random checkerboard, ϕ_1=0.5.

Ising model

The Ising model was originally formulated to model the spontaneous magnetization of a ferromagnet in the absence of an external field. This model considers an idealized system of interacting particles which are arranged on a regular, planar grid. Only one of two magnetic spin orientations can be prescribed to each particle, generally labeled up (+1) and down (-1). The

general assumption of the considered model is that each particle interacts only with its nearest neighbors.

Three microstructures obtained by Ising model are considered (Fig. 4.14.). Microstructures denoted as A, B and C have the volume fraction of phase 1 approximately equal to 0.5. Note that the digital images differ from each other, i.e. the microstructures have different sizes of clusters, such that microstructure A has the smallest clusters, while the largest clusters can be noticed in case of digital image C. The difference in size of clusters is caused by use of different parameters within the model.
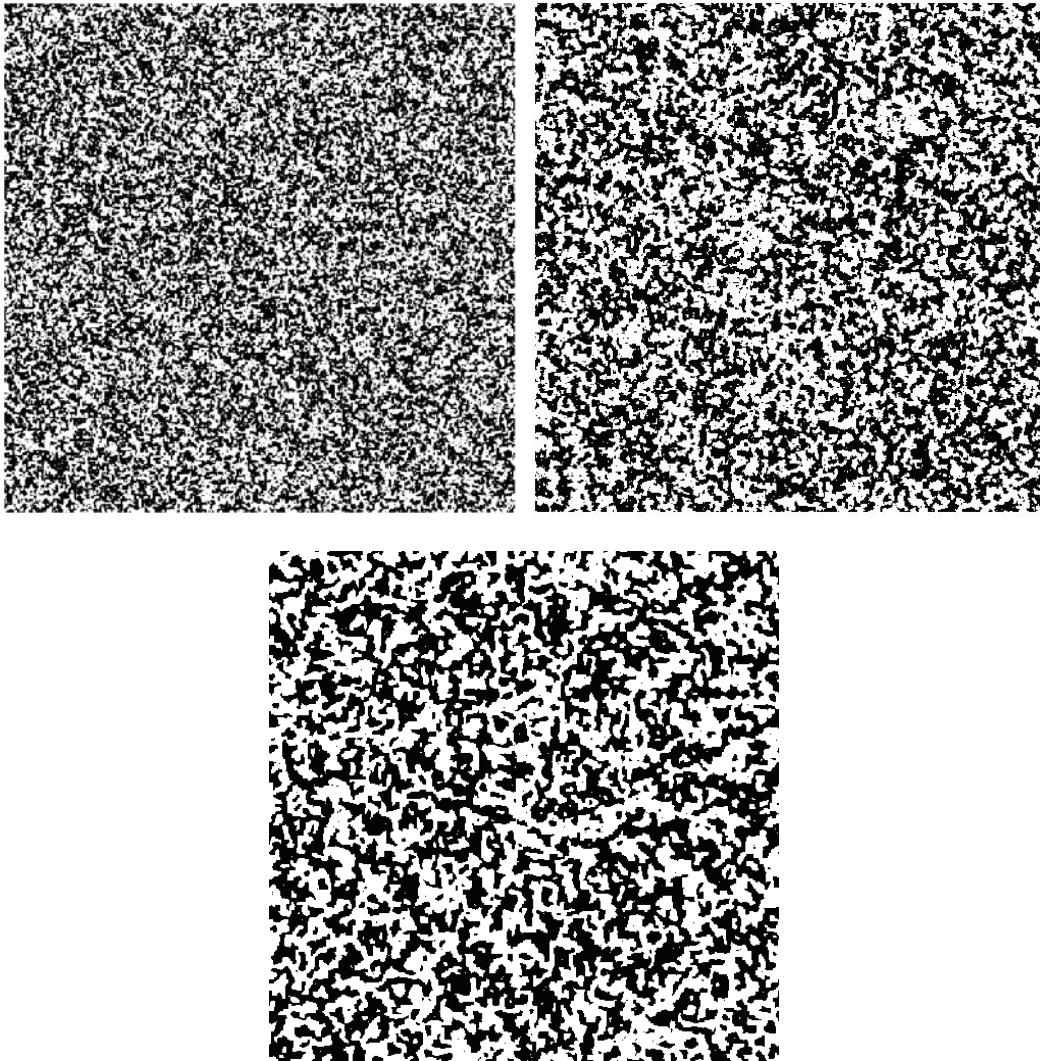
Fig. 4.14. The digital images (500×500 pixels) of microstructures generated via Ising model – $\phi_I{\approx}0.5$; top left: **A**, top right: **B**, bottom: **C**

It should be mentioned that for the microstructure generation process the Mathematica software algorithm, created in the *Institute of Geotechnics and Hydrotechnics of Wroclaw University of Technology*, was utilized. Roughly speaking the procedure of microstructure generation consists in assuming two states to each pixel: -1 or +1. Then, we draw one pixel from N^2 pixels contained in

the digital image. For the chosen pixel the change of state is proposed, i.e. if the pixel has the state +1 (-1) the change into −1 (+1) is suggested. The new value (+1 or −1) is accepted with certain probability P defined within the model. The acceptance consists in generating uniformly distributed random number $u \in [0,1]$ – if $u < P$ the change of state is accepted, otherwise the value assigned to the pixel is not changed.

In Fig. 4.15 the two-point probability functions determined for all types of microstructures are displayed. As it was in case of previous example, the two-point probability function was then utilized in order to evaluate the variance of local volume fraction. The latter is plotted against the number of pixels N (Fig. 4.16). Note that the variance is decreasing as the size of the sample is increasing.
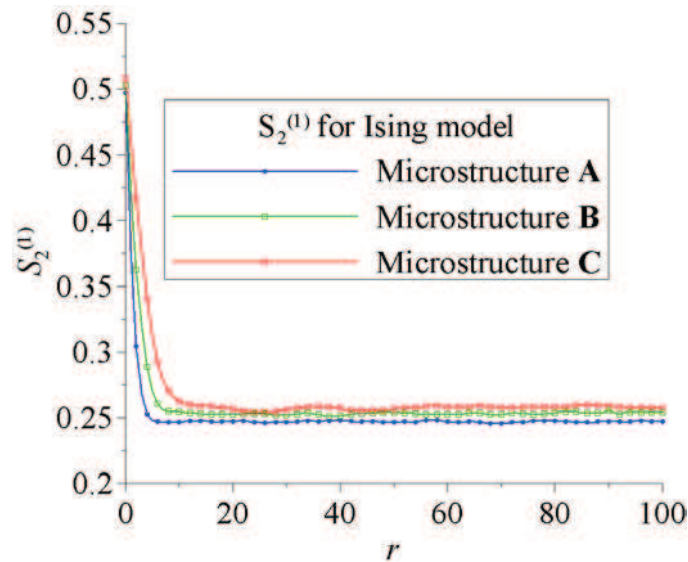
Fig. 4.15. Two-point probability function for Ising model plotted against r (in pixels)
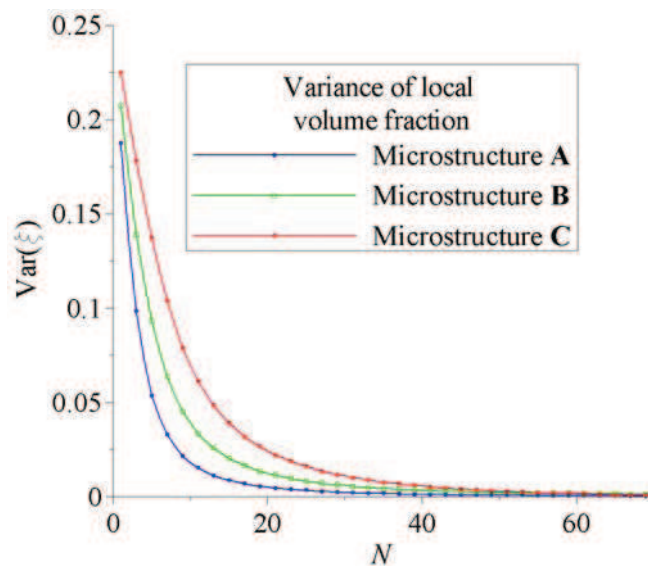
Fig. 4.16. The variance of local volume fraction against the number of pixels N (Ising model)

The results concerning the size of RVE are presented in Table 4.4 as well as 4.5. Note that results, expressed in terms of number of pixels, are divided into two groups. In third column the sizes of the sample, resulting from condition (4.35), are collected, i.e. the maximum value of $N_\xi = \sqrt{\|\Omega_0\|_\xi}$ and $N_\psi = \sqrt{\|\Omega_0\|_\psi}$ is presented. In fourth column the value of the sample size, $N_{l_c} = \sqrt{\|\Omega_0\|_{l_c}}$, according to correlation length condition (4.28), is displayed. Furthermore, it should be noted that the maximum value of those three is in bold and underline type.

Table 4.4. RVE size corresponding to error $\varepsilon = 3\%$ (Ising model)

Type of microstructure	ϕ_1	$\max\left[N_\xi; N_\psi\right]$	N_{l_c}
A		18	**<u>32</u>**
B	0.5	28	**<u>46</u>**
C		38	**<u>72</u>**

Table 4.5. RVE size corresponding to error $\varepsilon = 1\%$ (Ising model)

Type of microstructure	ϕ_1	$\max\left[N_\xi; N_\psi\right]$	N_{l_c}
A		30	**<u>40</u>**
B	0.5	49	**<u>60</u>**
C		55	**<u>78</u>**

We can observe that in case of Ising the size of RVE follows the correlation length condition. Note that the largest sizes of RVE are found to be associated with the type C microstructure – in case of this microstructure, phase 1 exhibits the largest clusters (see Fig. 4.14).

In Fig. 4.17 the comparison of the original two-point probability function, $S_2^{(1)}$, and its replica – mean value, $\overline{S_2^{(1)}}$ - are provided. We see that the original function, $S_2^{(1)}$, as well as the mean value (replica), $\overline{S_2^{(1)}}$, are in a very well agreement, regardless of the type of microstructure. Note that the simulations were performed for the RVE sizes corresponding to $\varepsilon=1\%$ (Table 4.5).
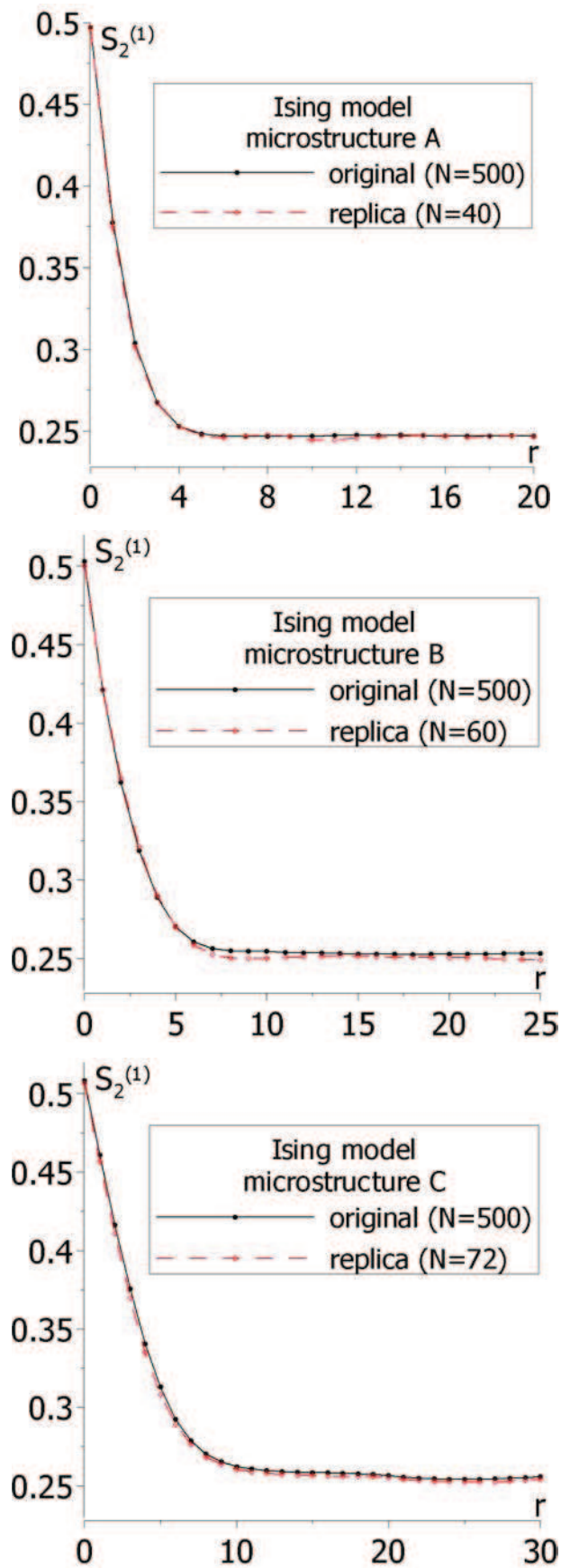
Fig. 4.17. Original $S_2^{(1)}$ and its replica – Ising model

System of overlapping disks

This type of microstructure was briefly described in previous chapter, where the microstructure statistical descriptors were presented. Roughly speaking, this type of microstructure consists of the matrix in which circle shape inclusions (disks) are embedded. Within the generation process the localization of each disk is independent of other particles localization – the disks are allowed to overlap. The digital images ($N \times N = 500 \times 500$ pixels) of the system of overlapping disks with different volume fraction are presented in Fig. 4.18.
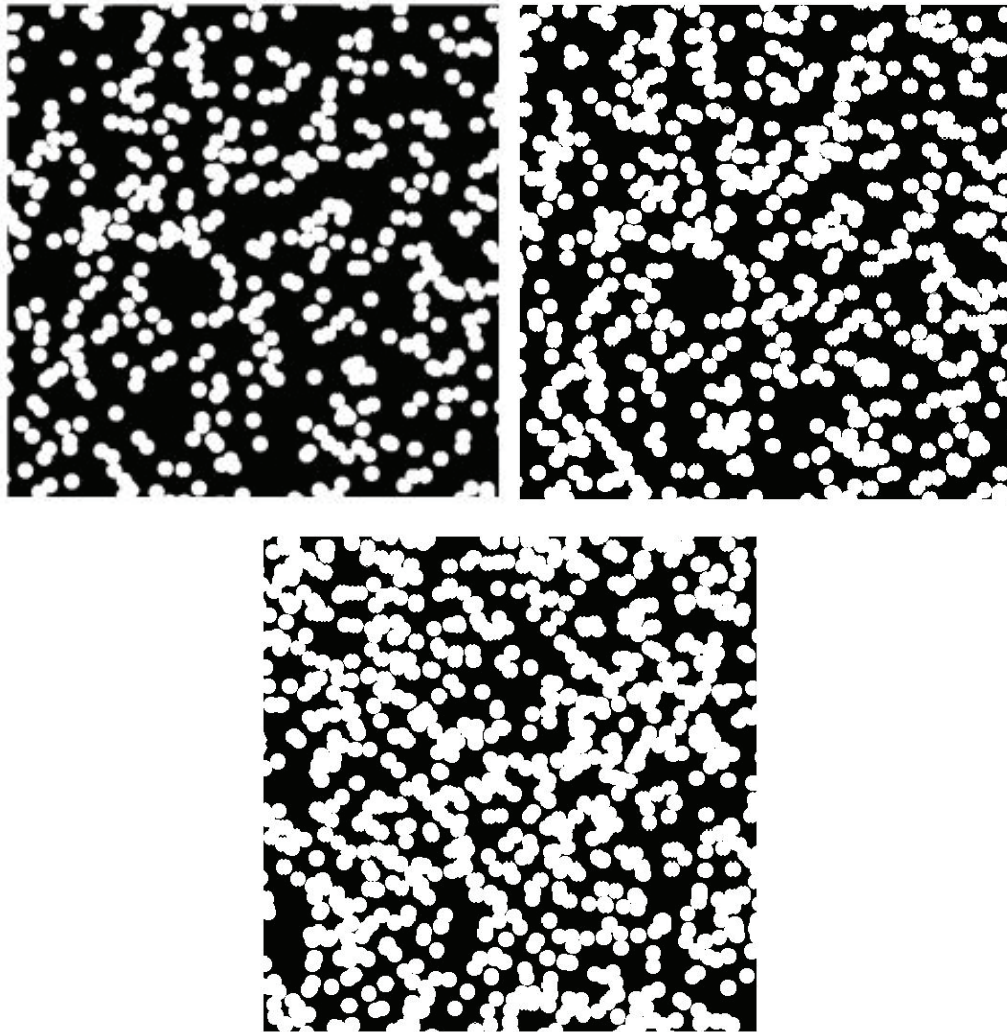
Fig. 4.18. The digital images (500×500 pixels) of the system of overlapping disks with different volume fraction of phase 1 - top left: ϕ_I=0.3, top right: ϕ_I=0.4, bottom: ϕ_I=0.5.

The two-point probability functions determined for considered microstructures are plotted against the distance r which is expressed in terms of pixels (Fig. 4.19). As before, $S_2^{(1)}$ was then utilized in order to determine the variance of local volume fraction which is graphically presented in Fig. 4.20. Of course, the variance is decreasing as the size of the sample is increasing.
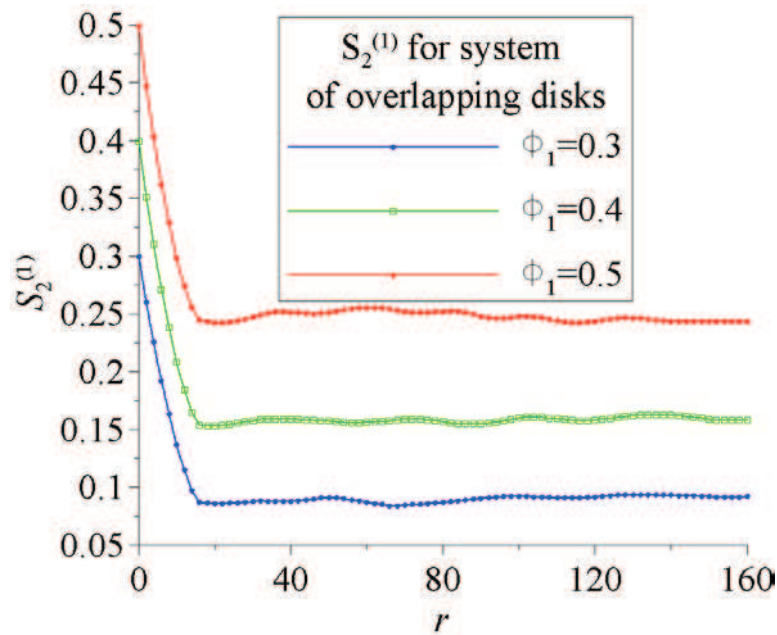
Fig. 4.19. Two-point probability function for the system of overlapping disks (distance r in pixels)
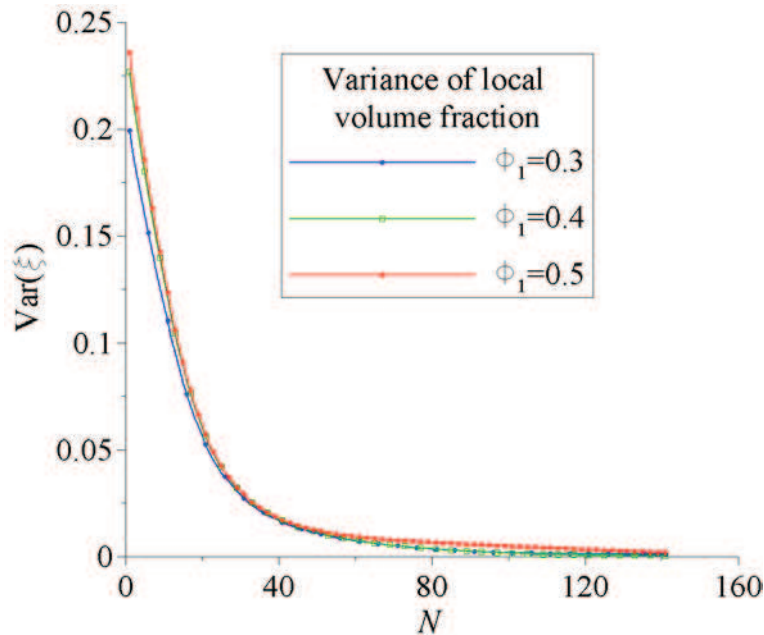
Fig. 4.20. The variance of local volume fraction, for the system of overlapping disks, plotted against N

It should be mentioned, however, that due to the geometry discretization process as well as due to the numerical error resulting from two-point probability determination, the profile of $S_2^{(1)}$ exhibits oscillations about the value of ϕ_1^2 (Fig. 4.19). In general, for the system of overlapping disks, $S_2^{(1)}$ should rather monotonically decay to its asymptotic value, i.e. ϕ_1^2 - the disks are spatially uncorrelated. The above implies that the evaluation of the correlation lengths was quite difficult task and its values are rather roughly determined. All the results concerning the system of overlapping disks are collected in Tables 4.6 and 4.7.

Table 4.6. RVE size corresponding to error $\varepsilon = 3\%$ (system of overlapping disks)

ϕ_1	$\max\left[N_\xi; N_\psi\right]$	N_{l_c}
0.3	87	**<u>210</u>**
0.4	73	**<u>240</u>**
0.5	70	**<u>224</u>**

Table 4.7. RVE size corresponding to error $\varepsilon = 1\%$ (system of overlapping disks)

ϕ_1	$\max\left[N_\xi; N_\psi\right]$	N_{l_c}
0.3	154	**<u>280</u>**
0.4	103	**<u>320</u>**
0.5	98	**<u>286</u>**

In Figs. 4.21-4.23 the two-point probability original functions and the replicas are graphically presented. Note that the chosen RVE size, for which the simulations were carried out, is *N*=160 – less then the results displayed in Tables 4.6-4.7. This choice is justified by the problem concerning original $S_2^{(1)}$ functions described above. Furthermore, for the RVE sizes displayed in Tables 4.6-4.7, larger original microstructure image would be required. In other words, for 500×500 digital image of original microstructure, sampling with windows, for instance 320×320, doesn't make sense in the view of randomness of the process.
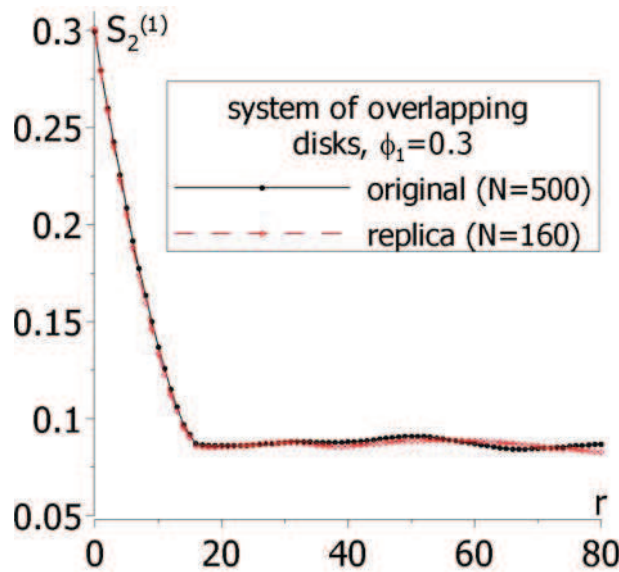
Fig. 4.21. Original $S_2^{(1)}$ and its replica – system of overlapping disks, ϕ_1=0.3
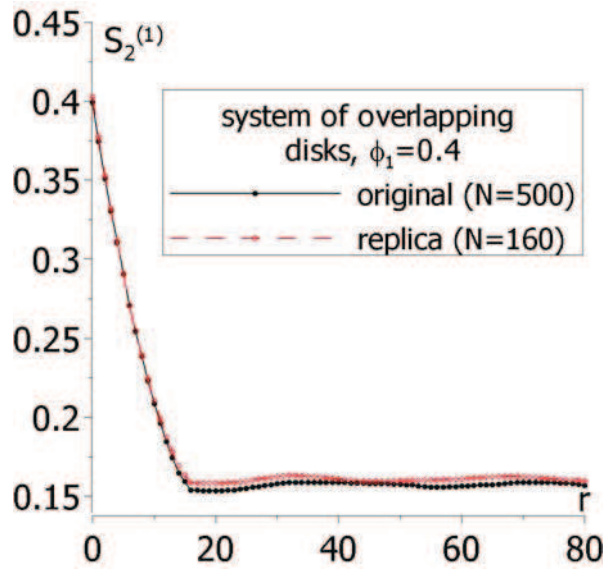
Fig. 4.22. Original $S_2^{(1)}$ and its replica – system of overlapping disks, ϕ_1=0.4
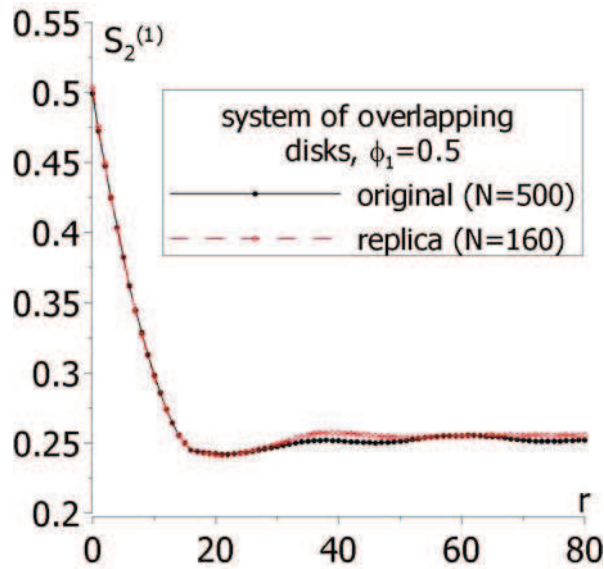
Fig. 4.23. Original $S_2^{(1)}$ and its replica – system of overlapping disks, ϕ_1=0.5

System of non-overlapping disks

As it was in case of overlapping disks, brief presentation of the system of non-overlapping disks was provided in chapter 3. The two-point probability as well as lineal-path function for this type of microstructure were evaluated and discussed. As before, the microstructure consists of matrix in which disks are embedded, however, this time disks are not allowed to overlap, i.e. during the generation process, except the first disk, localization of the remaining ones depends on the position of previously generated inclusions. Three digital images (consisted of 250,000 pixels) with different volume fractions are presented in Fig. 4.24. Corresponding two-point probability functions are presented graphically in Fig. 4.25.
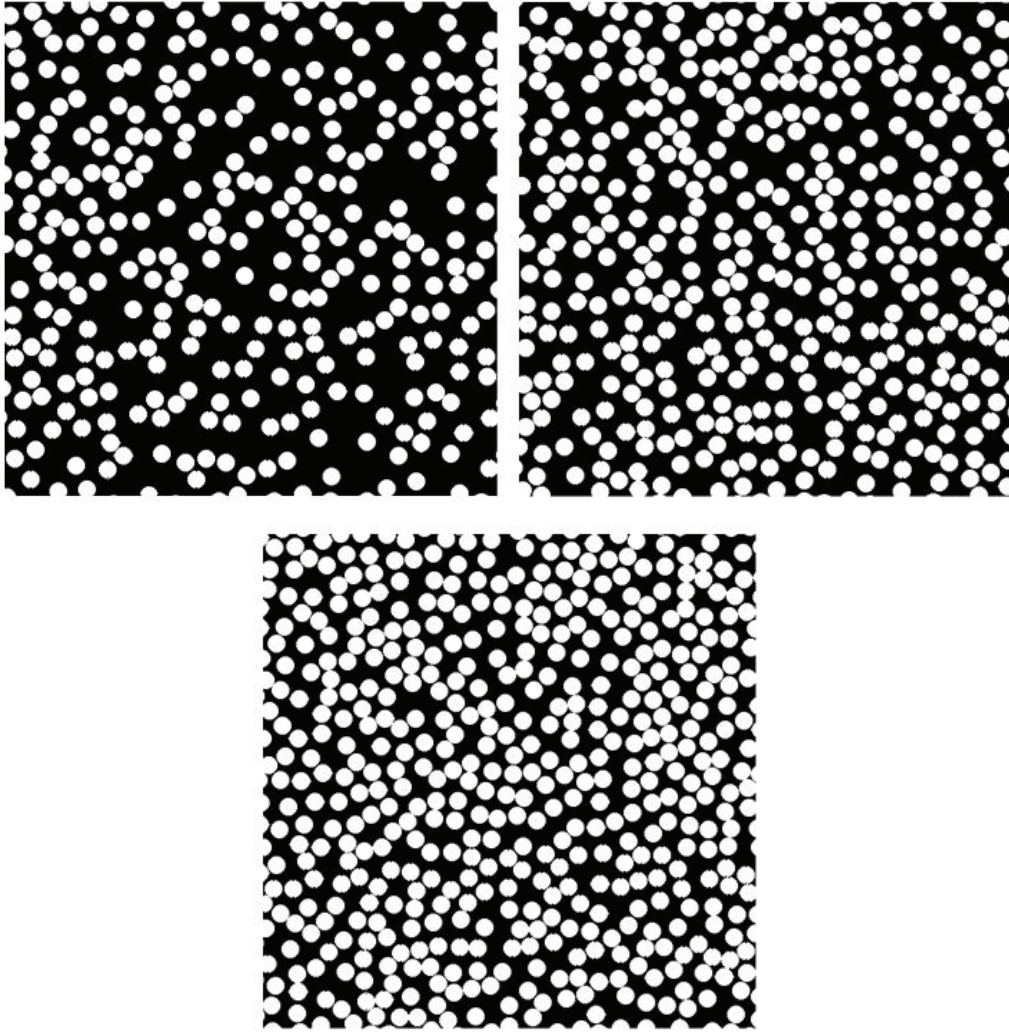
Fig. 4.24. The digital images (500×500 pixels) of the system of non-overlapping disks with different volume fraction of phase 1 - top left: ϕ_1=0.3, top right: ϕ_1=0.4, bottom: ϕ_1=0.5. Disk diameter D=18l.
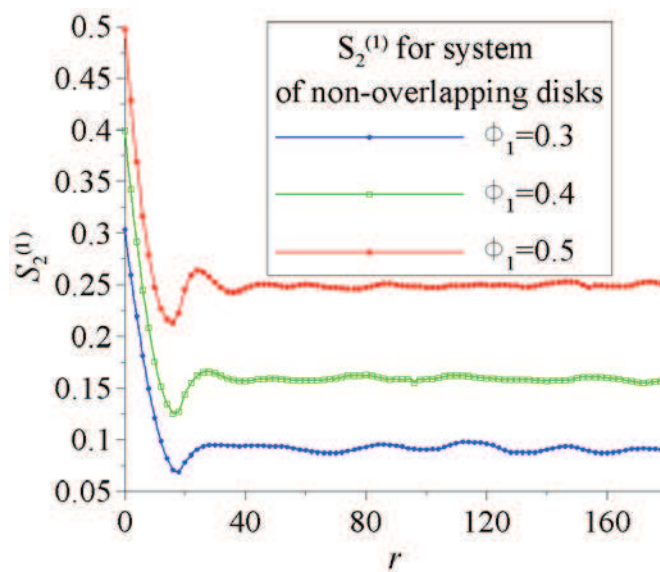
Fig. 4.25. Two-point probability function for the system of non-overlapping disks (distance r in pixels)

One can simply notice that the profile of $S_2^{(1)}$ is different comparing to the one evaluated for the system of overlapping disks (Fig. 4.19). In general, for the system of non-overlapping disks, $S_2^{(1)}$ should exhibit oscillations about the value of ϕ_1^2. This oscillations, however, should be vanishing as the distance r is increasing. Nevertheless, this is not observed for $S_2^{(1)}$ displayed in Fig. 4.25. Once again, it is caused by the geometry discretization process as well as the numerical error of $S_2^{(1)}$ estimation and therefore the correlation lengths had to be rather roughly determined.

In Fig. 4.26 the variance of local volume fraction is plotted against the number of pixels N. We see that the course of the function is the same as in previous examples, i.e. the variance is decreasing as the size of the sample is increasing.
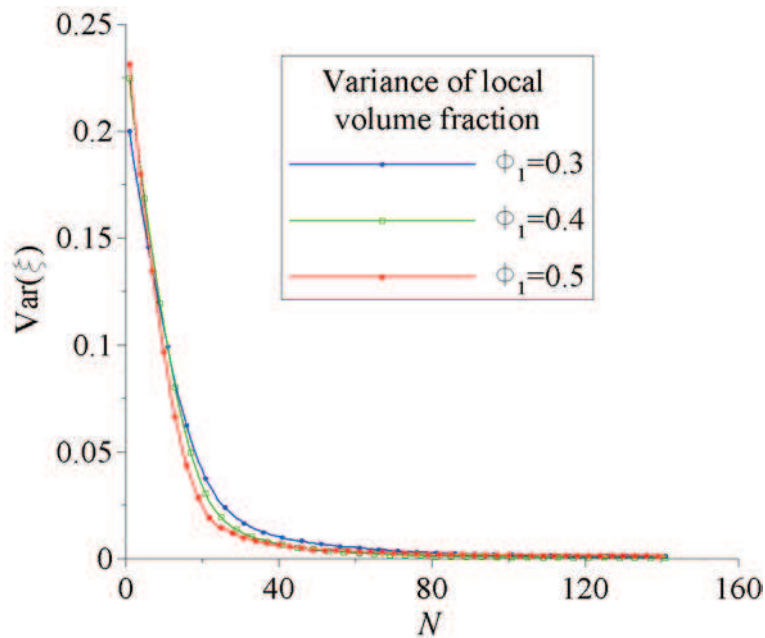
Fig. 4.26. The variance of local volume fraction for the system of non-overlapping disks against the number of pixels N

In Tables 4.8-4.9 the RVE sizes evaluated for different volume fractions are presented. As it was in case of overlapping disks, the correlation length condition yields maximum value of RVE size.

Table 4.8. RVE size corresponding to error $\varepsilon = 3\%$ (system of non-overlapping disks)

ϕ_1	$\max\left[N_\xi; N_\psi\right]$	N_{l_c}
0.3	78	**260**
0.4	47	**200**
0.5	37	**180**

Table 4.9. RVE size corresponding to error $\varepsilon = 1\%$ (system of non-overlapping disks)

ϕ_I	$\max\left[N_\xi; N_\psi\right]$	N_{l_c}
0.3	135	**330**
0.4	72	**240**
0.5	69	**330**

Figs. 4.27-4.29 provide the original two-point probability function as well as its replica determined for different values of volume fraction ϕ_I. It can be seen, that the mean value, $\overline{S_2^{(1)}}$, is a "good" replica of original function $S_2^{(1)}$. Note that, as it was in case of overlapping disks, the RVE size utilized within simulations is $N=160$.
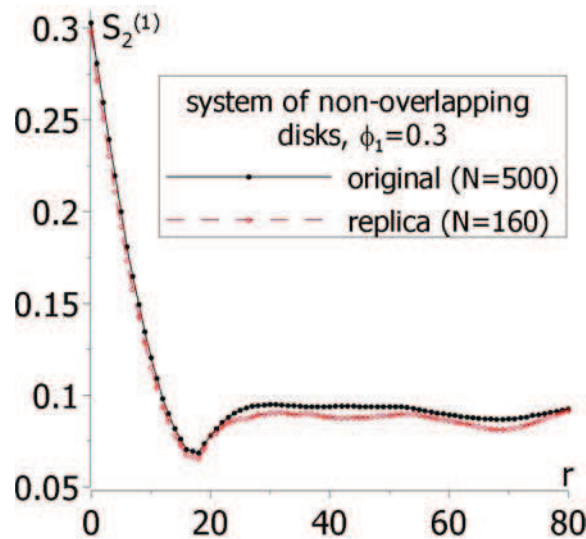
Fig. 4.27. Original $S_2^{(1)}$ and its replica: system of non-overlapping disks, $\phi_1=0.3$
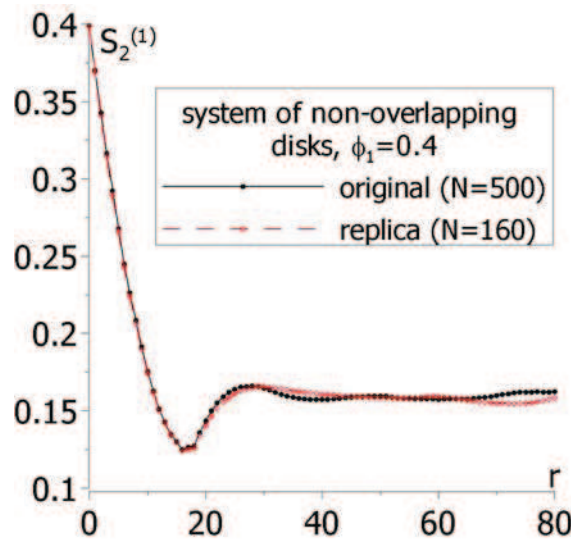
Fig. 4.28. Original $S_2^{(1)}$ and its replica: system of non-overlapping disks, $\phi_1=0.4$
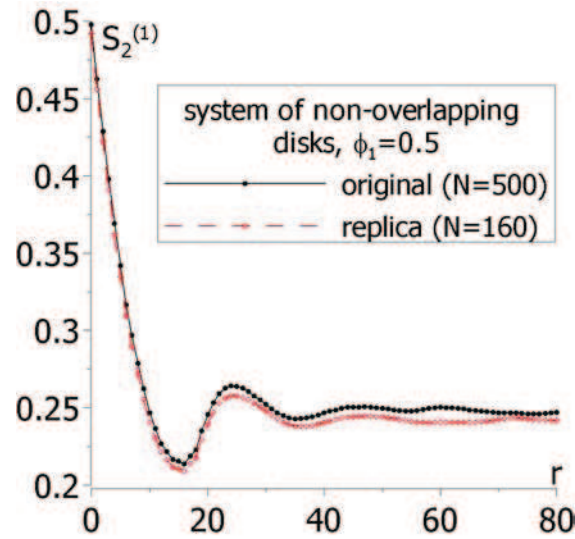
Fig. 4.29. Original $S_2^{(1)}$ and its replica: system of non-overlapping disks, ϕ_1=0.5

4.3.4. Reconstructed microstructures

This section deals with microstructures obtained via two-point probability mathematical reconstruction procedure. Roughly speaking, the reconstruction process consists in finding such realization for which the calculated two-point correlation function, $\widetilde{S_2^{(i)}}$, best matches the target two-point correlation function $S_2^{(i)}$ (Yeong & Torquato, 1998a, 1998b). The target function can be established e.g. in the way of laboratory experiments or theoretical models.

Starting from some initial realization, preserving volume fractions of phases, the microstructure is evolved towards $S_2^{(i)}$ by minimizing the energy E, which at any time step, is defined as:

$$E = \sum_r \left[\widetilde{S_2^{(i)}}(r) - S_2^{(i)}(r) \right]^2 \tag{4.83}$$

The minimization of E (at any time step) is performed by simulating annealing algorithm (Kirkpatrick *et.al.*, 1983). Namely, the states of two arbitrarily chosen pixels of different phases are interchanged - white pixel is changed into black one, while black pixel is filled with white colour. Interchanging the states of two pixels causes the change in energy, such that $E \to \overline{E}$. Therefore the difference between two states can be calculated, i.e.

$$\Delta E = \overline{E} - E \tag{4.84}$$

Then the phase interchange is accepted with some probability

$$P_{\Delta E} = \begin{cases} 1, & \Delta E \leq 0 \\ \exp(-\Delta E/T), & \Delta E > 0 \end{cases} \tag{4.85}$$

where *T* is the fictitious temperature and its actual value is defined by the cooling schedule procedure applied. The solution is obtained as T->0.

Debye microstructure

We start our considerations with the Debye random medium for which the target two-point correlation function is as follows:

$$S_2^{(1)}(r) = \phi_1\phi_2 \exp(-r/a) + \phi_1^2 \tag{4.86}$$

Reconstruction process begins with the initial configuration of pixels in the random checkerboard arrangement. Then, by interchanging pixels states, the system is evolved towards the target function. In Fig. 4.30 some chosen stages of reconstruction procedure are displayed.
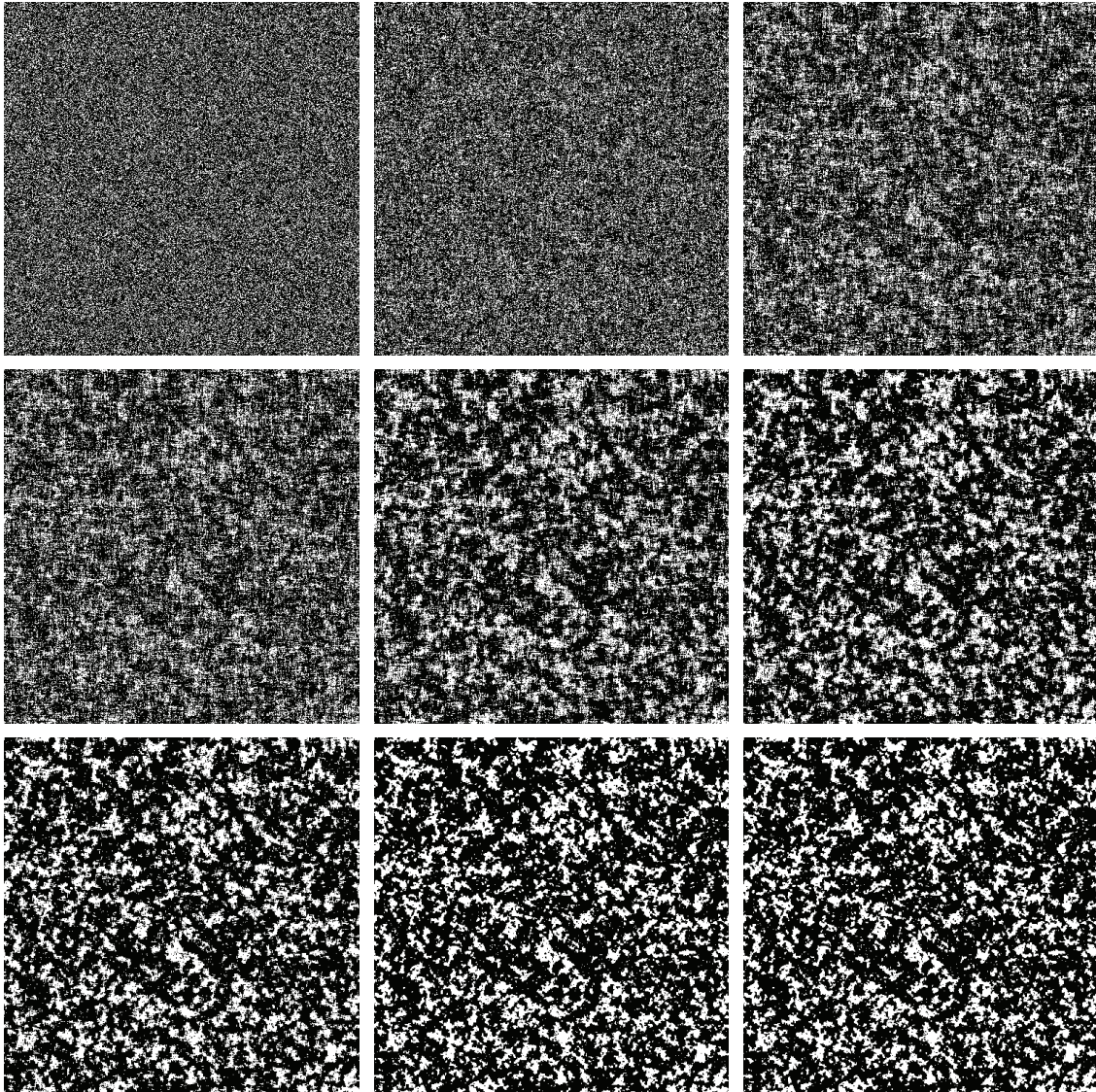
Fig. 4.30. Visualization of reconstruction procedure stages. Top left: initial configuration of pixels in the random checkerboard arrangement. Bottom right: reconstruction of a Debye random medium (*a*=3, ϕ_1=0.3).

Fig. 4.31 presents the digital images of reconstructed random media with different volume fractions. The two-point probability functions corresponding to these digital images are shown in Fig. 4.32.
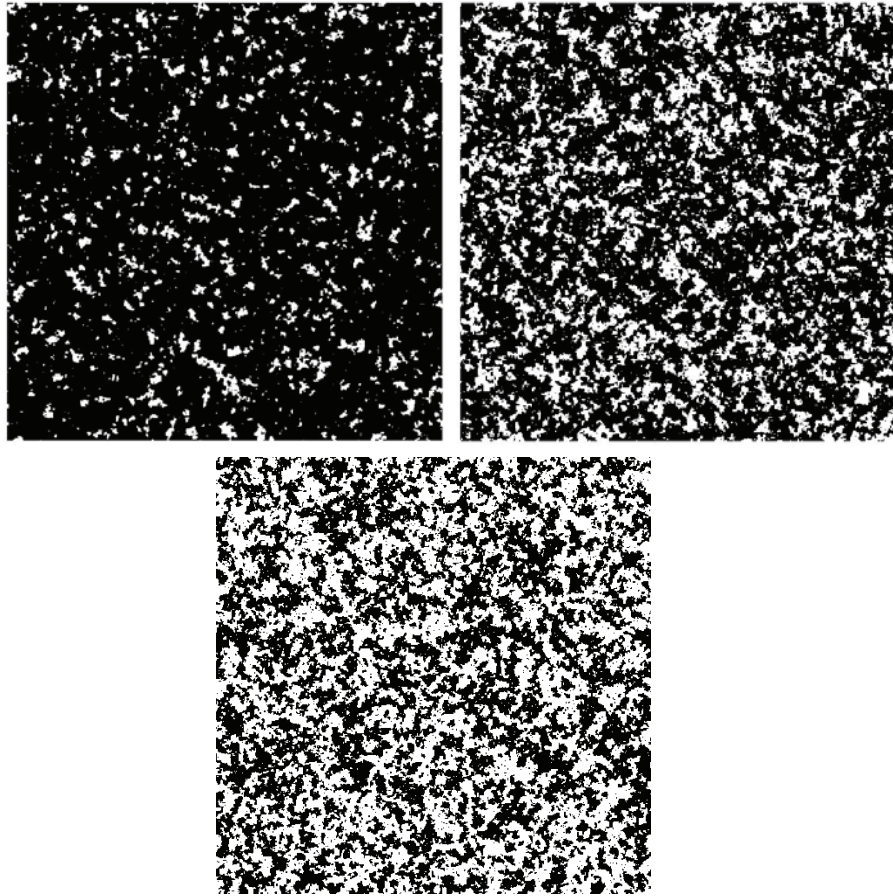
Fig. 4.31. Digital images (500×500 pixels) of reconstructed Debye random medium: a.) $\phi_I=0.1$, b.) $\phi_I=0.3$, c.) $\phi_I=0.5$.
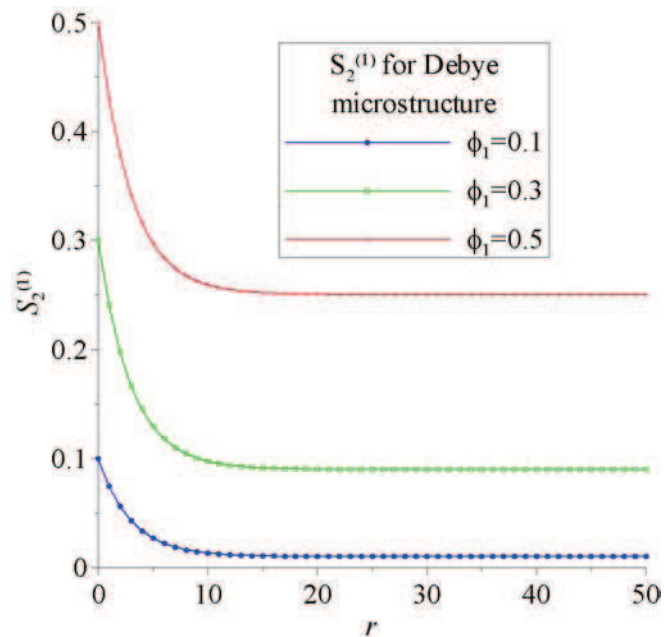
Fig. 4.32. Two-point probability function for Debye random medium (distance r in pixels)

In Tables 4.10 and 4.11 the RVE sizes evaluated for different volume fractions are presented. Note that for all microstructures the maximum sample size is the one corresponding to the condition given by (4.35).

Table 4.10. RVE size corresponding to error $\varepsilon = 3\%$ (Debye microstructure)

ϕ_1	$\max\left[N_\xi; N_\psi\right]$	N_{l_c}
0.1	**<u>133</u>**	40
0.3	**<u>64</u>**	40
0.5	**<u>41</u>**	40

Table 4.11. RVE size corresponding to error $\varepsilon = 1\%$ (Debye microstructure)

ϕ_1	$\max\left[N_\xi; N_\psi\right]$	N_{l_c}
0.1	**<u>224</u>**	50
0.3	**<u>114</u>**	50
0.5	**<u>73</u>**	50

The original two-point probability functions, as well as, their replica are shown below, in Figs. 4.33 – 4.35. It can be seen that both functions are in a very well agreement.
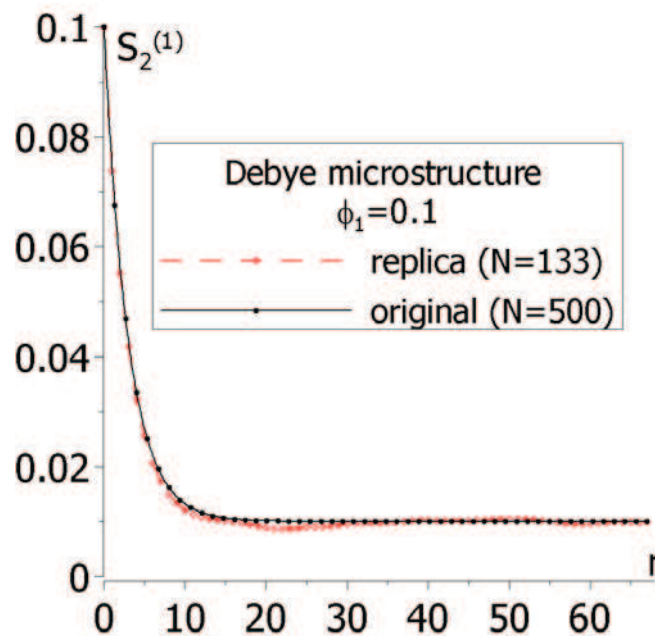
Fig. 4.33. Original $S_2^{(1)}$ and its replica: Debye microstructure, ϕ_1=0.1.
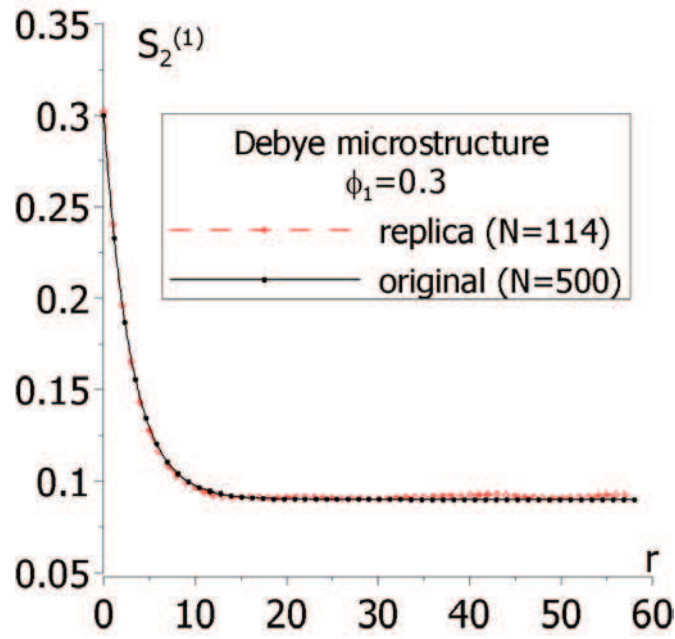
Fig. 4.34. Original $S_2^{(1)}$ and its replica: Debye microstructure, ϕ_1=0.3.
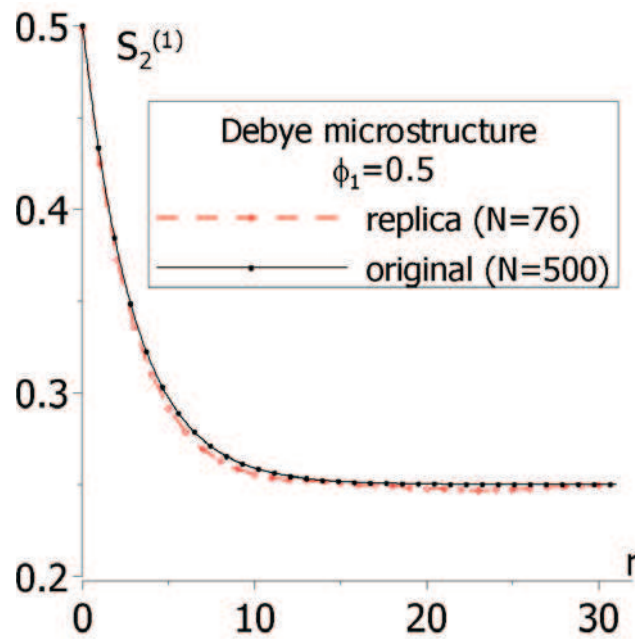
Fig. 4.35. Original $S_2^{(1)}$ and its replica: Debye microstructure, ϕ_1=0.5.

It should be mentioned that in case ϕ_1=0.1 the replica was obtained with the sample size equated to N= 133, so corresponding to relative error ε=3% (Table 4.10). For other volume fractions, i.e. 0.3 and 0.5, the sample sizes used are N=114 and N=73, respectively. These RVE sizes correspond to error of estimation ε=1% (see Table 4.11)

Modified Debye microstructure

Now we focus on the modified Debye random medium for which the target two-point correlation function is given by following relation:

$$S_2^{(1)}(r) = \phi_1 \phi_2 \exp(-r/a) \frac{\sin(qr)}{qr} + \phi_1^2 ; \quad q = \frac{2\pi}{b} \tag{4.87}$$

The digital images of the microstructures corresponding to the target function (4.87) are shown in Fig. 4.36. The resolution of images is 500 x 500 pixels. Furthermore, the microstructures are obtained for the following values of parameters involved in (4.87), i.e. a=32 and b=8.
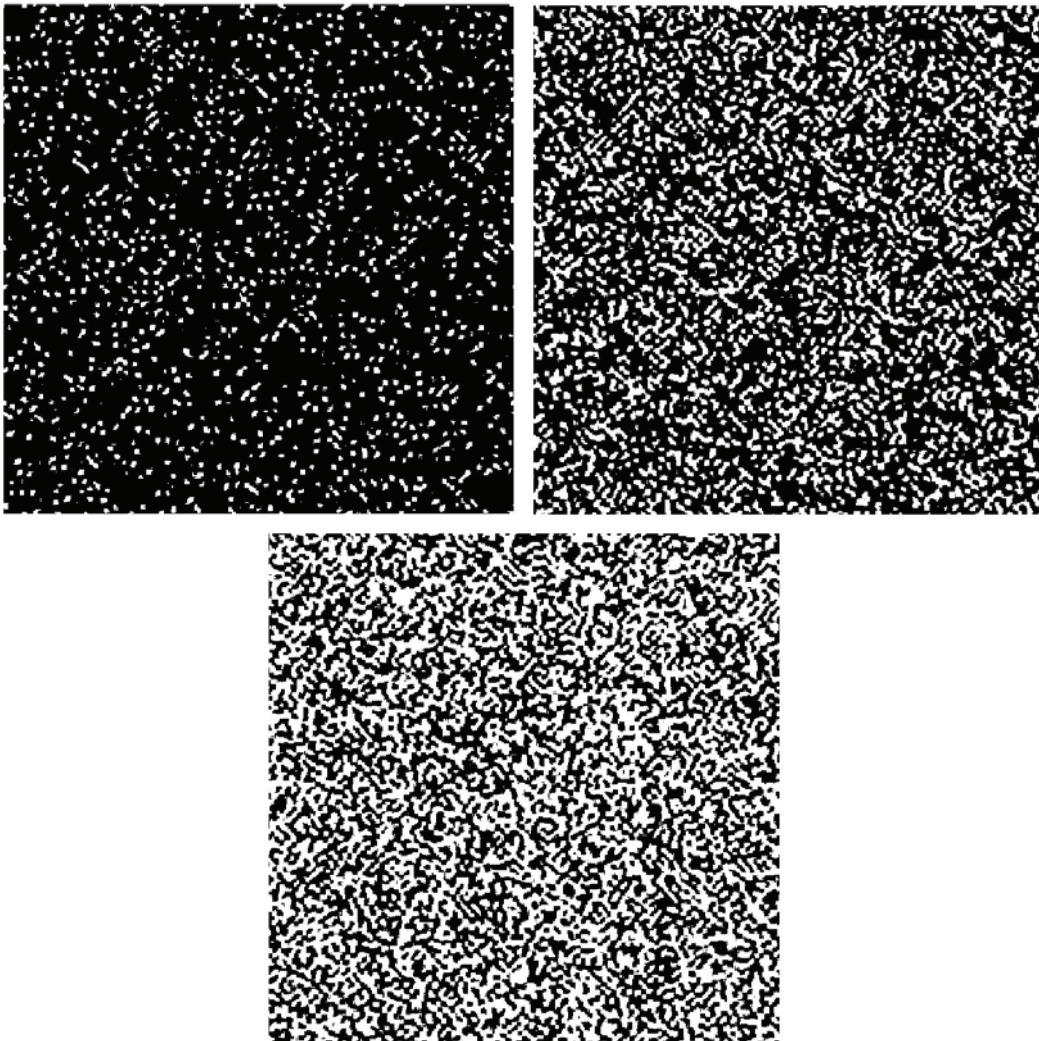
Fig. 4.36. Digital images (500×500 pixels) of modified Debye random medium - top left: ϕ_1=0.1,top right: ϕ_1=0.3, bottom: ϕ_1=0.5.

The two-point probability functions determined for different volume fractions are presented graphically in Fig. 4.37. Note that $S_2^{(1)}$ exhibits oscillations about the value of ϕ_1^2. Nevertheless, the

evaluation of correlation length can be performed with no doubts. This is due to fact, that the oscillations are vanishing (decreasing) as the distance r is increasing.
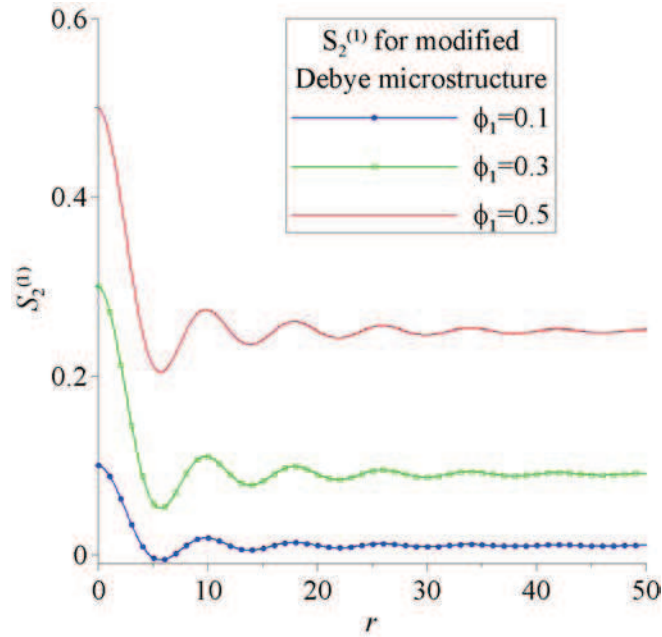
Fig. 4.37. Two-point probability function for modified Debye medium (distance r in pixels)

In Tables 4.12 and 4.13 the RVE sizes evaluated for different volume fractions are presented. The original two-point probability functions, as well as, their replicas are shown below, in Fig. 4.38.

Table 4.12. RVE size corresponding to error $\varepsilon = 3\%$ (modified Debye microstructure)

ϕ_1	$\max\left[N_\xi; N_\psi\right]$	N_{l_c}
0.1	57	**68**
0.3	30	**68**
0.5	21	**68**

Table 4.13. RVE size corresponding to error $\varepsilon = 1\%$ (modified Debye microstructure)

ϕ_1	$\max\left[N_\xi; N_\psi\right]$	N_{l_c}
0.1	**102**	100
0.3	54	**100**
0.5	35	**100**
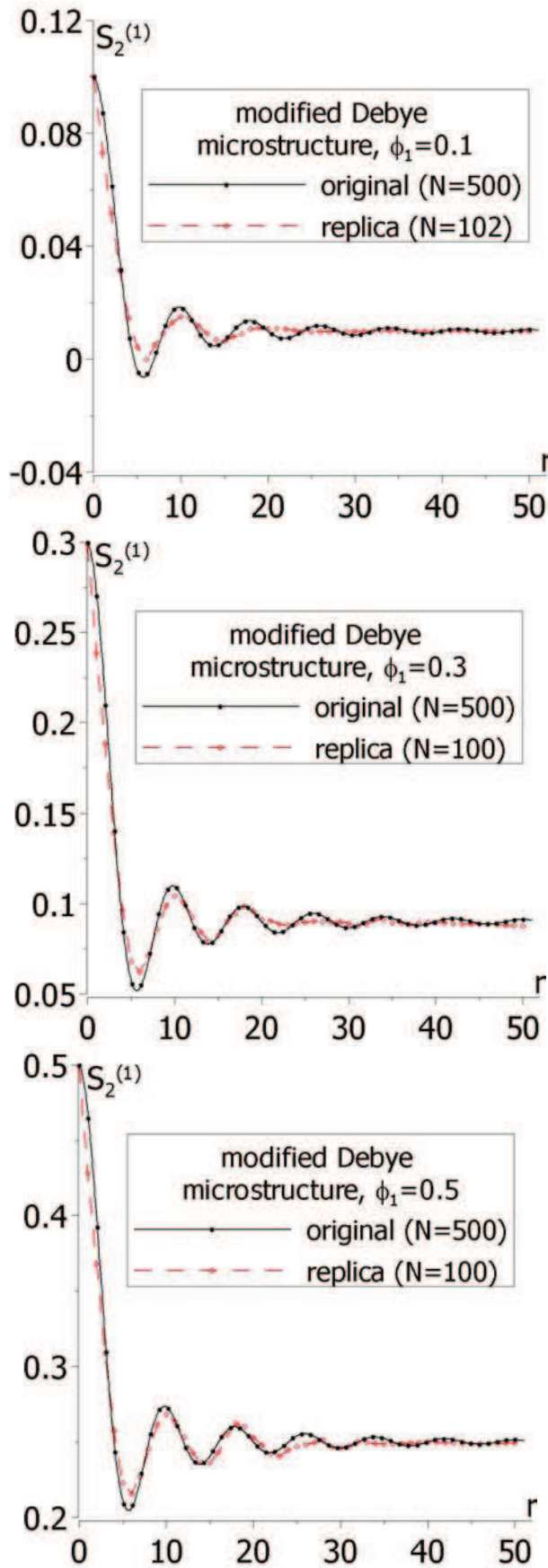
Fig. 4.38. Original $S_2^{(1)}$ function and their replicas: modified Debye microstructure.

Real materials

Fontainebleau sandstone

Within this section we investigate reconstructed microstructures of real materials. We begin our considerations with the Fontainebleau sandstone. The two-point correlation function for void phase can be approximated by the following relation (Jiao *et al.*, 2008):

$$S_2^{(1)}(r) = \left(0.77\exp(-r/3) + 0.23\exp(-r/6.5)\cos(0.2r)\right)\phi_1\phi_2 + \phi_1^2 \tag{4.88}$$

where $\phi_1 = 0.175$ and $\phi_2 = 0.825$ are the volume fractions of void and solid phases, respectively.

In Fig. 4.39. the digital image of 2D reconstructed realization of Fontainebleau sandstone is provided. The resolution of digital image is 500×500 pixels. The void phase is shown in white, whereas black pixels are associated with solid phase.
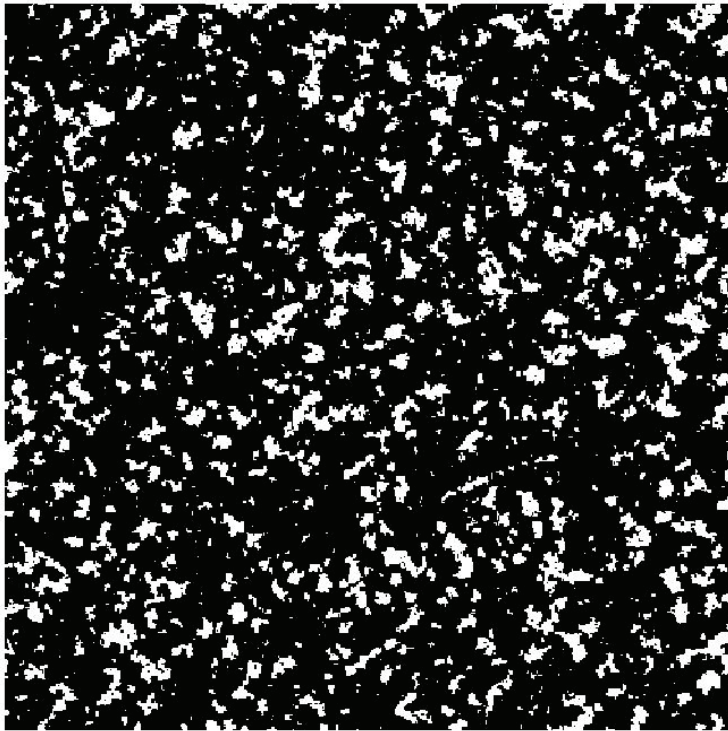
Fig. 4.39. Digital image (500×500 pixels) of the reconstructed 2D realization of the Fontainebleau sandstone.

The two-point correlation function of void phase is displayed in Fig. 4.40. It can be seen that the two-point probability function rather monotonically decays to its asymptotic value of ϕ_1^2. The oscillations about ϕ_1^2 are insignificant and therefore evaluation of the correlation length is quite an easy task.
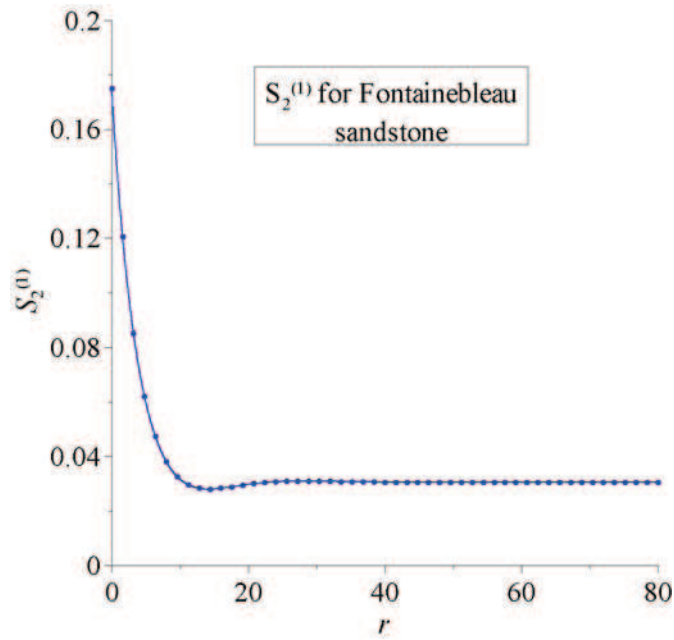
Fig. 4.40. Two-point probability function for Fontainebleau sandstone (distance *r* in pixels)

All the results concerning the size of RVE are collected in Table 4.14. Furthermore, for the size of RVE corresponding to $\varepsilon=1\%$, the replica of original two-point probability function was evaluated. This function is plotted against the distance *r* in Fig. 4.41.

Table 4.14. RVE size for reconstructed 2D realization of Fontainebleau sandstone

ϕ_I	$\max\left[N_\xi; N_\psi\right]$	N_{l_c}	ε
0.175	**77**	66	3%
	133	80	1%
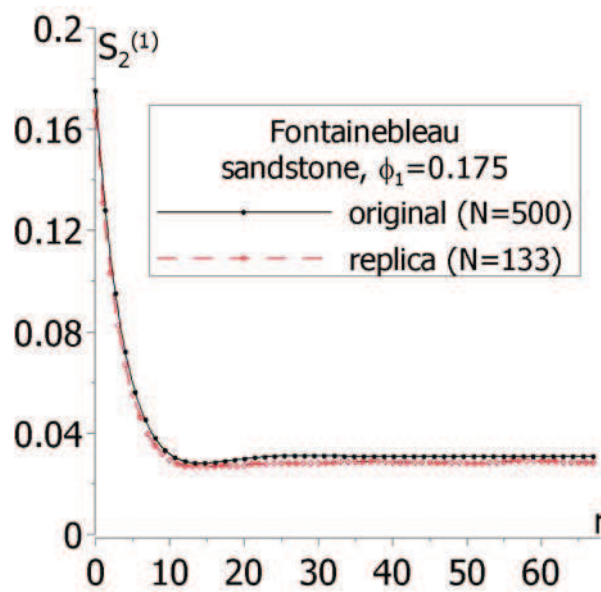
Fig. 4.41. Original $S_2^{(1)}$ function and its replica: Fontainebleau sandstone.

Boron-carbide/aluminum composite

Another example of real material is the boron-carbide/aluminum (B$_4$C/Al) composite. The two-point probability aluminum phase function can be approximated by (Jiao *et al.*, 2008):

$$S_2^{(1)}(r) = \left(0.81\exp(-r/3) + 0.19\exp(-r/10)\cos(0.22r)\right)\phi_1\phi_2 + \phi_1^2 \qquad (4.89)$$

where $\phi_1 = 0.353$ and $\phi_2 = 0.647$ are the volume fractions of aluminum (white) and boron-carbide (black) phases, respectively. The digital image (500×500 pixels) of 2D reconstructed realization of B$_4$C/Al is provided in Fig. 4.42, whereas $S_2^{(1)}$ is presented graphically in Fig. 4.43.
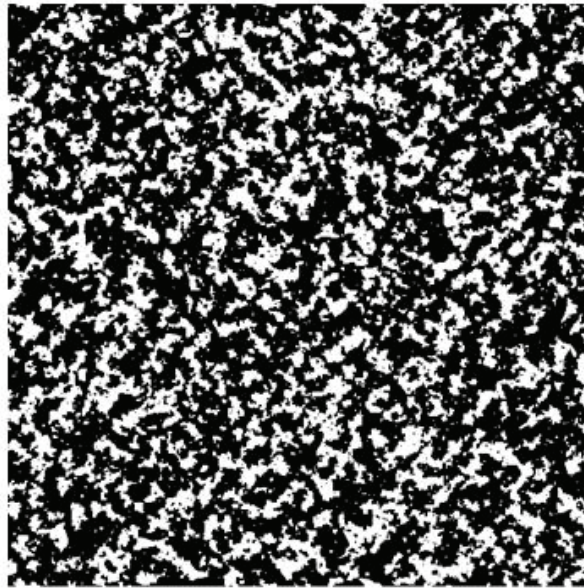
Fig. 4.42. Digital image (500×500 pixels) of the reconstructed 2D realization of boron-carbide/aluminum composite
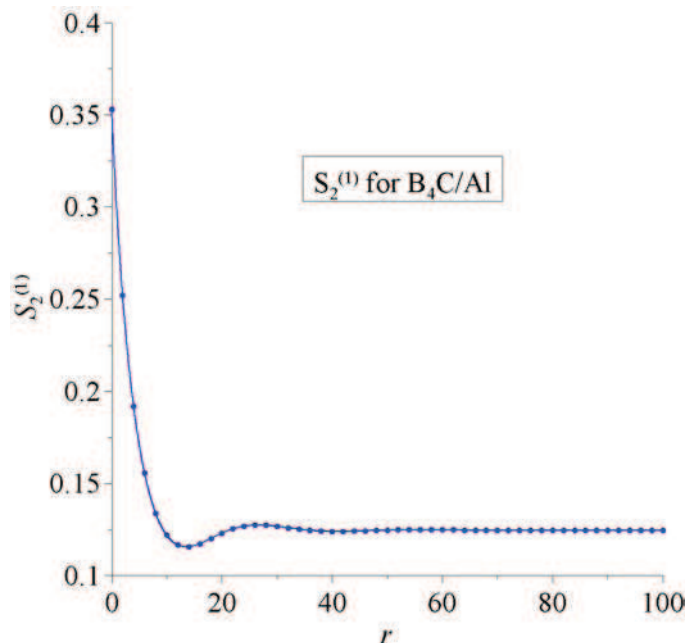
Fig. 4.43. Two-point probability function for boron-carbide/aluminum composite (distance r in pixels)

The results concerning the size of RVE for B4C/Al composite are collected in Table 4.15. Fig. 4.44 provides both original and replica of two-point probability function.

Table 4.15. RVE size for reconstructed 2D realization of B_4C/Al

ϕ_I	$\max\left[N_\xi; N_\psi\right]$	N_{l_c}	ε
0.353	44	**80**	3%
	77	**100**	1%
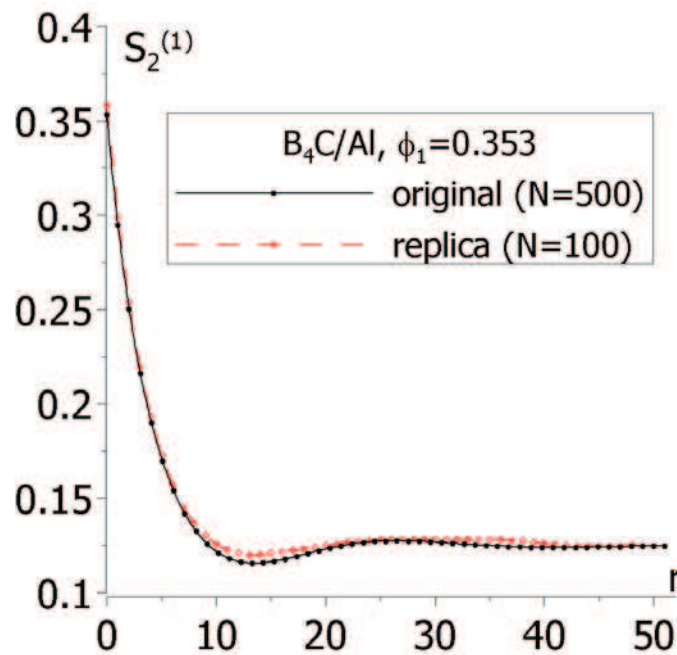
Fig. 4.44. Original $S_2^{(1)}$ function and its replica: B_4C/Al.

4.4. Remarks

In this chapter the criterion for the sample size to be representative with respect to microstructure geometry is proposed. The following definition of sample representativity has been adopted, i.e.:

A sample is representative with respect to geometry, if based on a knowledge of sample geometry, one can obtain a satisfactory replica of the two-point correlation function of random composite (statistically homogeneous), with definite value of statistical error tolerance.

Based on the main feature of the two-point probability function, i.e.: an existence of two fixed points of this microstructure descriptor $\left(S_2 = \phi \text{ at } r=0 \text{ and } S_2 = \phi^2 \text{ at } r \to \infty\right)$, the necessary criterion for the sample size to be representative with respect to composite geometry has been formulated

(4.36). The condition is an optimization one, namely of "max type". It involves three inequalities: two for limiting values of volume fraction variances of composite phases and the one for so called correlation length. Exact form of these requirements are presented by relations: (4.33), (4.34) and (4.28), respectively.

Validity and effectiveness of the criterion proposed has been tested by performing numerical simulations for a sequence of different types of composites. Two groups of random microstructures have been studied, i.e. *random cell models* group consisting of random checkerboard, system of overlapping disks, system of non-overlapping disks as well as *Ising* model. Another group consists of microstructures obtained via reconstruction procedure, e.g. Debye random medium as well as real materials, namely Fontainebleau sandstone, boron-carbide/aluminum (B$_4$C/Al). For all groups of microstructures the sizes of RVE were evaluated according to the criterion proposed, which consists in performing following steps:

- having a digital image of microstructure, evaluate the two-point probability function of an arbitrary phase – say phase 1- utilizing relations (4.22),

- determine the variance of local volume fraction given by (4.18) – apply the Monte Carlo approach (4.82),

- determine the functions: $\dfrac{Var(\xi)}{\langle \xi \rangle^2}$ and $\dfrac{Var(\xi)}{\langle \psi \rangle^2}$,

- set the wanted precision ε for the estimation and evaluate the size of the sample - as the number of pixels in a row and a column N - on the basis of relation (4.35),

- estimate the correlation length $l_c(\varepsilon)$,

- if the value of N is larger than $2l_c(\varepsilon)$, then the minimum RVE size is $N_{RVE} = N$, otherwise: $N_{RVE} = 2l_c(\varepsilon)$.

Having the minimum size N_{RVE} the replica of two-point probability function has been evaluated for each microstructure studied - well agreement between target two-point probability function and its replica has been observed. Therefore it can be stated that the criterion (4.36) is also a sufficient condition for the sample size to be representative with respect to two-point probability function. In particular, one can see that in case of microstructures for which $S_2^{(1)}$ rather monotonically decays to its asymptotic value of ϕ_1^2 (random checkerboard, Ising model, Debye microstructure, Fontainebleau sandstone) the convergence is very good and therefore the original function $S_2^{(1)}$ as well as the

mean value (replica), $\overline{S_2^{(1)}}$, are in a very well agreement. In case of microstructures, for which $S_2^{(1)}$ exhibits fluctuations about the value of ϕ_1^2 (system of both non-overlapping and overlapping disks, modified Debye medium, B$_4$C/Al composite), the replica $\overline{S_2^{(1)}}$ is a little bit less satisfactory - see Figs. 4.23, 4.27-4.29, 4.38, 4.44. This stems from the fact that the sample size used for calculations has been smaller than the one evaluated according the criterion proposed in order to preserve randomness of the process. In other words the original image size (500x500) was too small to perform Monte Carlo simulations with larger window sizes.

A separate problem, which has been not yet discussed, is the evaluation of the sufficient number of realizations n which one has to carry out in order to obtain good estimate of $S_2^{(1)}$. In other words, when calculating the mean $\overline{S_2^{(1)}}$, a primary question appears: *when the sampling should be stopped?*

A Central Limit Theorem (CLT) was utilized for the purpose of determination the sufficient number of realizations n. Note, that in case of two-point probability function the number of realizations should be estimated with respect to the convergence of $\overline{S_2^{(1)}}$ to both ϕ_1 and ϕ_1^2.

Utilizing relation (3.31) one can derive the number of realizations, which has to be performed in order to fit the first fixed point ϕ_1, as:

$$n_{\phi_1} = n \geq \left(\frac{\Phi^{-1}\left(1 - \alpha/2\right)}{\varepsilon_{rel}} \right)^2 \frac{Var(\xi)}{E(\xi)^2} \tag{4.90}$$

The number of realizations for fitting ϕ_1^2 is as follows:

$$n_{\phi_1^2} = n \geq \left(\frac{\Phi^{-1}\left(1 - \alpha/2\right)}{\varepsilon_{rel}} \right)^2 \frac{Var(\xi^2)}{E(\xi^2)^2} \tag{4.91}$$

It should be noted, that in case of relation (4.90) evaluation of n_{ϕ_1} is an easy task. The problem appears when the number of realizations has to be established with respect to relation (4.91) – the variance of ξ^2 is not known. Therefore, in what follows, we focus on the estimation of relation between $\frac{Var(\xi)}{E(\xi)^2}$ and $\frac{Var(\xi^2)}{E(\xi^2)^2}$.

It is easy to show that:

$$\frac{Var(\xi)}{E(\xi)^2} = E\left(\left[\frac{\xi - E(\xi)}{E(\xi)}\right]^2\right) \tag{4.92}$$

Following the definition of variance it is evident that:

$$Var(\xi^2) = E\left(\left[\xi^2 - E(\xi^2)\right]^2\right) \tag{4.93}$$

Note, if the sample is treated as the representative one, then according to the sample representativity criterion, relation (4.93) can be estimated as:

$$Var(\xi^2) \cong E\left(\left[\xi^2 - E(\xi)^2\right]^2\right) = E\left(\left[\xi - E(\xi)\right]^2\left[\xi + E(\xi)\right]^2\right) \tag{4.94}$$

and therefore

$$\frac{Var(\xi^2)}{E(\xi^2)^2} \cong E\left(\left[\frac{\xi - E(\xi)}{E(\xi)}\right]^2\left[\frac{\xi + E(\xi)}{E(\xi)}\right]^2\right) \tag{4.95}$$

Denoting the volume fraction of phase 1, corresponding to *j*-realization of microstructure, as ξ_j, relation (4.95) can be estimated as:

$$\frac{Var(\xi^2)}{E(\xi^2)^2} \cong \frac{1}{n}\sum_{i=1}^{n}\left[\frac{\xi_i - E(\xi)}{E(\xi)}\right]^2 \chi_i \tag{4.96}$$

where

$$\chi_i = \left[\frac{\xi_i + E(\xi)}{E(\xi)}\right]^2 = 1 + 2\frac{\xi_i}{E(\xi)} + \left(\frac{\xi_i}{E(\xi)}\right)^2 \tag{4.97}$$

Utilizing (4.97), the expectation of χ, can be calculated:

$$E(\chi) = E(1) + 2\frac{E(\xi)}{E(\xi)} + \frac{E(\xi^2)}{E(\xi)^2} \cong 4 \tag{4.98}$$

and hence

$$E(\chi) \cong \frac{1}{n}\sum_{i=1}^{n}\chi_i \cong 4 \tag{4.99}$$

On the other hand, basing on relation (4.92), we know that:

$$\frac{Var(\xi)}{E(\xi)^2} \cong \frac{1}{n}\sum_{i=1}^{n}\left[\frac{\xi_i - E(\xi)}{E(\xi)}\right]^2 \tag{4.100}$$

Therefore, recalling relation (4.90) as well as (4.91) we see that the number of realizations $n_{\phi_1^2}$, which one has to carry out, can be related to n_{ϕ_1} by following estimation:

$$n_{\phi_1^2} \cong 4n_{\phi_1} \tag{4.101}$$

In what follows, the estimation given by (4.101) is briefly verified. For that purpose a random checkerboard microstructure is once more utilized. We know that (see section 3.2.3):

$$E(\xi) = p \tag{4.102}$$

as well as

$$Var(\xi) = \frac{p(1-p)}{N^2} \tag{4.103}$$

and therefore

$$\frac{Var(\xi)}{E(\xi)^2} = \frac{(1-p)}{pN^2} \tag{4.104}$$

On the other hand, it can be shown, that:

$$\frac{Var(\xi^2)}{E(\xi^2)^2} = \frac{4p^3(1-p)}{N^2 p^4 + \dfrac{p^2(1-p)^2}{N^2} + 2p^3(1-p)} + \frac{6p^2(1-p) - 10p^3(1-p)}{N^4 p^4 + p^2(1-p)^2 + 2N^2 p^3(1-p)} + $$
$$+ \frac{p - 7p^2 + 12p^3 - 6p^4}{N^6 p^4 + N^2 p^2(1-p)^2 + 2N^4 p^3(1-p)} \tag{4.105}$$

Note that all algebraic transformations which lead to final form of relation (4.105) were omitted. Utilizing (4.104) as well (4.105) we obtain the following relation:

$$\lim_{N \to \infty} \frac{Var(\xi^2)}{E(\xi^2)^2} = \left[\lim_{N \to \infty} \frac{Var(\xi)}{E(\xi)^2} \right] \cdot 4 \tag{4.106}$$

In Fig. 4.45 the ratio

$$\left[\frac{Var(\xi^2)}{E(\xi^2)^2} \right] \bigg/ \left[\frac{Var(\xi)}{E(\xi)^2} \right] \tag{4.107}$$

is plotted against the sample size N.

It can be seen that as N is increasing the ratio (4.107) converges towards the value of 4, regardless of the volume fraction p. Note that this convergence is rather fast, however, it depends on the value of p. Nevertheless, relation (4.106) as well as the results displayed in Fig. 4.45 confirm that the number of realizations $n_{\phi_1^2}$ can be estimated basing on relation (4.101).
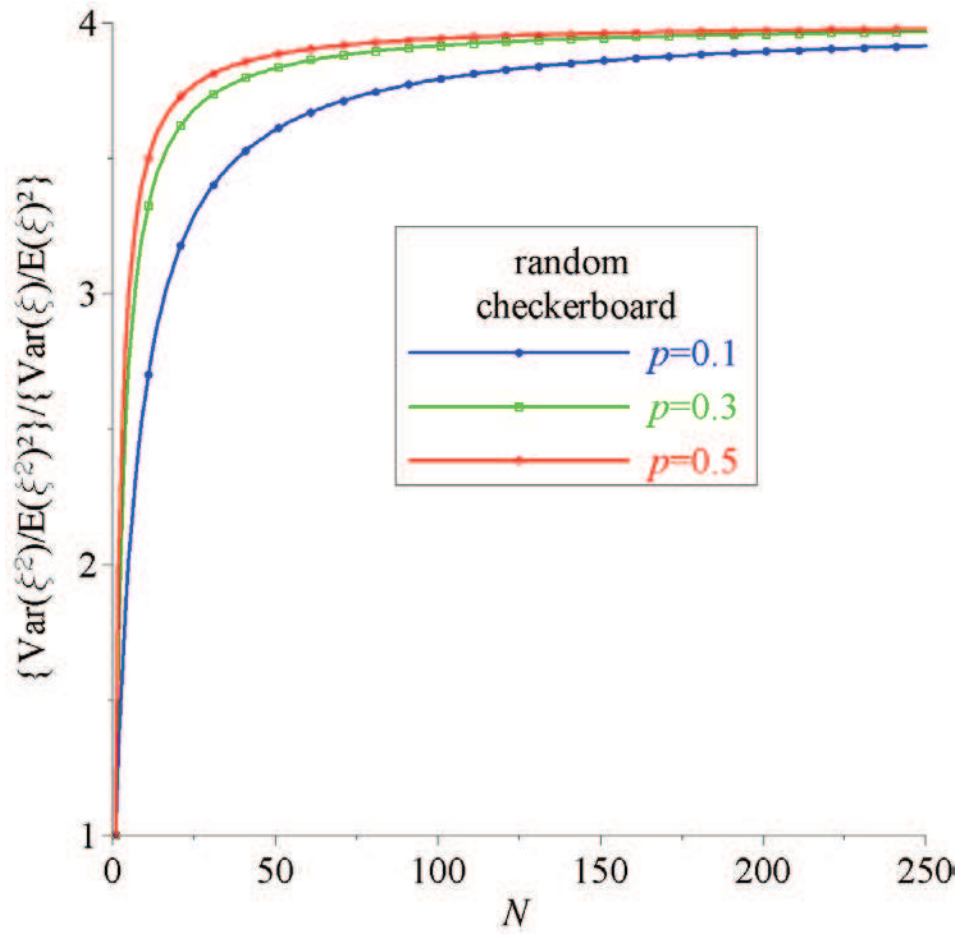
Fig. 4.45. The ratio (4.107) as a function of the sample size *N*.

5. Formulation of the condition for RVE size to be representative with respect to overall transport properties

On the basis of two-point probability properties, the condition for RVE size, with respect to microstructure geometry, has been formulated in previous chapter. It has been stated - and numerically verified - that fitting the fixed points of two-point probability function by $\overline{S_2^{(i)}}$ (averaged over sufficient number of realizations) guarantees that $\overline{S_2^{(i)}}$ converges towards original two-point correlation function $S_2^{(i)}$. In other words, we verified whether $\overline{S_2^{(1)}}$, evaluated for previously quantified RVE, could be treated as the *replica* of original function, $S_2^{(1)}$.

It is evident that the size of RVE is strongly affected by the type of analyzed physical property - it was shown, on the basis of random checkerboard, that different sizes of RVE are associated with, for instance, volume fraction and transport properties. Furthermore, Kanit *et al.* (2003) pointed out that the size of RVE is strongly affected by the contrast in mechanical properties of phases. This fact was also confirmed in author's paper where random two-phase checkerboard was studied (Różański *et al.* 2009). As a result, it was stated that considering size of RVE for transport processes leads to decreasing its size if compared to the size yielding from geometrical representativity condition. Therefore, in this chapter we focus on the formulation of the criterion governing the sample representativity with respect to overall transport properties. However, before the methodology is outlined some remarks concerning the quantification of RVE, found in recent literature, are provided.

As it was mentioned in chapter 2 a lot of attempt has been made in order to quantify RVE on the basis of statistical and numerical analysis. In (Stroeven *et al.*, 2004) an approach to quantify the size of RVE, for materials consisting of particles in a matrix, has been proposed. The influence of several criteria (peak load, dissipated energy and strain concentration factor) on the size of RVE has been considered. The proposed methodology is based on both statistical and numerical analysis. It should be mentioned that a simple statistical test which has been employed to express the fluctuations of analyzed quantities can be successfully used for an arbitrary physical property. In what follows the methodology is briefly outlined.

Within the statistical test (Stroeven *et al*., 2004) some important assumptions have been made:

- the infinite size sample is cut into an infinite number of much smaller specimens,
- the measured property or, in other words, mechanical response of *j*-specimen is denoted as x_j.
- x_j is normally distributed with mean μ and variance σ^2,
- μ is equal to the response of infinite body.

Statistical test have been performed by studying the variable possessing a *Student-t* distribution with *n-1* degrees of freedom, i.e.

$$t = \frac{\left(\bar{x} - \mu\right)}{s \Big/ \sqrt{n-1}} \tag{5.1}$$

The expectation as well as standard deviation are estimated as:

$$\bar{x} = \frac{1}{n}\sum_{j=1}^{n} x_j \tag{5.2}$$

and

$$s^2 = \frac{1}{n-1}\sum_{j=1}^{n}\left(x_j - \bar{x}\right)^2 \tag{5.3}$$

Assuming α to be the significance level, we have that

$$P\left(|t| < t_\alpha\right) = 1 - \alpha \tag{5.4}$$

or equivalently

$$P\left(\bar{x} - \Delta < \mu < \bar{x} + \Delta\right) = 1 - \alpha \tag{5.5}$$

Note that in relation above, the range of deviation Δ is expressed as:

$$\Delta = t_\alpha \frac{s}{\sqrt{n-1}} \tag{5.6}$$

and therefore the interval whose end points are $\bar{x} \pm \Delta$ is a $(1-\alpha)\cdot100\%$ confidence interval for μ.

It has been proposed to "*define the size of an RVE to be such that the response of an RVE will (with a given likelihood) not deviate more than a certain percentage from the response of a 'true' infinite body*". For instance, if we assume $\beta\cdot100\%$ as a desired precision, than relation (5.6) can be expressed as:

$$n-1 \approx \left(\frac{2\varepsilon t_\alpha}{\beta}\right)^2 \tag{5.7}$$

Relation (5.7) is obtained by replacing μ with its estimate $\bar{x}$. Furthermore, ε is a coefficient of variation defined as:

$$\varepsilon = \frac{s}{\bar{x}} \tag{5.8}$$

Note that the value of t_α, which is obtained form the *Student-t* distribution tables, depends on the value of *n*. Therefore, a procedure of RVE size determination is an iterative scheme. In general, having a sample of certain size *N*, the methodology consists in estimating *n* from relation (5.7) (such that the average value of measured property $\bar{x}$ only slightly differs - with acceptable deviation - from μ) and then RVE is treated as the sample which size is *n* times larger than the size of current specimen *N*. It should be emphasized that, for each sample, numerical analysis, such as that of finite element method, have to be performed in order to determine the value of x_j.

Different statistical approach for the quantification of RVE has been proposed by Gitman *et al.* (2007). The methodology is based on the simple *Chi-square* statistical criterion. As in case of previously presented methodology this one is also an iterative procedure. In general, it can be a sequence of following steps:

1. Generate several (*n*) sample realizations of certain size.
2. Using numerical tools, say finite element method, determine the value of analyzed property for each realization.
3. Evaluate the value of *Chi-square* coefficient as

$$\chi^2 = \sum_{j=1}^{n} \frac{\left(x_j - \bar{x}\right)^2}{\bar{x}} \tag{5.9}$$

   Note x_j is normalized with respect to its mean.
4. Compare the calculated value of *Chi-square* coefficient (5.9) with table value, corresponding to desired accuracy; if the obtained accuracy is satisfactory, the size of current sample is the RVE size, otherwise repeat the procedure starting from (2) – the method is graphically presented in Fig. 5.1.

It should be strongly emphasized that none of methods presented above incorporate information on the microstructure into the RVE size determination procedure. This information is obviously implicitly contained in numerical calculations - it influences the mechanical response x_j evaluated for each sample. Nevertheless, the size of RVE is not an explicit function of any statistical information concerning the microstructure morphology.

A procedure which involves information on microstructure morphology has been formulated by Kanit *et al.* (2003) who proposed a methodology for determination RVE size on the basis of the microstructural descriptor, namely the integral range (for more details concerning this microstructural descriptor see, for instance: Lantuéjoul, 2002). The methodology has been applied to two-phase 3D Voronoï mosaic. Linear elasticity as well as thermal conductivity problems have been investigated.
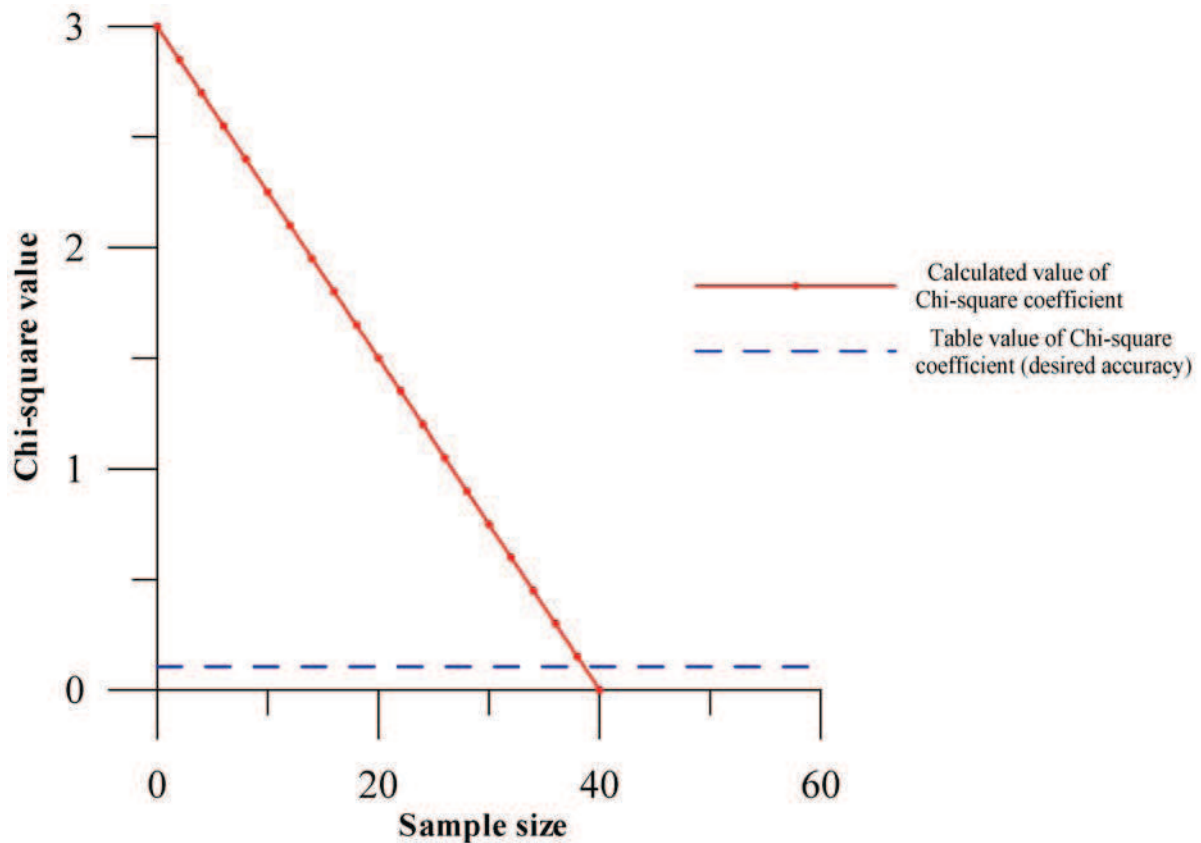
Fig. 5.1. Illustrative presentation of methodology proposed in (Gitman *et al.* 2007)

As mentioned in chapter 2, Kanit *et al.* (2003) pointed out that the size of RVE *" (...) must be considered as a function of five parameters: the physical property, the contrast of properties, the volume fractions of components, the wanted relative precision for the estimation of the effective property and the number of realizations of the microstructure associated with computations that one is ready to carry out"*. Furthermore it has been stated that: "*effective linear properties of random composites can be determined not only by numerical simulations on large volume elements of heterogeneous material, but also as mean values of apparent properties of rather small volumes, providing that a sufficient number of realizations is considered*". The validation of the methodology, concerning two materials from food industry, has been performed by Kanit *et al.* (2006).

As mentioned, the methodology proposed by Kanit *et al.* (2003) is based on the notion of integral range, A^{int}. For large sample, i.e. if $\|\Omega_0\| \gg A^{\text{int}}$, the variance of local volume fraction can be defined as:

$$Var\left(\xi\right) = \frac{\phi_1 \phi_2}{\|\Omega_0\|} A^{\text{int}} \qquad (5.10)$$

Therefore using relation (4.18) we have that

$$A^{\text{int}} = \lim_{\substack{a \to \infty \\ b \to \infty}} \frac{4 \int_0^a \int_0^b \left(S_2^{(1)}(r) - \phi_1^2\right)(a-x)(b-y)\,dxdy}{\|\Omega_0\| \phi_1 \phi_2} \qquad (5.11)$$

Utilising the properties of correlation length (4.21), the approximation of A^{int} can be expressed as:

$$A^{\text{int}} \cong \frac{4 \int_0^{l_c} \int_0^{l_c} \left(S_2^{(1)}(r) - \phi_1^2\right)dxdy}{\phi_1 \phi_2} \qquad (5.12)$$

Nevertheless, within the method proposed by Kanit *et al.* (2003) the integral range is determined on the basis of numerical simulations. This quantity is evaluated by fitting $\dfrac{Var\left(\xi\right)}{\phi_1 \phi_2}$ as a function of the inverse volume size $\dfrac{1}{\|\Omega_0\|}$. Then, the slope provides the value of integral range A^{int} - see relation (5.10).

Note, equation (5.10) relates the variance of local volume fraction with the value of integral range A^{int}. In case of elastic modules as well as thermal conductivity a power law model has been proposed such that:

$$Var\left(k\right) = \phi_1 \phi_2 \left(k_1 - k_2\right)^2 \left(\frac{A^{\text{int}}}{\|\Omega_0\|}\right)^{\alpha_m} \qquad (5.13)$$

where k_1 and k_2 denote the properties (elastic modules or thermal conductivity coefficients) of phases.

In general, the method formulated by (Kanit *et al.*, 2003) can be described by following steps:

1. Generate several (4-5) microstructure realizations of different sizes V.

2. Prescribe, say periodic boundary conditions, perform numerical calculations and determine apparent properties.

3. Evaluate both mean value and variance of apparent property for each volume size; the sufficient number of realizations, which have to be performed, for given size V can be calculated using the sampling rule:

$$\varepsilon_{abs} = \frac{2\sqrt{Var(k)}}{\sqrt{n}} \tag{5.14}$$

4. Determine the value of integral range and the power α_m in model (5.13).

5. Setting the desired accuracy as well as the number of realizations, the size of RVE can be evaluated from the following relation:

$$n = 4\phi_1\phi_2\left(\frac{k_1 - k_2}{\varepsilon_{abs}}\right)^2\left(\frac{A^{int}}{V}\right)^{\alpha_m} \tag{5.15}$$

Relation (5.15) is the result of the substitution (5.13) into (5.14). It should be noted that the size of RVE is strongly influenced by the value of integral range which has been found to depend (in case of effective linear properties) "*on the volume fraction, the contrast in properties, and the type of boundary conditions*" – for more details see (Kanit *et al.*, 2003).

It has to be strongly emphasized that all methods presented above require the large number of numerical calculations for the determination of the RVE size, i.e. one has to evaluate the values of mechanical response corresponding to *j*-realization of microstructure. Usually large number of realizations has to be considered and therefore the process of RVE size determination may require large computational cost (time).

Furthermore, as mentioned by Kanit *et al.* (2003) "(...) *the chosen volume V^{RVE} cannot be taken as small as one may wish, because there exists in general a bias in the estimation of the effective properties (...); the mean apparent properties computed on finite size domains do not coincide with the effective ones if the domain size is too small*". This fact was also indicated when the representativity of random checkerboard was studied. It was shown that there exist some threshold value of the sample size below which the mean value does not converge towards the effective property (note Fig. 3.25 is once again displayed below - Fig. 5.2).

The general disadvantage of presented methods is that they do not provide the condition for the minimum size of sample to be treated as the representative one for considered microstructure. Therefore, in what follows, the method providing the RVE size to be representative with respect to overall transport properties is formulated.
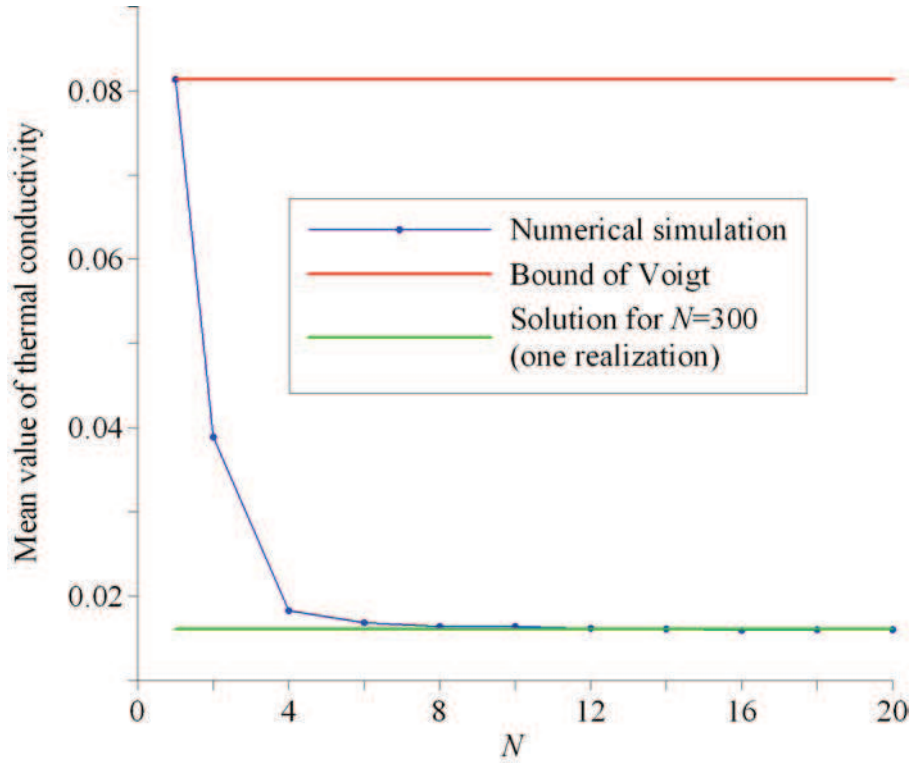
Fig. 5.2. Mean value of thermal conductivity $\bar{k}$ [W/mK] plotted against the size of sample.

5.1. Fluctuations of local Voigt and Reuss estimates

As it was shown in chapter 4 when moving sampling window from point to point, the volume fraction of phases strongly fluctuates and hence it becomes a random variable (Fig. 4.1). Note that fluctuations of local volume fraction implies that estimates of both Voigt and Reuss are changing - depending on window localization **x**. Thus, we define a new random variable, i.e. *local Voigt/Reuss estimate*, denoted as $\xi_\lambda(\mathbf{x})$, which relates to the value of Voigt/Reuss estimate corresponding to sample with position **x**. Therefore, we focus on fluctuations of local Voigt and Reuss estimates. As it was in case of local volume fraction, two-phase random medium is considered. Furthermore, we assume that phase 1 (phase 2) has a transport property k_1 (k_2).

Let introduce now a following indicator function:

$$I_\lambda(\mathbf{x}) = \begin{cases} \lambda_1, & \text{if } \mathbf{x} \in \mathcal{V}_1 \\ \lambda_2, & \text{if } \mathbf{x} \in \mathcal{V}_2 \end{cases} \tag{5.16}$$

where both λ_1 and λ_2 take different values depending on the estimate (Voigt or Reuss) considered.

In case of Voigt estimate

$$\lambda_1 = k_1 \text{ and } \lambda_2 = k_2, \tag{5.17}$$

whereas for Reuss estimation we have that:

113

$$\lambda_1 = \frac{1}{k_1} \text{ and } \lambda_2 = \frac{1}{k_2} \tag{5.18}$$

Utilizing (4.2-4.4) local Voigt/Reuss estimation can be defined as:

$$\xi_\lambda(\mathbf{x}) = \frac{1}{\|\Omega_0\|}\int_\Omega I_\lambda(\mathbf{y}) H(\mathbf{y}-\mathbf{x})\, d\mathbf{y} = \frac{1}{\|\Omega_0\|}\int_\Omega I_\lambda(\mathbf{x}+\mathbf{r}) H(\mathbf{r})\, d\mathbf{r} \tag{5.19}$$

If we recall ergodic hypothesis one can simply equate the ensemble average of ξ_λ to the volume average in the limit of infinitely large volume, i.e.:

$$\overline{\langle \xi_\lambda \rangle} = \lambda_1 \phi_1 + \lambda_2 \phi_2 \tag{5.20}$$

As it was in case of local volume fraction, in what follows, the variance of ξ_λ is studied. Following the variance definition as well as utilizing (5.20) the variance of local Voigt/Reuss estimate is as follows

$$Var(\xi_\lambda) = \overline{\langle \xi_\lambda^2 \rangle} - \left(\overline{\langle \xi_\lambda \rangle}\right)^2 = \overline{\langle \xi_\lambda^2 \rangle} - \left(\lambda_1 \phi_1 + \lambda_2 \phi_2\right)^2 \tag{5.21}$$

Once again, it can be seen, that in order to calculate $Var(\xi_\lambda)$ the value of $\overline{\langle \xi_\lambda^2 \rangle}$ should be first determined. This quantity can be simply expressed as:

$$\overline{\langle \xi_\lambda^2 \rangle} = \lim_{\|\Omega\|\to\infty} \frac{1}{\|\Omega\|}\frac{1}{\|\Omega_0\|^2}\int_\Omega\int_\Omega\int_\Omega I_\lambda(\mathbf{x}+\mathbf{r}) I_\lambda(\mathbf{x}+\mathbf{z}) H(\mathbf{r}) H(\mathbf{z})\, d\mathbf{r}\, d\mathbf{z}\, d\mathbf{x} \tag{5.22}$$

Relation (5.22) can be rewritten in the following form

$$\overline{\langle \xi_\lambda^2 \rangle} = \frac{1}{\|\Omega_0\|^2}\int_\Omega\int_\Omega S_2\left(|\mathbf{r}-\mathbf{z}|, \lambda_1, \lambda_2\right) H(\mathbf{r}) H(\mathbf{z})\, d\mathbf{r}\, d\mathbf{z} \tag{5.23}$$

where $S_2\left(|\mathbf{r}-\mathbf{z}|, \lambda_1, \lambda_2\right)$ is the modified two-point correlation function defined as:

$$S_2\left(|\mathbf{r}-\mathbf{z}|, \lambda_1, \lambda_2\right) = \lim_{\|\Omega\|\to\infty} \frac{1}{\|\Omega\|}\int_\Omega I_\lambda(\mathbf{x}+\mathbf{r}) I_\lambda(\mathbf{x}+\mathbf{z})\, d\mathbf{x} \tag{5.24}$$

Note, this correlation function, which is similar to the two-point probability one (3.9), is presented, in details, in section 5.2.

Making use of substitution $\mathbf{t} = \mathbf{r} - \mathbf{z}$ and utilizing (4.12) as well as (4.15) one simply gets:

$$Var(\xi_\lambda) = \frac{1}{\|\Omega_0\|^2}\int_\Omega \left(S_2\left(\mathbf{t}, \lambda_1, \lambda_2\right) - \overline{\langle \xi_\lambda \rangle}^2\right) \vartheta_{int}(\mathbf{t}, a, b)\, dt \tag{5.25}$$

Substituting (4.13) into relation (5.25) and performing simple algebraic transformation one obtains the final form of the local Voigt/Reuss estimate variance, i.e.:

$$\text{Var}\{\xi_\lambda\} = \frac{4}{\|\Omega_0\|^2} \int_0^a \int_0^b \left(S_2\left(\mathbf{t}, \lambda_1, \lambda_2\right) - \overline{\langle \xi_\lambda \rangle}^2 \right)\left(a - t_x\right)\left(b - t_y\right) dx dy \tag{5.26}$$

In expression (5.26) a modified two-point correlation function plays a central role, i.e. given its values one can simply calculate the variance of local Voigt/Reuss estimate. However, as it will be shown in next section, in case of two phase medium, $S_2\left(\mathbf{t}, \lambda_1, \lambda_2\right)$ can be determined on the basis of two-point correlation function for arbitrary phase, $S_2^{(i)}$.

5.2. Modified two-point correlation function

We focus now on the modified two-point correlation function which has been introduced in previous section. It will be shown that (for two phase medium) $S_2\left(\mathbf{t}, \lambda_1, \lambda_2\right)$ is related to the two-point probability function $S_2\left(\mathbf{t}\right)$ by simple algebraic relation.

Note that indicator function (5.16) can be expressed in terms of (3.5) such that:

$$I_\lambda\left(\mathbf{x}\right) = \lambda_1 I^{(1)}\left(\mathbf{x}\right) + \lambda_2 I^{(2)}\left(\mathbf{x}\right) \tag{5.27}$$

and hence the modified two-point correlation function given by (5.24) has the following form:

$$S_2\left(\mathbf{t}, \lambda_1, \lambda_2\right) = \lim_{\|\Omega\| \to \infty} \frac{1}{\|\Omega\|} \int_\Omega I_\lambda\left(\mathbf{x}\right) I_\lambda\left(\mathbf{x} + \mathbf{t}\right) d\mathbf{x} =$$
$$= \lim_{\|\Omega\| \to \infty} \frac{1}{\|\Omega\|} \int_\Omega \left(\lambda_1 I^{(1)}\left(\mathbf{x}\right) + \lambda_2 I^{(2)}\left(\mathbf{x}\right)\right)\left(\lambda_1 I^{(1)}\left(\mathbf{x} + \mathbf{t}\right) + \lambda_2 I^{(2)}\left(\mathbf{x} + \mathbf{t}\right)\right) d\mathbf{x} \tag{5.28}$$

Utilizing the definition of two-point probability, given by (3.13), it is easy to show that:

$$S_2\left(\mathbf{t}, \lambda_1, \lambda_2\right) = \lambda_1^2 S_2^{(1)}\left(\mathbf{t}\right) + \lambda_2^2 S_2^{(2)}\left(\mathbf{t}\right) + \lambda_1 \lambda_2 S_2^{(12)}\left(\mathbf{t}\right) \tag{5.29}$$

Recalling now the assumption concerning statistical isotropy causes that it is meaningful to substitute (3.16) into (5.29). After some simple algebraic transformations one gets:

$$S_2\left(t, \lambda_1, \lambda_2\right) = \lambda_1^2 S_2^{(1)}\left(t\right) + \lambda_2^2 S_2^{(2)}\left(t\right) + \lambda_1 \lambda_2 \left(1 - S_2^{(1)}\left(t\right) - S_2^{(2)}\left(t\right)\right) \tag{5.30}$$

As it can be seen, the modified two-point correlation function can be successfully calculated on the basis of the two-point probability functions $S_2^{(1)}$ and $S_2^{(2)}$. Furthermore, taking into account that the modified two-point correlation function can be related to $S_2^{(1)}$ and $S_2^{(2)}$ via relation (5.30) it is evident that one should also be able to express the variance of Voigt/Reuss estimate (5.26) as a function of these quantities.

In what follows we focus on the expression $\left(S_2\left(t,\lambda_1,\lambda_2\right) - \overline{\langle\xi_\lambda\rangle}^2 \right)$ which is a part of integral (5.26). Utilizing (5.30) as well as (5.20) we have that:

$$S_2\left(t,\lambda_1,\lambda_2\right) - \overline{\langle\xi_\lambda\rangle}^2 = \lambda_1^2\left(S_2^{(1)}(t)-\phi_1^2\right) + \lambda_2^2\left(S_2^{(2)}(t)-\phi_2^2\right) + \lambda_1\lambda_2\left(1-S_2^{(1)}(t)-S_2^{(2)}(t)-2\phi_1\phi_2\right) \quad (5.31)$$

Taking into account following relation

$$2\phi_1\phi_2 = \phi_1\left(1-\phi_1\right) + \phi_2\left(1-\phi_2\right) = 1-\phi_1^2-\phi_2^2 \quad (5.32)$$

equation (5.31) can be rewritten as

$$S_2\left(t,\lambda_1,\lambda_2\right) - \overline{\langle\xi_\lambda\rangle}^2 = \left(\lambda_1-\lambda_2\right)\left[\lambda_1\chi^{(1)}(t) - \lambda_2\chi^{(2)}(t)\right] \quad (5.33)$$

where $\chi^{(i)}(t)$ is the autocovariance function defined as (Torquato, 2002):

$$\chi^{(i)}(t) = S_2^{(i)}(t) - \phi_i^2 \quad (5.34)$$

Following Torquato (2002), we have that, in case of two-phase medium, the autocovariance function

$$\chi(t) \equiv S_2^{(1)}(t) - \phi_1^2 = S_2^{(2)}(t) - \phi_2^2 \quad (5.35)$$

for phase 1 is equal to that for phase 2. Therefore relation (5.33) can be rewritten as

$$S_2\left(t,\lambda_1,\lambda_2\right) - \overline{\langle\xi_\lambda\rangle}^2 = \left(\lambda_1-\lambda_2\right)^2 \chi^{(1)}(t) \quad (5.36)$$

or in equivalent form:

$$S_2\left(t,\lambda_1,\lambda_2\right) - \overline{\langle\xi_\lambda\rangle}^2 = \left(\lambda_1-\lambda_2\right)^2 \chi^{(2)}(t) \quad (5.37)$$

Observing relations above we see that $\left(S_2\left(t,\lambda_1,\lambda_2\right) - \overline{\langle\xi_\lambda\rangle}^2 \right)$ can be related to the autocovariance function $\chi(t)$ which takes the same values for both phases. Therefore, hereafter we can take into account only one arbitrary phase, say phase 1, and hence the variance of local Voigt/Reuss estimate (5.26) is as follows

$$\mathrm{Var}\{\xi_\lambda\} = \left(\lambda_1-\lambda_2\right)^2 \frac{4}{\left\|\Omega_0\right\|^2} \int_0^a\int_0^b\left(S_2^{(1)}(t)-\phi_1^2\right)\left(a-t_x\right)\left(b-t_y\right)dxdy \quad (5.38)$$

Substituting (5.36) in the relation (5.38) as well as utilizing the relation which defines the variance of local volume fraction (4.18), leads to

$$\mathrm{Var}\{\xi_\lambda\} = \left(\lambda_1-\lambda_2\right)^2 \mathrm{Var}\{\xi\} \quad (5.39)$$

Note that (5.39) relates the variance of local Voigt/Reuss estimate to the one of local volume fraction which is given by (4.18).

5.3. Modified sample representativity criterion

In case of two-point probability function it was shown that, irrespective of the function profile, two points are common $\left(S_2^{(i)} \left(r = 0 \right) = \phi_i \quad \text{and} \quad S_2^{(i)} \left(r \to \infty \right) = \phi_i^2 \right)$, regardless of the medium considered. These points have been denoted as the fixed points of two-point probability function. On the basis of these properties, geometrical representativity condition (expressed as the relative error) has been formulated – see relation (4.33). Furthermore, it has been postulated and numerically verified that the mean value (averaged over sufficient number of realizations), $\overline{S_2^{(i)}}$, evaluated for the size of RVE determined via relation (4.36), converges towards original two-point correlation function $S_2^{(i)}$, and hence, $\overline{S_2^{(i)}}$ can be treated as the *replica* of original function, $S_2^{(i)}$.

In the same manner the condition for the modified two-point correlation function can be formulated. Note, according to (5.36), the modified correlation function can be presented as:

$$S_2\left(t,\lambda_1,\lambda_2\right) = \left(\lambda_1 - \lambda_2\right)^2 \chi^{(1)}\left(t\right) + \overline{\left\langle \xi_\lambda \right\rangle}^2 \tag{5.40}$$

Taking into account (5.20) the above relation can be also rewritten as:

$$S_2\left(t,\lambda_1,\lambda_2\right) = \left(\lambda_1 - \lambda_2\right)^2 \left(S_2^{(1)}\left(t\right) - \phi_1^2\right) + \left(\lambda_1\phi_1 + \lambda_2\phi_2\right)^2 \tag{5.41}$$

It is evident, from the above relation, that the fixed points of the modified two-point correlation function are due to the fixed points of the two-point probability function, i.e.:

$$S_2\left(t \to 0, \lambda_1, \lambda_2\right) = \lambda_1^2 \phi_1 + \lambda_2^2 \phi_2 \tag{5.42}$$

and

$$S_2\left(t \to \infty, \lambda_1, \lambda_2\right) = \left(\lambda_1\phi_1 + \lambda_2\phi_2\right)^2 \tag{5.43}$$

The correlation length is defined, for given error of estimation ε, by the following condition:

$$\forall t \geq l_p\left(\varepsilon\right) \Rightarrow \left| \frac{S_2\left(t,\lambda_1,\lambda_2\right) - \left(\lambda_1\phi_1 + \lambda_2\phi_2\right)^2}{\left(\lambda_1\phi_1 + \lambda_2\phi_2\right)^2} \right| \leq \varepsilon \tag{5.44}$$

or equivalently, due to (5.41), as:

$$\forall t \geq l_p\left(\varepsilon\right) \Rightarrow \frac{\left(\lambda_1 - \lambda_2\right)^2 \phi_1^2}{\left(\lambda_1\phi_1 + \lambda_2\phi_2\right)^2} \left| \frac{S_2^{(1)}\left(t\right) - \phi_1^2}{\phi_1^2} \right| \leq \varepsilon \tag{5.45}$$

Since λ can attain values k or $1/k$, therefore, the correlation length is the maximum of two correlation lengths corresponding to Voigt and Reuss estimates, i.e.:

$$l_p\left(\varepsilon\right) = \max\left\{ l_p^{Voigt}\left(\varepsilon\right), l_p^{Reuss}\left(\varepsilon\right) \right\} \tag{5.46}$$

where:

$$\forall t \geq l_p^{Voigt}(\varepsilon) \Rightarrow \frac{(k_1 - k_2)^2 \phi_1^2}{(k_1\phi_1 + k_2\phi_2)^2} \left| \frac{S_2^{(1)}(t) - \phi_1^2}{\phi_1^2} \right| \leq \varepsilon \tag{5.47}$$

$$\forall t \geq l_p^{Reuss}(\varepsilon) \Rightarrow \frac{(1/k_1 - 1/k_2)^2 \phi_1^2}{(1/k_1\phi_1 + 1/k_2\phi_2)^2} \left| \frac{S_2^{(1)}(t) - \phi_1^2}{\phi_1^2} \right| \leq \varepsilon \tag{5.48}$$

It can be proved by introducing a parameter $\theta = k_2/k_1$ ($k_1 > 0$) that, due to (5.46), (5.47) and (5.48), the correlation length $l_p(\varepsilon)$ is the smallest value fulfilling the following relation:

$$\forall t \geq l_p(\varepsilon) \Rightarrow \max \left\{ \frac{(1-\theta)^2 \phi_1^2}{(\phi_1 + \theta\phi_2)^2}, \frac{\left(1 - \frac{1}{\theta}\right)^2 \phi_1^2}{\left(\phi_1 + \frac{1}{\theta}\phi_2\right)^2} \right\} \left| \frac{S_2^{(1)}(t) - \phi_1^2}{\phi_1^2} \right| \leq \varepsilon \tag{5.49}$$

The above relation can be simplified to more compact form by noting that, for $\theta \in (0,1]$, the following inequality holds true:

$$\frac{(1-\theta)^2 \phi_1^2}{(\phi_1 + \theta\phi_2)^2} \geq \frac{\left(1 - \frac{1}{\theta}\right)^2 \phi_1^2}{\left(\phi_1 + \frac{1}{\theta}\phi_2\right)^2} \tag{5.50}$$

Therefore

$$\max \left\{ \frac{(1-\theta)^2 \phi_1^2}{(\phi_1 + \theta\phi_2)^2}, \frac{\left(1 - \frac{1}{\theta}\right)^2 \phi_1^2}{\left(\phi_1 + \frac{1}{\theta}\phi_2\right)^2} \right\} = \frac{(1 - a(\theta))^2 \phi_1^2}{(\phi_1 + a(\theta)\phi_2)^2} \quad \text{where} \quad a(\theta) = \min\left\{\theta, \frac{1}{\theta}\right\} \tag{5.51}$$

and the correlation length $l_p(\varepsilon)$ is finally defined as:

$$\forall t \geq l_p(\varepsilon) \Rightarrow \frac{(1 - a(\theta))^2 \phi_1^2}{(\phi_1 + a(\theta)\phi_2)^2} \left| \frac{S_2^{(1)}(t) - \phi_1^2}{\phi_1^2} \right| \leq \varepsilon \tag{5.52}$$

Basing on considerations provided in previous chapter, one can conclude immediately, that in order to fit the fixed points of modified correlation function, the sample size, expressed in terms of the number of pixels, should satisfy the following inequality:

$$N_{\min} \geq 2l_p(\varepsilon) \tag{5.53}$$

The first fixed point, $S_2(t \to 0, \lambda_1, \lambda_2) = \lambda_1^2 \phi_1 + \lambda_2^2 \phi_2$, is always assured, since the mean value of volume fraction converges towards macroscopic volume fraction, regardless of the sample size

used. The condition resulting from the second fixed point is formulated in the same manner as in the previous chapter, i.e.:

$$\frac{\left|\left\langle \xi_\lambda^2 \right\rangle_{N_{min}} - S_2\left(l_p\left(\varepsilon\right), \lambda_1, \lambda_2\right)\right|}{S_2\left(l_p\left(\varepsilon\right), \lambda_1, \lambda_2\right)} = \frac{\left|\left\langle \xi_\lambda^2 \right\rangle_{N_{min}} - \overline{\left\langle \xi_\lambda \right\rangle}_{N_{min}}^2\right|}{\overline{\left\langle \xi_\lambda \right\rangle}_{N_{min}}^2} = \frac{Var\left\{\xi_\lambda\right\}}{\left(\lambda_1\phi_1 + \lambda_2\phi_2\right)^2} \leq \varepsilon \tag{5.54}$$

Taking into account the equation (5.39), the above inequality can be transformed to:

$$\frac{Var\left\{\xi_\lambda\right\}}{\left(\lambda_1\phi_1 + \lambda_2\phi_2\right)^2} = \frac{\left(\lambda_1 - \lambda_2\right)^2}{\left(\lambda_1\phi_1 + \lambda_2\phi_2\right)^2} Var\left\{\xi\right\} \leq \varepsilon \tag{5.55}$$

The above can be treated as the relative error of Voigt/Reuss estimate. The sample size should be simultaneously representative in the view of both estimates: Voigt and Reuss. Therefore the size of RVE should be evaluated as the maximum value of aforementioned estimates, i.e.:

$$\max\left\{\frac{\left(k_1 - k_2\right)^2}{\left(k_1\phi_1 + k_2\phi_2\right)^2}, \frac{\left(1/k_1 - 1/k_2\right)^2}{\left(1/k_1\phi_1 + 1/k_2\phi_2\right)^2}\right\} Var\left\{\xi\right\} \leq \varepsilon \tag{5.56}$$

Therefore, the general condition for minimum size of the sample assuring the satisfactory replica of both Voigt and Reuss modified two-point correlation functions is as follows:

$$\left\|\Omega_0\right\|^\# \geq \max\left[\left\|\Omega_0\right\|_{Voigt}; \left\|\Omega_0\right\|_{Reuss}; \left\|\Omega_0\right\|_{l_p}\right] \tag{5.57}$$

where

$$\left\|\Omega_0\right\|_{Voigt} = \frac{2\left|k_1 - k_2\right|}{\left(k_1\phi_1 + k_2\phi_2\right)} \sqrt{\frac{\int_0^a \int_0^b \left(S_2^{(1)}\left(t\right) - \phi_1^2\right)\left(a - t_x\right)\left(b - t_y\right)dxdy}{\varepsilon}} \tag{5.58}$$

$$\left\|\Omega_0\right\|_{Reuss} = \frac{2k_1k_2\left|\frac{1}{k_1} - \frac{1}{k_2}\right|}{\left(k_1\phi_2 + k_2\phi_1\right)} \sqrt{\frac{\int_0^a \int_0^b \left(S_2^{(1)}\left(t\right) - \phi_1^2\right)\left(a - t_x\right)\left(b - t_y\right)dxdy}{\varepsilon}} \tag{5.59}$$

and

$$\left\|\Omega_0\right\|_{l_p} = 4l_p^2\left(\varepsilon\right) \tag{5.60}$$

Note that the size of the sample, namely $\left\|\Omega_0\right\|_{Voigt}$ as well as $\left\|\Omega_0\right\|_{Reuss}$, can also be expressed – explicitly - as a function of contrast in mechanical properties , i.e.: $\Theta = \dfrac{k_2}{k_1}$. Then

$$\left\|\Omega_0\right\|_{\text{Voigt}} = \frac{2\left|1-\Theta\right|}{\left(\phi_1+\phi_2\Theta\right)}\sqrt{\frac{\int\limits_0^a\int\limits_0^b\left(S_2^{(1)}(t)-\phi_1^2\right)\left(a-t_x\right)\left(b-t_y\right)dxdy}{\varepsilon}} \tag{5.61}$$

$$\left\|\Omega_0\right\|_{\text{Reuss}} = \frac{2\left|1-\Theta\right|}{\left(\phi_2+\phi_1\Theta\right)}\sqrt{\frac{\int\limits_0^a\int\limits_0^b\left(S_2^{(1)}(t)-\phi_1^2\right)\left(a-t_x\right)\left(b-t_y\right)dxdy}{\varepsilon}} \tag{5.62}$$

Let us investigate, in addition, relation between minimum RVE size resulting from the criterion (5.57) and that from (4.36) proposed in the previous chapter.

First, note that:

$$\max\left\{\frac{\left(k_1-k_2\right)^2}{\left(k_1\phi_1+k_2\phi_2\right)^2},\frac{\left(1/k_1-1/k_2\right)^2}{\left(1/k_1\phi_1+1/k_2\phi_2\right)^2}\right\}Var\{\xi\}=\max\left\{\frac{\left(1-\theta\right)^2\phi_1^2}{\left(\phi_1+\theta\phi_2\right)^2},\frac{\left(1-1/\theta\right)^2\phi_1^2}{\left(\phi_1+1/\theta\phi_2\right)^2}\right\}\frac{Var\{\xi\}}{\phi_1^2} \tag{5.63}$$

By virtue of (5.51) and $\overline{\langle\xi\rangle}^2=\phi_1^2$, the above relation can be also presented as:

$$\max\left\{\frac{\left(k_1-k_2\right)^2}{\left(k_1\phi_1+k_2\phi_2\right)^2},\frac{\left(1/k_1-1/k_2\right)^2}{\left(1/k_1\phi_1+1/k_2\phi_2\right)^2}\right\}Var\{\xi\}=\frac{\left(1-a(\theta)\right)^2\phi_1^2}{\left(\phi_1+a(\theta)\phi_2\right)^2}\frac{Var\{\xi\}}{\overline{\langle\xi\rangle}^2} \tag{5.64}$$

Therefore the condition (5.56) is equivalent to:

$$\frac{\left(1-a(\theta)\right)^2\phi_1^2}{\left(\phi_1+a(\theta)\phi_2\right)^2}\frac{Var\{\xi\}}{\overline{\langle\xi\rangle}^2}\leq\varepsilon \tag{5.65}$$

or

$$\frac{Var\{\xi\}}{\overline{\langle\xi\rangle}^2}\leq\varepsilon b(\theta)\quad\text{with}\quad b(\theta)=\frac{\left(\phi_1+a(\theta)\phi_2\right)^2}{\left(1-a(\theta)\right)^2\phi_1^2} \tag{5.66}$$

The relation (5.52) for the correlation length $l_p(\varepsilon)$ can be presented also in a similar form:

$$\forall t\geq l_p(\varepsilon)\Rightarrow\left|\frac{S_2^{(1)}(t)-\phi_1^2}{\phi_1^2}\right|\leq\varepsilon b(\theta) \tag{5.67}$$

Now, comparing the definition (4.21) for correlation length $l_c(\varepsilon)$ with the definition (5.67) for correlation length $l_p(\varepsilon)$ one can immediately conclude that:

$$l_p(\varepsilon)=l_c\left(\varepsilon b(\theta)\right) \tag{5.68}$$

so

$$\left\|\Omega_o(\varepsilon)\right\|_{l_p}=\left\|\Omega_o\left(\varepsilon b(\theta)\right)\right\|_{l_c} \tag{5.69}$$

As a consequence of (5.66) and (4.33) we get:

$$\max \left[\left\| \Omega_0 \left(\varepsilon \right) \right\|_{\text{Voigt}} ; \left\| \Omega_0 \left(\varepsilon \right) \right\|_{\text{Reuss}} \right] = \max \left[\left\| \Omega_0 \left(\varepsilon b \left(\theta \right) \right) \right\|_{\xi} ; \left\| \Omega_0 \left(\varepsilon b \left(\theta \right) \right) \right\|_{\Psi} \right] \qquad (5.70)$$

Finally, comparing the criterion (5.57) with (4.36) the following final relation is obtained:

$$\left\| \Omega_0 \left(\varepsilon \right) \right\|^{\#} = \left\| \Omega_0 \left(\varepsilon b \left(\theta \right) \right) \right\|^{*} \qquad (5.71)$$

The above relation states that the minimum RVE size preserving the replica (with tolerance error ε) of modified two-point correlation function corresponds exactly to RVE size preserving replica of two-point probability function determined for tolerance error equated to $\varepsilon b \left(\theta \right)$.

It can be also shown, by simple arguments, that $b \left(\theta \right)$ is a monotonic function of $a \left(\theta \right)$ and its maximum is attained at $a \left(\theta \right) = 0$ whereas the minimum at $a \left(\theta \right) = 1$. More precisely:

$$a \left(\theta \right) = 0 \Rightarrow b \left(\theta \right) = 1 \quad \text{or} \quad \lim_{\substack{\theta \to 0 \\ \theta \to \infty}} b \left(\theta \right) = 1 \qquad (5.72)$$

$$\lim_{a(\theta) \to 1} b \left(\theta \right) = \infty \quad \text{or} \quad \lim_{\theta \to 1} b \left(\theta \right) = \infty \qquad (5.73)$$

The size of RVE which is determined on the basis of geometrical criterion (4.36) is the maximum one, i.e. the condition (5.57) yields the size of the sample which is - more or less - decreased depending on the value of Θ.

The condition (5.57) formulated in this chapter guarantees a satisfactory replica of the modified two-point correlation function if the size of the sample used fulfils the requirements of this criterion. The main goal of the thesis is, however, formulation of the condition for a sample size to be representative with respect to overall transport properties. Since the sample size determined according (5.57) guarantees, in addition, a satisfactory replica of microstructure morphology, with tolerance error $\varepsilon b \left(\theta \right)$, so it should also assure the proper determination of overall transport properties. So we postulate that a sample, fulfilling the criterion (5.57), is also representative with respect to overall transport properties. Numerical validation of this postulate is the aim of the chapter 6 of the thesis.

5.4. Analytical solution: checkerboard

Now let us recall the example of random checkerboard. Basing on this type of random microstructure the difference between two conditions will be presented. In what follows, we focus on the determination of the size of RVE to be representative with respect to overall transport properties.

Utilizing (3.48) as well as (3.49), the sample sizes, following Voigt and Reuss estimates, can be expressed as:

$$\left\|\Omega_0\right\|_{\text{Voigt}} = \frac{\left(k_1 - k_2\right)^2}{\left(k_1\left(1-p\right)+k_2 p\right)^2} \frac{p\left(1-p\right)}{\varepsilon}$$

$$\left\|\Omega_0\right\|_{\text{Reuss}} = \frac{\left(\dfrac{1}{k_1} - \dfrac{1}{k_2}\right)^2}{\left(\dfrac{1-p}{k_1} - \dfrac{p}{k_2}\right)^2} \frac{p\left(1-p\right)}{\varepsilon} \tag{5.74}$$

or in the equivalent form:

$$\left\|\Omega_0\right\|_{\text{Voigt}} = \frac{\left(1-\Theta\right)^2}{\left(1-p+p\Theta\right)^2} \frac{p\left(1-p\right)}{\varepsilon}$$

$$\left\|\Omega_0\right\|_{\text{Reuss}} = \frac{\left(1-\Theta\right)^2}{\left(p+\left(1-p\right)\Theta\right)^2} \frac{p\left(1-p\right)}{\varepsilon} \tag{5.75}$$

Furthermore, as it is shown in plots (Fig. 5.3, Fig. 5.4) of modified two-point correlation function, the correlation length $l_p = 1$. Substituting (5.75) in the relation (5.57) we obtain the final condition for the RVE size in case of random checkerboard, i.e.

$$\left\|\Omega_0\right\|^{\#} \geq \max\left[\frac{\left(1-\Theta\right)^2}{\left(1-p+p\Theta\right)^2} \frac{p\left(1-p\right)}{\varepsilon}; \ \frac{\left(1-\Theta\right)^2}{\left(p+\left(1-p\right)\Theta\right)^2} \frac{p\left(1-p\right)}{\varepsilon}; \ 4\right] \tag{5.76}$$

Assuming that RVE is a square shape digital image, one can express the size of RVE in terms of the number of pixels in a row and in a column, $N^{\#} = \sqrt{\left\|\Omega_0\right\|^{\#}}$, and hence:

$$N^{\#} \geq \max\left[\frac{\left|1-\Theta\right|}{\left(1-p+p\Theta\right)}\sqrt{\frac{p\left(1-p\right)}{\varepsilon}}; \ \frac{\left|1-\Theta\right|}{\left(p+\left(1-p\right)\Theta\right)}\sqrt{\frac{p\left(1-p\right)}{\varepsilon}}; \ 2\right] \tag{5.77}$$

In Fig. 5.3, S_2^{Voigt} as well as S_2^{Reuss} are plotted against the distance r which is expressed in pixels. Note, these functions were evaluated with assumption that $k_1 = 1$, and therefore $k_2 = \Theta$. Only two plots presenting the case of volume fraction 0.1 as well as $\Theta = 5$ and $\Theta = 10$ are presented.

In Figs. 5.4-5.6 the size of RVE corresponding to criterion (5.77) is plotted against the contrast in mechanical properties, $\Theta = \dfrac{k_2}{k_1}$. The results correspond to different values of volume fraction p and error ε.
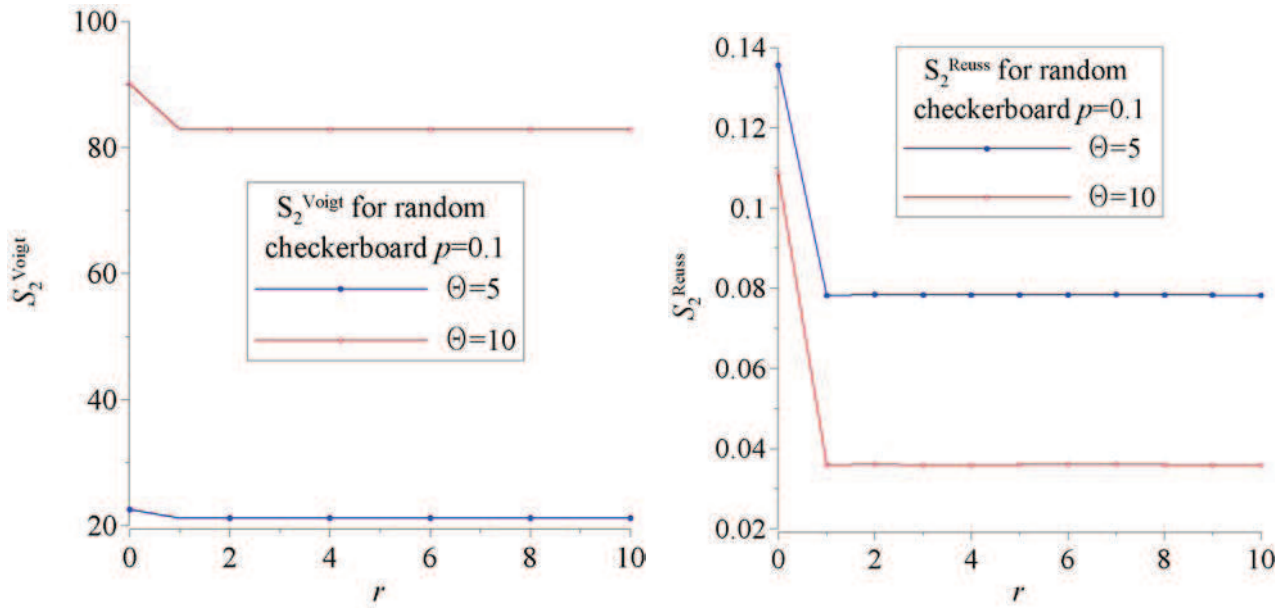
Fig. 5.3. Modified two-point correlation function; left: S_2^{Voigt}, right: S_2^{Reuss}.
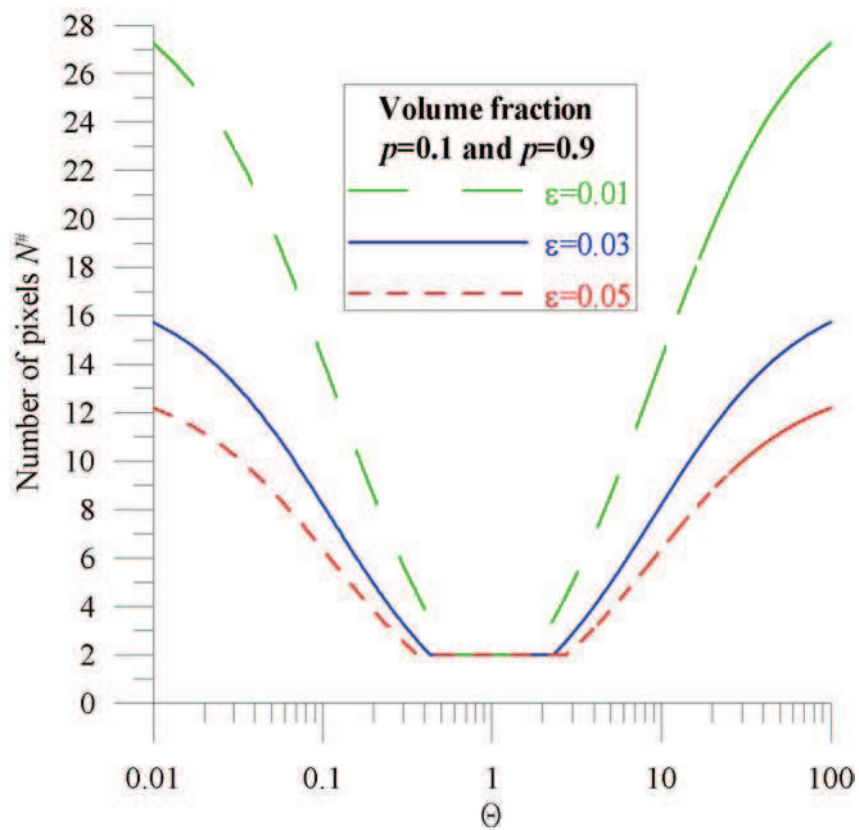
Fig. 5.4. The size of RVE plotted against the contrast in properties Θ (p=0.1).
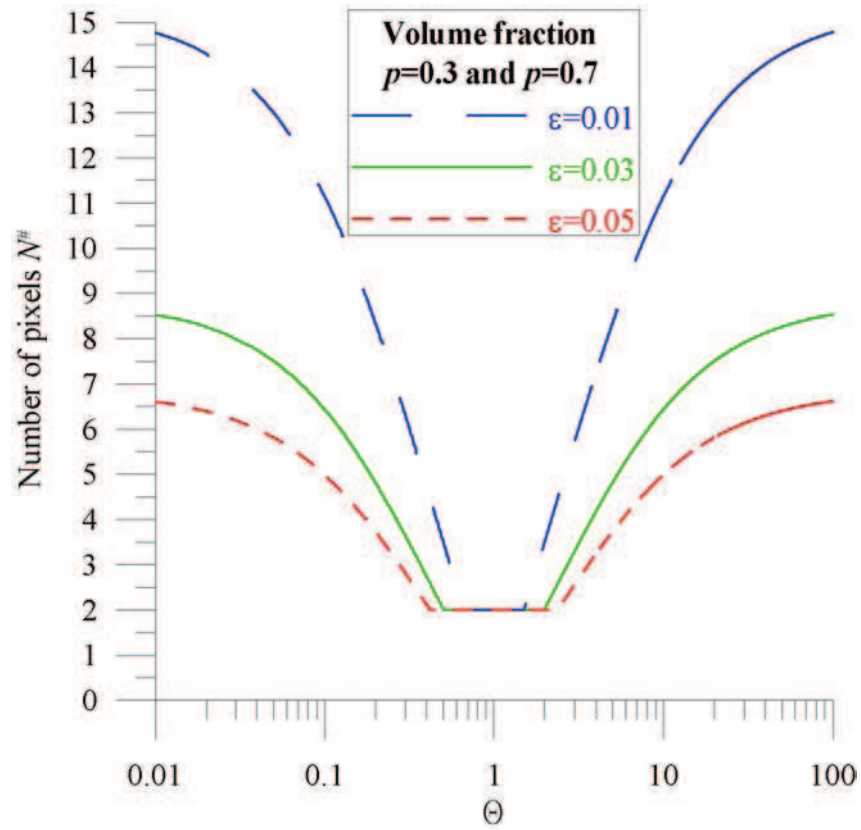
Fig. 5.5. The size of RVE plotted against the contrast in properties Θ (*p*=0.3).
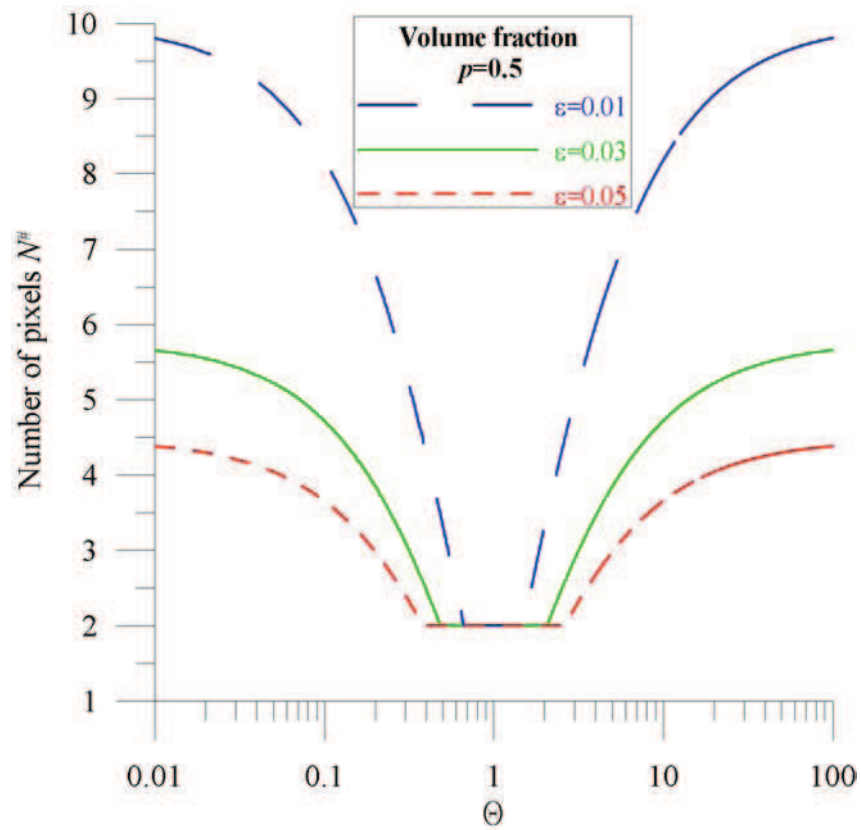
Fig. 5.6. The size of RVE plotted against the contrast in properties Θ (*p*=0.5).

As it was in case of geometrical representativity condition, one can observe that the larger value of ε, the smaller RVE size is evaluated to be representative. Moreover, note that the condition (5.77) is a symmetrical function of Θ. with the symmetry axis in $\Theta = 1$. It means that for fixed value of p, the size of RVE is the same for the value of contrast Θ and $\frac{1}{\Theta}$.

Figures 5.7-5.10 present the number of pixels $N^{\#}$ plotted against the value of volume fraction p. Each graph provides the results obtained for different values of contrast in mechanical properties, i.e. Θ ranges from 10 up to 1000. The results correspond to the value of error ε=0.01. Note, that each figure provides, in addition, the number of pixels N^* determined according to geometrical representativity criterion (4.36). Observing results one can simply notice that the number of pixels is a symmetrical function of p having symmetry axis in p=0.5. It can be also seen that the larger value of Θ, the larger size of RVE is required. Furthermore, we see that the size of RVE, determined on the basis of criterion (5.77), is never larger than the one obtained from the geometrical representativity condition, however, the value of $N^{\#}$ strongly depends on the contrast in mechanical properties, i.e. for $\Theta = 10$ we have that $N^{\#} \ll N^*$ while in case of $\Theta = 1000$ both criterions yield almost the same result, i.e. $N^{\#} \approx N^*$.
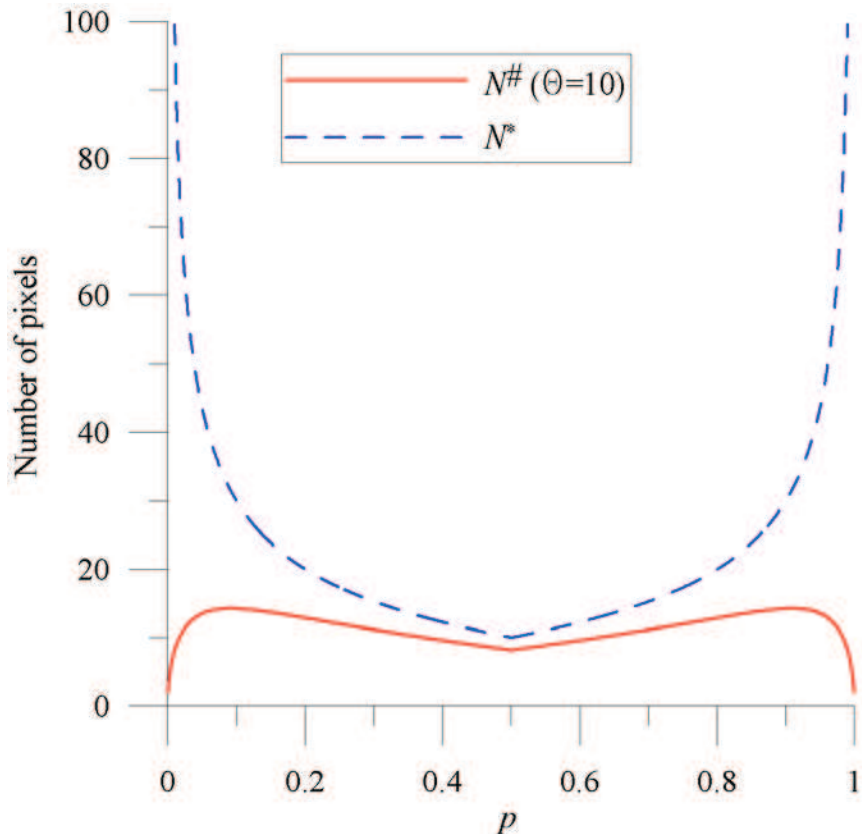
Fig. 5.7. The sizes of RVE $N^{\#}$ (Θ=10) and N^* plotted against the volume fraction p.
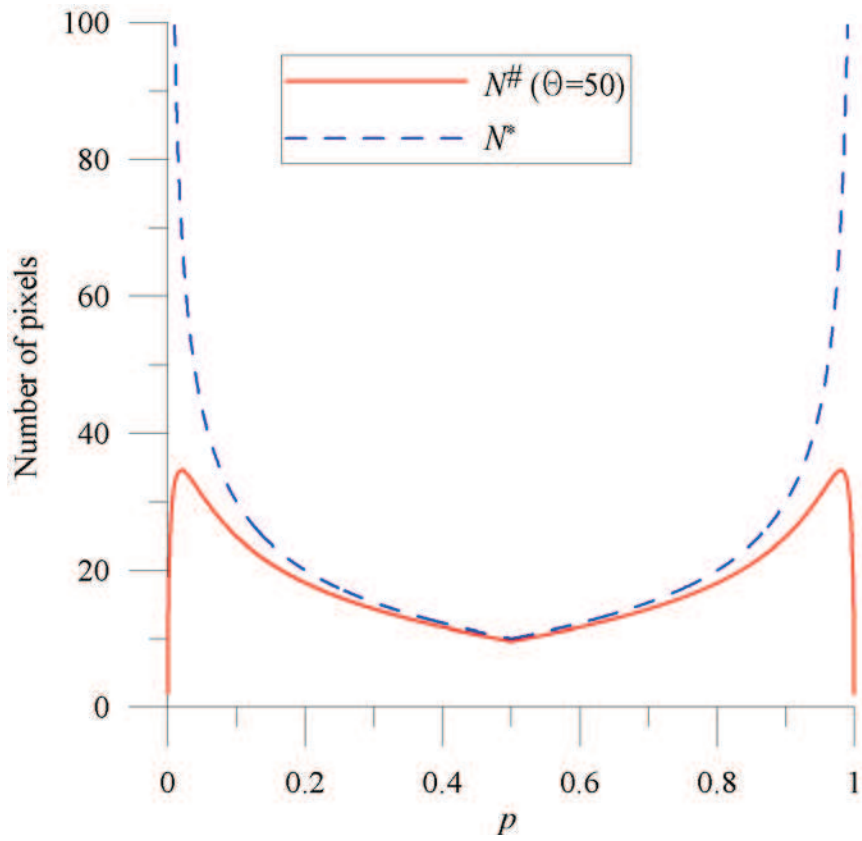
Fig. 5.8. The sizes of RVE $N^{\#}$ (Θ=50) and N^{*} plotted against the volume fraction p.
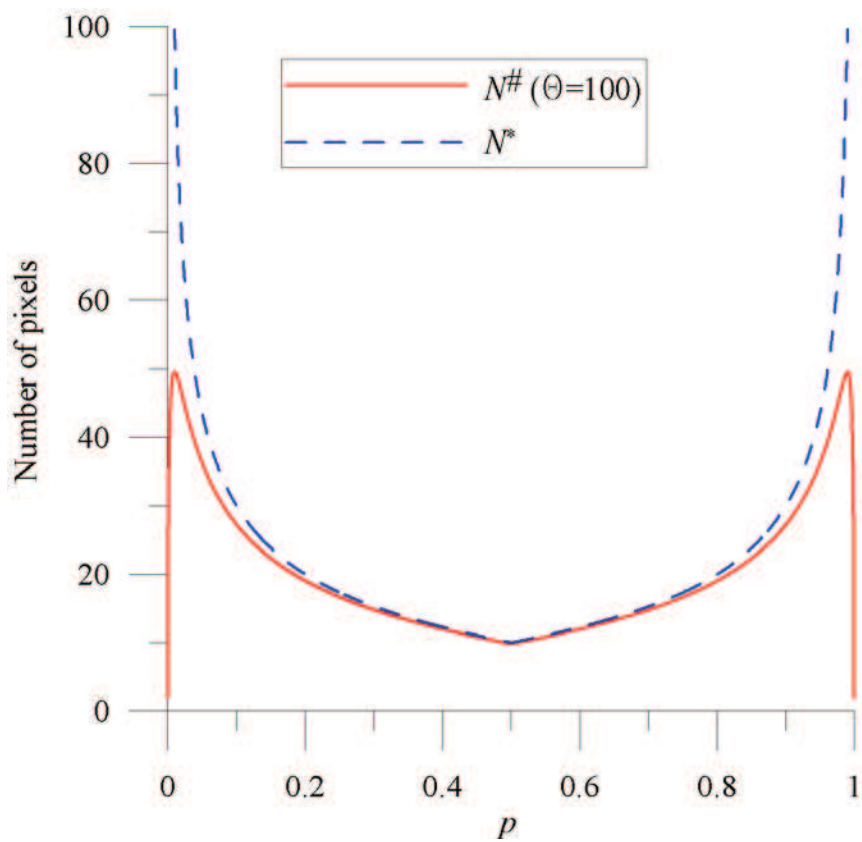
Fig. 5.9. The sizes of RVE $N^{\#}$ (Θ=100) and N^{*} plotted against the volume fraction p.
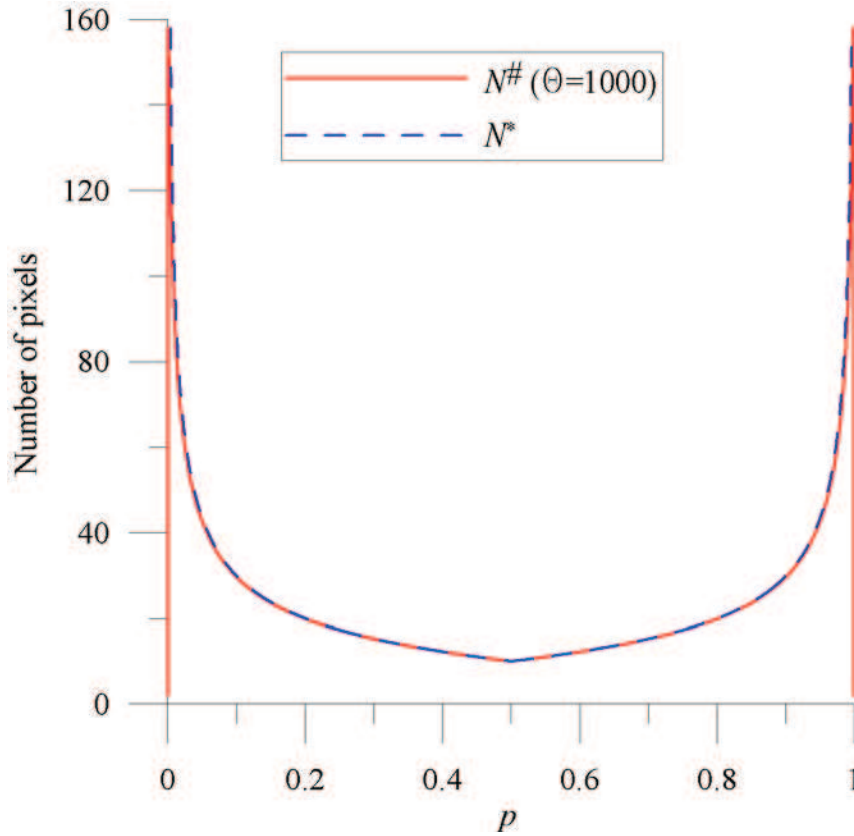
Fig. 5.10. The sizes of RVE $N^{\#}$ (Θ=1000) and N^{*} plotted against the volume fraction p.

Note that regardless of Θ the difference between $N^{\#}$ and N^{*} can be observed in case of limiting values of p, i.e. when $p \rightarrow 0$ and $p \rightarrow 1$. To understand this fact, one should imagine the microstructure with the volume fraction $\phi_2 \approx 0$ ($\phi_2 \approx 1$). Then the probability of finding phase 2 in arbitrary localization is $p \approx 0 \, (1 - p \approx 1)$. Therefore, considering geometrical representativity, the size of RVE, N^{*}, should be very large in order to be representative for phase 2. On the other hand, if one focuses on mechanical properties of such microstructure it is obvious that effective property is nearly equal that of phase 1, i.e. $K^{\mathrm{eff}} \approx k_1$, and hence, the size of RVE, $N^{\#}$, can consist even of only one pixel – we find phase 1 with approximately 100% probability.

Once again it should be emphasized that – if digital images are considered - the size of RVE has to be an integer value. The smallest possible RVE size is 1 pixel. In Fig. 5.11 the size of RVE, given by $N = \lfloor N^{\#} \rfloor + 1$, is plotted against the volume fraction p. The results presented in figure below correspond to the ones displayed in Fig. 5.7. Note, due to the symmetry axis (p=0.5) p ranges from 0 to 0.5.
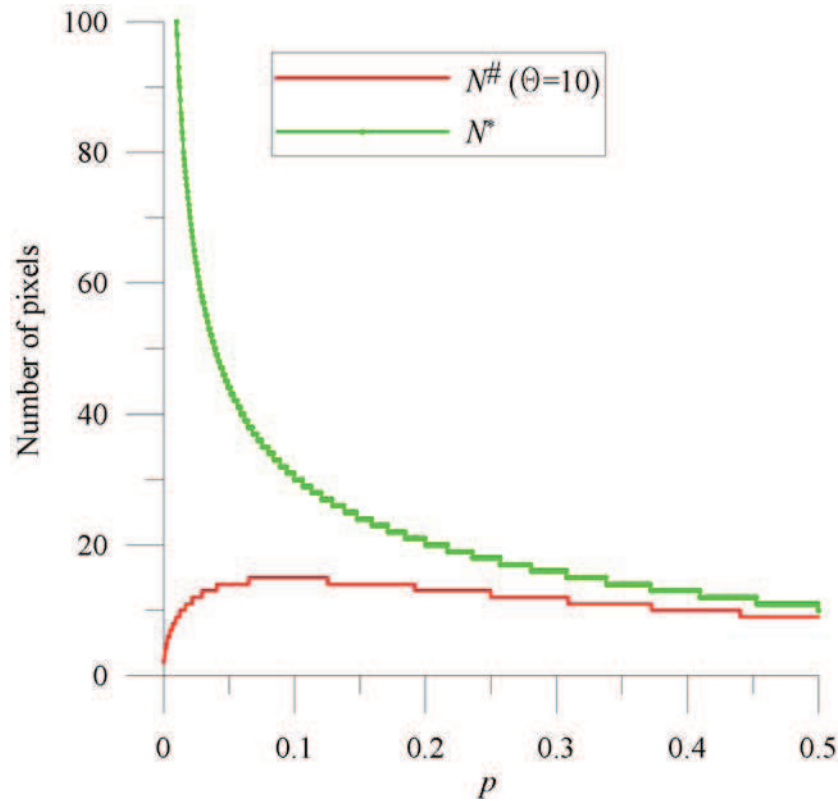
Fig. 5.11. The size of RVE given by $N = \lfloor N^{\#} \rfloor + 1$ as a function of volume fraction p.

5.5. Remarks

A lot of attempt has been made recently in order to quantify the RVE on the basis of statistical and numerical analysis. Stroeven *et al.* (2004) proposed an approach to quantify the size of RVE on the basis of *Student-t* distribution properties. Gitman *et al.* (2007) have formulated an algorithm based on the simple *Chi-square* criterion. None of them however involves information on microstructure morphology. The method which incorporates information on microstructure is the one formulated by Kanit *et al.* (2003). Within proposed method the notion of integral range plays a central role. The definition of aforementioned microstructural descriptor is given by (5.11).

The general disadvantage of all these methods is that they involve, in order to determine the size of RVE, a large number of numerical calculations, for instance the one of finite element. Therefore, within this chapter, an original method providing the RVE size with respect to overall transport properties has been formulated. The condition has been derived based on a modified two-point correlation function. This function, in contrast to two-point probability function, i.e. $S_2^{(i)}(r)$, depends not only on the distance between two points r, but also on mechanical properties associated with medium phases.

Within proposed method the general requirement is that

$$\max\left[\frac{\text{Var}\{\xi_k\}}{\langle\xi_k\rangle^2};\frac{\text{Var}\{\xi_{1/k}\}}{\langle\xi_{1/k}\rangle^2}\right]\leq\varepsilon \tag{5.78}$$

where $\text{Var}\{\xi_k\}$ and $\text{Var}\{\xi_{1/k}\}$ are the variances of local Voigt and Reuss estimate, respectively. Furthermore, $\overline{\langle\xi_k\rangle}=k_1\phi_1+k_2\phi_2$ and $\overline{\langle\xi_{1/k}\rangle}=\frac{1}{k_1}\phi_1+\frac{1}{k_2}\phi_2$ - see relation (5.20).

It has been derived that the variances of local Voigt and Reuss estimates are related to the variance of local porosity by relation (5.39). The above implies that the minimum RVE size resulting from (5.78) can be successfully evaluated on the basis of local volume fraction variance and therefore an integral (4.18) plays a central role. As in case of geometrical representativity condition, it is also postulated that the sample size should be larger than or equal to two times correlation length l_p of modified two-point correlation function. Note that l_p is treated as the maximum of two correlation lengths corresponding to S_2^{Voigt} and S_2^{Reuss} (see (5.52)). Therefore, the final form of the condition for the minimum size of RVE with respect to overall transport properties is the maximum value of three quantities, i.e. $\|\Omega_0\|^\# \geq \max\left[\|\Omega_0\|_{\text{Voigt}};\|\Omega_0\|_{\text{Reuss}};\|\Omega_0\|_{l_p}\right]$ - see relations (5.58), (5.59) and (5.60).

It has been also pointed out that the geometrical criterion, derived in chapter 4, yields the maximum sample size, whereas, the size of RVE established on the basis of condition based on modified two-point correlation function can only be decreased depending on the value of contrast in mechanical properties.

One can expect a large advantage comparing proposed method to other methods which were briefly presented in the beginning of this chapter. It should be strongly emphasized that within proposed algorithm none numerical simulations (finite element, etc.) are necessary in order to determine the size of RVE. Within the method proposed in this work, the minimum size can be simply evaluated basing on the morphology of microstructure expressed by two-point correlation function.

Next chapter provides a numerical validation of proposed methodology.

6. Numerical validation of the sample representativity criterion

In what follows a validation of the condition regarding the sample representativity with respect to overall transport properties is provided. The method proposed in previous chapter is verified on the basis of several numerical calculations. As in case of geometrical representativity criterion, two different groups of two-phase microstructures, namely *random cell models* as well as *reconstructed microstructures* are considered. The results are presented in the same order as in section 4.3, i.e. random checkerboard, Ising model based microstructure, system of overlapping disks, system of non-overlapping disks, Debye and modified Debye random medium, Fontainebleau sandstone, boron-carbide/aluminum composite.

Before results are provided, in next section the numerical technique, utilized for the purpose of validation tests, is formulated. The numerical method is devoted to the solution of the boundary value problem (2.6). It should be mentioned that, in particular, the methodology, outlined below, is available for use on digital images.

6.1. Pixel based finite volume scheme

There exist nowadays a large number of techniques which provide the images of real materials, e.g. synchrotron-based tomography, magnetic resonance imaging, scanning tunnelling electron microscopy or confocal microscopy. In general, these techniques provide two- or three-dimensional images of considered materials. Such digital images are usually regarded as the collections of non-overlapping elements (pixels in 2D; voxels in 3D) having marked colour intensities which indicate the material phases (Garboczi *et al.* 1999). The size of pixel (voxel) characterizes the spatial resolution of image, i.e. if the size of pixel (voxel) decreases (the number of pixels (voxels) per unit length increases) the spatial resolution of image increases.

Digital images are usually a grey-scale ones, i.e. the pixels (voxels) can have up to 256 different intensities (shades of grey colour) varying from black (0) to white (255) – see Fig. 6.1 (left panel). In case of two-phase materials the grey-scale images are often reduced to binary ones. The process which turns grey-scale image into binary one is referred to as the *thresholding*. This procedure

consists in assigning white colour to the pixel if the grey value is lighter than the threshold one or the black colour otherwise (see right panel of Fig. 6.1).

First attempts (made by author) in order to solve the boundary value problem (2.6) have been based on the re-formulation of the *Generalized Method of Cells* (GMC) which had been first proposed by Aboudi (1991). GMC has been originally formulated for elastic composites (for more details, see: Paley & Aboudi 1992; Aboudi 1995; Łydżba *et al.* 2007). Nevertheless, due to some deficiencies of this method, which have been widely studied by Gan *et al.* (2000), the application of this method to the boundary value problem (2.6) has been failed. Finally, the method which is provided below, is based on the *Finite Volume Method* (FVM). Note that the finite volume scheme is often referred to as the "*cell centred difference scheme*" (Eymard et al., 2003).
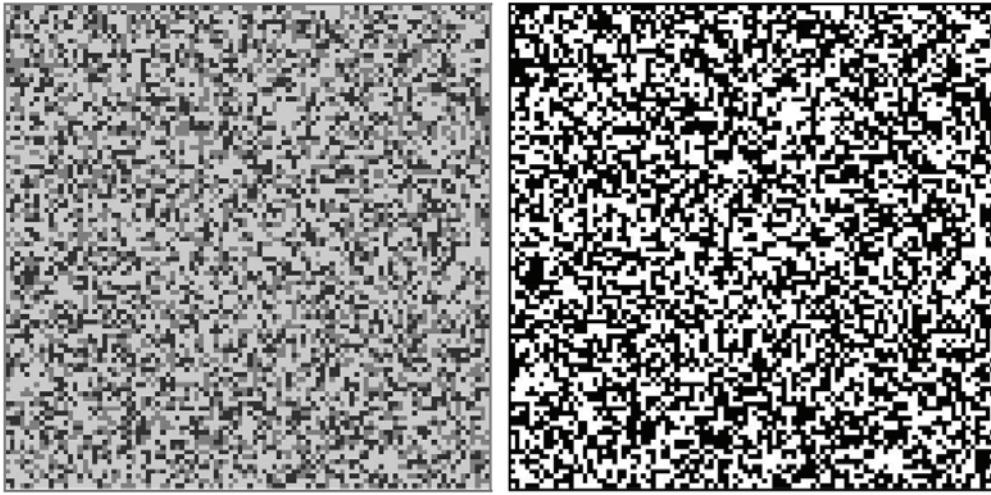
Fig. 6.1. Digital images – left: grey-scale image obtained from a specific random process; right: the same image after thresholding procedure

Consider now a certain RVE which is composed of large number of voxels such that each (α, β, γ) voxel contains only one material of constitutive properties. The number of voxels in the volume is $N_\alpha N_\beta N_\gamma$. The lengths of a single voxel edges are l_α, l_β, l_γ which corresponds to the local coordinate axis y_1, y_2, y_3, respectively (Fig. 6.2).

Recall now the mass conservation equation (2.4) which describes the diffusion process presented in section 2.1. According to the finite volume scheme this equation must be satisfied for each voxel (control volume), i.e.:

$$\frac{\partial q_i^{(\alpha,\beta,\gamma)}}{\partial y_i} = 0 \tag{6.1}$$

where $q_i^{(\alpha,\beta,\gamma)}$ is a y_i component of the mass flux vector of the diffusing substance, whereas y_i is a local coordinate axis with origin in the central point of (α, β, γ) voxel.
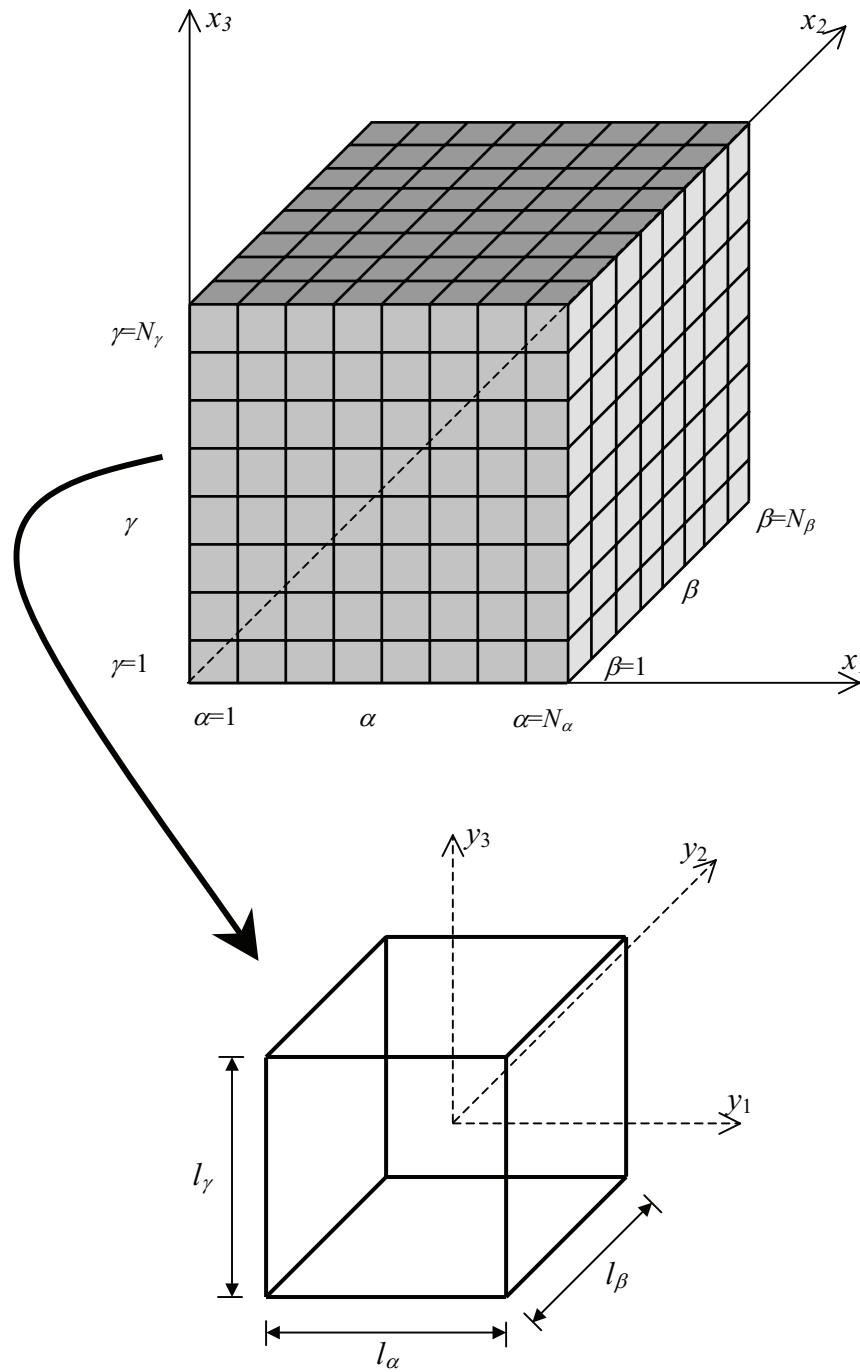
Fig. 6.2. Top: RVE composed of a large number of voxels; bottom: single (α, β, γ) voxel.

Following the divergence theorem, which relates the outward flux of a vector field through a surface to a volume integral of divergence on the region inside the surface, equation (6.1) can be rewritten in the equivalent form:

$$\int\limits_{S_1^+} q_i^{(\alpha,\beta,\gamma)} n_i dS + \int\limits_{S_1^-} q_i^{(\alpha,\beta,\gamma)} n_i dS + \int\limits_{S_2^+} q_i^{(\alpha,\beta,\gamma)} n_i dS +$$

$$+ \int\limits_{S_2^-} q_i^{(\alpha,\beta,\gamma)} n_i dS + \int\limits_{S_3^+} q_i^{(\alpha,\beta,\gamma)} n_i dS + \int\limits_{S_3^-} q_i^{(\alpha,\beta,\gamma)} n_i dS = 0 \tag{6.2}$$

In the equation above n_i stands for the y_i component of the unit normal vector and $S_i^{\pm}$ describes the surface of voxel's side which is perpendicular to local coordinate y_i. The superscript "+" ("-") appears when the outward-pointing normal vector n_i possesses the same (opposite) orientation as y_i (Fig. 6.3).
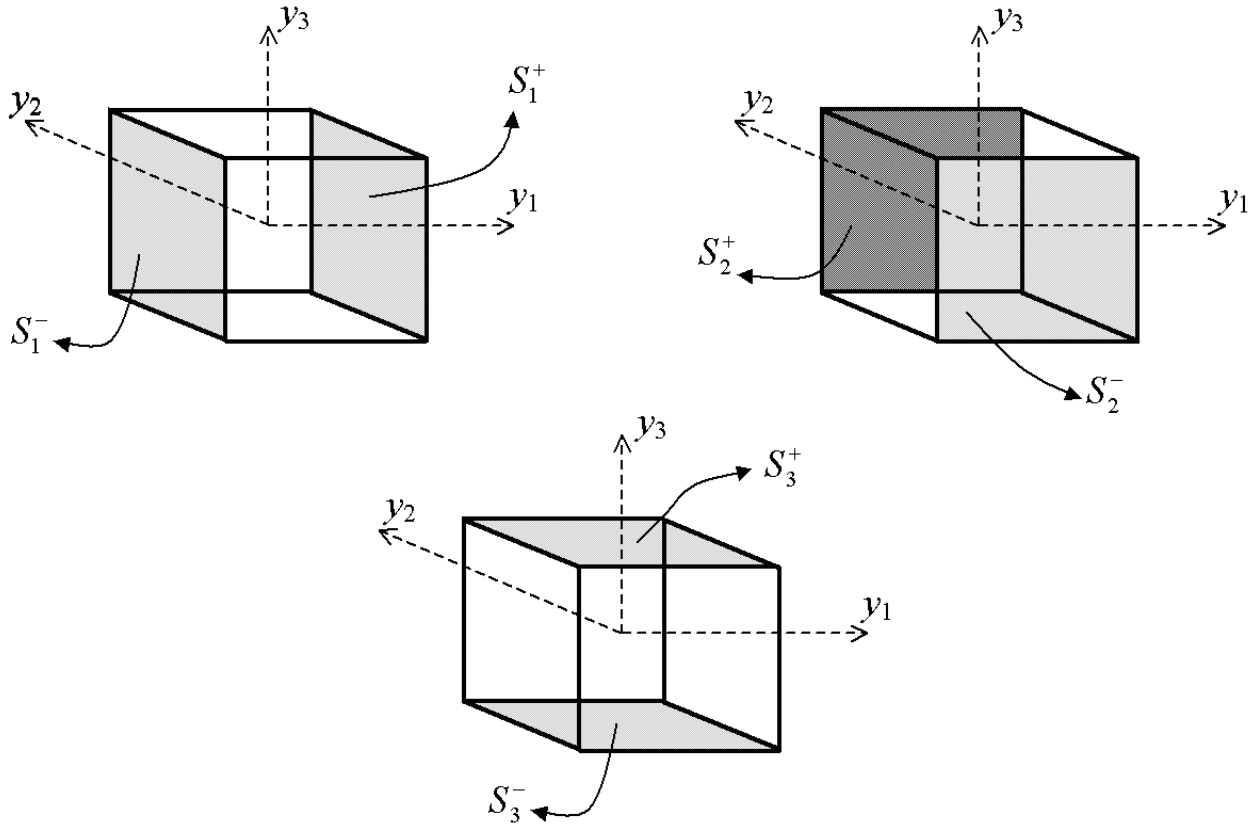
Fig. 6.3. Single (α, β, γ) voxel and notations

For brevity of further considerations it is assumed that voxels (control volumes) as well as RVE are cubes. Hence: $l_\alpha = l_\beta = l_\gamma = l$ and $N_\alpha = N_\beta = N_\gamma = N$. Then, performing some simple algebraic transformations equation (6.2) can be written as:

$$\left\langle q_1^{(\alpha,\beta,\gamma)} \right\rangle_{S_1^+} - \left\langle q_1^{(\alpha,\beta,\gamma)} \right\rangle_{S_1^-} + \left\langle q_2^{(\alpha,\beta,\gamma)} \right\rangle_{S_2^+} - \left\langle q_2^{(\alpha,\beta,\gamma)} \right\rangle_{S_2^-} + \left\langle q_3^{(\alpha,\beta,\gamma)} \right\rangle_{S_3^+} - \left\langle q_3^{(\alpha,\beta,\gamma)} \right\rangle_{S_3^-} = 0 \tag{6.3}$$

where $<*>_S$ is the surface averaging operator.
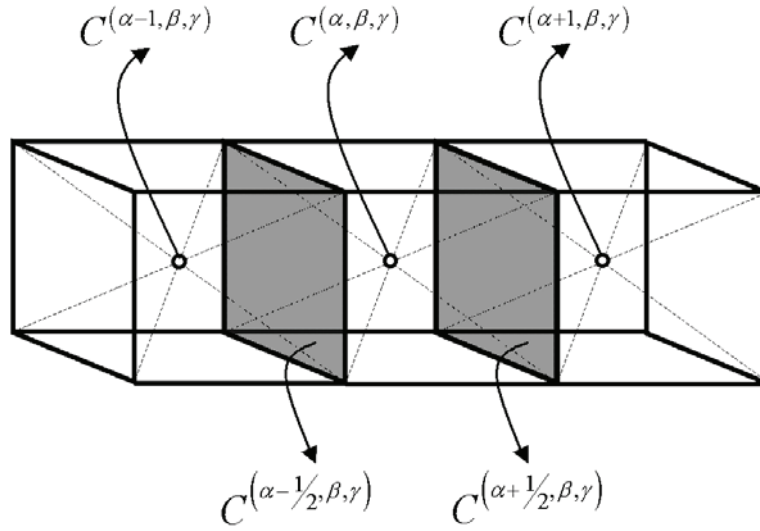
Fig. 6.4. Approximation of concentration C between voxels

Consider now the continuity of the fluxes on the interfaces between neighbouring voxels in y_1 direction. Let introduce auxiliary unknowns $C^{(\alpha-\frac{1}{2},\beta,\gamma)}$ and $C^{(\alpha+\frac{1}{2},\beta,\gamma)}$ which are approximations of C on the interfaces across control volumes (Fig. 6.4). Then, using the finite difference principle, expressions regarding the continuity of the fluxes, can be written in the following form:

$$-D^{(\alpha-1,\beta,\gamma)}\frac{C^{(\alpha-\frac{1}{2},\beta,\gamma)}-C^{(\alpha-1,\beta,\gamma)}}{l/2} = -D^{(\alpha,\beta,\gamma)}\frac{C^{(\alpha,\beta,\gamma)}-C^{(\alpha-\frac{1}{2},\beta,\gamma)}}{l/2} \tag{6.4}$$

$$-D^{(\alpha,\beta,\gamma)}\frac{C^{(\alpha+\frac{1}{2},\beta,\gamma)}-C^{(\alpha,\beta,\gamma)}}{l/2} = -D^{(\alpha+1,\beta,\gamma)}\frac{C^{(\alpha+1,\beta,\gamma)}-C^{(\alpha+\frac{1}{2},\beta,\gamma)}}{l/2} \tag{6.5}$$

Equations (6.4) and (6.5) yield the values of concentration C on the interfaces:

$$C^{(\alpha-\frac{1}{2},\beta,\gamma)} = \frac{D^{(\alpha-1,\beta,\gamma)}C^{(\alpha-1,\beta,\gamma)}+D^{(\alpha,\beta,\gamma)}C^{(\alpha,\beta,\gamma)}}{D^{(\alpha-1,\beta,\gamma)}+D^{(\alpha,\beta,\gamma)}} \tag{6.6}$$

$$C^{(\alpha+\frac{1}{2},\beta,\gamma)} = \frac{D^{(\alpha,\beta,\gamma)}C^{(\alpha,\beta,\gamma)}+D^{(\alpha+1,\beta,\gamma)}C^{(\alpha+1,\beta,\gamma)}}{D^{(\alpha,\beta,\gamma)}+D^{(\alpha+1,\beta,\gamma)}} \tag{6.7}$$

Utilizing (6.6) and (6.7) the formulas representing the fluxes across S_1^+ and S_1^- take the following form:

$$\begin{aligned}
\left\langle q_1^{(\alpha,\beta,\gamma)}\right\rangle_{S_1^+} &= -\frac{2D^{(\alpha,\beta,\gamma)}D^{(\alpha+1,\beta,\gamma)}}{D^{(\alpha,\beta,\gamma)}+D^{(\alpha+1,\beta,\gamma)}}\frac{C^{(\alpha+1,\beta,\gamma)}-C^{(\alpha,\beta,\gamma)}}{l} \\
\left\langle q_1^{(\alpha,\beta,\gamma)}\right\rangle_{S_1^-} &= -\frac{2D^{(\alpha-1,\beta,\gamma)}D^{(\alpha,\beta,\gamma)}}{D^{(\alpha-1,\beta,\gamma)}+D^{(\alpha,\beta,\gamma)}}\frac{C^{(\alpha,\beta,\gamma)}-C^{(\alpha-1,\beta,\gamma)}}{l}
\end{aligned} \tag{6.8}$$

Note that equations (6.8) involve the harmonic mean value of D. Such approximation is widely used in case of composite materials due to its well handling of abrupt property changes by keeping

"good" representation of the flux across interfaces (Patankar 1980; Eymard *et al.* 2003; Prapainop & Maneeratana 2004).

By the analogy to (6.8) the fluxes across $S_2^\pm$ and $S_3^\pm$ interfaces can be defined as:

$$
\begin{aligned}
\left\langle q_2^{(\alpha,\beta,\gamma)} \right\rangle_{S_2^+} &= -\frac{2D^{(\alpha,\beta,\gamma)}D^{(\alpha,\beta+1,\gamma)}}{D^{(\alpha,\beta,\gamma)}+D^{(\alpha,\beta+1,\gamma)}}\frac{C^{(\alpha,\beta+1,\gamma)}-C^{(\alpha,\beta,\gamma)}}{l} \\[2mm]
\left\langle q_2^{(\alpha,\beta,\gamma)} \right\rangle_{S_2^-} &= -\frac{2D^{(\alpha,\beta-1,\gamma)}D^{(\alpha,\beta,\gamma)}}{D^{(\alpha,\beta-1,\gamma)}+D^{(\alpha,\beta,\gamma)}}\frac{C^{(\alpha,\beta,\gamma)}-C^{(\alpha,\beta-1,\gamma)}}{l} \\[2mm]
\left\langle q_3^{(\alpha,\beta,\gamma)} \right\rangle_{S_3^+} &= -\frac{2D^{(\alpha,\beta,\gamma)}D^{(\alpha,\beta,\gamma+1)}}{D^{(\alpha,\beta,\gamma)}+D^{(\alpha,\beta,\gamma+1)}}\frac{C^{(\alpha,\beta,\gamma+1)}-C^{(\alpha,\beta,\gamma)}}{l} \\[2mm]
\left\langle q_3^{(\alpha,\beta,\gamma)} \right\rangle_{S_3^-} &= -\frac{2D^{(\alpha,\beta,\gamma-1)}D^{(\alpha,\beta,\gamma)}}{D^{(\alpha,\beta,\gamma-1)}+D^{(\alpha,\beta,\gamma)}}\frac{C^{(\alpha,\beta,\gamma)}-C^{(\alpha,\beta,\gamma-1)}}{l}
\end{aligned}
\tag{6.9}
$$

Substituting now (6.8) and (6.9) in the relation (6.3) leads to:

$$
\begin{aligned}
&a^{(\alpha+1,\beta,\gamma)}C^{(\alpha+1,\beta,\gamma)} + a^{(\alpha-1,\beta,\gamma)}C^{(\alpha-1,\beta,\gamma)} + a^{(\alpha,\beta+1,\gamma)}C^{(\alpha,\beta+1,\gamma)} + \\
&+a^{(\alpha,\beta-1,\gamma)}C^{(\alpha,\beta-1,\gamma)} + a^{(\alpha,\beta,\gamma+1)}C^{(\alpha,\beta,\gamma+1)} + a^{(\alpha,\beta,\gamma-1)}C^{(\alpha,\beta,\gamma-1)} - \\
&-\left(a^{(\alpha+1,\beta,\gamma)} + a^{(\alpha-1,\beta,\gamma)} + a^{(\alpha,\beta+1,\gamma)} + a^{(\alpha,\beta-1,\gamma)} + a^{(\alpha,\beta,\gamma+1)} + a^{(\alpha,\beta,\gamma-1)}\right)C^{(\alpha,\beta,\gamma)} = 0
\end{aligned}
\tag{6.10}
$$

where for given (α, β, γ) voxel:

$$
a^{(p,q,r)} = -\frac{1}{l}\left(\frac{2D^{(\alpha,\beta,\gamma)}D^{(p,q,r)}}{D^{(\alpha,\beta,\gamma)}+D^{(p,q,r)}}\right)
\tag{6.11}
$$

Relations (6.8) and (6.9) are valid for "interior" voxels, i.e. the ones for which $\alpha = 2,...,N-1$, $\beta = 2,...,N-1$ and $\gamma = 2,...,N-1$, and hence (6.10) is a system of $(N-2)^3$ equations. Nevertheless, the number of unknown values of concentration C is N^3. Missing $(6N^2 - 12N + 8)$ equations are determined by involving "exterior" voxels ($\alpha = 1$, $\alpha = N$, $\beta = 1$, $\beta = N$, $\gamma = 1$, $\gamma = N$) in the relation (6.3). In this case, in addition, the boundary conditions are taken into account. Three different types of boundary conditions with regard to the concentration C can be imposed on ∂V_{RVE}, i.e. uniform gradient of concentration (UGBC), uniform mass flux (UFBC) or periodic boundary conditions (PBC). None the less, in this work only PBC are studied. It results from the fact that this type of boundary conditions best simulates the infinite medium limit – the RVE is regarded as the unit cell which is repeated in all directions forming the infinite continuous body. Furthermore, the mechanical response obtained for PBC is always between the ones determined for UGBC and UFBC.

Taking into account PBC, the fluxes on opposite faces of RVE are equal, and hence they can be written in the following form:

$$\left\langle q_1^{(1,\beta,\gamma)} \right\rangle_{S_1^-} = \left\langle q_1^{(N,\beta,\gamma)} \right\rangle_{S_1^+} = -\frac{2D^{(1,\beta,\gamma)}D^{(N,\beta,\gamma)}}{D^{(1,\beta,\gamma)}+D^{(N,\beta,\gamma)}} \frac{C^{(1,\beta,\gamma)}-C^{(N,\beta,\gamma)}+\left\langle G_1 \right\rangle Nl}{l}$$

$$\left\langle q_2^{(\alpha,1,\gamma)} \right\rangle_{S_2^-} = \left\langle q_2^{(\alpha,N,\gamma)} \right\rangle_{S_2^+} = -\frac{2D^{(\alpha,1,\gamma)}D^{(\alpha,N,\gamma)}}{D^{(\alpha,1,\gamma)}+D^{(\alpha,N,\gamma)}} \frac{C^{(\alpha,1,\gamma)}-C^{(\alpha,N,\gamma)}+\left\langle G_2 \right\rangle Nl}{l} \qquad (6.12)$$

$$\left\langle q_3^{(\alpha,\beta,1)} \right\rangle_{S_3^-} = \left\langle q_3^{(\alpha,\beta,N)} \right\rangle_{S_3^+} = -\frac{2D^{(\alpha,\beta,1)}D^{(\alpha,\beta,N)}}{D^{(\alpha,\beta,1)}+D^{(\alpha,\beta,N)}} \frac{C^{(\alpha,\beta,1)}-C^{(\alpha,\beta,N)}+\left\langle G_3 \right\rangle Nl}{l}$$

where $\left\langle G_i \right\rangle$ stands for the x_i component of macroscopic gradient of concentration C. For instance, the mass conservation equation (6.3) in case of $(1,1,1)$ voxel has the following form:

$$a^{(2,1,1)}C^{(2,1,1)}+a^{(N,1,1)}C^{(N,1,1)}+a^{(1,2,1)}C^{(1,2,1)}+a^{(1,N,1)}C^{(1,N,1)}+a^{(1,1,2)}C^{(1,1,2)}+$$

$$+a^{(1,1,N)}C^{(1,1,N)}-\left(a^{(2,1,1)}+a^{(N,1,1)}+a^{(1,2,1)}+a^{(1,N,1)}+a^{(1,1,2)}+a^{(1,1,N)}\right)C^{(1,1,1)}= \qquad (6.13)$$

$$= a^{(N,1,1)}\left\langle G_1 \right\rangle Nl + a^{(1,N,1)}\left\langle G_2 \right\rangle Nl + a^{(1,1,N)}\left\langle G_3 \right\rangle Nl$$

All mass conservation equations concerning "exterior" and "interior" voxels lead to a system of N^3 linear equations with N^3 unknown values of C at the centre of each voxel. The system of equations can be written in a matrix form

$$\mathbf{ZC} = \mathbf{F} \qquad (6.14)$$

where $\mathbf{Z}$ is a $\left(N^3 \times N^3\right)$ matrix which elements are functions of both geometry and diffusion coefficients of appropriate voxels (6.11), $\mathbf{C}$ is the vector containing N^3 unknown values of concentration C and the constituents of vector $\mathbf{F}$ are the functions of both transport properties and macroscopic gradient of C (see right side of eq. (6.13)). Note that due to the finite volume computational scheme, each row of matrix $\mathbf{Z}$ has only seven non-zero elements.

On the basis of macroscopic flux $\left\langle \mathbf{q} \right\rangle$, which due to PBC, has the form:

$$\left\langle q_1 \right\rangle = \frac{1}{N^2}\sum_{\beta=1}^{N}\sum_{\gamma=1}^{N}\left\langle q_1^{(N,\beta,\gamma)} \right\rangle_{S_1^+}$$

$$\left\langle q_2 \right\rangle = \frac{1}{N^2}\sum_{\alpha=1}^{N}\sum_{\gamma=1}^{N}\left\langle q_2^{(\alpha,N,\gamma)} \right\rangle_{S_2^+} \qquad (6.15)$$

$$\left\langle q_3 \right\rangle = \frac{1}{N^2}\sum_{\alpha=1}^{N}\sum_{\beta=1}^{N}\left\langle q_3^{(\alpha,\beta,N)} \right\rangle_{S_3^+}$$

all elements of effective diffusion tensor can be established provided that the macroscopic gradient of C is the known loading. Then the elements of effective diffusion tensor are as follows:

$$D_{ij}^{\text{eff}} = -\frac{\left\langle q_i \right\rangle}{\left\langle G_j \right\rangle} \qquad (6.16)$$

Due to the form of equation (6.16) the reasonable assumption is to choose the unit macroscopic gradient $\langle G_j \rangle$. Then, effective property simply equals the macroscopic flux. Note that in order to determine all elements of effective diffusion tensor, the system of equations (6.14) has to be solved three times, independently, each time setting different values of macroscopic gradient constituents, i.e. *j*-component equal to one and the remaining ones equal to zero:

$$\langle \mathbf{G} \rangle = \{1, 0, 0\}^{\mathrm{T}}$$
$$\langle \mathbf{G} \rangle = \{0, 1, 0\}^{\mathrm{T}}$$
$$\langle \mathbf{G} \rangle = \{0, 0, 1\}^{\mathrm{T}}$$

(6.17)

In what follows a simple 2D example is provided in order to validate the numerical method outlined above. Thus, consider a diffusion process within a two-phase deterministic composite, such that its components are isotropic and the values of diffusion coefficients are as follows: $D_M=1$ [$m^2 s^{-1}$] for matrix and $D_I=100$ [$m^2 s^{-1}$] for inclusion. The RVE for considered composite is presented in Fig. 6.5.
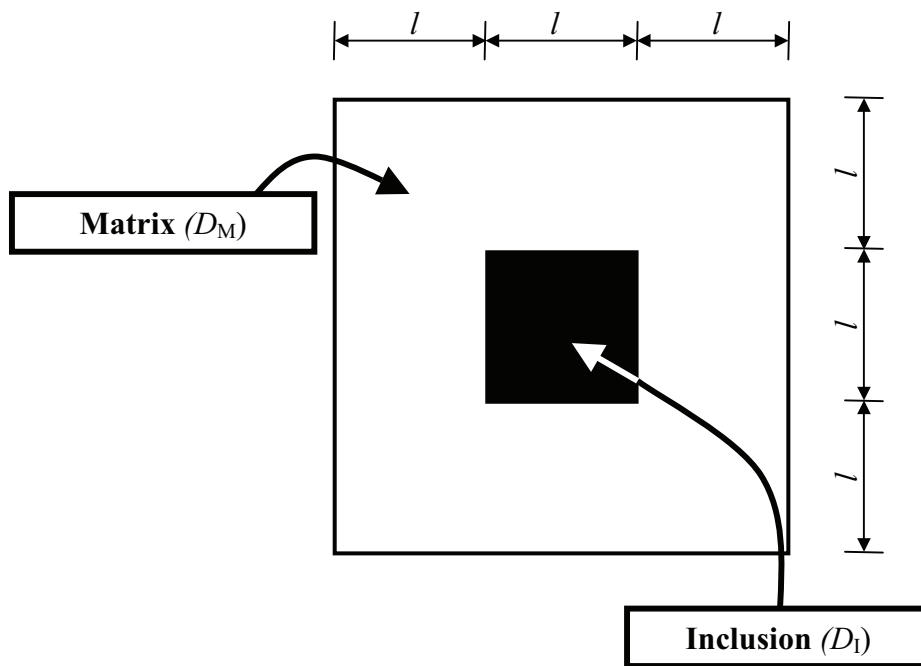
Fig. 6.5. Geometry of considered RVE

Note, that in 2D case, system of equations (6.14) reduces in a following way:

- **C** is a vector containing N^2 unknowns (values of concentration C in the central point of control volumes (pixels)),

- **Z** is a $\left(N^2 \times N^2 \right)$ matrix,

- each row of matrix **Z** has only five non-zero elements.

137

Furthermore, the relations expressing macroscopic fluxes (6.15) take the form:

$$\langle q_1 \rangle = \frac{1}{N^2} \sum_{\beta=1}^{N} \left\langle q_1^{(N,\beta)} \right\rangle_{S_1^+}$$

$$\langle q_2 \rangle = \frac{1}{N^2} \sum_{\alpha=1}^{N} \left\langle q_2^{(\alpha,N)} \right\rangle_{S_2^+}$$

(6.18)

In order to evaluate the effective diffusion tensor, in 2D case, the system of equations (6.14) has to be solved two times (three times for 3D case), independently, for different values of unit macroscopic gradient, i.e.: $\langle \mathbf{G} \rangle = \{1,0\}^{\mathrm{T}}$ and $\langle \mathbf{G} \rangle = \{0,1\}^{\mathrm{T}}$.

Numerical calculations have been performed for different mesh densities such that the number of control volumes has been changed form 9 ($N=3$) up to 90,000 ($N=300$). In Figure 6.6 three different mesh densities ($N=3$, $N=6$, $N=24$) are presented.
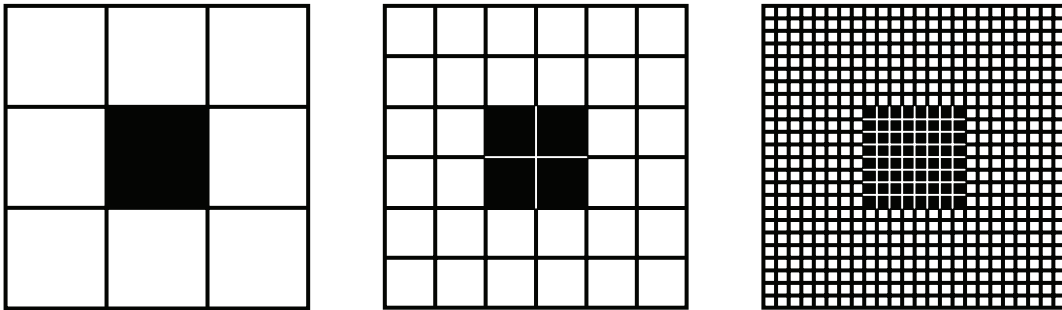
Fig. 6.6. RVE and finite volume mesh: a.) $N=3$ (9 pixels); b.) $N=6$ (36 pixels); c.) $N=24$ (576 pixels)

The results presented in Fig. 6.7 show the convergence of effective diffusion coefficient as a function of mesh density given by the number of control volumes in a row N.
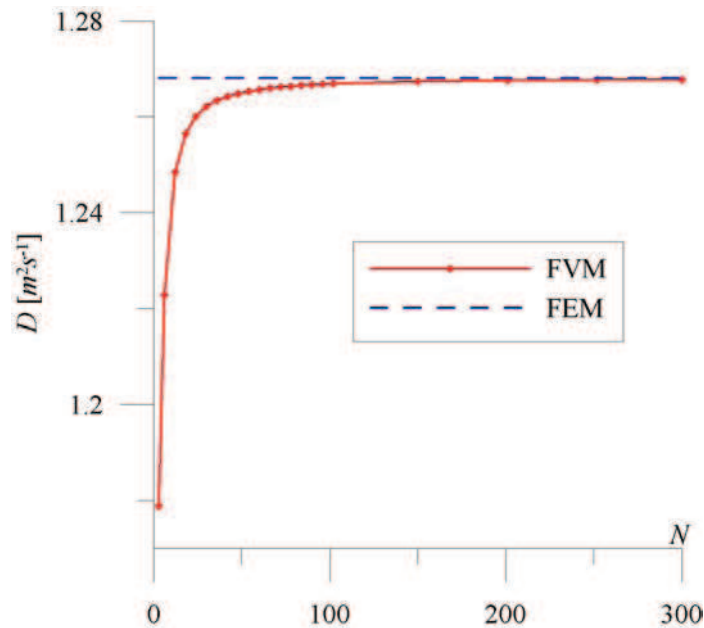
Fig. 6.7. Effect of mesh density (FVM) on the value of effective diffusion coefficient

It appears that one must use at least 328 control volumes ($N=18$), for the variation of effective diffusion coefficient to be less than 1%. Furthermore, in Fig. 6.7, the result evaluated by FE computations is also provided. The FE result was obtained utilising FlexPDE software with default re-meshing (FlexPDE, 2005) and corresponds to the mesh consisting of 6159 nodes (Fig. 6.8).
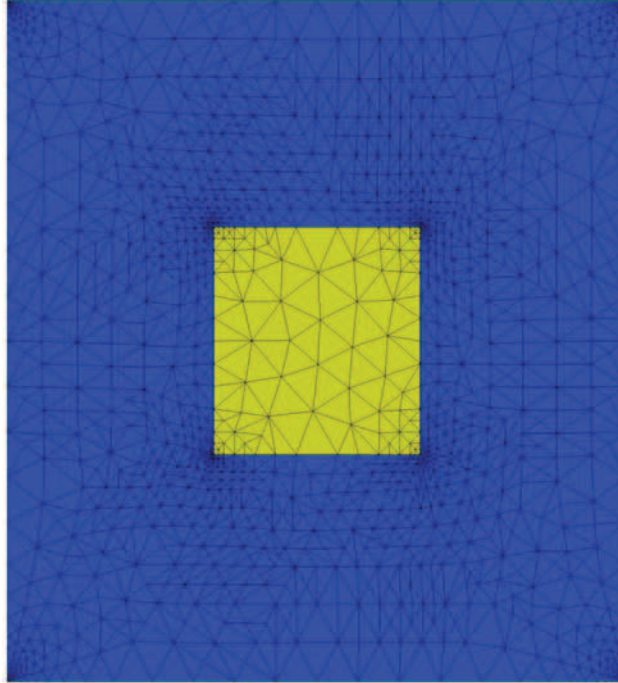
Fig. 6.8. Finite element mesh (6159 nodes) provided by FlexPDE (FlexPDE, 2005)

In Fig. 6.9 the relative error representing the discrepancy between FE result and its FV counterpart is presented. The value of relative error is less than 1% if the discretization of RVE is performed by at least 328 control volumes ($N=18$).
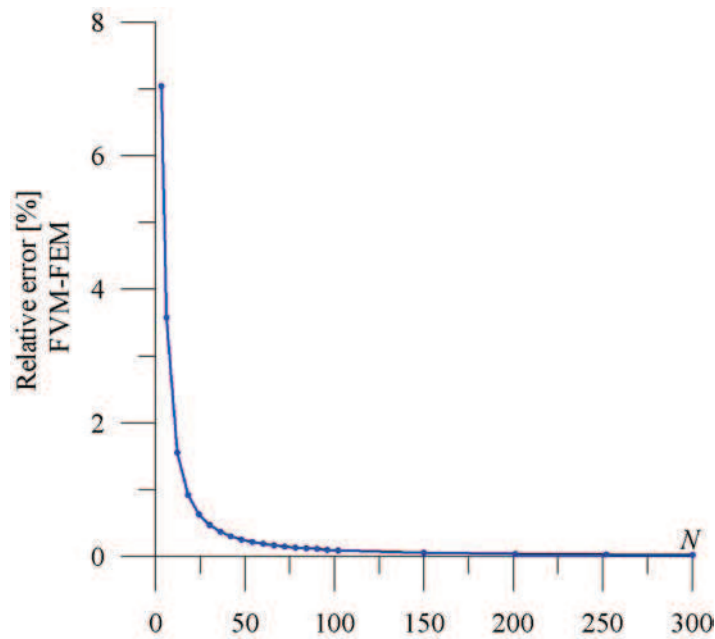
Fig. 6.9. Relative error between the result obtained by FE calculations and FV approach.

Note that within considered example contrast in mechanical properties is quite large, namely:
$\Theta = \dfrac{D_I}{D_M} = 100$. The influence of the contrast in properties on the numerical results as well as more

sophisticated investigations concerning numerical error and mesh density in relation to particular types of random microstructures are provided below.

Therefore, in what follows, the effect of mesh density (the number of control volumes used to mesh one pixel of digital image) is studied. The results concerning all considered microstructures are provided. It is investigated how the quantities like volume fraction, contrast in properties as well as the geometry influence the numerical result. Note, within all examples provided below thermal conductivity problem is considered. It is assumed that $k_I=1$ [W/mK] and hence, $k_2 = \Theta$ [W/mK].

Random checkerboard

We start our considerations with digital image of random checkerboard consisted of 10×10 pixels. As mentioned, each pixel is treated as control volume. Then, in each simulation step the number of control volumes is changed (such that the geometry of microstructure is kept unchanged – see Fig. 6.6) and numerical calculations are performed. The value of thermal conductivity coefficient as a function of the number of control volumes (in a row and column) is displayed in Fig. 6.10. Note, the results concerning two different volume fractions as well as three values of contrast in properties are presented.
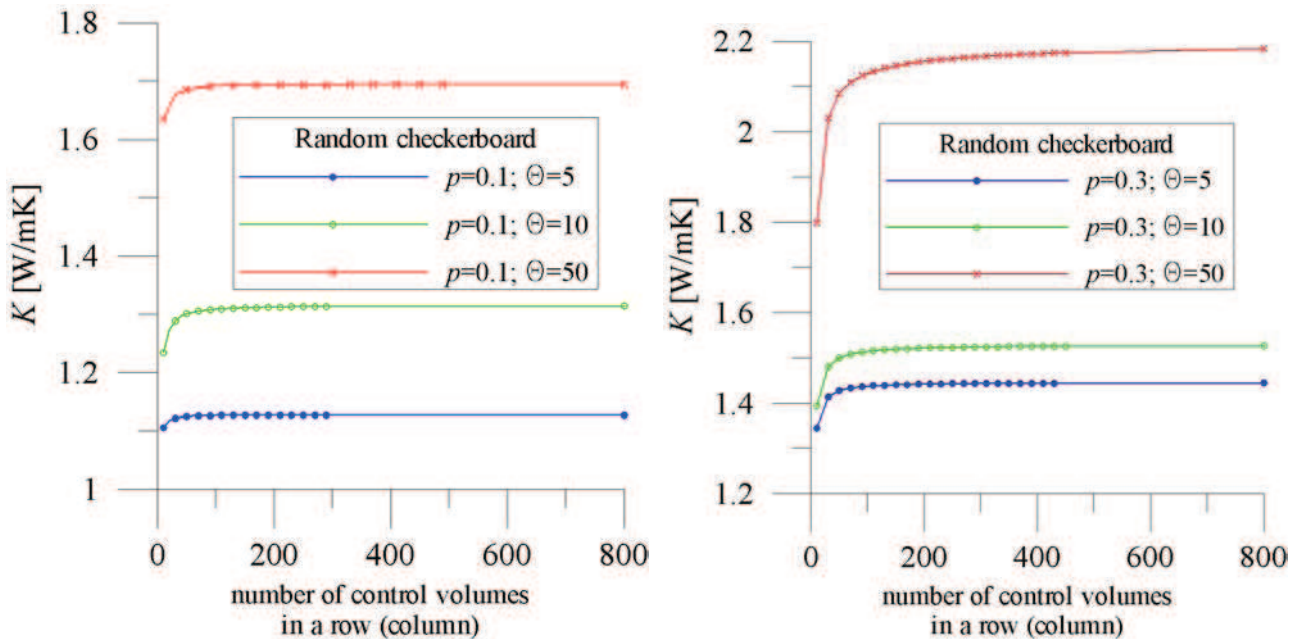
Fig. 6.10. Effect of mesh density on the numerical results – random checkerboard.

It can be seen that the convergence of the thermal conductivity coefficient is rather fast. However, the range of deviation is larger for *p*=0.3 than in case of *p*=0.1. Furthermore, in case of *p*=0.3 one can observe strong influence of contrast in properties on the number of control volumes. Nevertheless, in case of *p*=0.1 (for all considered values of Θ) as well as in case *p*=0.3 (for $\Theta = 5$ and $\Theta = 10$) it is reasonable to use 9-16 control volumes to "mesh" one pixel – such mesh density ensures the variation of the overall response to be approximately 1%. In case of *p*=0.3 ($\Theta = 50$) one should use about 25 control volumes.

Ising model

In case of Ising model, we focus on the microstructure type C (see Fig. 4.14 - bottom). Digital image consisted of 60×60 pixels (and control volumes) is first considered. As it was in case of random checkerboard, keeping the microstructure geometry unchanged, the number of control volumes per one pixel is increased. For each step – mesh density – the result concerning thermal conductivity coefficient is determined and recorded. Fig. 6.11 provides thermal conductivity coefficient as a function of the number of control volumes.
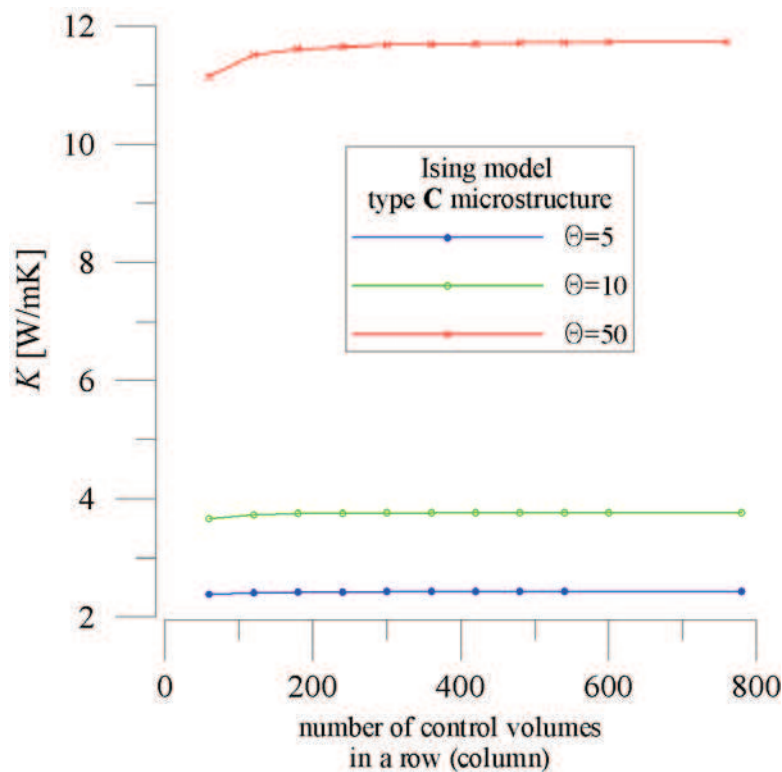
Fig. 6.11. Effect of mesh density on the numerical results – Ising model: type C microstructure.

As it was in case of previous example (random checkerboard) the largest mesh density is required in case of $\Theta = 50$. However, we can see a good convergence when a sample is consisted of 180×180 pixels. Therefore it seems to be reasonable to mesh each pixel with 9 control volumes.

System of overlapping disks

We consider now a microstructure consisted of overlapping disks. We focus on microstructure with volume fraction $\phi_I=0.5$ – it is depicted in Fig. 4.18 (bottom). Considerations are started with a digital image consisted of 50×50 pixels (control volumes). The process of mesh density analysis is analogous to the one described above. Fig. 6.12 shows values of thermal conductivity coefficient obtained for different mesh densities – number of control volumes per pixel.
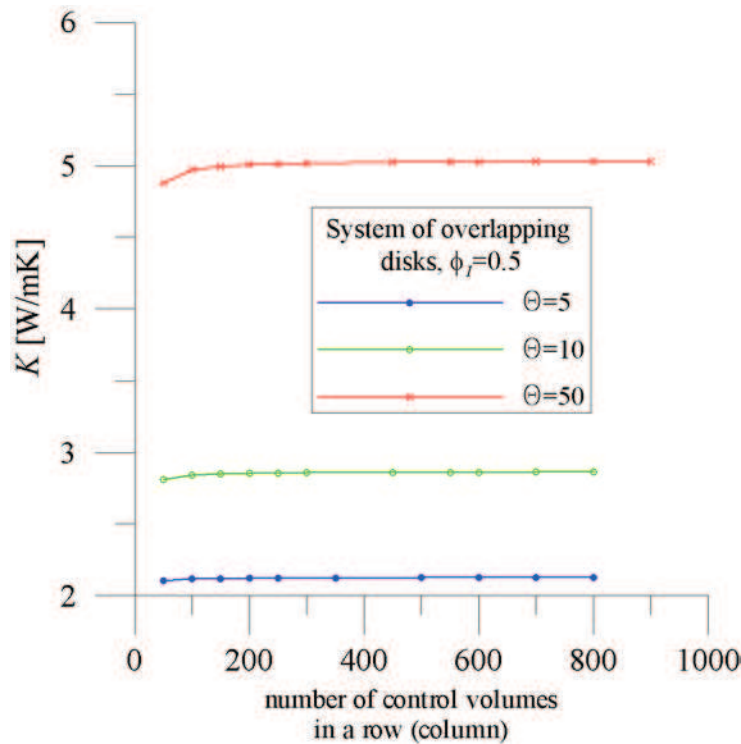
Fig. 6.12. Effect of mesh density on the numerical results – system of overlapping disks, $\phi_I=0.5$.

Observing results concerning system of overlapping disks (Fig. 6.12) it can be noticed that the largest number of control volumes per pixel is required in case of the largest value of Θ. In case of $\Theta = 5$ and $\Theta = 10$ obtained results yield similar, fast convergence. This correspond to the results established for random checkerboard and Ising model.

Fig. 6.12 also shows that one should use about 9-16 $\left(150\times150 - 200\times200\right)$ control volumes per pixel for the variation of thermal conductivity coefficient to be very small (approximately 1%), regardless of the value of contrast in properties Θ

System of non-overlapping disks

In case of system of non-overlapping disks mesh density analysis were performed for the microstructure presented in Fig. 4.24 (top right) – volume fraction $\phi_I=0.4$. A digital image consisted

of 60×60 pixels was first studied – thermal conductivity coefficient corresponding to the microstructure realization is displayed in Fig. 6.13. This figure shows also the values of thermal conductivity coefficient obtained for different mesh densities. It can be seen that mesh density analysis yield similar effect as in case of previous examples – the largest number of control volumes per pixel is required in case of the greatest value of contrast in properties.
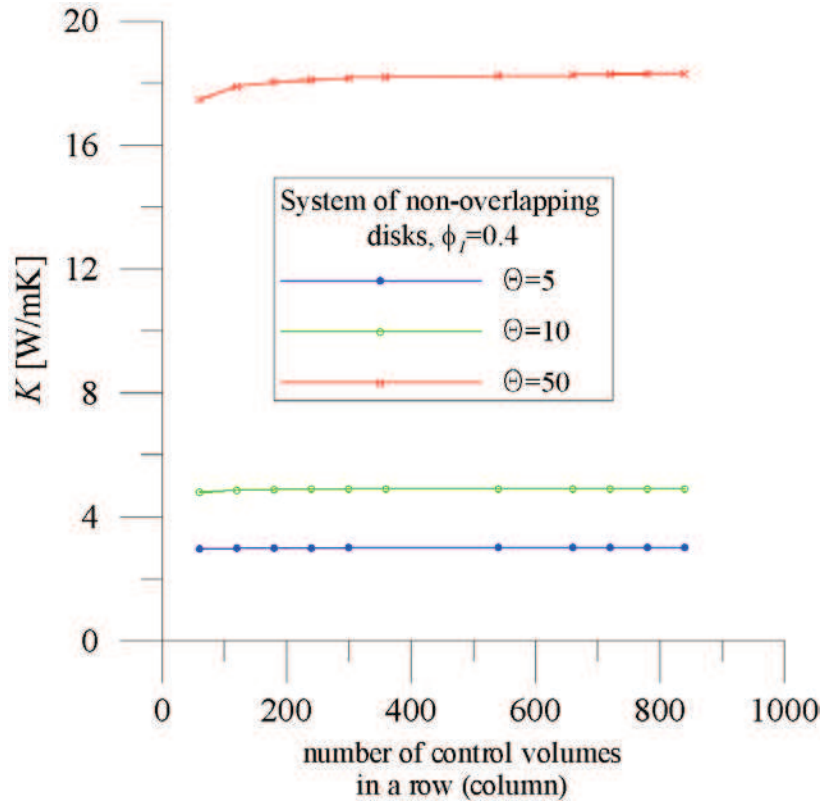
Fig. 6.13. Effect of mesh density on the numerical results – system of non-overlapping disks, ϕ_l=0.4.

Debye and modified Debye microstructures

In case of Debye as well as modified Debye random media two microstructures (digital images) consisting of 60×60 and 50×50 pixels, respectively, were reconstructed. Keeping the geometry of microstructure unchanged the mesh density analysis were performed. The results, namely thermal conductivity coefficients corresponding to different number of control volumes, are presented graphically in Fig. 6.14. Note left panel of aforementioned figure corresponds to Debye microstructure, whereas right panel displays results corresponding to modified Debye random microstructure.

Once again, it can be seen that the convergence of results is very fast. The largest deviation is observed in case of $\Theta = 50$. Furthermore, it seems to be reasonable to use 9-16 control volumes to mesh one pixel – such mesh density ensures the variation of the overall response to be approximately 1%.
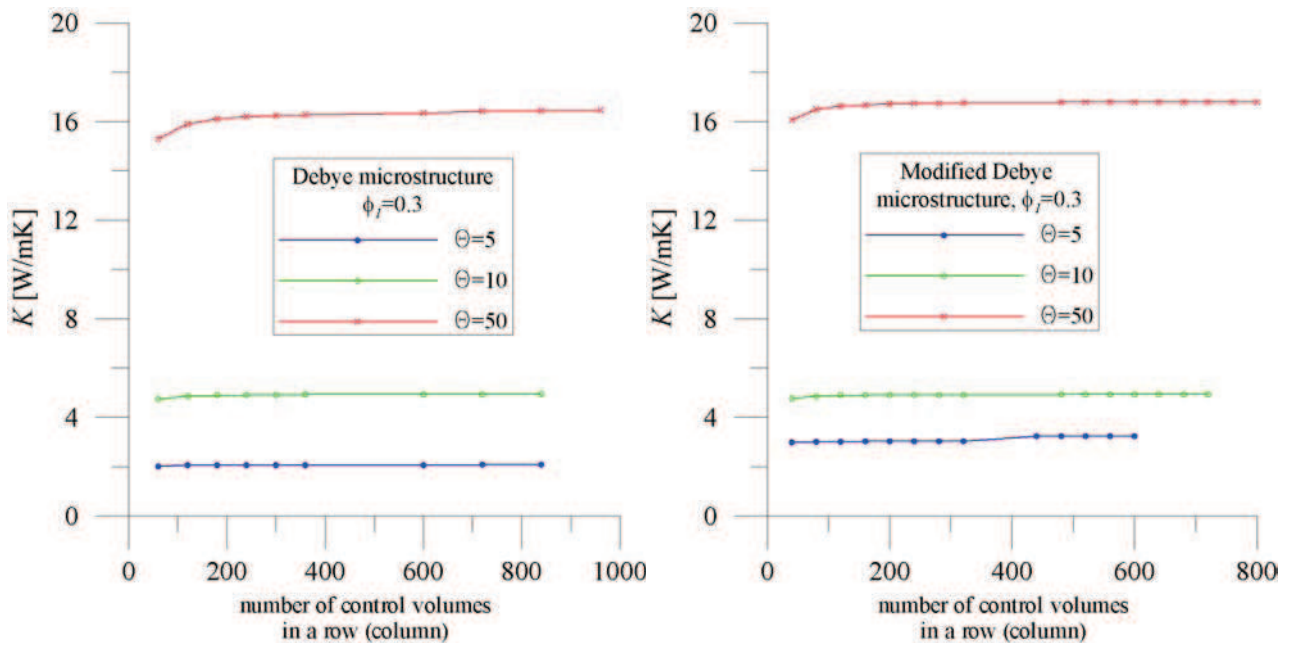
Fig. 6.14. Effect of mesh density on the numerical results – left: Debye microstructure, ϕ_1=0.3; right: modified Debye microstructure, ϕ_1=0.3

Real materials

Reconstructed microstructures of Fontainebleau sandstone 40×40 as well as boron-carbide/aluminum composite 50×50 were utilized for the purpose of mesh density analysis. Fig. 6.15 provides thermal conductivity coefficient as a function of the number of control volumes.
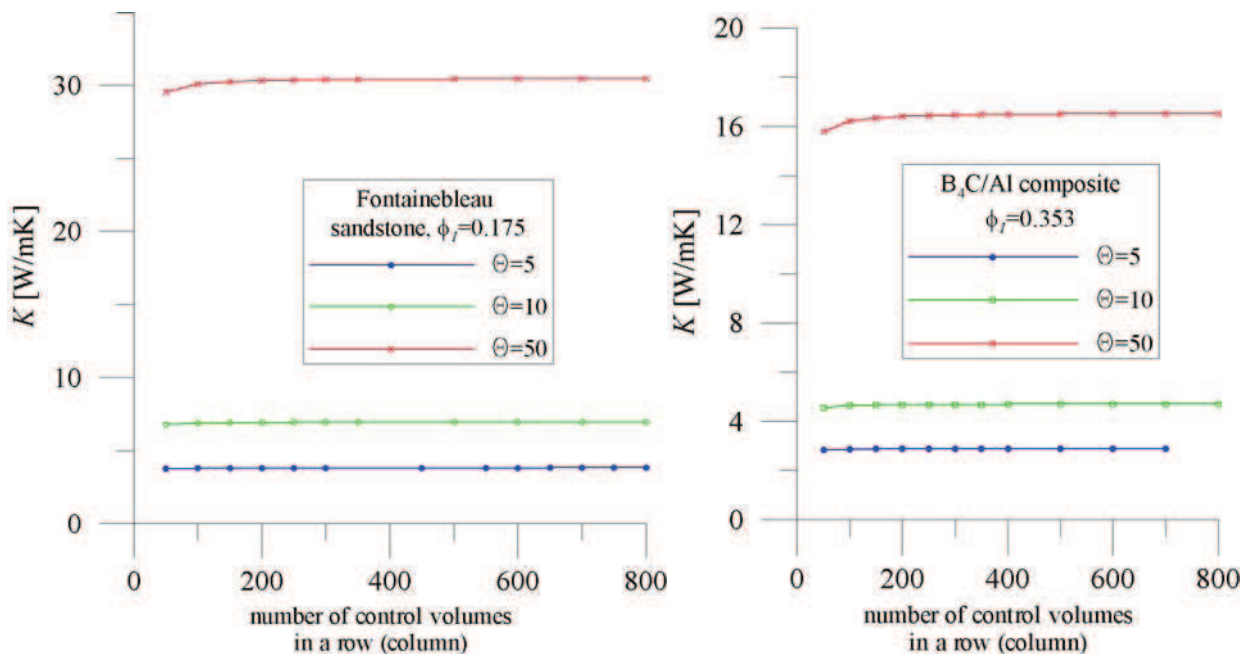
Fig. 6.15. Effect of mesh density on the numerical results – left: Fontainebleau sandstone; right: boron-carbide/aluminum composite.

As in case of previous examples the largest mesh density, in order to obtain the small variation of the overall response, corresponds to the largest value of contrast in properties. Nevertheless, for all values of Θ it is reasonable to mesh one pixel with 9-16 control volumes.

It should be strongly emphasized that results concerning mesh density analysis are utilised within numerical simulations presented in next sections. Due to limited hardware capabilities we use, for each type of microstructure, 9 control volumes to mesh one pixel. Furthermore, the sizes of RVE are determined for five different values of Θ (5, 10, 50, 100, 1000). Nevertheless, determination of effective thermal conductivity coefficients is performed for three values of Θ (5, 10, 50).

6.2. Random cell models

Random checkerboard

As it was in case of geometrical representativity criterion we begin our considerations with random checkerboard microstructure. In what follows two microstructures with volume fractions ϕ_I=0.1 and ϕ_I=0.3 are considered (see Fig. 4.10). In Figs. 6.16 and 6.17 modified two-point correlation functions are displayed. Note these functions are evaluated with assumption that k_1=1 and therefore $k_2 = \Theta$. As mentioned in chapter 5, for all considered values of Θ, the modified two-point correlation functions have the correlation length l_p=1 pixel. Furthermore, it can be simply seen that the value of S_2 yielding from Voigt estimate is greater than its counterpart corresponding to Reuss estimation.
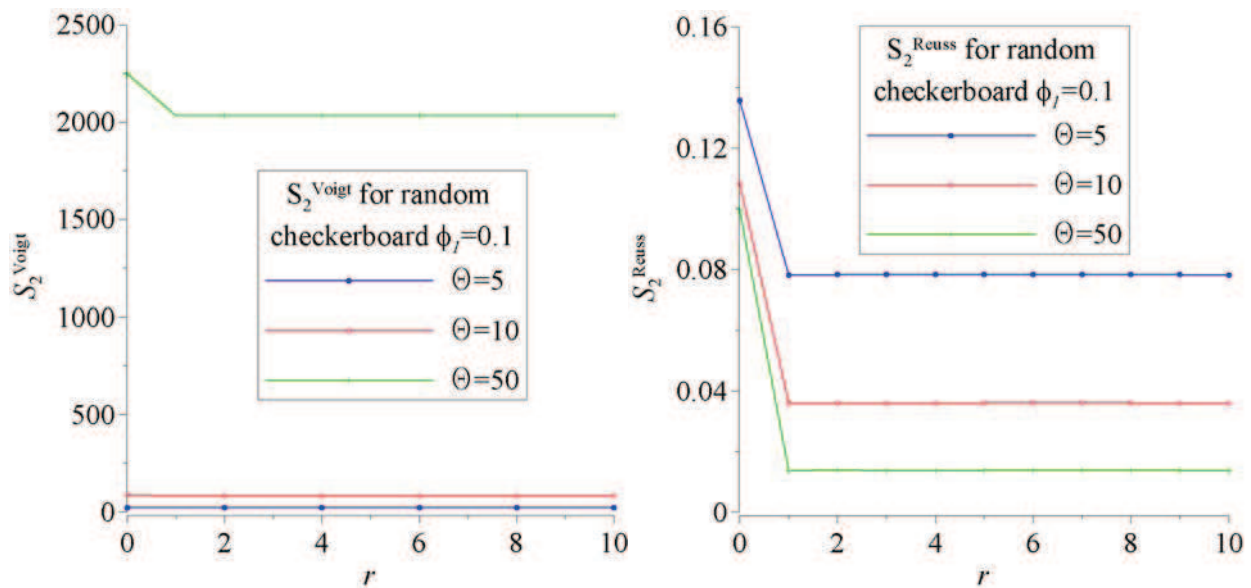
Fig. 6.16. Modified two-point correlation functions, left: S_2^{Voigt} ; right: S_2^{Reuss} - random checkerboard, ϕ_I=0.1
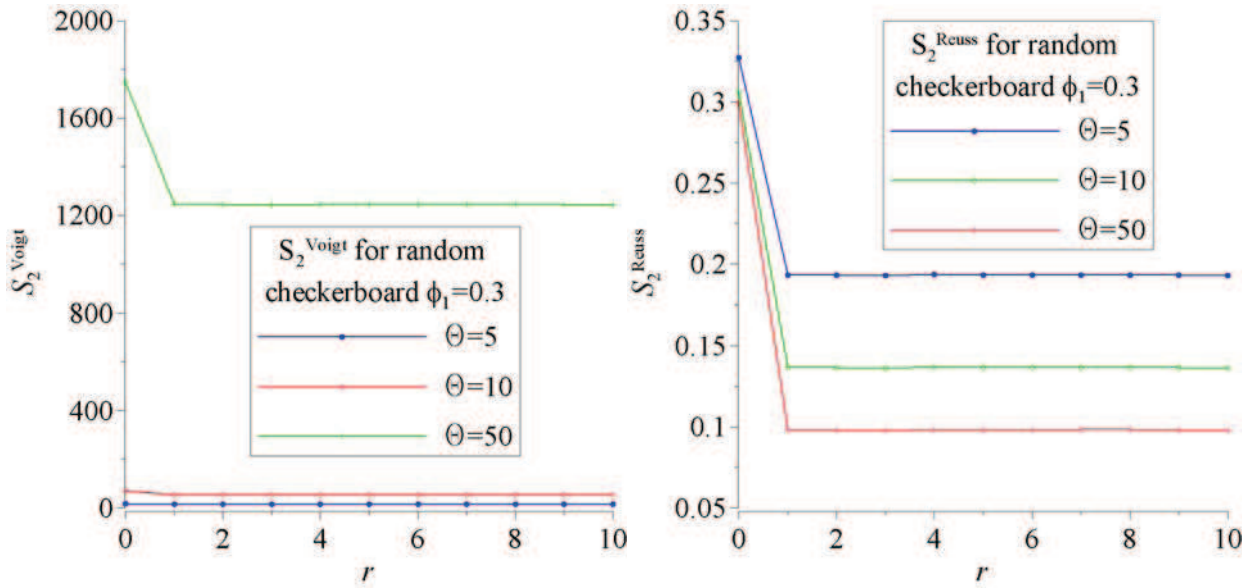
Fig. 6.17. Modified two-point correlation functions, left: S_2^{Voigt}; right: S_2^{Reuss} - random checkerboard, ϕ_I=0.3.

Figs. 6.18 as well as 6.19 provide variance of local Voigt and Reuss estimations plotted against the number of pixels expressed as N. We see that these functions are decreasing as the size of the sample is increasing. Furthermore, variance of local Voigt estimate yields greater values than the one corresponding to Reuss estimate.

The variances of local Voigt and Reuss estimates were utilized to determine the minimum RVE size according to relation (5.56). Note that in case of random checkerboard, due to chosen values of contrast in properties, it is not necessary to involve the condition resulting from the correlation length (5.53) – l_p=1 pixel.
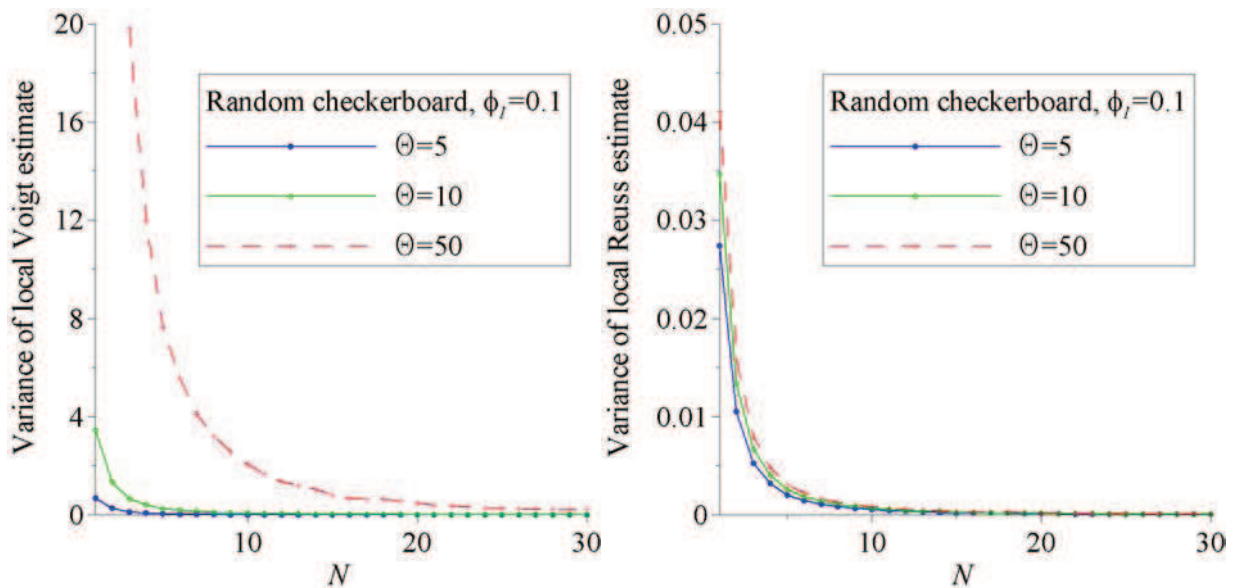
Fig. 6.18. Variance of local Voigt and Reuss estimates as a function of N - random checkerboard, ϕ_I=0.1.
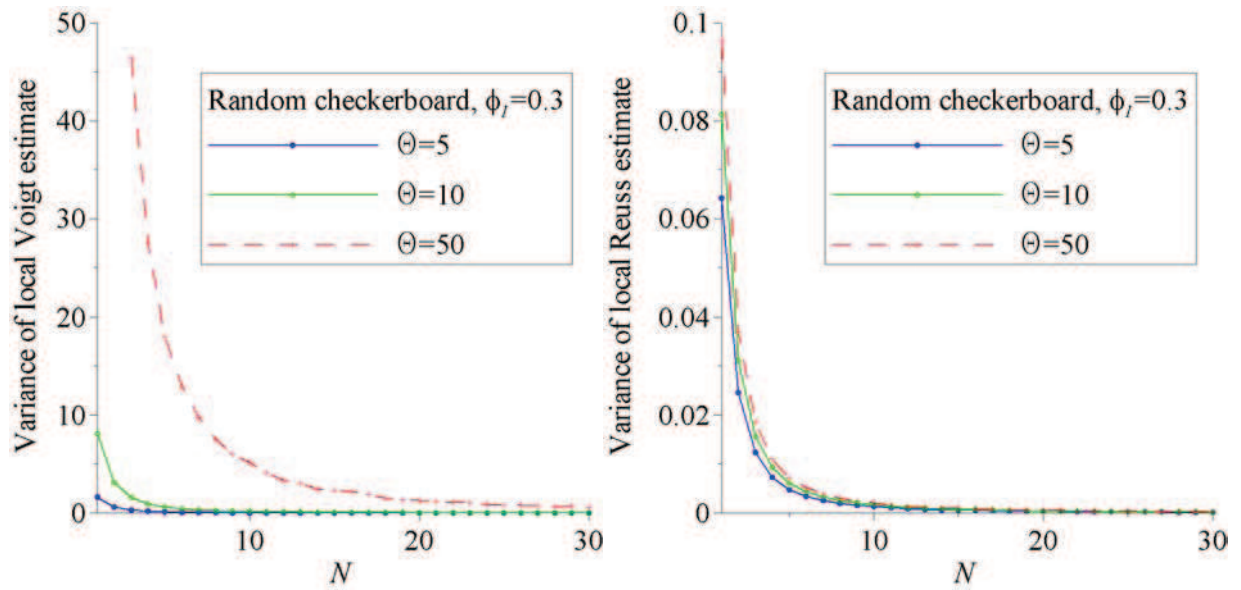
Fig. 6.19. Variance of local Voigt and Reuss estimates as a function of N - random checkerboard, ϕ_I=0.3.

In spite of some results concerning random checkerboard were discussed and presented graphically in previous chapters, in order to be more legible, they are provided once again and collected in Tables 6.1 and 6.2. Each table corresponds to fixed value of relative error ε, i.e. 3% and 1%. The results corresponding to different values of contrast in properties are provided.

Table 6.1. RVE size corresponding to error ε= 3% (random checkerboard microstructure)

Θ	ϕ_I	RVE size with respect to overall transport properties	RVE size with respect to microstructure geometry
		$N^{\#}$	N^{*}
5		5	
10		9	
50	0.1	14	18
100		16	
1000		18	
5		5	
10		7	
50	0.3	8	9
100		9	
1000		9	

Table 6.2. RVE size corresponding to error $\varepsilon = 1\%$ (random checkerboard microstructure)

Θ	ϕ_1	RVE size with respect to overall transport properties $N^{\#}$	RVE size with respect to microstructure geometry N^{*}
5		9	
10		15	
50	0.1	23	30
100		28	
1000		30	
5		9	
10		12	
50	0.3	14	16
100		15	
1000		16	

Observing results provided above one can simply notice that the size of RVE is increasing as the error of estimation is decreasing. Furthermore, for fixed value of volume fraction and ε, the size of RVE converges towards the one obtained with respect to microstructure geometry. Note that for $\Theta = 1000$ both conditions yields the same value of RVE size.

RVE sizes collected in Tables 6.1 and 6.2 were then utilized for the calculations of the mean values of thermal conductivity according to relation (3.25), i.e.

$$\overline{K} = \frac{1}{n}\sum_{j=1}^{n} K_j \tag{6.19}$$

where K_j is the thermal conductivity coefficient evaluated for j-realization (using numerical method presented in the beginning of this chapter) and n is the sufficient number of realizations.

A sufficient number of realizations was obtained on the basis of CLT (see section 3.2.2). It is simply treated as the maximum value yielding from two estimates, i.e.

$$n = \max\left[n_{\text{Voigt}} ; n_{\text{Reuss}} \right] \tag{6.20}$$

where

$$n_{\text{Voigt}} = n \geq \left(\frac{\Phi^{-1}\left(1 - \frac{\alpha}{2}\right)}{\varepsilon} \right)^2 \frac{Var(\xi_k)}{\langle \xi_k \rangle^2} \tag{6.21}$$

and

$$n_{\text{Reuss}} = n \geq \left(\frac{\Phi^{-1}\left(1 - \frac{\alpha}{2}\right)}{\varepsilon} \right)^2 \frac{Var\left(\xi_{1/k}\right)}{\left\langle \xi_{1/k} \right\rangle^2} \tag{6.22}$$

In Tables 6.3 and 6.4 the mean values of thermal conductivity coefficients, determined for three different values of contrast in properties, are provided. Table 6.3 (6.4) displays the results for the value of error ε=3% (ε=1%). Note that, the same value of error ε is chosen for the determination of the size of RVE (relation 5.57) as well as the number of realizations - relation (6.20).

It should be noted that the number of realizations n, determined for different values of contrast in properties as well as different values of volume fraction, is also presented. The values of n were obtained with assumption that the significance level is α=5%. Thus, according to the tables of normal distribution we have that $\Phi^{-1}(0.975) = 1.96$ and therefore:

$$n = \max\left[\frac{Var\left(\xi_k\right)}{\left\langle \xi_k \right\rangle^2}; \; \frac{Var\left(\xi_{1/k}\right)}{\left\langle \xi_{1/k} \right\rangle^2} \right]\left(\frac{1.96}{\varepsilon} \right)^2 \tag{6.23}$$

The last column of both Tables provides the result obtained for the RVE size for which only one realization is sufficient. This size is chosen assuming the estimation error ε=1%. This result is treated as the effective one for the considered microstructure. We see, for all values of volume fraction as well as contrast in properties, well agreement between $\overline{K}$ and K^{eff}. Nevertheless the relative error between these results is increasing as the contrast in properties is increasing. This is widely discussed in section 6.4 where some remarks are provided.

Table 6.3. Mean values of thermal conductivity coefficient corresponding to error ε = 3% (random checkerboard microstructure)

Θ	ϕ_I	Size of RVE (see Table 6.1)	Number of realizations n	$\overline{K}$ [W/mK]	K^{eff} [W/mK] (n=1, ε=1%)
5		5	111	4.193	4.183
10	0.1	9	103	7.896	7.839
50		14	129	36.416	36.078
5		5	106	2.888	2.886
10	0.3	7	103	4.578	4.527
50		8	131	14.673	14.169

Table 6.4. Mean values of thermal conductivity coefficient corresponding to error $\varepsilon = 1\%$ (random checkerboard microstructure)

Θ	ϕ_1	Size of RVE (see Table 6.2)	Number of realizations n	$\overline{K}$ [W/mK]	K^{eff} [W/mK] $(n=1, \varepsilon=1\%)$
5		9	337	4.195	4.183
10	0.1	15	288	7.869	7.839
50		23	347	36.125	36.078
5		9	317	2.889	2.886
10	0.3	12	317	4.528	4.527
50		14	379	14.446	14.169

In Fig. 6.20 the mean value of thermal conductivity coefficient is plotted against the size of the sample *N*. The results correspond to the case of volume fraction ϕ_1=0.3, contrast $\Theta =10$ and estimation error ε=1%. Furthermore, K^{eff} and bounds of Voigt/Reuss as well as Hashin – Shtrikman are also provided. It can be seen that as the sample size is increasing the difference between mean value of thermal conductivity $\overline{K}$ and K^{eff} is decreasing. As mentioned, this fact is widely discussed in section 6.4.
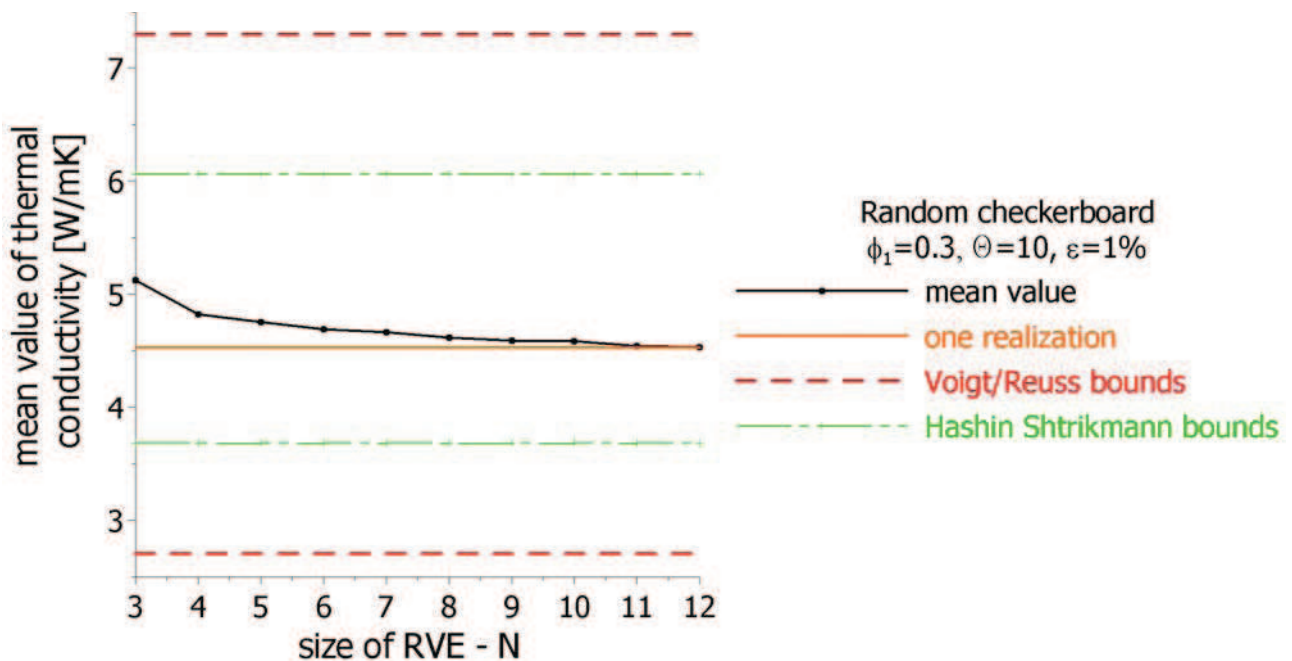
Fig. 6.20. Mean value of thermal conductivity [W/mK], Voigt/Reuss and Hashin-Shtrikmann bounds.

Ising model

We consider now the microstructure generated via Ising model. Focus is based on the type C microstructure (see. Fig. 4.14 - bottom) possessing the volume fraction of phase 1, $\phi_1 \approx 0.5$. In Figs. 6.21 and 6.22 modified two-point correlation functions S_2^{Voigt} as well as S_2^{Reuss} are displayed. As in case of random checkerboard these functions are evaluated with assumption that k_1=1 ($k_2 = \Theta$). It can be seen that the value of S_2^{Voigt} is always greater than its counterpart corresponding to Reuss estimation, S_2^{Reuss}.
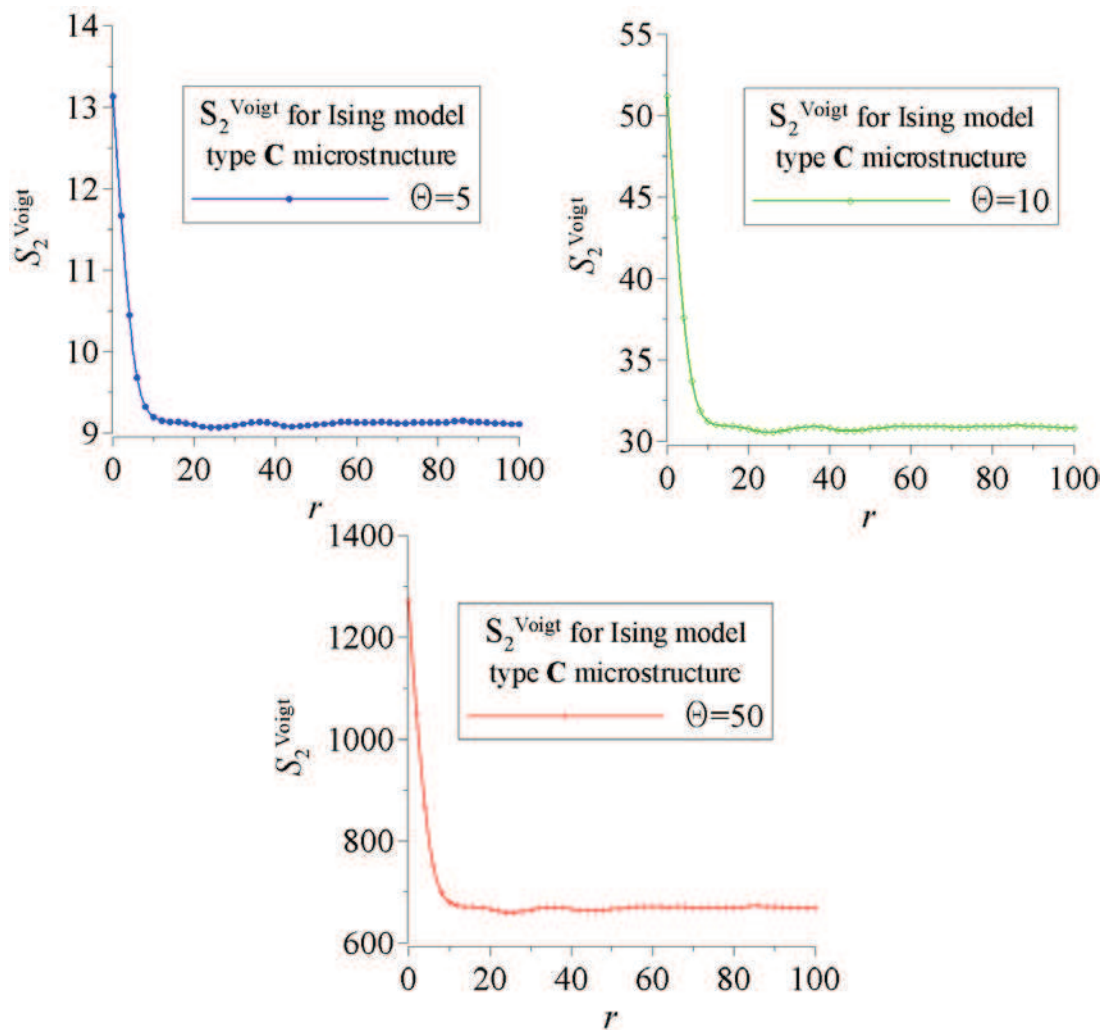
Fig. 6.21. Modified two-point correlation function, S_2^{Voigt}, for different values of contrast in properties

Figs. 6.23 as well as 6.24 provide variances of local Voigt and Reuss estimations, respectively. Note, the variances are plotted against the sample size expressed in terms of the number of pixels N. It can be seen that both variances are decreasing as the sample size is increasing. Furthermore, the greatest value of variance corresponds to the contrast in properties $\Theta = 50$.
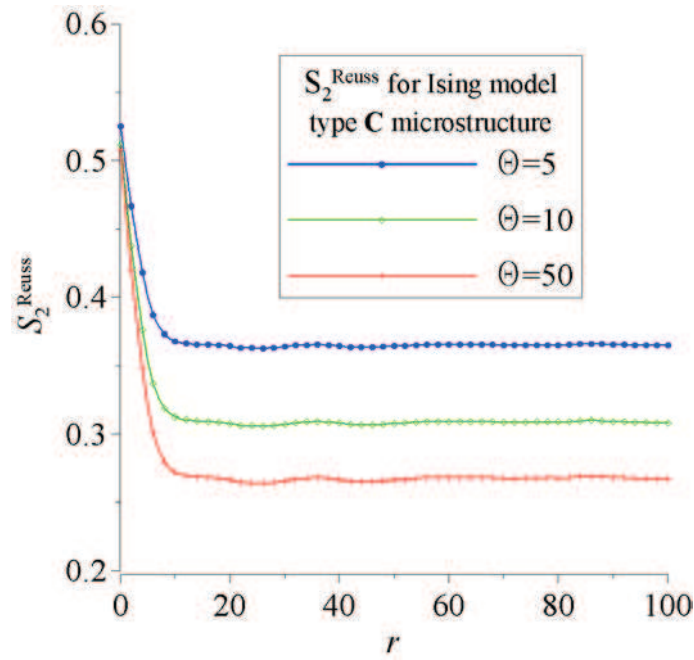
Fig. 6.22. Modified two-point correlation function, S_2^{Reuss}, for different values of contrast in properties
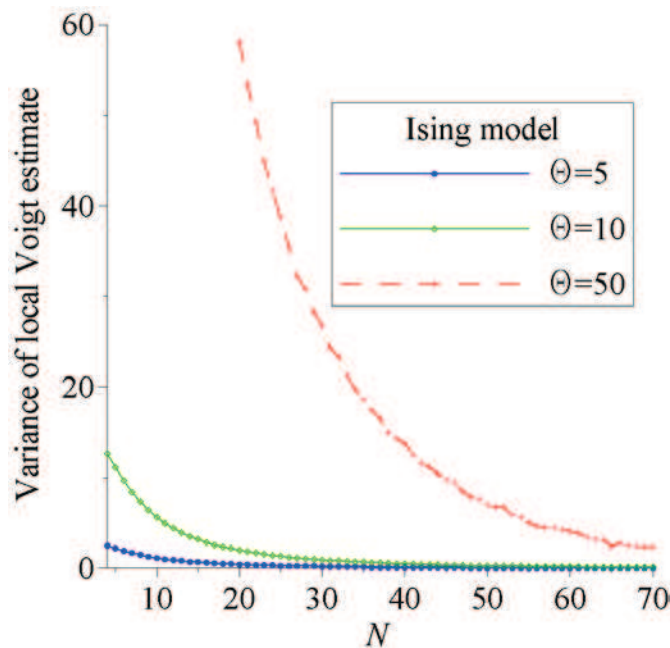
Fig. 6.23. Variance of local Voigt estimate as a function of N – Ising model.

Utilizing both variances, the size of sample were determined. These results are presented in Tables 6.5 and 6.6. The size of the sample yielding from the correlation length condition is presented in separate column. Speaking more clearly, in third column the size resulting from condition (5.52), is presented, i.e. the maximum value of $N_{\text{Voigt}} = \sqrt{\|\Omega_0\|_{\text{Voigt}}}$ and $N_{\text{Reuss}} = \sqrt{\|\Omega_0\|_{\text{Reuss}}}$. In fourth column the value of the sample size, $N_{l_p} = \sqrt{\|\Omega_0\|_{l_p}}$, according to correlation length condition (5.53), is displayed. Furthermore, it should be noted that the maximum

value of those three is in bold and underline type. Note, last two columns provide the size with respect to microstructure geometry.
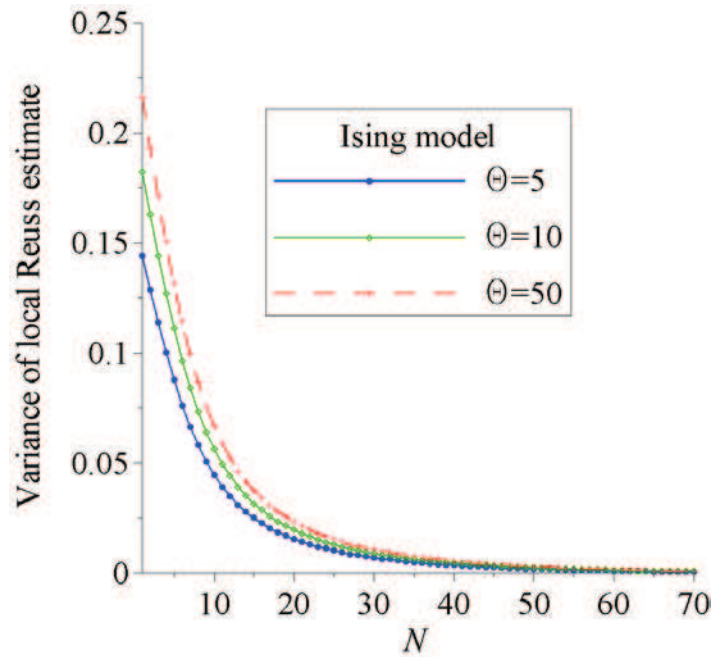
Fig. 6.24. Variance of local Reuss estimate as a function of N – Ising model.

Table 6.5. RVE size corresponding to error $\varepsilon= 3\%$ (Ising model – type C microstructure)

Θ	ϕ_I	RVE size with respect to overall transport properties		RVE size with respect to microstructure geometry	
		$\max\left[N_{\text{Voigt}};N_{\text{Reuss}}\right]$	N_{l_p}	$\max\left[N_\xi;N_\psi\right]$	N_{l_c}
5		**<u>26</u>**	18		
10		**<u>31</u>**	22		
50	0.5	**<u>36</u>**	28	38	**<u>72</u>**
100		**<u>37</u>**	34		
1000		**<u>38</u>**	38		

Table 6.6. RVE size corresponding to error $\varepsilon= 1\%$ (Ising model – type C microstructure)

Θ	ϕ_I	RVE size with respect to overall transport properties		RVE size with respect to microstructure geometry	
		$\max\left[N_{\text{Voigt}};N_{\text{Reuss}}\right]$	N_{l_p}	$\max\left[N_\xi;N_\psi\right]$	N_{l_c}
5		43	**<u>78</u>**		
10		48	**<u>78</u>**		
50	0.5	53	**<u>78</u>**	55	**<u>78</u>**
100		54	**<u>78</u>**		
1000		55	**<u>78</u>**		

In Table 6.7 the mean values of thermal conductivity coefficients, determined for three different values of contrast in properties, are provided. The results were obtained for two value of error ε=3% and ε=1%. Note, for all values of volume fraction as well as contrast in properties, well agreement between $\overline{K}$ and K^{eff} can be observed. Furthermore, as in case of random checkerboard, the relative error between these results is increasing as the contrast in properties is increasing. As mentioned - this is widely discussed in section 6.4.

Table 6.7. Mean values of thermal conductivity coefficient corresponding to different values of both error ε and contrast in properties Θ (Ising model – type C microstructure)

Θ	ϕ_l	ε	Size of RVE (see Tables 6.5 and 6.6)	Number of realizations n	$\overline{K}$ [W/mK]	K^{eff} [W/mK] (n=1, ε=1%)
5			26	62	2.291	2.173
10		3%	31	60	3.172	3.017
50			36	60	6.795	6.409
5	0.5		78	61	2.180	2.173
10		1%	78	94	3.022	3.017
50			78	127	6.536	6.409

Fig. 6.25 provides the value of $\overline{K}$ plotted against N. The results correspond to the case of Θ =10 and ε=3%. The value of K^{eff} as well as the bounds are also displayed. It can be seen that as the sample size is increasing the difference between mean value of thermal conductivity $\overline{K}$ and K^{eff} is decreasing.
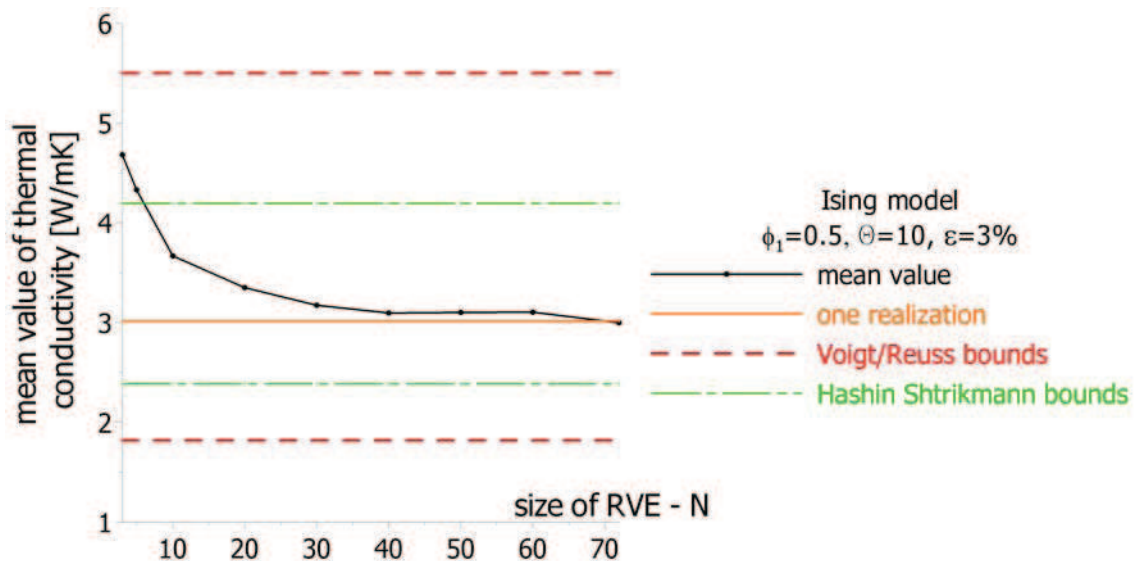
Fig. 6.25. Mean value of thermal conductivity [W/mK], Voigt/Reuss and Hashin-Shtrikman bounds.

System of overlapping disks

Figs. 6.26 and 6.27 provide modified two-point correlation functions S_2^{Voigt} as well as S_2^{Reuss} for the microstructure corresponding to the system or overlapping disks. Once again, the values of aforementioned functions are determined with following assumption: $k_1=1$ and $k_2 = \Theta$. As in previous examples, it can be seen that the value of S_2^{Voigt} is always greater than its counterpart corresponding to Reuss estimation, S_2^{Reuss}.

In Figs. 6.28 and 6.29 the variances corresponding to local Voigt as well as local Reuss estimations are graphically presented. Note, the variances are plotted against the sample size expressed in terms of the number of pixels N. Note, the functions are decreasing as the size N is increasing. Furthermore, the greatest value of variance of local Voigt/Reuss estimate corresponds to the greatest value of contrast in properties, i.e. $\Theta = 50$.
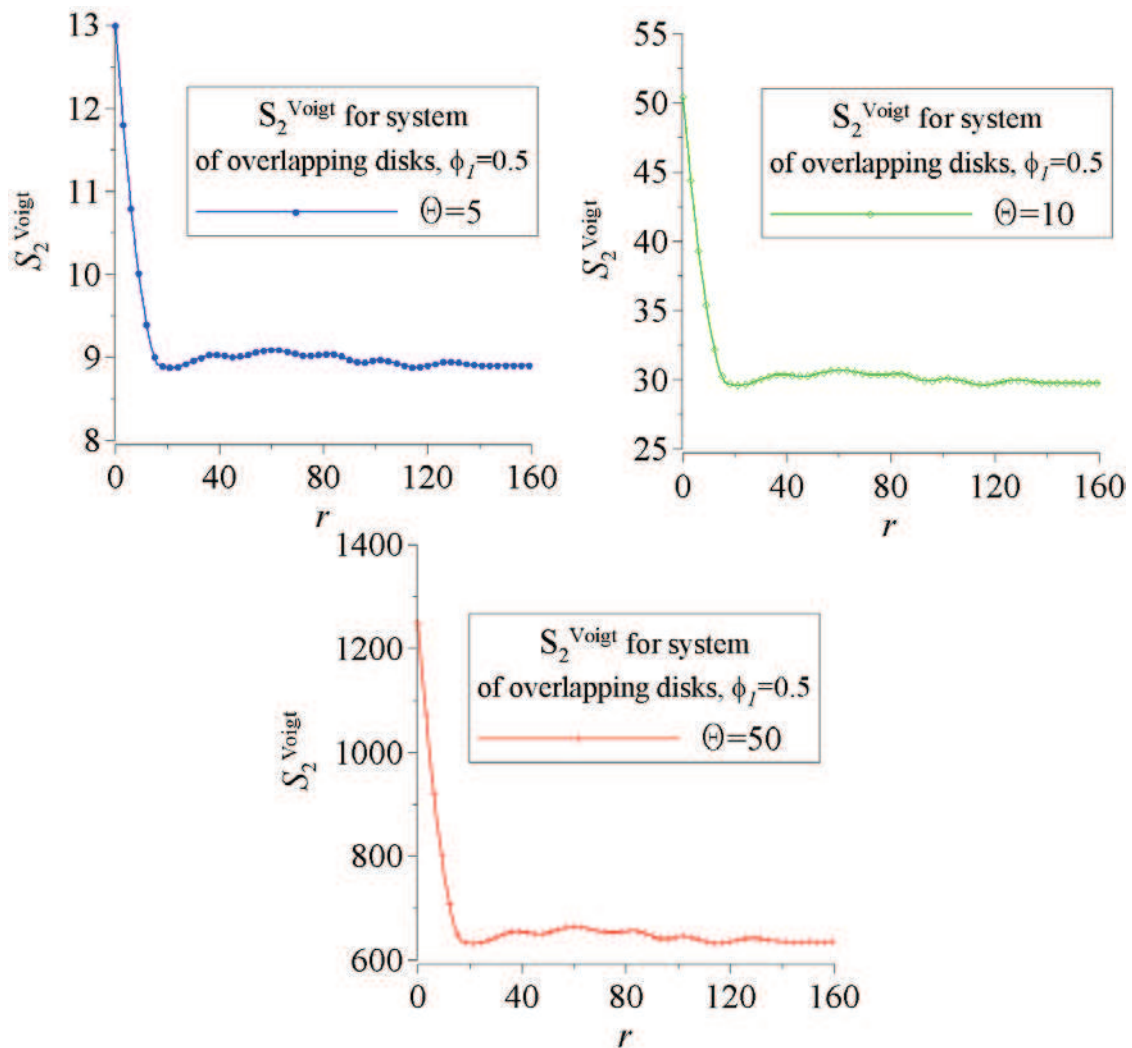
Fig. 6.26. Modified two-point correlation function, S_2^{Voigt}, for different values of contrast in properties.
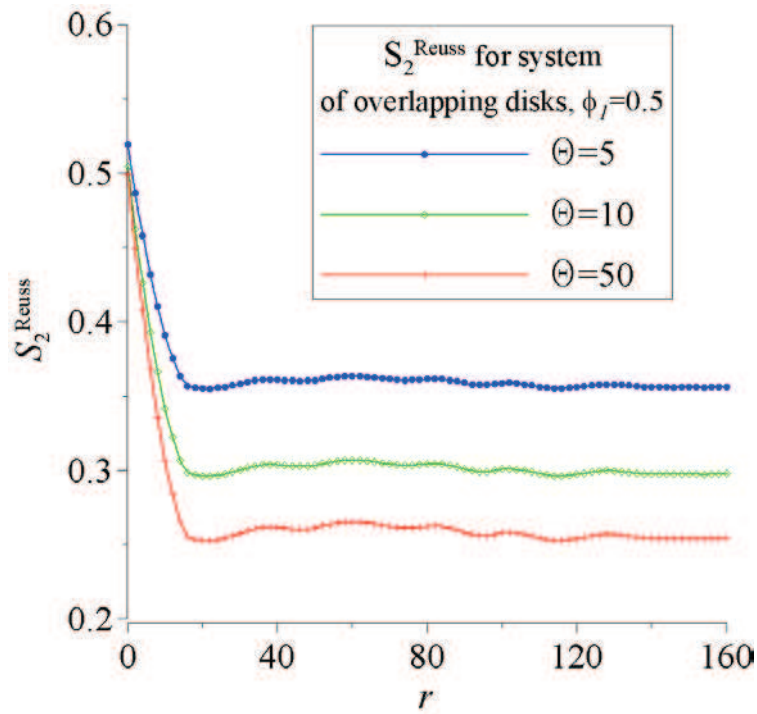
Fig. 6.27. Modified two-point correlation function, S_2^{Reuss}, for different values of contrast in properties
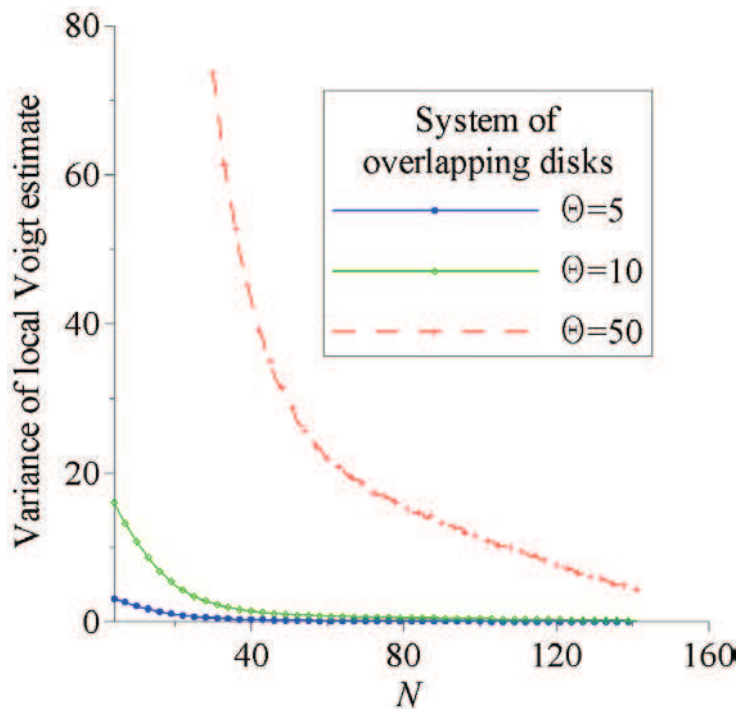
Fig. 6.28. Variance of local Voigt estimate as a function of N – system of overlapping disks.

The sizes of RVE evaluated for the system of overlapping disks are collected in Tables 6.8 and 6.9. Note, as before, the results are determined for five different values of contrast in properties as well as two values of error ε. Moreover, RVE sizes evaluated with respect to both overall transport properties and microstructure geometry are provided. It can be seen that as the contrast in properties, i.e. Θ, is increasing the size evaluated as $\max\left[N_{\text{Voigt}};N_{\text{Reuss}}\right]$ converges towards the one

obtained from geometrical criterion, namely: $\max\left[N_\xi; N_\psi\right]$ - this was also observed in case of previously considered examples.
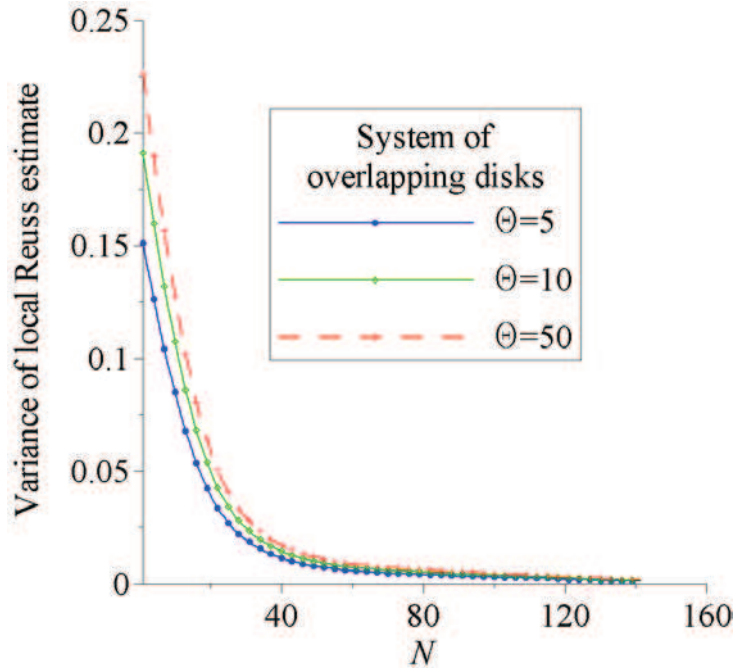
Fig. 6.29. Variance of local Reuss estimate as a function of N – system of overlapping disks.

Table 6.8. RVE size corresponding to error ε= 3% (system of overlapping disks)

Θ	ϕ_1	RVE size with respect to overall transport properties		RVE size with respect to microstructure geometry	
		$\max\left[N_{\text{Voigt}}; N_{\text{Reuss}}\right]$	N_{l_p}	$\max\left[N_\xi; N_\psi\right]$	N_{l_c}
5		**<u>42</u>**	28		
10		**<u>52</u>**	28		
50	0.5	**<u>67</u>**	28	70	**<u>224</u>**
100		**<u>69</u>**	44		
1000		**<u>70</u>**	44		

Table 6.9. RVE size corresponding to error ε= 1% (system of overlapping disks)

Θ	ϕ_1	RVE size with respect to overall transport properties		RVE size with respect to microstructure geometry	
		$\max\left[N_{\text{Voigt}}; N_{\text{Reuss}}\right]$	N_{l_p}	$\max\left[N_\xi; N_\psi\right]$	N_{l_c}
5		74	**<u>286</u>**		
10		84	**<u>286</u>**		
50	0.5	92	**<u>286</u>**	98	**<u>286</u>**
100		96	**<u>286</u>**		
1000		98	**<u>286</u>**		

In Table 6.10 the mean values of thermal conductivity coefficients, determined for three different values of contrast in properties, are provided. As in case of previous microstructures, we see that both results, i.e. $\overline{K}$ as well as K^{eff} are in a very well agreement.

Nevertheless, the size of RVE cannot be chosen as small as one may wish – this is observed in Fig. 6.30 where mean value of thermal conductivity coefficient is plotted against N. The results correspond to the case of $\Theta = 10$ and estimation error ε=3%.

Table 6.10. Mean values of thermal conductivity coefficient corresponding to different values of both error ε and contrast in properties Θ (system of overlapping disks)

Θ	ϕ_1	ε	Size of RVE (see Tables 6.8 and 6.9)	Number of realizations n	$\overline{K}$ [W/mK]	K^{eff} [W/mK] (n=1, ε=1%)
5			42	118	2.311	2.296
10		3%	52	204	3.418	3.419
50			67	212	9.587	9.866
5	0.5		286	37	2.284	2.296
10		1%	286	59	3.432	3.419
50			286	78	9.702	9.866
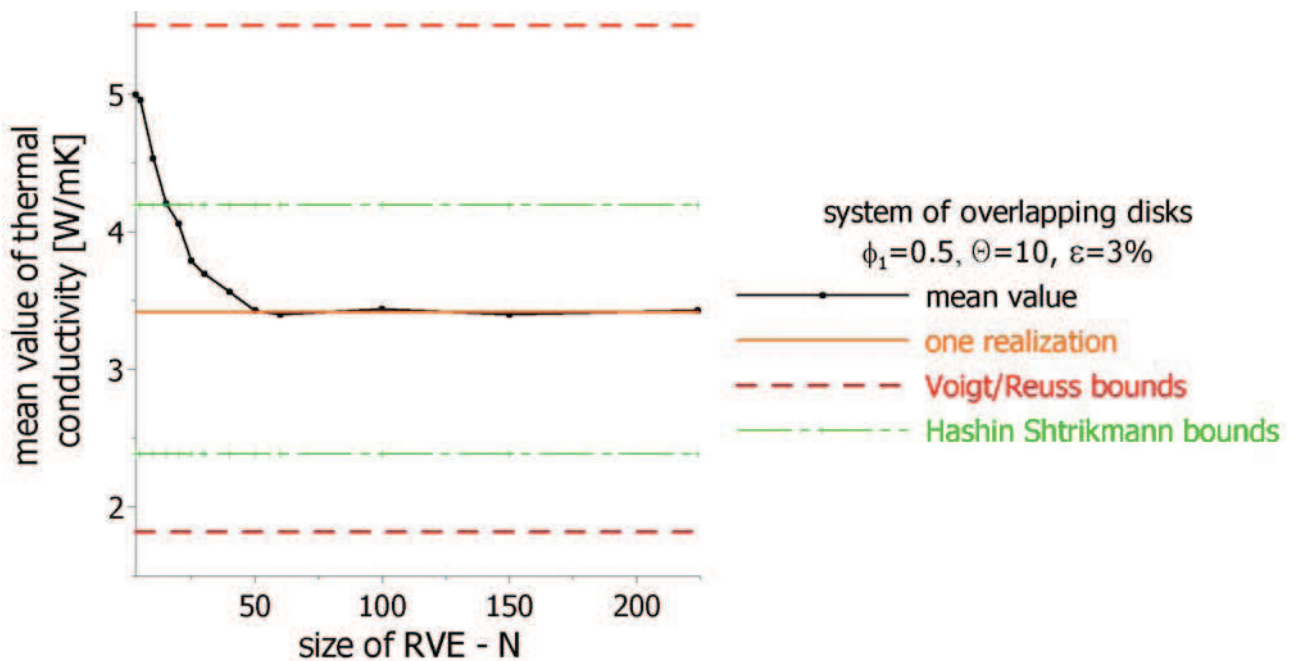
Fig. 6.30. Mean value of thermal conductivity [W/mK], Voigt/Reuss and Hashin-Shtrikman bounds.

System of non-overlapping disks

We focus now on the microstructure corresponding to the system of non-overlapping disks. The results are presented in the same order as in case of previous examples. First, modified two-point correlation functions are presented – see Figs. 6.31 and 6.32.
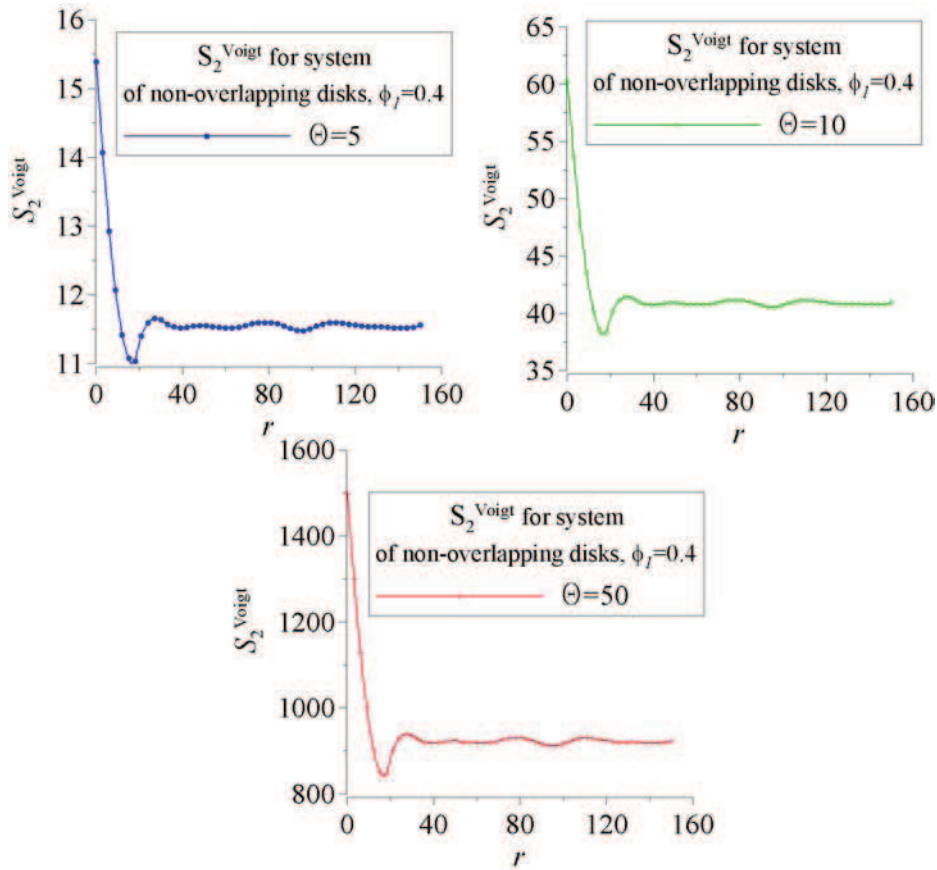
Fig. 6.31. Modified two-point correlation function, S_2^{Voigt}, for different values of contrast in properties.
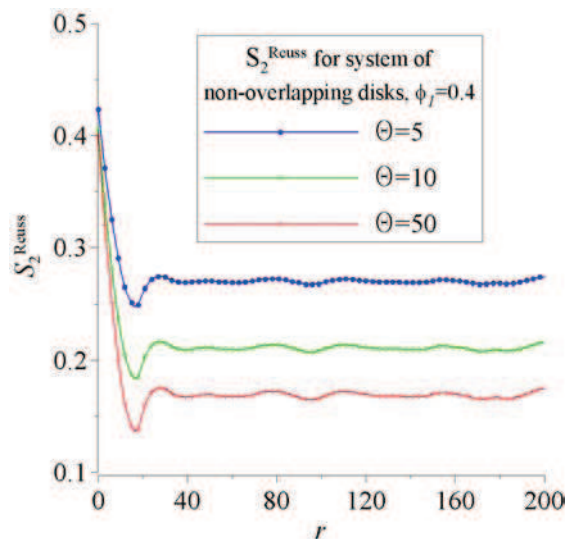
Fig. 6.32. Modified two-point correlation function, S_2^{Reuss}, for different values of contrast in properties

In Fig. 6.33 as well as 6.34 the variance of local Voigt and Reuss estimates are presented, respectively. As before, this quantities are plotted against the size of the sample *N*.
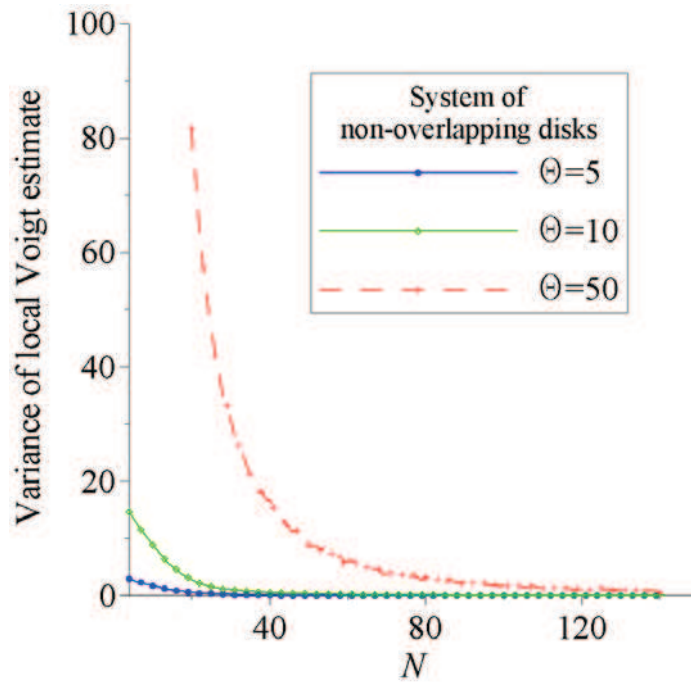
Fig. 6.33. Variance of local Voigt estimate as a function of *N* – system of non-overlapping disks.
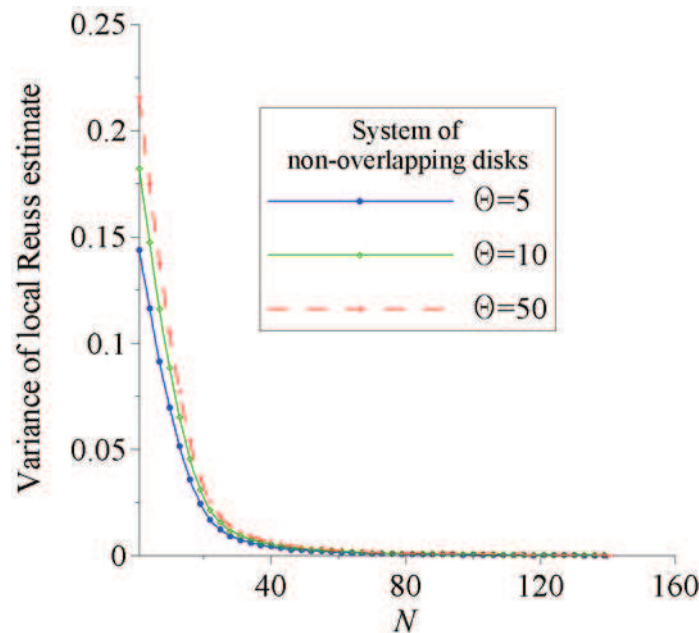
Fig. 6.34. Variance of local Reuss estimate as a function of *N* – system of non-overlapping disks.

The sizes of RVE evaluated with respect to both overall transport properties and microstructure geometry are provided below - see Tables 6.11 and 6.12. Note, as before, the results are determined for different values of contrast in properties Θ (5, 10, 50, 100, 1000) as well as two values of error ε, i.e. 1% and 3%. In Table 6.13 the mean values of thermal conductivity coefficients, determined

for three different values of contrast in properties (5, 10, 50), are provided. As in case of previous microstructures, we see that both results, namely mean value $\overline{K}$ as well as K^{eff} are in a very well agreement.

Table 6.11. RVE size corresponding to error $\varepsilon= 3\%$ (system of non-overlapping disks)

Θ	ϕ_l	RVE size with respect to overall transport properties		RVE size with respect to microstructure geometry	
		$\max\left[N_{\text{Voigt}}; N_{\text{Reuss}}\right]$	N_{l_p}	$\max\left[N_\xi; N_\psi\right]$	N_{l_c}
5		31	**42**		
10		37	**44**		
50	0.4	44	**194**	47	**200**
100		46	**194**		
1000		47	**194**		

Table 6.12. RVE size corresponding to error $\varepsilon= 1\%$ (system of non-overlapping disks)

Θ	ϕ_l	RVE size with respect to overall transport properties		RVE size with respect to microstructure geometry	
		$\max\left[N_{\text{Voigt}}; N_{\text{Reuss}}\right]$	N_{l_p}	$\max\left[N_\xi; N_\psi\right]$	N_{l_c}
5		48	**240**		
10		59	**240**		
50	0.4	69	**240**	72	**240**
100		70	**240**		
1000		72	**240**		

Table 6.13. Mean values of thermal conductivity coefficient corresponding to different values of both error ε and contrast in properties Θ (system of non-overlapping disks)

Θ	ϕ_l	ε	Size of RVE (see Tables 6.11 and 6.12)	Number of realizations n	$\overline{K}$ [W/mK]	K^{eff} [W/mK] ($n=1$, $\varepsilon=1\%$)
5			42	91	2.753	2.778
10		3%	44	166	4.551	4.581
50	0.4		194	14	17.964	18.311
5			240	22	2.776	2.778
10		1%	240	35	4.644	4.581
50			240	58	18.023	18.311

Fig. 6.35 provides the value of $\overline{K}$ plotted against the size of the sample expressed in terms of the number of pixels in a row and in a column, N. The results correspond to the case of $\Theta = 10$ and $\varepsilon = 3\%$. The value of K^{eff} as well as the bounds of Voigt/Reuss and Hashin-Shtrikman are also displayed. It can be seen that as the sample size is increasing the difference between mean value of thermal conductivity $\overline{K}$ and K^{eff} is decreasing – this was also observed for previously considered random cell models.
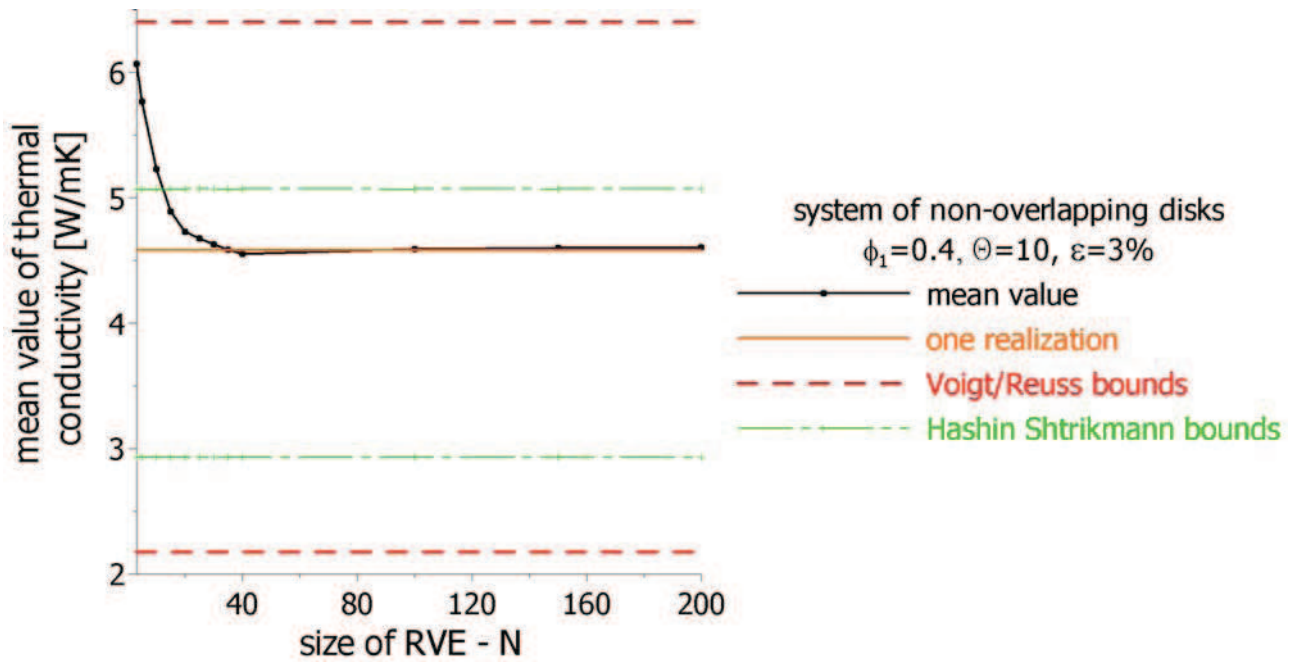
Fig. 6.35. Mean value of thermal conductivity [W/mK], Voigt/Reuss and Hashin-Shtrikman bounds.

6.3. Reconstructed microstructures

Debye microstructure

In case of reconstructed microstructures we begin our considerations with Debye random medium. Figs. 6.36 and 6.37 provide modified two-point correlation functions S_2^{Voigt} as well as S_2^{Reuss}. As in case of previously considered examples, aforementioned functions are determined with assumption that $k_1 = 1$.

In Figs. 6.38 and 6.39 the variances corresponding to local Voigt as well as local Reuss estimations are graphically presented. Once again, the variances are plotted against the sample size which is expressed by the number of pixels in a row (and in a column) N. Note, the functions are

decreasing as the size N is increasing. Furthermore, the greatest value of variance is obtained for the value of contrast in properties $\Theta = 50$.
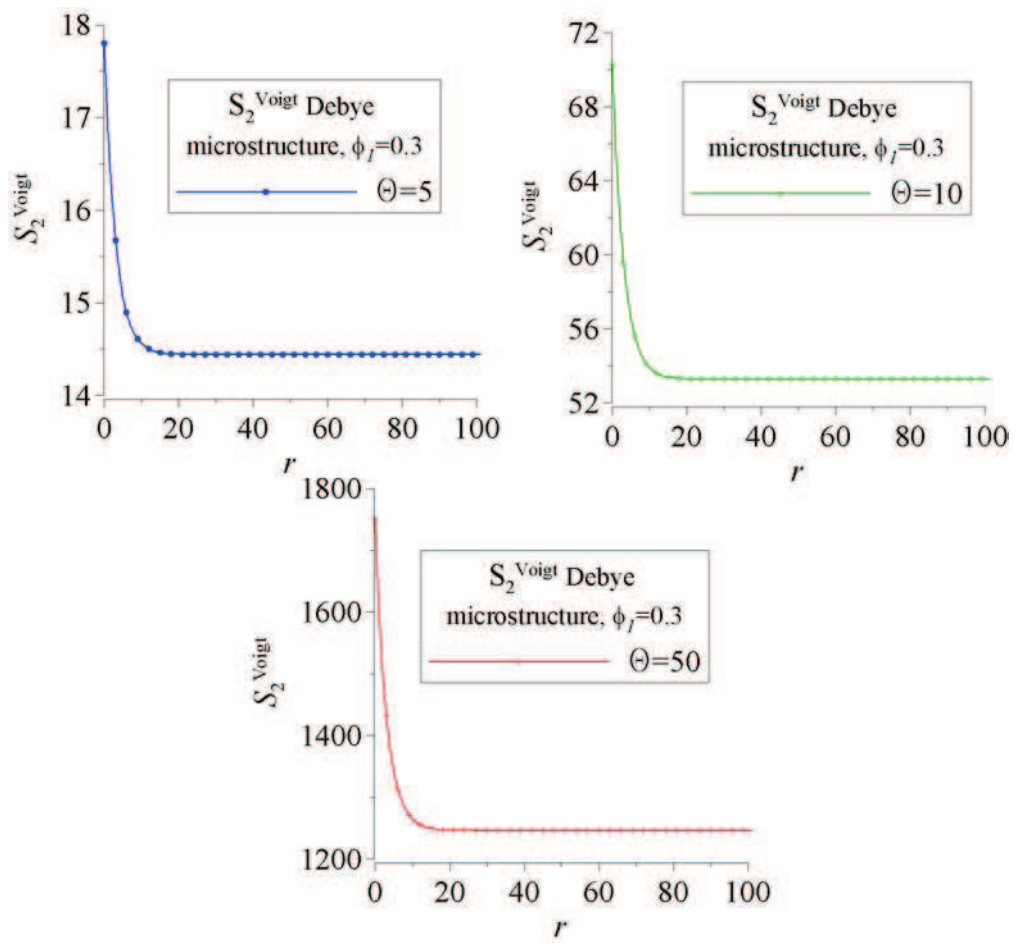
Fig. 6.36. Modified two-point correlation function, S_2^{Voigt}, for different values of contrast in properties.
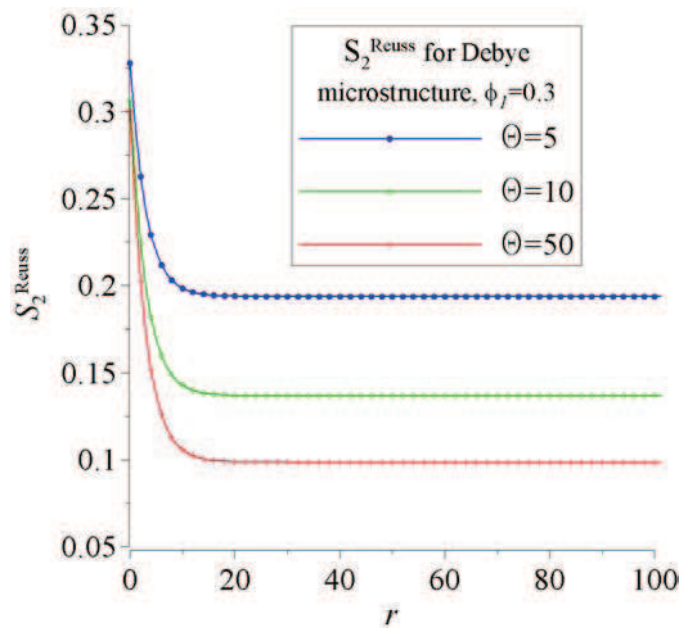
Fig. 6.37. Modified two-point correlation function, S_2^{Reuss}, for different values of contrast in properties
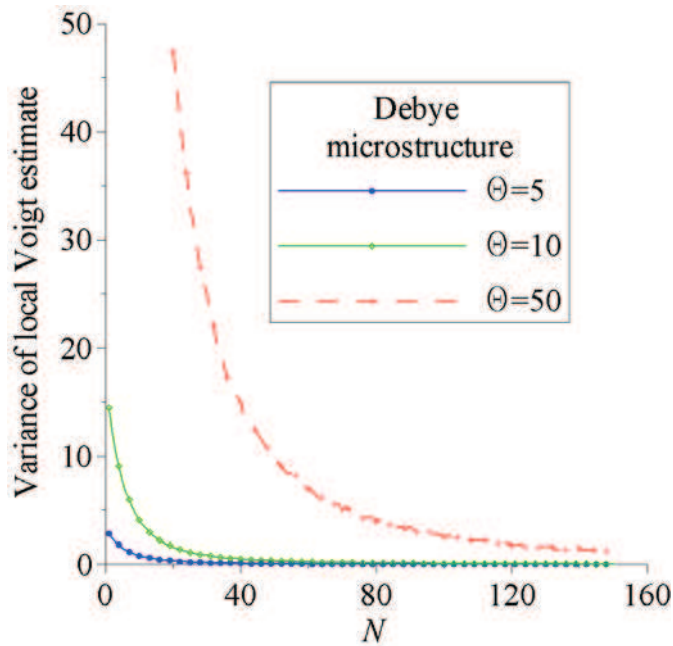
Fig. 6.38. Variance of local Voigt estimate as a function of N – Debye microstructure.
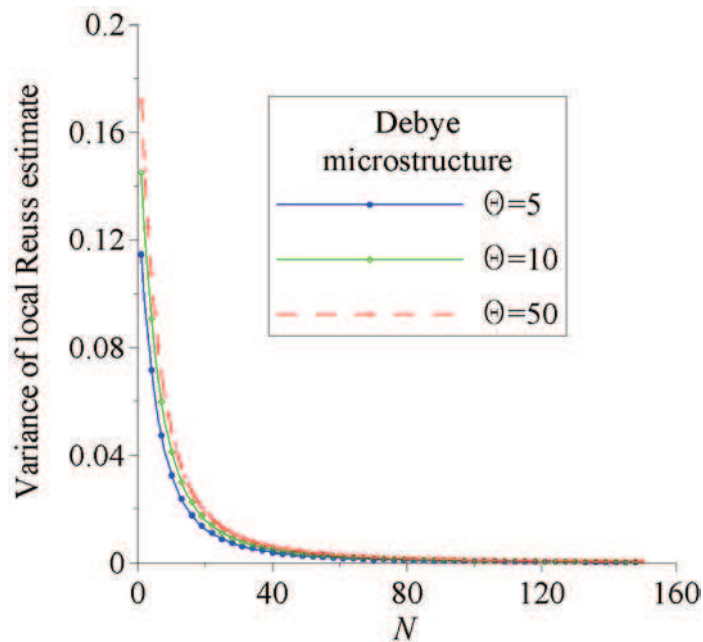
Fig. 6.39. Variance of local Reuss estimate as a function of N – Debye microstructure.

Tables 6.14 and 6.15 provide the sizes of RVE evaluated with respect to both overall transport properties and microstructure geometry. As in case of previously considered examples the results are determined for different values of contrast in properties Θ (5, 10, 50, 100, 1000) as well as two values of error ε, i.e. 1% and 3%.

In Table 6.16 the mean values of thermal conductivity coefficients, determined for three different values of contrast in properties (5, 10, 50), are provided. Once again, one can simply notice that both results, namely mean value $\overline{K}$ as well as K^{eff}, are in a very well agreement.

Table 6.14. RVE size corresponding to error $\varepsilon = 3\%$ (Debye microstructure)

Θ	ϕ_l	RVE size with respect to overall transport properties		RVE size with respect to microstructure geometry	
		$\max\left[N_{\text{Voigt}}; N_{\text{Reuss}}\right]$	N_{l_p}	$\max\left[N_{\xi}; N_{\psi}\right]$	N_{l_c}
5		**34**	20		
10		**46**	24		
50	0.3	**59**	26	**64**	40
100		**62**	28		
1000		**64**	28		

Table 6.15. RVE size corresponding to error $\varepsilon = 1\%$ (Debye microstructure)

Θ	ϕ_l	RVE size with respect to overall transport properties		RVE size with respect to microstructure geometry	
		$\max\left[N_{\text{Voigt}}; N_{\text{Reuss}}\right]$	N_{l_p}	$\max\left[N_{\xi}; N_{\psi}\right]$	N_{l_c}
5		**59**	28		
10		**81**	30		
50	0.3	**103**	34	**114**	50
100		**112**	36		
1000		**114**	38		

Table 6.16. Mean values of thermal conductivity coefficient corresponding to different values of both error ε and contrast in properties Θ (Debye microstructure)

Θ	ϕ_l	ε	Size of RVE (see Tables 6.14 and 6.15)	Number of realizations n	$\overline{K}$ [W/mK]	K^{eff} [W/mK] ($n=1$, $\varepsilon=1\%$)
5			34	124	3.092	3.058
10		3%	46	123	5.117	5.009
50			59	124	18.676	18.130
5	0.3		59	378	3.070	3.058
10		1%	81	405	5.065	5.009
50			103	377	18.230	18.130

In Fig. 6.40 the mean value of thermal conductivity coefficient, namely $\overline{K}$, is plotted against the size of the sample N. The results correspond to the case of $\Theta = 10$ and $\varepsilon = 3\%$. The value of K^{eff} as

well as the bounds of Voigt/Reuss and Hashin-Shtrikman are also presented. Once again, it can be seen that as the sample size N is increasing the difference between $\overline{K}$ and K^{eff} is decreasing – this was also observed for previously considered random microstructures.
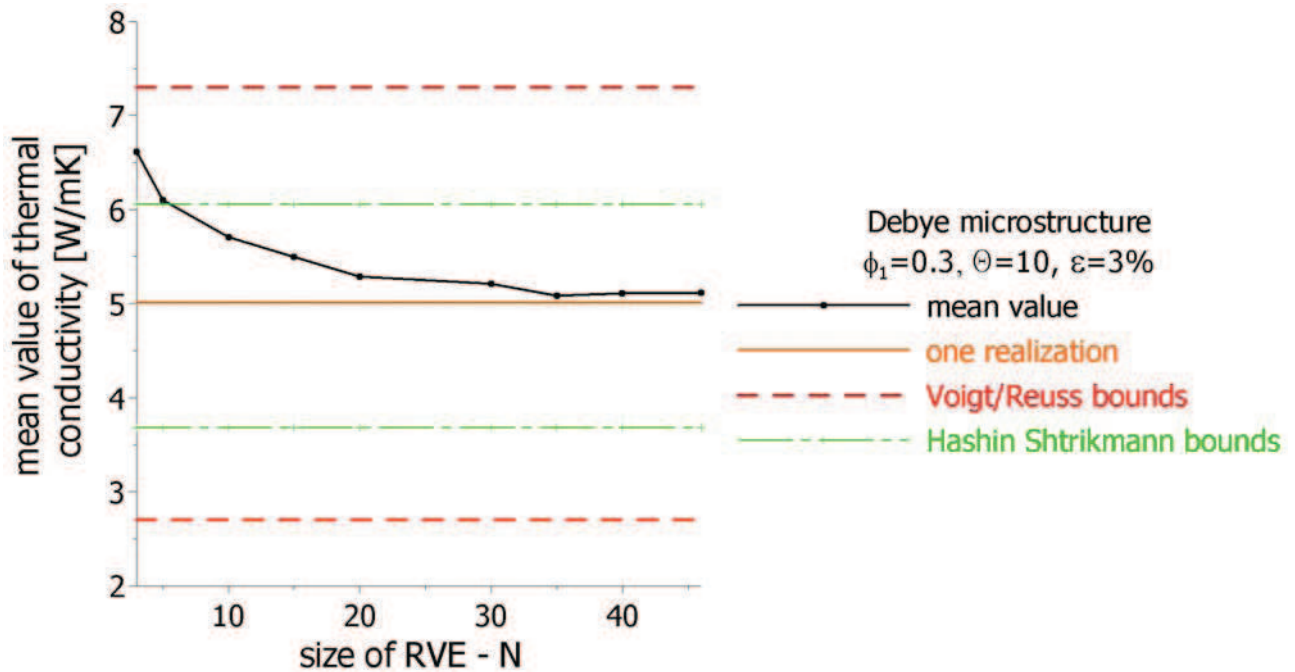
Fig. 6.40. Mean value of thermal conductivity [W/mK], Voigt/Reuss and Hashin-Shtrikman bounds.

Modified Debye microstructure

A microstructure corresponding to the modified Debye random medium is now considered. Once again the results are presented in the same order as in case of previous examples. Therefore, modified two-point correlation functions for both estimations (Voigt and Reuss) are , first, presented – see Figs. 6.41 and 6.42. As before thermal conductivity coefficient for phase one is k_1=1 and hence $k_2 = \Theta$.

In Figs. 6.43 and 6.44 the variances corresponding to local Voigt as well as local Reuss estimations are graphically presented. As before, these quantities are plotted against the sample size which is expressed in terms of the number of pixels in a row (and in a column) N. Note, the aforementioned functions are decreasing as the size of the sample N is increasing. Furthermore, the greatest value of variance of local Voigt/Reuss estimate corresponds to the greatest value of contrast in properties, i.e. $\Theta = 50$ - this was also observed for previously considered examples.
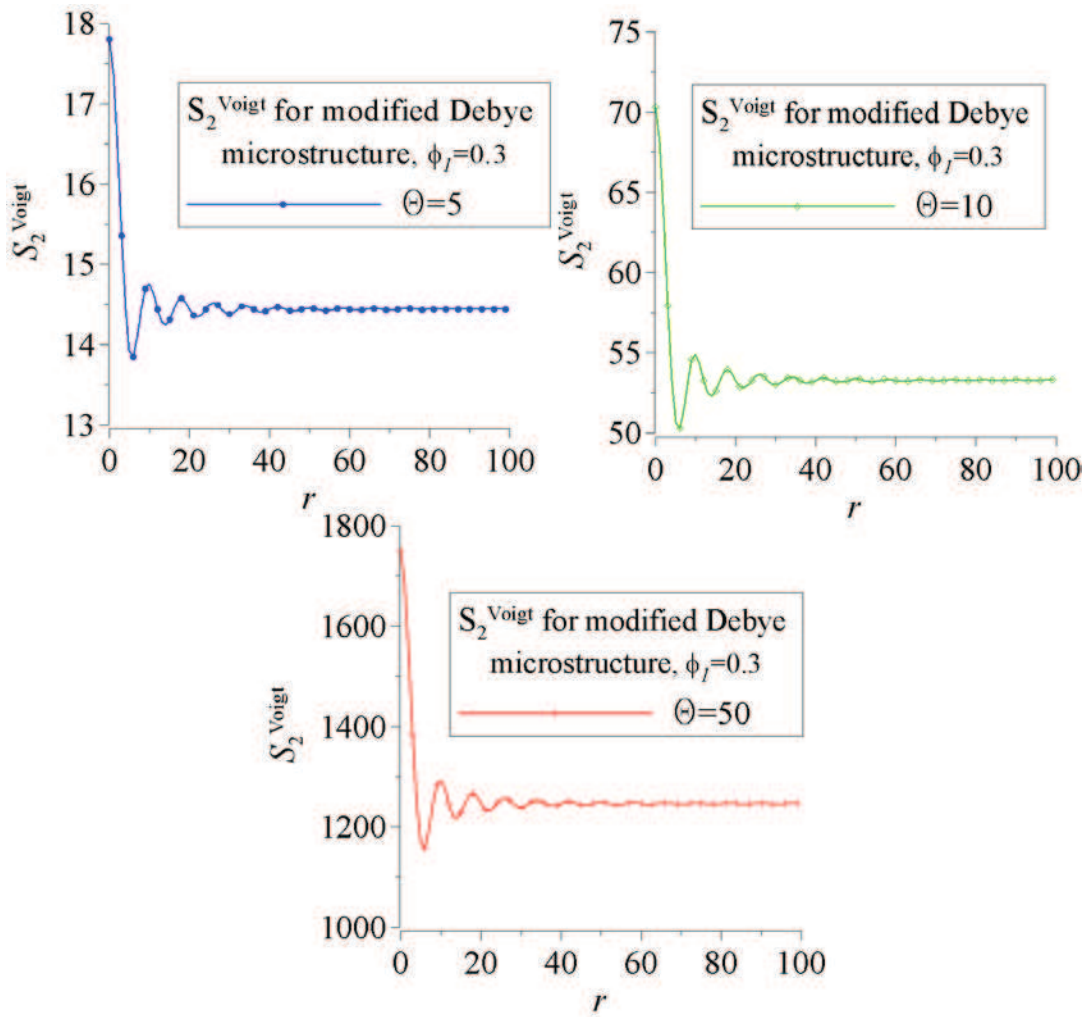
Fig. 6.41. Modified two-point correlation function, S_2^{Voigt}, for different values of contrast in properties.
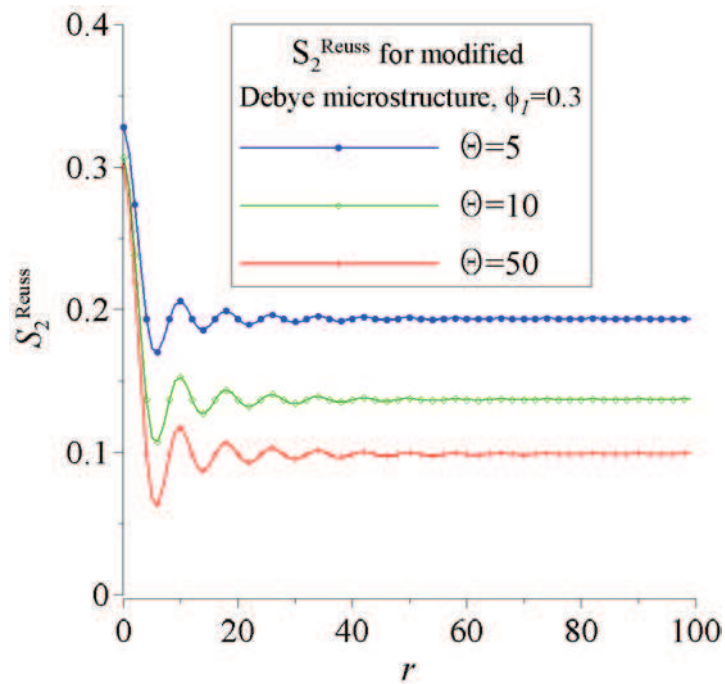
Fig. 6.42. Modified two-point correlation function, S_2^{Reuss}, for different values of contrast in properties
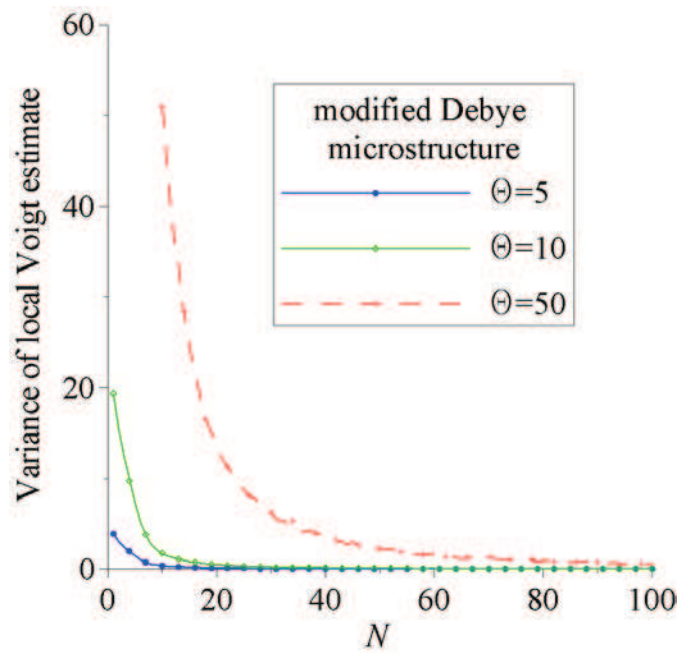
Fig. 6.43. Variance of local Voigt estimate as a function of N – modified Debye microstructure.
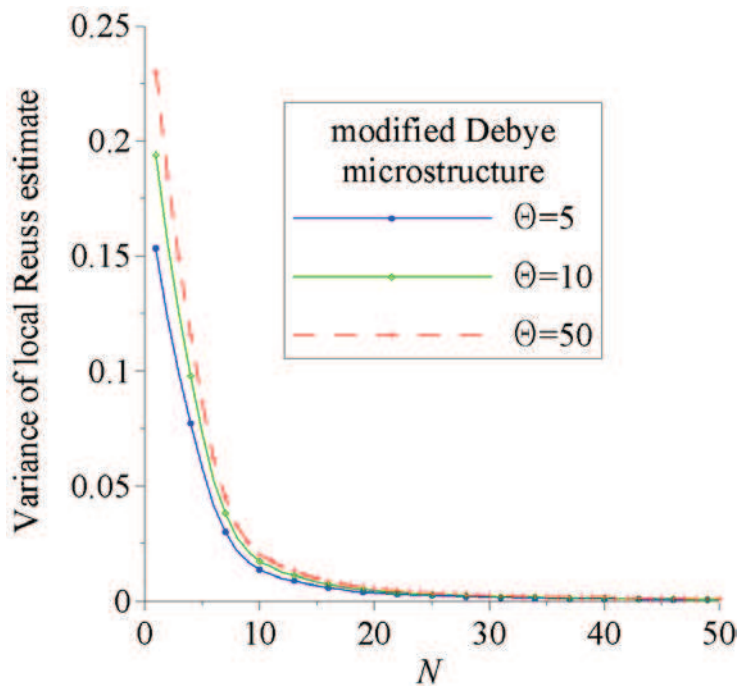
Fig. 6.44. Variance of local Voigt estimate as a function of N – modified Debye microstructure.

The sizes of RVE evaluated for considered microstructure are collected in Tables 6.17 and 6.18. Note, as before, the results are determined for different values of contrast in properties as well as different values of estimation error ε. The results concerning RVE sizes evaluated with respect to both overall transport properties and microstructure geometry are provided. In Table 6.19 the mean values of thermal conductivity coefficients, determined for three different values of contrast in properties (5, 10, 50), are presented. Once again, one can simply notice that both results, i.e. $\overline{K}$ as

well as K^{eff}, converge to each other. Fig. 6.45 shows the values of mean value of thermal conductivity coefficient determined for the sample sizes N smaller than RVE. The results correspond to the case of $\Theta = 10$ and $\varepsilon = 3\%$.

Table 6.17. RVE size corresponding to error $\varepsilon = 3\%$ (modified Debye microstructure)

Θ	ϕ_I	RVE size with respect to overall transport properties		RVE size with respect to microstructure geometry	
		$\max\left[N_{\text{Voigt}}; N_{\text{Reuss}}\right]$	N_{l_p}	$\max\left[N_{\xi}; N_{\psi}\right]$	N_{l_c}
5		17	**38**		
10		23	**46**		
50	0.3	28	**62**	30	**68**
100		30	**68**		
1000		30	**68**		

Table 6.18. RVE size corresponding to error $\varepsilon = 1\%$ (modified Debye microstructure)

Θ	ϕ_I	RVE size with respect to overall transport properties		RVE size with respect to microstructure geometry	
		$\max\left[N_{\text{Voigt}}; N_{\text{Reuss}}\right]$	N_{l_p}	$\max\left[N_{\xi}; N_{\psi}\right]$	N_{l_c}
5		30	**62**		
10		39	**78**		
50	0.3	47	**100**	54	**100**
100		52	**100**		
1000		54	**100**		

Table 6.19. Mean values of thermal conductivity coefficient corresponding to different values of both error ε and contrast in properties Θ (modified Debye microstructure)

Θ	ϕ_I	ε	Size of RVE (see Tables 6.17 and 6.18)	Number of realizations n	$\overline{K}$ [W/mK]	K^{eff} [W/mK] (n=1, ε=1%)
5			38	26	3.063	3.098
10		3%	46	31	5.192	5.179
50	0.3		62	27	19.651	19.963
5			62	81	3.088	3.098
10		1%	78	92	5.108	5.179
50			100	92	19.762	19.963
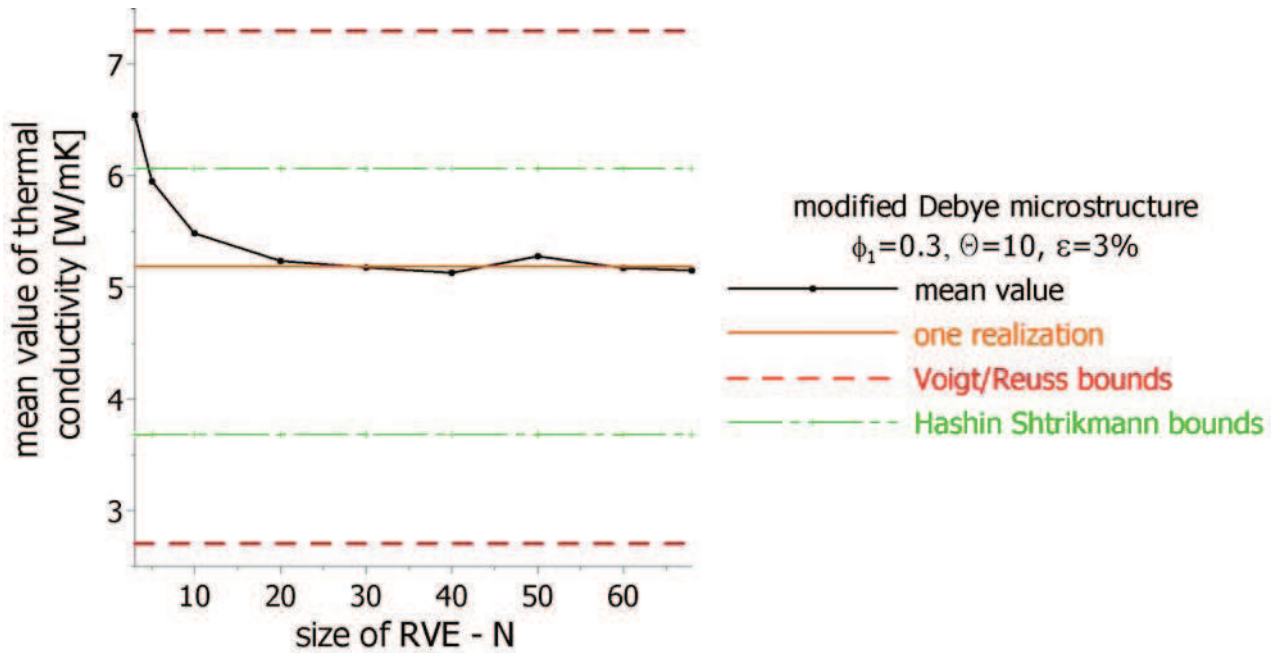
Fig. 6.45. Mean value of thermal conductivity [W/mK], Voigt/Reuss and Hashin-Shtrikman bounds.

Fontainebleau sandstone

The results concerning Fontainebleau sandstone microstructure are in the same order as for previously considered ones. Figs. 6.46 and 6.47 show the modified two-point correlation functions.
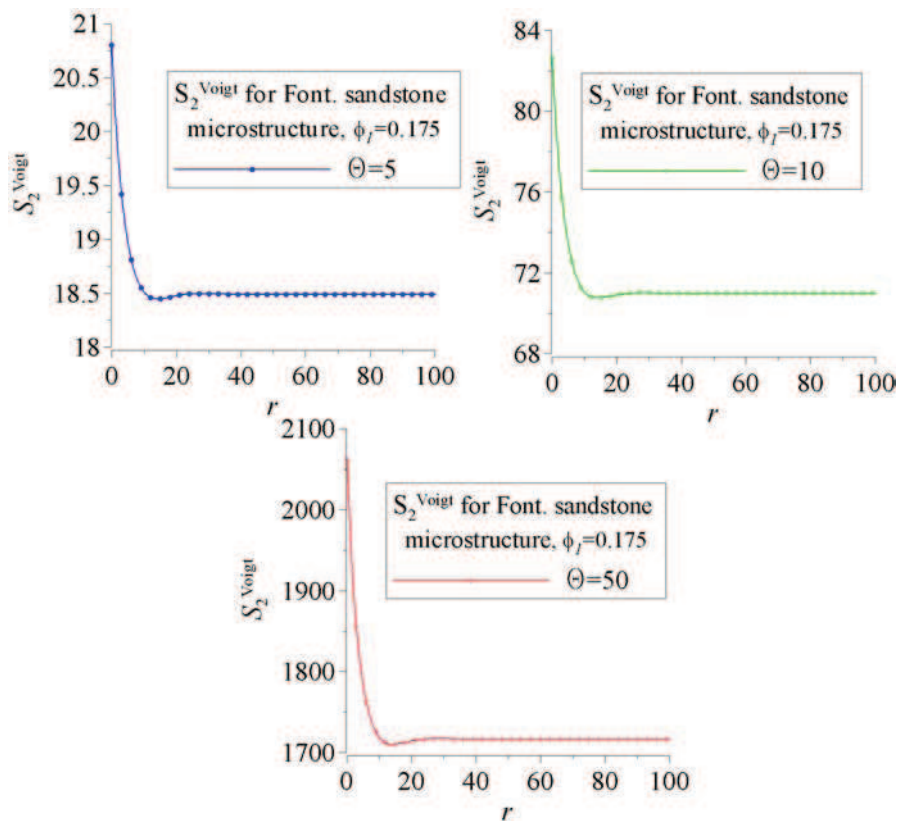
Fig. 6.46. Modified two-point correlation function, S_2^{Voigt} , for different values of contrast in properties.
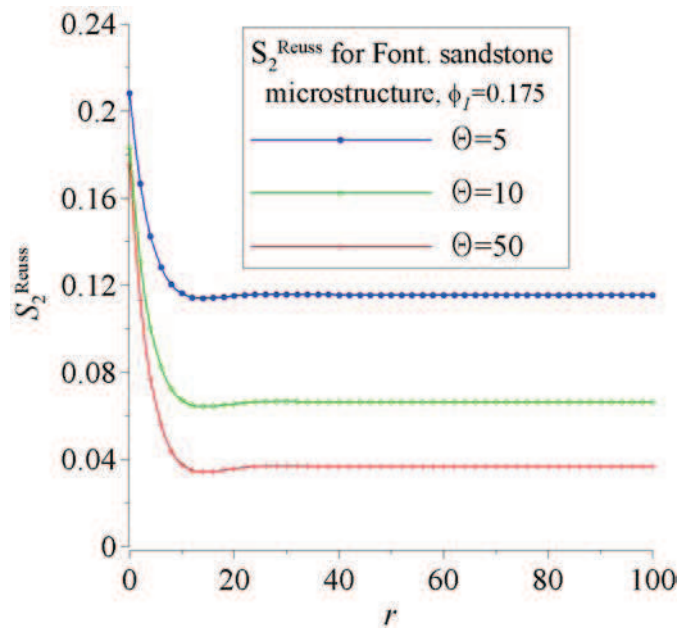
Fig. 6.47. Modified two-point correlation function, S_2^{Reuss}, for different values of contrast in properties

In Figs. 6.48 and 6.49 the variances corresponding to local Voigt as well as local Reuss estimations are graphically presented. Once again, the variances are plotted against the sample size which is expressed by the number of pixels in a row (and in a column) N.

Tables 6.20 and 6.21 provide the sizes of RVE evaluated with respect to both overall transport properties and microstructure geometry. As in case of previously considered examples the results are determined for different values of contrast in properties Θ (5, 10, 50, 100, 1000) as well as two values of error ε, i.e. 1% and 3%. In Table 6.22 the mean values of thermal conductivity coefficients, determined for three different values of contrast in properties (5, 10, 50), are provided.
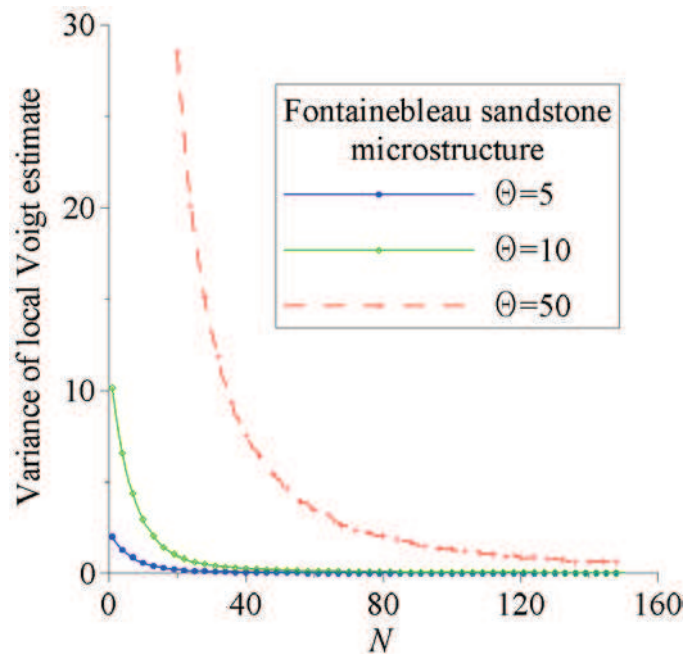
Fig. 6.48. Variance of local Voigt estimate as a function of N – Fontainebleau sandstone microstructure.
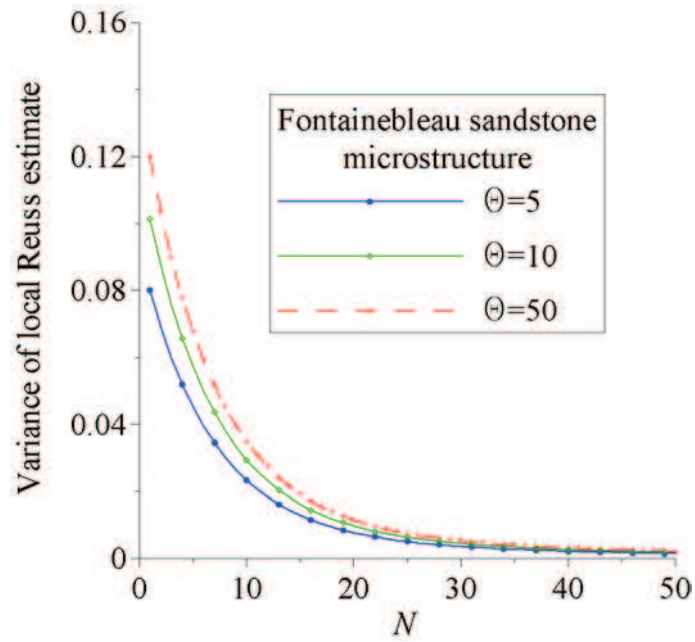
Fig. 6.49. Variance of local Voigt estimate as a function of N – Fontainebleau sandstone microstructure.

Table 6.20. RVE size corresponding to error $\varepsilon = 3\%$ (Fontainebleau sandstone)

Θ	ϕ_I	RVE size with respect to overall transport properties		RVE size with respect to microstructure geometry	
		$\max\left[N_{\text{Voigt}}; N_{\text{Reuss}}\right]$	N_{l_p}	$\max\left[N_\xi; N_\psi\right]$	N_{l_c}
5		**31**	18		
10		**46**	20		
50	0.175	**68**	40	**77**	66
100		**72**	40		
1000		**77**	40		

Table 6.21. RVE size corresponding to error $\varepsilon = 1\%$ (Fontainebleau sandstone)

Θ	ϕ_I	RVE size with respect to overall transport properties		RVE size with respect to microstructure geometry	
		$\max\left[N_{\text{Voigt}}; N_{\text{Reuss}}\right]$	N_{l_p}	$\max\left[N_\xi; N_\psi\right]$	N_{l_c}
5		**54**	36		
10		**81**	42		
50	0.175	**119**	44	**133**	80
100		**128**	44		
1000		**133**	44		

Table 6.22. Mean values of thermal conductivity coefficient corresponding to different values of both error ε and contrast in properties Θ (Fontainebleau sandstone)

Θ	ϕ_1	ε	Size of RVE (see Tables 6.20 and 6.21)	Number of realizations n	$\overline{K}$ [W/mK]	K^{eff} [W/mK] (n=1, ε=1%)
5			31	132	3.851	3.779
10		3%	46	128	6.976	6.814
50			68	122	30.135	29.516
5	0.175		54	398	3.826	3.779
10		1%	81	378	6.865	6.814
50			119	367	30.108	29.516

Fig. 6.50 provides the mean value of thermal conductivity coefficient $\overline{K}$ plotted against the sample size N. All results correspond to the case of $\Theta = 10$ and ε=3%. The value of K^{eff} as well as the bounds of Voigt/Reuss and Hashin-Shtrikman are also displayed. Once again, it can be seen that as the sample size N is increasing the difference between mean value of thermal conductivity $\overline{K}$ and K^{eff} is decreasing.
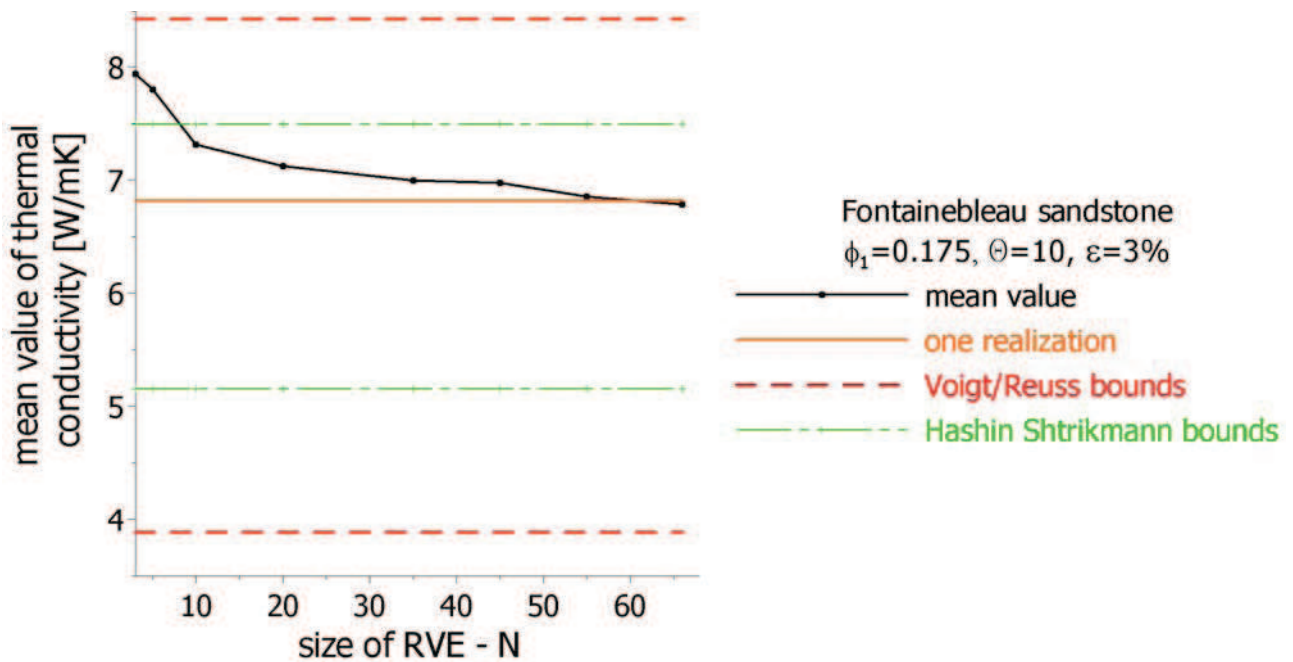
Fig. 6.50. Mean value of thermal conductivity [W/mK], Voigt/Reuss and Hashin-Shtrikman bounds.

Boron-carbide/aluminum composite

As before the modified two-point correlation functions corresponding to Voigt and Reuss estimates are first presented – see Fig 6.51 and 6.52. The variances corresponding to local Voigt as well as local Reuss estimations are graphically presented in Fig. 6.53 and 6.54.
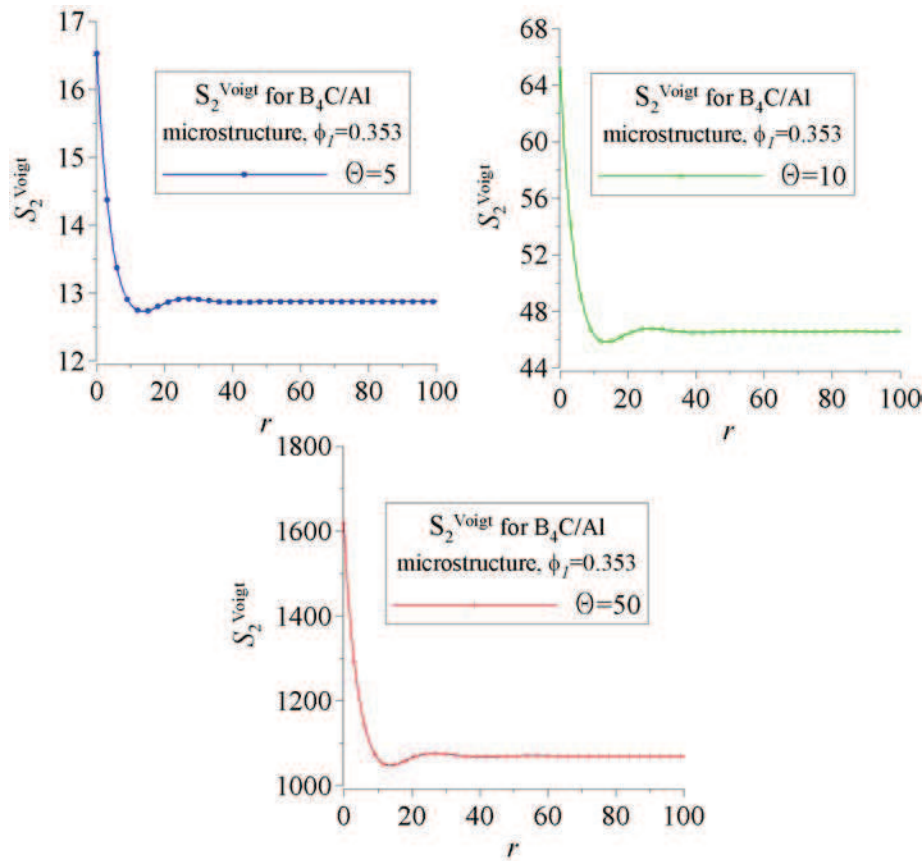
Fig. 6.51. Modified two-point correlation function, S_2^{Voigt}, for different values of contrast in properties.
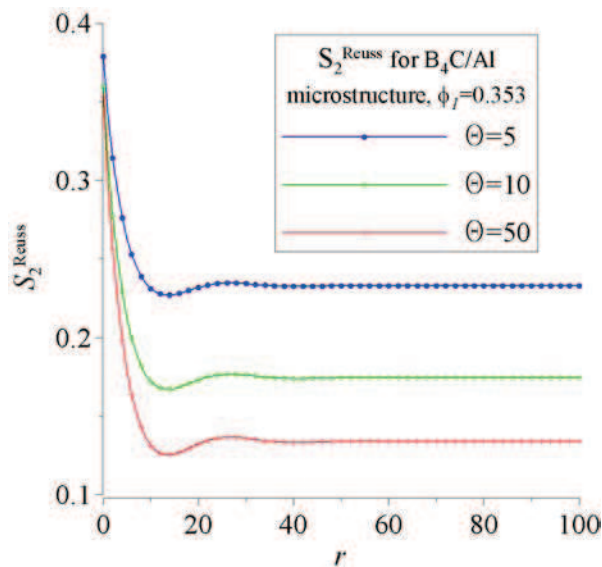
Fig. 6.52. Modified two-point correlation function, S_2^{Reuss}, for different values of contrast in properties
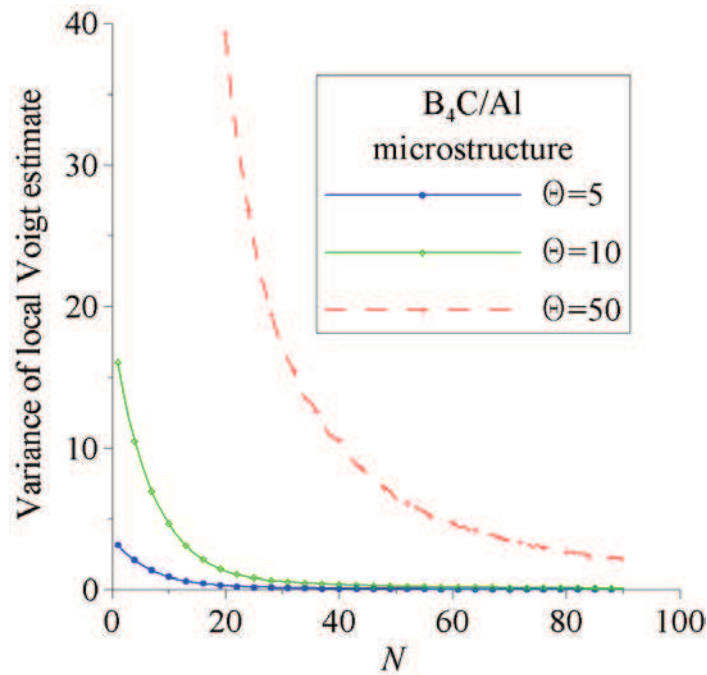
Fig. 6.53. Variance of local Voigt estimate as a function of N – B_4C/Al composite.
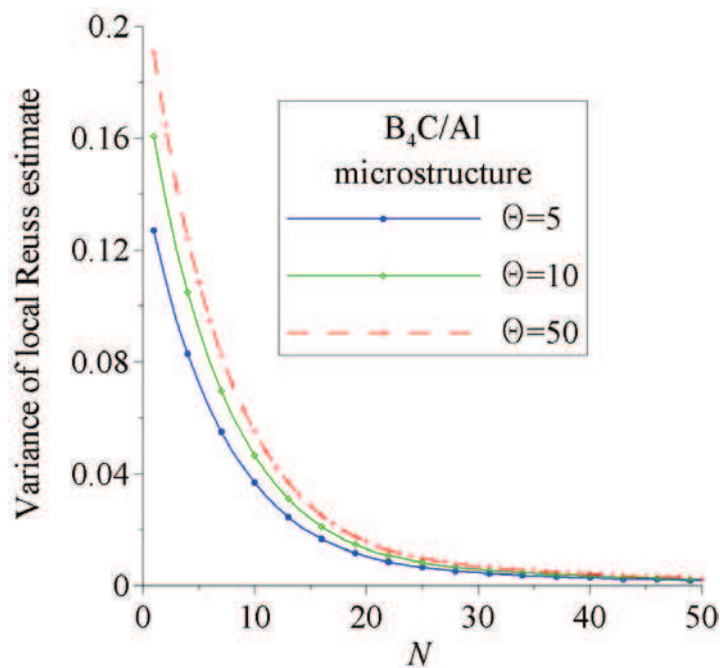
Fig. 6.54. Variance of local Reuss estimate as a function of N – B_4C/Al composite.

Tables 6.23 and 6.24 provide the sizes of RVE evaluated with respect to both overall transport properties and microstructure geometry. The results correspond to different values of contrast in properties Θ (5, 10, 50, 100, 1000) as well as different values of error ε, i.e. 1% and 3%.

In Table 6.25 mean values of thermal conductivity coefficients, determined for three different values of contrast in properties (5, 10, 50), are provided. Once again, we observe well agreement between mean values $\overline{K}$ and the result which is treated as the effective property, namely K^{eff}.

Table 6.23. RVE size corresponding to error ε= 3% (B$_4$C/Al)

Θ	ϕ_I	RVE size with respect to overall transport properties		RVE size with respect to microstructure geometry	
		$\max\left[N_{\text{Voigt}};N_{\text{Reuss}}\right]$	N_{l_p}	$\max\left[N_\xi;N_\psi\right]$	N_{l_c}
5		**25**	16		
10		30	**34**		
50	0.353	**40**	36	44	**80**
100		**42**	38		
1000		**44**	38		

Table 6.24. RVE size corresponding to error ε= 1% (B$_4$C/Al)

Θ	ϕ_I	RVE size with respect to overall transport properties		RVE size with respect to microstructure geometry	
		$\max\left[N_{\text{Voigt}};N_{\text{Reuss}}\right]$	N_{l_p}	$\max\left[N_\xi;N_\psi\right]$	N_{l_c}
5		**44**	38		
10		54	**60**		
50	0.353	**70**	64	77	**100**
100		**75**	64		
1000		**77**	66		

Table 6.25 Mean values of thermal conductivity coefficient corresponding to different values of both error ε and contrast in properties Θ (B$_4$C/Al)

Θ	ϕ_I	ε	Size of RVE (see Tables 6.23 and 6.24)	Number of realizations n	$\overline{K}$ [W/mK]	K^{eff} [W/mK] (n=1, ε=1%)
5			25	144	2.893	2.803
10		3%	34	128	4.485	4.403
50	0.353		40	140	13.807	13.550
5			44	439	2.852	2.803
10		1%	60	398	4.480	4.403
50			70	452	13.681	13.550

Fig. 6.55 provides the mean value of thermal conductivity coefficient plotted against sample size
N. The results correspond to the case of Θ =10 and ε=3%. Once again the value of effective thermal

conductivity coefficient, i.e. K^{eff} as well as the bounds of Voigt/Reuss and Hashin/Shtrikman are also presented. It can be seen that as the sample size is increasing the difference between mean value of thermal conductivity $\overline{K}$ and K^{eff} is decreasing.
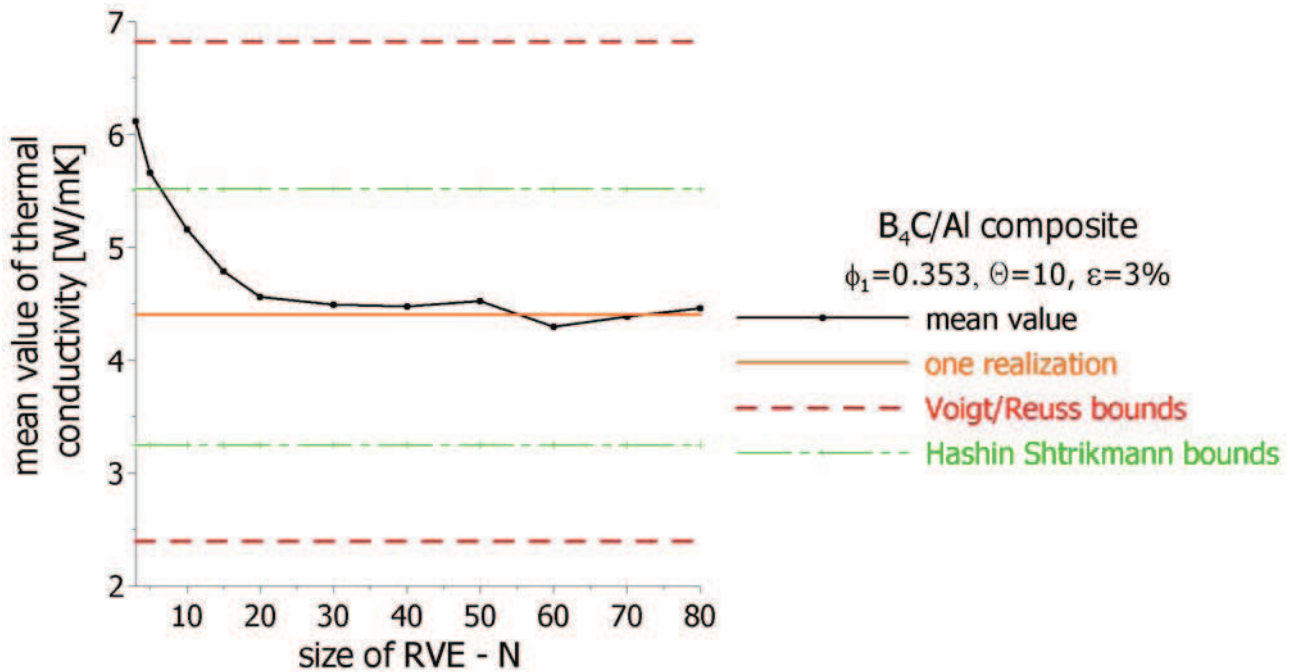
Fig. 6.55. Mean value of thermal conductivity [W/mK], Voigt/Reuss and Hashin-Shtrikman bounds.

6.4. Remarks

Numerical method (based on finite volume scheme) which has been formulated in section 6.1 is devoted to solve the boundary value problem (2.6). This method is applied for use on digital images. Even though the boundary value problem as well as numerical technique have been formulated for the diffusion problem, other classes of transport phenomena (see Table 2.1) can be solved in the same manner.

The validation of proposed method, on the basis of simple 2D diffusion problem, has also been performed. The results, for single deterministic microstructure, are in a very well agreement with those of FE calculations. More sophisticated studies regarding the numerical error as well as mesh density in the view of particular random microstructures have also been carried out – the results concerning the influence of contrast in properties, volume fraction of phases as well as microstructure geometry on the value of thermal conductivity coefficient were provided.

Furthermore, it should be noted that all calculations performed by pixel based finite volume scheme have been performed by the algorithm which had been written, by the author, in C++ code. Moreover, in order to solve the system of linear equations (6.14) the conjugate gradient method has

been utilized. Additionally, in an attempt to increase the rate of convergence and hence to accelerate computations the typical precondition of matrix $\mathbf{Z}$ has been performed (see Zohdi & Wriggers 2005).

In this chapter a numerical validation of the RVE size with respect to overall transport properties has been provided. As in case of geometrical representativity criterion all considered examples were split into two groups: *random cell models* and *reconstructed microstructures*. Following results provided in section 6.2 and 6.3 several conclusions can be stated:

- within all considered examples the variances of local Voigt and Reuss estimates are decreasing as the size of the sample is increasing,

- observing results one can simply notice that the size of RVE is increasing as the error of estimation ε is decreasing,

- it can be seen that as the contrast in properties Θ is increasing the size evaluated as $\max\left[N_{\text{Voigt}}; N_{\text{Reuss}}\right]$ (relation 5.56) converges towards the one obtained from geometrical criterion, i.e. $\max\left[N_{\xi}; N_{\psi}\right]$ (relation 4.35) - this was observed in case of all considered examples; furthermore for the value of $\Theta = 1000$ both criterions yield the same result,

- for chosen values of contrast in properties (5, 10, 50) the mean values of thermal conductivity coefficients (averaged over sufficient number of realizations *n*) are in a very well agreement with K^{eff} (the result corresponding to RVE size for which only one realization is sufficient and error of estimation is ε=1%),

- the relative error between $\overline{K}$ and K^{eff} is usually increasing as the contrast in properties is increasing – this may be caused by not sufficient mesh density - numerical analysis shown that in some cases (especially for $\Theta = 50$) one should use about 16 or even 25 control volumes to mesh one pixel; in all considered examples only 9 control volumes have been used.

Before further conclusions are stated, first, some remarks concerning the error of estimation are provided. Consider an arbitrary microstructure and assume that the size of the sample is $N \ll \infty$. Let the mean value of effective property (averaged over sufficient number of realizations) be denoted as $\overline{K}$. Furthermore, the expectation of overall property, for chosen size $N \ll \infty$, is K_N, whereas the response for infinite body - effective property - is K^{eff}.

It is evident that according to central limit theorem, for chosen sample size $N \ll \infty$, the mean value $\overline{K}$ should satisfy following relation (with given probability):

$$\left| \overline{K} - K_N \right| \le \varepsilon_{abs} \tag{6.24}$$

Utilizing relation (3.35) we can rewrite (6.24) as

$$\left(1 - \varepsilon_{rel}\right) K_N \le \overline{K} \le \left(1 + \varepsilon_{rel}\right) K_N \tag{6.25}$$

On the other hand, for given sample size $N \ll \infty$, the overall response, i.e. K_N differs from the infinite body result, K^{eff}, such that:

$$\left(1 - \varepsilon\right) K^{\mathrm{eff}} \le K_N \le \left(1 + \varepsilon\right) K^{\mathrm{eff}} \tag{6.26}$$

and therefore utilising (6.25) we obtain:

$$\left(1 - \varepsilon_{rel}\right)\left(1 - \varepsilon\right) K^{\mathrm{eff}} \le \overline{K} \le \left(1 + \varepsilon_{rel}\right)\left(1 + \varepsilon\right) K^{\mathrm{eff}} \tag{6.27}$$

Assuming that $\varepsilon_{rel}\varepsilon$ is the higher order negligible term we can express (6.27) in the following form:

$$\left(1 - \varepsilon_{rel} - \varepsilon\right) K^{\mathrm{eff}} \le \overline{K} \le \left(1 + \varepsilon_{rel} + \varepsilon\right) K^{\mathrm{eff}} \tag{6.28}$$

Note that within all calculations provided in previous section we assumed that $\varepsilon_{rel} = \varepsilon$ and hence the error of estimation is as follows:

$$\left(1 - 2\varepsilon\right) K^{\mathrm{eff}} \le \overline{K} \le \left(1 + 2\varepsilon\right) K^{\mathrm{eff}} \tag{6.29}$$

Therefore the relative error between mean value averaged over sufficient number of realizations and the effective property should be less than 2ε, i.e.

$$\frac{\left| \overline{K} - K^{\mathrm{eff}} \right|}{K^{\mathrm{eff}}} \le 2\varepsilon \tag{6.30}$$

It should be noted that for all considered microstructures relative error (6.30) is less than the limiting accuracy 2ε – see Tables: 6.3, 6.4, 6.7, 6.10, 6.13, 6.16, 6.19, 6.22, and 6.25.

In Table 6.26 relative errors calculated according to relation (6.30) are provided. Note that results are obtained for all considered microstructures. Furthermore, for each microstructure two relative errors are determined, i.e. the one corresponding to the size evaluated as $\max\left[N_{\mathrm{Voigt}}; N_{\mathrm{Reuss}} \right]$ and the second one corresponding to the size resulting from correlation length condition N_{l_p}. The number of pixels corresponding to both criterions as well as the limiting accuracy 2ε are also provided. It should be mentioned that all results presented below have been obtained for the case of $\Theta = 10$.

Table 6.26. Relative error between mean value $\overline{K}$ and effective thermal conductivity coefficient K^{eff}.

Type of microstructure	Relative error $\dfrac{\left\|\overline{K}-K^{\text{eff}}\right\|}{K^{\text{eff}}}*100\%$		Limiting accuracy (2ε)
	$\max\left[N_{\text{Voigt}};N_{\text{Reuss}}\right]$	N_{l_p}	
Random checkerboard, $\phi_1=0.3$	0.02 %	13.17 %	2%
	12 pixels	3 pixels	
Ising model type C microstructure	5.14 %	11.12 %	6%
	31 pixels	22 pixels	
System of overlapping disks	0.03 %	9.21 %	6%
	52 pixels	28 pixels	
System of non-overlapping disks	0.66 %	0.65 %	6%
	37 pixels	44 pixels	
Debye microstructure	2.16 %	6.21 %	6%
	46 pixels	24 pixels	
Modified Debye microstructure	1.07 %	0.25 %	6%
	23 pixels	46 pixels	
Fontainebleau sandstone	2.38 %	6.11 %	6%
	46 pixels	20 pixels	
B$_4$C/Al	2.07 %	1.86 %	6%
	30 pixels	34 pixels	

Observing results above (Table 6.26), one can simply notice that for all considered microstructures the relative error satisfies the condition (6.30). Furthermore, it can be seen that in many cases the relative error yields quite large margin of tolerance. On the other hand, if we focus for instance on relative error corresponding to Ising model, we see that $\max\left[N_{\text{Voigt}};N_{\text{Reuss}}\right]=31$ pixels and the relative error is 5.14% - it only slightly differs from limiting value 2ε=6%. Decreasing the size of RVE to N=26 pixels causes that the relative error is 7.13 %. This fact can also be observed for other microstructures, particularly in case of $\Theta=50$ and ε=1% (see for

instance Table 6.4, ϕ_1=0.3 – the relative error is 1.95%, while limiting accuracy is 2%). Therefore the size of RVE resulting from the condition derived cannot be decreased.

7. Final conclusions

At the end of this work, what should be strongly emphasized, only general – most important – conclusions are provided. Detailed remarks, concerning all aspects considered in this work, are formulated after each chapter.

It has been found in this work that effective transport properties of random heterogeneous materials can be successfully determined as mean values averaged over sufficient number of microstructure realizations. Furthermore, it has been shown, on the basis of numerical (chapter 6) and analytical results (random checkerboard – chapter 3), that the size of the sample should be chosen very carefully, i.e. if one chooses the size which is not large enough, the mean value does not coincide with effective property.

The methodology of RVE size determination, which has been formulated in this work, is based on the microstructural descriptor, namely the two-point correlation function. Note that the condition for RVE size has been formulated with respect to microstructure geometry (chapter 4) and with respect to overall transport properties (chapter 5), separately. A validation of proposed methods has been performed by considering different types of random microstructures, i.e. random checkerboard, Ising model microstructures, system of non-overlapping and overlapping disks, Debye (and modified Debye) model, Fontainebleau sandstone microstructure and boron-carbide/aluminum composite.

It appeared that in case of overall transport properties the size of RVE is a function of several parameters: the morphology of microstructure, volume fractions of phases which constitute the medium, contrast in properties, number of performed realizations as well as a desired accuracy. Note that this conclusion is consistent with the one presented by Kanit *et al.* (2003) who proposed the methodology of RVE size determination in which the notion of *integral range* plays a central role.

It should be strongly emphasized that method proposed by Kanit *et al.* (2003) (as well as other methods presented in chapter 5) requires large number of numerical simulations. In other words, for the evaluation of RVE size, one has to determine the values of mechanical responses corresponding

to several realizations of different sizes. Usually large number of realizations has to be considered, and therefore, the process of RVE size determination may require large computational (time) cost. Furthermore, none of aforementioned methods provides a condition for the minimum size of the sample, which can be treated as the representative one for given microstructure morphology.

What is remarkable, a method which has been proposed in this work, utilizes the microstructure morphology (contained within the two-point correlation function), and therefore, it gives the possibility of RVE size determination with no large number of numerical calculations. In other words, the main advantage, comparing to aforementioned methods, is that one does not have to evaluate mechanical responses corresponding to large number of microstructure realizations – for RVE size determination, numerical calculations like those of FE or other methods, are not necessary.

The above implies that the process of determination of effective transport properties of two-phase random composites (on the basis of microstructure digital images) can be summarized in three simple steps:

1.) Determine the minimum size of RVE using proposed method, i.e.:

- having a digital image of microstructure, evaluate the two-point probability function of an arbitrary phase, say phase 1, using relations (4.22),

- determine the variance of local volume fraction $\left(\mathrm{Var}\{\xi\}\right)$ given by (4.70) – apply the Monte Carlo approach (4.82),

- evaluate the variance of both local Voigt $\left(\mathrm{Var}\{\xi_k\}\right)$ and local Reuss $\left(\mathrm{Var}\{\xi_{1/k}\}\right)$ estimates – use relation (5.39),

- set the wanted precision ε for the estimation and evaluate the minimum size of RVE which satisfies the inequality (5.53) and (5.56),

- choose RVE size - larger than or equal to the minimum one determined according the condition (5.57).

2.) Determine - for previously chosen RVE size - sufficient number of realizations *n*:

- set the significance level α as well as desired accuracy ε and determine the sufficient number of realizations *n* applying central limit theorem – relations (6.20) - (6.22); note,

in this work the significance level is $\alpha=0.05$, and therefore, the number of realizations has been evaluated as:

$$n \geq \max \left[\frac{Var(\xi_k)}{\langle \xi_k \rangle^2}; \frac{Var(\xi_{1/k})}{\langle \xi_{1/k} \rangle^2} \right] \left(\frac{1.96}{\varepsilon} \right)^2 \tag{7.1}$$

3.) Using numerical tool (for instance pixel based finite volume scheme) determine the effective property as the mean value, averaged over sufficient number of realizations *n*:

- prescribe periodic boundary conditions to each *j*-realization,
- evaluate transport property corresponding to each microstructure realization, K_j,
- determine effective property as mean value, i.e.

$$\overline{K} = \sum_{j=1}^{n} K_j \tag{7.2}$$

As a final conclusion it should strongly emphasized that, even though a methodology has been formulated and validated only on the basis of 2D microstructures, it is possible to investigate real 3D materials. Note that the numerical method, namely pixel based finite volume scheme, has been formulated for 3D case. Furthermore, in case of RVE size determination as well as evaluation of the sufficient number of realizations a variance of local volume fraction plays a central role. In case of 3D microstructures – cube consisted of N^3 pixels – it can be expressed as:

$$Var_{3D}(\xi) = \frac{8}{\|\Omega_0\|^3} \int_0^N \int_0^N \int_0^N \left(S_2^{(1)} \left(\sqrt{x^2 + y^2 + z^2} \right) - \phi_1^2 \right) (N-x)(N-y)(N-z) \, dxdydz \tag{7.3}$$

Moreover, a Monte Carlo approach (presented in section 4.3.2) can be also successfully applied for the calculation of (7.3). Comparing to 2D case, the only change is that one has to evaluate additional non-uniformly distributed random number, say $Z(Q_i)$, and then the MC estimator of (7.3) is as follows:

$$Var_{3D}(\xi) \approx \frac{1}{n} \sum_{i=1}^{n} \left(S_2^{(1)} \left(\sqrt{X(Q_i)^2 + Y(Q_i)^2 + Z(Q_i)^2} \right) - \phi_1^2 \right) \tag{7.4}$$

This work should be regarded as an introduction to the problem of numerical determination of effective properties of random composites. The aim of future works will be an application of proposed method to the problem of other classes of linear composites (effective elastic properties – for instance) as well as non-linear ones.

8. References

Aboudi J.: *Mechanics of Composite Materials: A Unified Micromechanics Approach*, Elsevier, New York, 1991.

Aboudi J.: *Micromechanical Analysis of Thermo-Inelastic Multiphase Short-Fiber Composites*, Composites Engineering, Vol. 5, 1995, pp. 839-850.

Beran M.J.: *Statistical Continuum Theories*, Monographs in Statistical Physics, Interscience Publishers, 1968.

Berryman J. G.: *Relationship between specific surface area and spatial correlation functions for anisotropic porous media*, J. Math. Phys., Vol. 28, 1987, pp. 244.

Berryman J. G., Blair S.C.: *Use of digital image analysis to estimate fluid permeability of porous materials: Application of two-point correlation function.* Journal of Applied Physics, Vol. 60(6), 1986, pp.1930-1938.

Berryman J.G., Milton G.W.: *Microgeometry of random composites and porous media*, J. Phys. D: Appl. Phys., Vol. 21, 1988, pp.87-94.

Bristow J.R.*: Microcracks, and the static and dynamic elastic constants of annealed and heavily cold-worked metals*, J. Appl. Phys., Vol. 11, 1960, pp.81-85.

Brown W.F. Jr.: *Solid Mixture Permittivies*, J.Chem.Phys.,Vol.23, 1955, pp. 1514-1517.

Debye P., Anderson H.R., Brumberger H.: *Scattering by an inhomogeneous solid II. The correlation function and its applications,* J. Appl. Phys., Vol. 28, 1957, pp. 679-683.

Dormieux L., Kondo D., Ulm F.J.: *Microporomechanics*, John Wiley & Sons, 2006.

Dormieux L., Ulm F.J. (eds.): Applied Micromechanics of Porous Materials, Springer, 2005.

Drugan W.J., Willis J.R.: *A micromechanics-based nonlocal constitutive equation and estimates of representative volume element size ofr elastic composites*, J. Mech. Phys., Vol. 44, 1996, pp.497-524.

Du X., Ostoja-Starzewski M.: *On the size of representative volume element for Darcy law in random media*, Proc.R.Soc. London A, Vol. 462, 2006, pp. 2949-2963.

Dvorak G.J., Benveniste Y.: *On transformation strains and uniform fields in multiphase elastic media*, Proc. R. Soc. Lond. A, Vol. 437, 1992, pp.291.

Eymard R., Gallouët T., Herbin R.: *Finite Volume Methods* (2003) - this manuscript is an update of the preprint n0 97-19 du LATP, UMR 6632, Marseille, September 1997 which appeared in Handbook of Numerical Analysis, P.G. Ciarlet, J.L. Lions eds, Vol. 7, pp 713-1020.

Fehske H., Schneider R., Weiße A. (Eds.): *Computational Many-Particle Physics*, Lect. Notes Phys. 739, Springer Berlin Heidelberg, 2008.

Feller W.: *An Introduction to Probability Theory And Its Applications*, John Wiley and Sons, New York, 1961.

Fishman G.S.: *Monte Carlo: Concepts, Algorithms, and Applications*, Springer-Verlag, New York, 1996.

FlexPDE, *User Guide Version 5.0*, PDE Solutions Inc., 2005.

Gan H., Orozco C.E., Herakovich C.T.: *A strain - compatible method for micromechanical analysis of multi - phase composites,* Int J Solids Struct, Vol. 37, 2000, pp. 5097-5122.

Garboczi E.J., Bentz D.P. Martys N.S.: *Experimental Methods for Porous Media*, Academic Press, New York, 1999.

Gitman I.M., Askes H., Sluys L.J.: *Representative volume: existence and size determination*, Eng Fract Mech, Vol. 74, 2007, pp.2518.

Graham S., Yang N.: *Representative volumes of materials based on microstructural statistics*, Scripta Materialia, 48, 2003, pp.269-274.

Grufman C., Fernand E.: Determining a representative volume element capturing the morphology of fibre reinforced polymer composites, Compos Sci Technol, Vol. 67, 2007, pp.766-775.

Gusev A.A.: *Representative volume element size for elastic composites: a numerical study*, J. Mech. Phys. Solids, Vol. 45, 1997, pp.1449–1459.

Hashin Z., Shtrikman S.: *A variational approach to the theory of elastic behavior of multiphase materials*, J. Mech. Phys. Solids, Vol. 11, 1963, pp.127.

Hashin Z.: *Analysis of composite materials – a survey*, ASME J. Appl. Mech., Vol. 50, 1983, pp.481-505

Janke W.: *Pseudo random number: generation and quality checks*, Lecture Notes John von Neumann Institute for Computing, Vol. 10, 2002, pp.447.

Kalos M.H., Whitlock P.A.: *Monte Carlo Methods. Second Edition*, Wiley-VCH Verlag, Weinheim, 2008.

Kanit T., Forest S., Galliet I., Mounoury V., Jeulin D.: *Determination of the size of the representative volume element for random composites: statistical and numerical approach*, Int J Solids Struct, Vol. 40, 2003, pp.3647.

Kanit T., N'Guyen F., Forest S., Jeulin D., Reed M., Singleton S.: *Apparent and effective physical properties of heterogeneous materials: Representativity of samples of two materials form food industry*, Comput. Methods Appl. Mech. Engrg, 195 (33-36), 2006, pp.3960-3982.

Kirkpatrick S., Gelatt C.D., Vecchi M.P.; *Optimization by simulated annealing*, Science, 220, 1983, pp. 671-680.

Lado F., Torquato S.: *Two-point probability function for distributions of oriented hard ellipsoids*, J.Chem.Phys., Vol. 93, 1990, pp. 5912-5917.

Lantuéjoul C.: *Geostatistical Simulation Models And Algorithms*, Springer, Berlin, 2002.

Levin V.M.: *On the coefficients of thermal expansion of heterogeneous materials*, Mech. Solids 2, 1967, pp.58–61.

Lu B., Torquato S.: *Local volume fraction fluctuations in heterogeneous media*, J. Chem. Phys. 93 (5), 1990, pp. 3452-3459.

Lu B., Torquato S.: *Lineal-path function for random heterogeneous materials*, Phys Rev A, Vol. 45 (2), 1992, pp. 922-929.

Łydżba D.: *Applications of asymptotic homogenization method in soil and rock mechanics*, Scientific Papers of the Institute of Geotechnics and Hydrotechnics of the Wroclaw University of Technology, 2002 (in polish).

Łydżba D., Różański A.: *Random composites: numerical prediction of the effective transport properties, Geotechnika w budownictwie i górnictwie*. XXX Zimowa Szkoła Mechaniki Górotworu i Geoinżynierii, Szklarska Poręba, 11-16 marca 2007, Wrocław: Oficyna Wydaw. PWr, 2007, pp. 441-450 (in polish).

Łydżba D., Różański A.: *Statistical characterization of geometrical measures of random microstructures: definitions, properties and applications*, Górnictwo i Geoinżynieria, 2009, Vol. 33 (1), pp.399-410 (in polish).

Łydżba D., Różański A., Kawa M.: *Generalized Method of Cells – computationally more efficient formulation*, Scientific Papers of the Wroclaw University of Technology 2007, pp. 154-164 (in polish).

Mathematica: *Wolfram Mathematica Tutorial Collection*, 2008

Milton G.W.: *Bounds on the electromagnetic, elastic and other properties of two component composites*, Phys. Rev. Lett., Vol. 46, No. 8, 1981a, pp. 542-545.

Milton G.W.: *Bounds on the transport and optical properties of a two-component composite material*, J. Appl. Phys., 52, 1981b, pp.5294-5304.

Milton G.W.: *Concerning bounds on the transport and mechanical properties of multicomponent composite materials*, Appl. Phys. A26, 1981c, pp.125-130.

Milton G.W.: *The theory of composites,* Cambridge University Press, 2002.

Paley M., Aboudi J.: *Micromechanical Analysis of Composites by the Generalized Method of Cells*, Mechanics of Materials, Vol. 14, 1992, pp. 127-139.

Patankar S.: *Numerical Heat Transfer and Fluid Flow*, Hemisphere Publishing Corporation, New York, 1980.

Prapainop R., Maneeratana K.: *Simulation of ice formation by the finite volume method*, Songklanakarin Journal of Science and Technology, Vol.26 (1), 2004, pp. 55-70.

Povirk G.L.: *Incorporation of microstructural information into model of two-phase materials*, Acta Metall. Mater., 43 (8), 1995, pp. 3199-3206.

Quintanilla J., Torquato S.: *Lineal measures of clustering in overlapping particle systems*, Phys Rev E, Vol. 54(4), 1996, pp. 4027-4036.

Quintanilla J., Torquato S.: *Local volume fraction fluctuations in random media*, J. Chem. Phys. 106 (7), 1997, pp. 2741-2751.

Quintanilla J., Torquato S.: *Local volume fraction fluctuations in periodic heterogeneous media*, J. Chem. Phys. 110 (6), 1999, pp. 3215-3219.

Różański A., Łydżba D.: *Some remarks on the size of representative volume element (RVE) in case of 2D lattice model*, Górnictwo i Geoinżynieria, 2009, Vol. 33 (1), pp.507-517 (in polish).

Rózański A., Łydżba D., Shao J.F.: *Numerical evaluation of effective transport properties of random cell models: two-point probability approach*, Proceedings of the 3rd International Symposium GeoProc 2008, Lille, 1st-5th June, 2008, pp.345.

Rózański A., Łydżba D., Shao J.F.: *Numerical determination of minimum size of RVE for random composite materials: two-point probability approach*, Proceedings of the First International Symposium on Computational Geomechanics, COMGEO I, Juan les Pins, France, 29 April - 1 May, 2009 / eds S. Pietruszczak *et al.*, Rhodes : IC2E International Centre for Computational Engineering, 2009, pp.26-37.

Sab K.: *On the homogenization and the simulation of random materials*, Eur. J. Mech. Solids, Vol. 11, 1992, pp.585.

Sejnoha M., Zeman J.: *Micromechanical Analysis of Random Composites*, Czech Technical University, 2000.

Sen A.K., Torquato S.: *Effective conductivity of anisotropic two-phase composite media*, Phys. Rev. B, 39, 1989, pp.4504-4515.

Stroeven M., Askes H., Sluys L.J.: *Numerical determination of representative volumes for granular materials*, Comput Meth Appl Mech Engng, Vol. 193, 2004, pp.3221.

Suquet P.: *Elements of homogenization for inealastic solid mechanics*, in: Homogenization technique for composite media, Lecture Notes in Physics, 272, Springer,1987.

Suquet P.: *Continuum micromechanics*, CISM Courses and Lectures No. 377, Springer-Verlag, 1997.

Sviercoski R.F., Travis B.J.: *Analytical effective coefficient for block inclusions: Numerical results for linear flow*, Transp. Porous Media, 2007 (submitted for publication)

Thomas M., Boyard N., Perez L., Jarny Y., Delaunay D.: *Representative volume element of anisotropic unidirectional carbon-epoxy composite with high-fibre volume fraction*, Compos Sci Technol, Vol. 68, 2008, pp.3184.

Torquato S.: *Effective electrical conductivity of two-phase disordered composite media*, J. Appl. Phys., Vol. 58, 1985, pp.3790-3797.

Torquato S.: *Random Heterogeneous Materials. Microstructure and Macroscopic Properties*, Springer-Verlag, New York, 2002.

Torquato S., Stell G.: *Microstructure of two-phase random media, I: The n-point probability functions*, J. Chem. Phys., Vol. 77, 1982, pp.2071.

Torquato S., Sen A.K.: *Conductivity tensor of anisotropic composite media from the microstructure*, J. Appl. Phys., 67, 1990, pp. 1145-1155.

van Mier J.G.M.: *Fracture Processes of Concrete*, USA: CRC Press, Inc., 1997.

Willis J.R.: *Bounds and self-consistent estimates for the overall properties of anisotropic composites*, J. Mech. Phys. Solids, Vol. 25, 1977, pp.185-202.

Yeong C.L.Y., Torquato S.: *Reconstructing random media*, Phys. Rev. E, Vol. 57, 1998a, pp.495.

Yeong C.L.Y., Torquato S.: *Reconstructing random media II. Three dimensional media from two-dimensional cuts*, Phys. Rev. E, Vol. 58, 1998b, pp.224.

Zaoui A.: *Approximate statistical modeling and applications, in: Homogenization Techniques for Composite Media*, Lecture Notes in Physics, Springer-Verlag, Berlin, 1987.

Zeman J., Sejnoha M.: *Numerical evaluation of effective elastic properties of graphite fiber tow impregnated by polymer matrix*, J. Mech. Phys. Solids, Vol. 49, 2001, pp.69.

Zhao H.F., Hu G.K., Lu T.J.: *Cross property relations for two-phase planar composites*, Comp. Mat. Sc., Vol. 35, 2006, pp.408.

Zohdi T.I., Wriggers P., Huet C., *A method of substracting large-scale computational micromechanical problems*, Comput. Methods Appl. Mech. Engrg., Vol. 190, 2001, pp.5639

Zohdi T.I., Wriggers P.: *Introduction to Computational Micromechanics*, Springer-Verlag, Berlin, 2005.